

Measurement of differential cross sections for the production of top quark pairs and of additional jets in lepton + jets events from pp collisions at $\sqrt{s} = 13$ TeV

A. M. Sirunyan *et al.*^{*}
(CMS Collaboration)

(Received 23 March 2018; published 15 June 2018)

Differential and double-differential cross sections for the production of top quark pairs in proton-proton collisions at $\sqrt{s} = 13$ TeV are measured as a function of kinematic variables of the top quarks and the top quark-antiquark ($t\bar{t}$) system. In addition, kinematic variables and multiplicities of jets associated with the $t\bar{t}$ production are measured. This analysis is based on data collected by the CMS experiment at the LHC in 2016 corresponding to an integrated luminosity of 35.8 fb^{-1} . The measurements are performed in the lepton + jets decay channels with a single muon or electron and jets in the final state. The differential cross sections are presented at the particle level, within a phase space close to the experimental acceptance, and at the parton level in the full phase space. The results are compared to several standard model predictions that use different methods and approximations. The kinematic variables of the top quarks and the $t\bar{t}$ system are reasonably described in general, though none predict all the measured distributions. In particular, the transverse momentum distribution of the top quarks is more steeply falling than predicted. The kinematic distributions and multiplicities of jets are adequately modeled by certain combinations of next-to-leading-order calculations and parton shower models.

DOI: 10.1103/PhysRevD.97.112003

I. INTRODUCTION

Measurements of differential production cross sections of top quark pairs ($t\bar{t}$) provide important information for testing the standard model and searching for phenomena beyond the standard model. Precise theoretical predictions of these measurements are challenging since higher-order effects of quantum chromodynamics (QCD) and electro-weak (EW) corrections [1] are important. Moreover, the generation of $t\bar{t}$ events requires a realistic modeling of the parton shower (PS). The measured kinematic properties and multiplicities of jets allow for a detailed comparison of different PS models to the data and provide insight into their tuning.

In this paper, differential and double-differential production cross sections as a function of kinematic variables of the top quarks and the $t\bar{t}$ system are reported. In addition, measurements of multiplicities and kinematic properties of jets in $t\bar{t}$ events are presented. The measurements are based on proton-proton (pp) collision data at a center-of-mass energy of 13 TeV corresponding to an integrated luminosity

of 35.8 fb^{-1} [2]. The data were recorded by the CMS experiment at the CERN LHC in 2016. Only $t\bar{t}$ decays into the $\ell + \text{jets}$ ($\ell = e, \mu$) final state are considered, where, after the decay of each top quark into a bottom quark and a W boson, one of the W bosons decays hadronically and the other one leptonically. Hence, the experimental signature consists of two jets coming from the hadronization of b quarks (b jets), two jets from a hadronically decaying W boson, a transverse momentum imbalance associated with the neutrino from the leptonically decaying W boson, and a single isolated muon or electron.

This measurement continues a series of differential $t\bar{t}$ production cross section measurements in pp collisions at the LHC. Previous measurements of differential cross sections at $\sqrt{s} = 7$ TeV [3,4] and 8 TeV [5–11] have been performed in various $t\bar{t}$ decay channels. First measurements at 13 TeV are available [12–14]. Previous studies of multiplicities and kinematic properties of jets in $t\bar{t}$ events can be found in Refs. [15–17]. With about 15 times more data and an improved understanding of systematic uncertainties, we provide an update and extension to the previous CMS analysis in the $\ell + \text{jets}$ channel at 13 TeV [18].

We measure differential cross sections defined in two ways: at the particle level and the parton level. For the particle-level measurement a proxy of the top quark is defined based on experimentally accessible quantities, such as properties of jets, which are made up of quasistable

*Full author list given at the end of the article.

Published by the American Physical Society under the terms of the [Creative Commons Attribution 4.0 International license](#). Further distribution of this work must maintain attribution to the author(s) and the published article's title, journal citation, and DOI. Funded by SCOAP³.

particles with a mean lifetime greater than 30 ps. These quantities are described by theoretical predictions that require modeling of the PS and hadronization, in addition to the matrix-element calculations. The kinematic requirements on these objects are chosen to closely reproduce the experimental acceptance. Muons and electrons stemming from τ lepton decays are not treated separately and can contribute to the particle-level signal. A detailed definition of particle-level objects is given in Sec. III. The particle-level approach has the advantage that it reduces theoretical uncertainties in the experimental results by avoiding theory-based extrapolations from the experimentally accessible portion of the phase space to the full range, and from jets to partons.

For the parton-level measurement top quarks in the $\ell + \text{jets}$ decay channel are defined as signal directly before their decays into a bottom quark and a W boson. The $\tau + \text{jets}$ decay channel is not considered here as signal even in cases where the τ lepton decays into a muon or electron. No restriction on the phase space is applied for parton-level top quarks. The corrections and extrapolations used in this measurement are based on a next-to-leading-order (NLO) calculation of $t\bar{t}$ production, combined with a simulation of the PS.

For both particle- and parton-level measurements the $t\bar{t}$ system is reconstructed at the detector level with a likelihood-based approach using the top quark and W boson mass constraints to identify the corresponding top quark decay products. The differential cross sections are measured at the particle and parton levels as a function of the transverse momentum p_T and the absolute rapidity $|y|$ of the top quarks, separately for the hadronically (labeled t_h) and leptonically (labeled t_ℓ) decaying W bosons, and the p_T , $|y|$, and invariant mass M of the $t\bar{t}$ system. In addition, the differential cross sections at the parton level are determined as a function of the lower- and higher- p_T values of the top quarks in an event. Double-differential cross sections for the following combinations of variables are determined at both levels: $|y(t_h)|$ vs. $p_T(t_h)$, $M(t\bar{t})$ vs. $|y(t\bar{t})|$, and $p_T(t_h)$ vs. $M(t\bar{t})$. At particle level, the differential cross sections as a function of $p_T(t_h)$, $p_T(t\bar{t})$, and $M(t\bar{t})$ are measured in bins of jet multiplicity. Using the four jets identified as the $t\bar{t}$ decay products and the four highest- p_T additional jets, the cross sections are determined as a function of the jet p_T and absolute pseudorapidity $|\eta|$, the minimal separation ΔR_{j_i} of jets from another jet in the $t\bar{t}$ system, and the separation ΔR_t of jets from the closest top quark. Here $\Delta R = \sqrt{(\Delta\phi)^2 + (\Delta\eta)^2}$, where $\Delta\phi$ and $\Delta\eta$ are the differences in azimuthal angle (in radians) and pseudorapidity between the directions of the two objects. Finally, we determine the gap fraction, defined as the fraction of events that do not contain jets above a given p_T threshold, and the jet multiplicities for various thresholds of the jet p_T .

This paper is organized as follows: In Sec. II, we provide a description of the signal and background simulations,

followed by the definition of the particle-level top quarks in Sec. III. After a short overview of the CMS detector and the particle reconstruction in Sec. IV, we describe the object and event selections in Sec. V. Section VI contains a detailed description of the reconstruction of the $t\bar{t}$ system. Details on the background estimation and the unfolding are presented in Secs. VII and VIII. After a discussion of systematic uncertainties in Sec. IX, the differential cross sections as a function of observables of the top quark and the $t\bar{t}$ system are presented in Sec. X. Finally, observables involving jets are discussed in Sec. XI. The results are summarized in Sec. XII.

II. SIGNAL AND BACKGROUND MODELING

The Monte Carlo generator POWHEG [19–22] (v2,hvq) is used to calculate the production of $t\bar{t}$ events at NLO accuracy in QCD. The renormalization μ_r and factorization μ_f scales are set to the transverse mass $m_T = \sqrt{m_t^2 + p_T^2}$ of the top quark, where a top quark mass $m_t = 172.5$ GeV is used in all simulations. The result is combined with the PS simulations of PYTHIA8 [23,24] (v8.219) using the underlying event tune CUETP8M2T4 [25,26], and of HERWIG++ [27] (v2.7.1) using the tune E5SC [28]. In addition, MADGRAPH 5_AMC@NLO [29] (v2.2.2) (MG5_AMC@NLO) is used to produce a simulation of $t\bar{t}$ events with additional partons. All processes with up to two additional partons are calculated at NLO and combined with the PYTHIA8 PS simulation using the FxFx [30] algorithm. The scales are selected as $\mu_r = \mu_f = \frac{1}{2}(m_T(t) + m_T(\bar{t}))$. The default parametrization of the parton distribution functions (PDFs) used in all simulations is NNPDF30_nlo_as_0118 [31]. The simulations are normalized to an inclusive $t\bar{t}$ production cross section of 832^{+40}_{-46} pb [32]. This value is calculated with next-to-NLO (NNLO) accuracy, including the resummation of next-to-next-to-leading-logarithmic soft-gluon terms. Its uncertainty is evaluated by varying the choice of μ_r and μ_f and by propagating uncertainties in the PDFs.

Distributions that correspond to variations in the PDFs or the scales μ_r and μ_f are obtained by applying different event weights. These distributions are used for the corresponding uncertainty estimates. For additional uncertainty estimations we use POWHEG+PYTHIA8 simulations with top quark masses of 171.5 and 173.5 GeV, with initial and final PS scales varied up and down by a factor of two, with variations of the underlying event tune, and a simulation with an alternative color-reconnection model.

The main backgrounds are simulated using the same techniques. The MG5_AMC@NLO generator is used for the simulation of W boson production in association with jets, t -channel single top quark production, and Drell–Yan (DY) production in association with jets. The generator POWHEG [33] is used for the simulation of single top quark associated production with a W boson (tW), and PYTHIA8 is used for multijet production. In all cases, the PS and the

hadronization are described by PYTHIA8. The W boson and DY backgrounds are normalized to their NNLO cross sections calculated with FEWZ [34] (v3.1). The t -channel single top quark production is normalized to the NLO calculation obtained from HATHOR [35] (v2.1). The production of tW is normalized to the NLO calculation [36], and the multijet simulation is normalized to the LO calculation obtained with PYTHIA8 [24].

The detector response is simulated using GEANT4 [37]. The simulations include multiple pp interactions per bunch crossing (pileup). The simulated events are weighted, depending on their number of pileup interactions, to reproduce the measured pileup distribution. Finally, the same reconstruction algorithms that are applied to the data are used for the simulated events.

III. PARTICLE-LEVEL TOP QUARK DEFINITION

The definitions of particle-level objects constructed from quasi-stable simulated particles, obtained from the predictions of $t\bar{t}$ event generators before any detector simulation, are summarized below. These particle-level objects are further used to define the particle-level top quarks. Detailed studies on particle-level definitions can be found in Ref. [38].

- (i) All simulated muons and electrons are corrected for effects of bremsstrahlung by adding the photon momenta to the momentum of the closest lepton if their separation is $\Delta R < 0.1$. All photons are considered for the momentum correction. A corrected lepton is selected if it fulfills the isolation requirement that the p_T sum of all quasi-stable particles, excluding corrected leptons and neutrinos, within $\Delta R = 0.4$ is less than 35% of the corrected lepton p_T . In addition, we require the lepton to have $p_T > 15$ GeV and $|\eta| < 2.4$.
- (ii) Simulated photons with $p_T > 15$ GeV and $|\eta| < 2.4$ that are not used in the momentum correction of a lepton are considered if their isolation, defined analogously to the lepton isolation, is below 25%.
- (iii) All neutrinos are selected including those stemming from decays of hadrons.
- (iv) Jets are clustered by the anti- k_T jet algorithm [39,40] with a distance parameter of 0.4. All quasistable particles with the exception of neutrinos are clustered. Jets with $p_T > 25$ GeV and $|\eta| < 2.4$ are selected if there is no isolated lepton or photon, as defined above, within $\Delta R = 0.4$.
- (v) b jets at the particle level are defined as those jets that contain a b hadron. As a result of the short lifetime of b hadrons, these are not quasistable particles and only their decay products should be considered for the jet clustering. However, to allow their association with a jet, the b hadrons are also included with their momenta scaled down to a negligible value. This preserves the information of

their directions, but removes their impact on the jet clustering.

Based on the invariant masses of these objects, we construct a pair of particle-level top quarks in the $\ell +$ jets final state. Events with exactly one muon or electron with $p_T > 30$ GeV and $|\eta| < 2.4$ are selected. Simulated events with an additional muon or electron with $p_T > 15$ GeV and $|\eta| < 2.4$ are rejected. We take the sum of the four-momenta of all neutrinos as the neutrino candidate momentum p_ν from the leptonically decaying top quark and find the permutation of jets that minimizes the quantity

$$\begin{aligned} & [M(p_\nu + p_\ell + p_{b_\ell}) - m_t]^2 + [M(p_{j_{w1}} + p_{j_{w2}}) - m_W]^2 \\ & + [M(p_{j_{w1}} + p_{j_{w2}} + p_{b_h}) - m_t]^2, \end{aligned} \quad (1)$$

where $p_{j_{w1,2}}$ are the four-momenta of two light-flavor jet candidates, considered as the decay products of the hadronically decaying W boson; $p_{b_{\ell,h}}$ are the four-momenta of two b jet candidates; p_ℓ is the four-momentum of the lepton; and $m_W = 80.4$ GeV [41] is the mass of the W boson. All jets with $p_T > 25$ GeV and $|\eta| < 2.4$ are considered. At least four jets are required, of which at least two must be b jets. The remaining jets with $p_T > 30$ GeV and $|\eta| < 2.4$ are defined as additional jets.

Events with a hadronically and a leptonically decaying particle-level top quark are not required to be $\ell +$ jets events at the parton level, e.g., $t\bar{t}$ dilepton events with additional jets can be identified as $\ell +$ jets event at the particle level if one lepton fails to pass the selection. As an example, the comparison between the $p_T(t_h)$ distributions at the particle and parton levels are shown in Fig. 1 and demonstrates the direct relation between particle-level and parton-level top quarks.

To obtain an unambiguous nomenclature for the jets, we define j_{w1} to be the jet in the W boson decay with the higher p_T . The additional jets j_i are sorted by their transverse momenta where j_1 has the highest p_T .

IV. THE CMS DETECTOR

The central feature of the CMS detector is a superconducting solenoid of 6 m internal diameter, providing a magnetic field of 3.8 T. Within the solenoid volume are a silicon pixel and strip tracker, a lead tungstate crystal electromagnetic calorimeter (ECAL), and a brass and scintillator hadron calorimeter (HCAL), each composed of a barrel and two endcap sections. Forward calorimeters extend the η coverage provided by the barrel and endcap detectors. Muons are measured in gas-ionization detectors embedded in the steel flux-return yoke outside the solenoid. A more detailed description of the CMS detector, together with a definition of the coordinate system and relevant kinematic variables, can be found in Ref. [42].

The particle-flow (PF) event algorithm [43] reconstructs and identifies each individual particle with an optimized

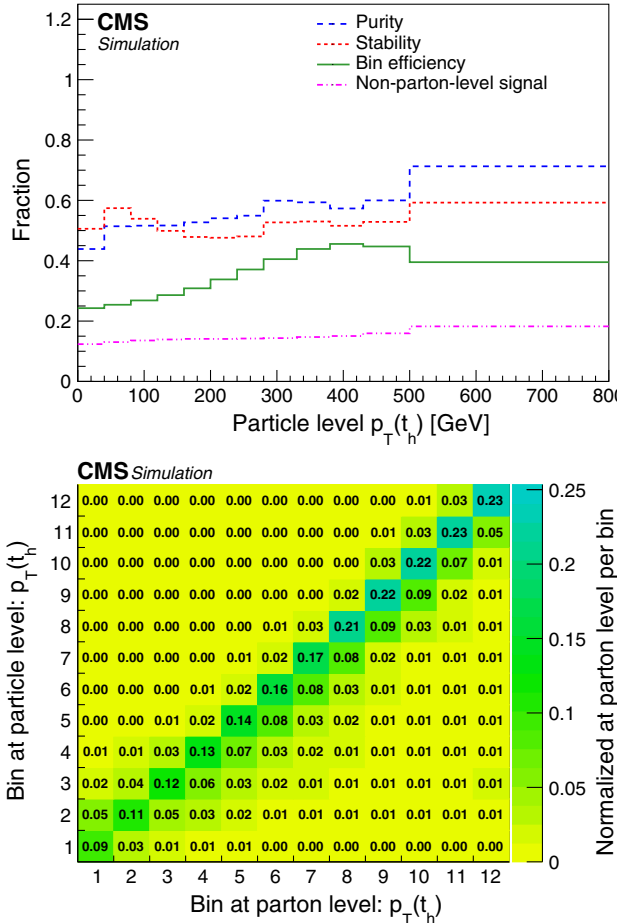


FIG. 1. Comparison between the $p_T(t_h)$ distributions at the particle and parton level, extracted from the POWHEG+PYTHIA8 simulation. Left: fraction of parton-level top quarks in the same p_T bin at the particle level (purity), fraction of particle-level top quarks in the same p_T bin at the parton level (stability), ratio of the number of particle- to parton-level top quarks (bin efficiency), and fraction of events with a particle-level top quark pair that are not considered as signal events at the parton level (non-parton-level signal). Right: p_T -bin migrations between particle and parton level. The p_T range of the bins can be taken from the left panel. Each column is normalized such that the sum of its entries corresponds to the fraction of particle-level events in this bin at the parton level in the full phase space.

combination of information from the various elements of the CMS detector. The energy of muons is obtained from the curvature of the corresponding track. The energy of electrons is determined from a combination of the electron momentum at the primary interaction vertex as determined by the tracker, the energy of the corresponding ECAL cluster, and the energy sum of all bremsstrahlung photons spatially compatible with originating from the electron track. The energy of photons is directly obtained from the ECAL measurement, corrected for zero-suppression effects. The energy of charged hadrons is determined from a combination of their momentum measured in the tracker

and the matching ECAL and HCAL energy deposits, corrected for zero-suppression effects and for the response function of the calorimeters to hadronic showers. Finally, the energy of neutral hadrons is obtained from the corresponding corrected ECAL and HCAL energy.

V. PHYSICS OBJECT RECONSTRUCTION AND EVENT SELECTION

The measurements presented in this paper depend on the reconstruction and identification of muons, electrons, jets, and missing transverse momentum associated with a neutrino. Muons and electrons are selected if they are compatible with originating from the primary vertex, which, among the reconstructed primary vertices, is the one with the largest value of summed physics-object p_T^2 . The physics objects are jets, clustered using the jet finding algorithm [39,40] with the tracks assigned to the primary vertex as inputs, and the associated missing transverse momentum, taken as the negative vector sum of the \vec{p}_T of those jets.

Since leptons from $t\bar{t}$ decays are typically isolated, a requirement on the lepton isolation is used to reject leptons produced in decays of hadrons. The lepton isolation variables are defined as the sum of the p_T of neutral hadrons, charged hadrons, and photon PF candidates within a cone of $\Delta R = 0.4$ for muons and $\Delta R = 0.3$ for electrons. It is required to be less than 15% (6%) of the muon (electron) p_T . Event-by-event corrections are applied to maintain a pileup-independent isolation efficiency. The muon and electron reconstruction and selection efficiencies are measured in the data using tag-and-probe techniques [44–46]. Depending on the p_T and η , their product is 75–85% for muons and 50–80% for electrons.

Jets are clustered from PF objects using the anti- k_T jet algorithm with a distance parameter of 0.4 implemented in the FASTJET package [40]. Charged particles originating from a pileup interaction vertex are excluded. The total energy of the jets is corrected for energy depositions from pileup. In addition, p_T - and η -dependent corrections are applied to correct for the detector response effects [47]. If an isolated lepton with $p_T > 15$ GeV within $\Delta R = 0.4$ around a jet exists, the jet is assumed to represent the isolated lepton and is removed from further consideration.

For the identification of b jets, the combined secondary vertex algorithm [48] is used. It provides a discriminant between b and non- b jets based on the combined information of secondary vertices and the impact parameter of tracks at the primary vertex. A jet is identified as a b jet if the associated value of the discriminant exceeds a threshold criterion with an efficiency of about 63% and a combined charm and light-flavor jet rejection probability of 97%.

The missing transverse momentum \vec{p}_T^{miss} is calculated as the negative of the vectorial sum of transverse momenta of all PF candidates in the event. Jet energy corrections are also propagated to improve the measurement of \vec{p}_T^{miss} .

Events considered for this analysis are selected by single-lepton triggers. These require $p_T > 24$ GeV for muons and $p_T > 27$ GeV for electrons, as well as various quality and isolation criteria.

To reduce the background contributions and optimize the $t\bar{t}$ reconstruction, additional requirements are imposed on the recorded events. Events with exactly one muon or electron with $p_T > 30$ GeV and $|\eta| < 2.4$ are selected. No additional muons or electrons with $p_T > 15$ GeV and $|\eta| < 2.4$ are allowed. In addition to the lepton, at least four jets with $p_T > 30$ GeV and $|\eta| < 2.4$ are required. At least two of these jets must be identified as b jets.

We compare several kinematic distributions in the data to the simulation separately for the muon and electron channels to verify that there are no unexpected differences. The ratios of the measured to the expected event yields in the two channels agree within the uncertainty in the lepton reconstruction and selection efficiencies. In the remaining steps of the analysis, the two channels are combined by adding their distributions.

VI. RECONSTRUCTION OF THE TOP QUARK-ANTIQUARK SYSTEM

The reconstruction of the $t\bar{t}$ system follows closely the methods used in Ref. [18]. The goal is the correct identification of detector-level objects as parton- or particle-level top quark decay products. In the simulation, a jet or lepton at the particle level can be spatially matched to the corresponding detector-level object. If no one-to-one assignment to a corresponding detector-level object is possible for any of the objects in the particle-level $t\bar{t}$ system, the event is considered as “nonreconstructable” in the particle-level measurement. For the parton-level measurement a quark from the $t\bar{t}$ decay is assigned to the detector-level jet with the highest p_T within $\Delta R = 0.4$ around the parton. If no one-to-one correspondence at detector level is found for any of these quarks or the leptons, the event is “nonreconstructable” in the parton-level measurement. In particular, this includes events with merged topologies where at least two quarks are matched to the same jet. Based on these relations between detector level and parton or particle level, the efficiencies of the $t\bar{t}$ reconstruction are studied. A detailed discussion on the relationship between quantities at the parton or particle level and detector level is presented in Sec. VIII.

For the reconstruction all possible permutations of assigning detector-level jets to the corresponding $t\bar{t}$ decay products are tested and a likelihood that a certain permutation is correct is evaluated. Permutations are considered only if the two jets with the highest b identification probabilities are the two b jet candidates. In each event, the permutation with the highest likelihood is selected. The likelihoods are evaluated separately for the particle- and the parton-level measurements.

For each tested permutation the neutrino four-momentum p_ν is reconstructed using the algorithm of Ref. [49]. The idea is to find all possible solutions for the three components of the neutrino momentum vector using the two mass constraints $(p_\nu + p_\ell)^2 = m_W^2$ and $(p_\nu + p_\ell + p_{b_\ell})^2 = m_t^2$. Each equation describes an ellipsoid in the three-dimensional momentum space of the neutrino. The intersection of these two ellipsoids is usually an ellipse. We select p_ν as the point on the ellipse for which the distance $D_{\nu,\min}$ between the ellipse projection onto the transverse plane and \vec{p}_T^{miss} is minimal. This algorithm leads to a unique solution for the longitudinal neutrino momentum and an improved resolution of its transverse component. For the cases where the invariant mass of the lepton and b_ℓ candidate is above m_t , no solution can be found and the corresponding permutation is discarded. The minimum distance $D_{\nu,\min}$ is also used to identify the correct b_ℓ , as described below.

The value of $D_{\nu,\min}$ from the neutrino reconstruction and the mass constraints on the hadronically decaying top quark are combined in a likelihood function λ , given by

$$-\log[\lambda] = -\log[P_m(m_2, m_3)] - \log[P_\nu(D_{\nu,\min})], \quad (2)$$

where P_m is the two-dimensional probability density of the invariant masses of W bosons and top quarks that are correctly reconstructed, based on the matching criteria described above. The value of λ is maximized to select the permutation of jets. The probability density P_m is calculated as a function of the invariant mass of the two jets, m_2 , tested as the W boson decay products, and the invariant mass of the three jets, m_3 , tested as the decay products of the hadronically decaying top quark. The distributions for the correct jet assignments, taken from the POWHEG+PYTHIA8 simulation and normalized to unit area, are shown in Fig. 2 (upper) for the particle- and parton-level measurements. This part of the likelihood function is sensitive to the correct reconstruction of the hadronically decaying top quark. Permutations with probabilities less than 0.1% of the maximum value of the probability density P_m are rejected. This selection criterion discards less than 1% of the correctly reconstructed events. Especially in the parton-level measurement, it removes events that are incompatible with the hypothesis of a hadronically decaying top quark and reduces the background contribution. This is caused by the stringent mass constraints for a parton-level top quark, where, in contrast to the particle-level top quark, close compatibility with the top quark and W boson masses are required.

The probability density P_ν describes the distribution of $D_{\nu,\min}$ for a correctly selected b_ℓ . In Fig. 2 (lower), the normalized distributions of $D_{\nu,\min}$ for b_ℓ and for other jets are shown. On average, the distance $D_{\nu,\min}$ for a correctly selected b_ℓ is smaller and has a smaller tail compared to the distance obtained for other jets. Permutations with values of

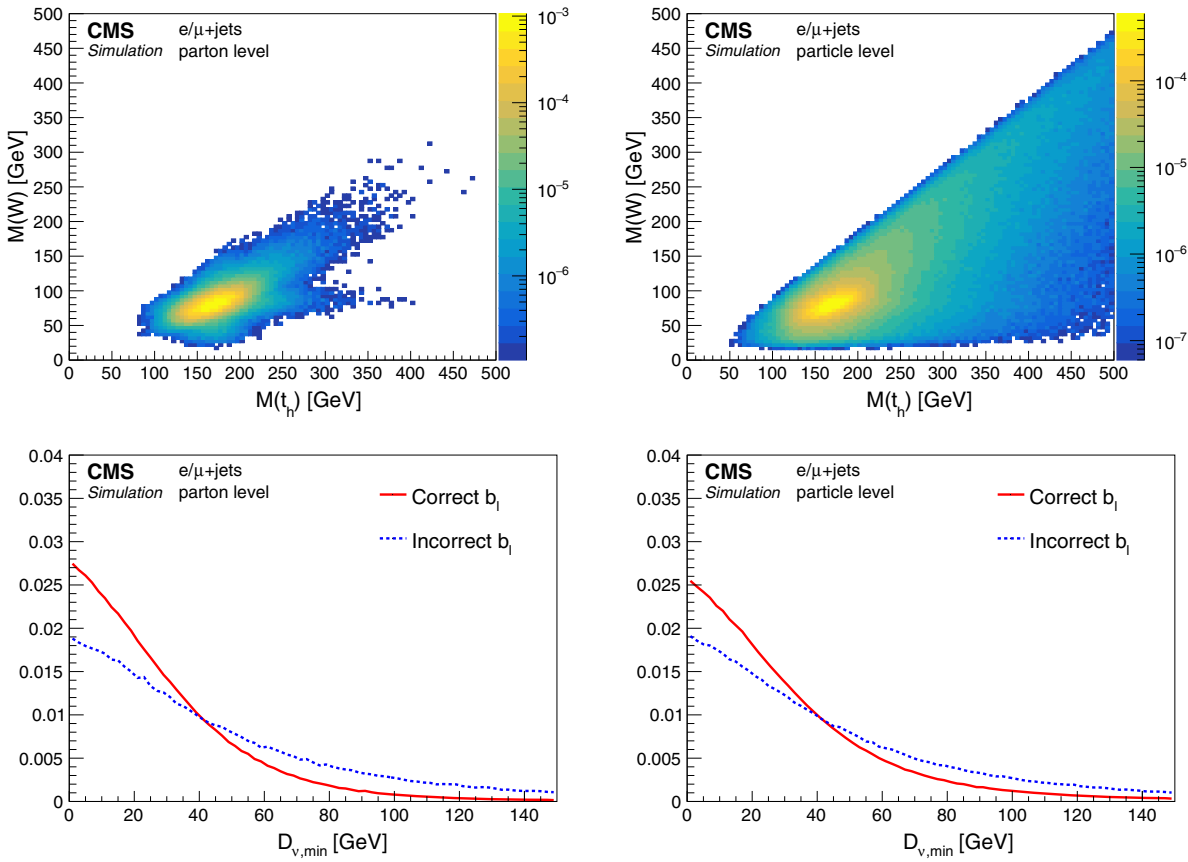


FIG. 2. Upper: normalized two-dimensional mass distribution of the correctly reconstructed hadronically decaying W bosons $M(W)$ and the correctly reconstructed top quarks $M(t_h)$ for the (left) parton- and the (right) particle-level measurements. Lower: normalized distributions of the distance $D_{\nu,\min}$ for correctly and incorrectly selected b jets from the leptonically decaying top quarks. The distributions are taken from the POWHEG+PYTHIA8 $t\bar{t}$ simulation.

$D_{\nu,\min} > 150$ GeV are rejected since they are very unlikely to originate from a correct b_j association. This part of the likelihood function is sensitive to the correct reconstruction of the leptonically decaying top quark.

Since the likelihood function λ combines the probabilities from the reconstruction of the leptonically and hadronically decaying top quarks, it provides information on the reconstruction of the whole $t\bar{t}$ system. The

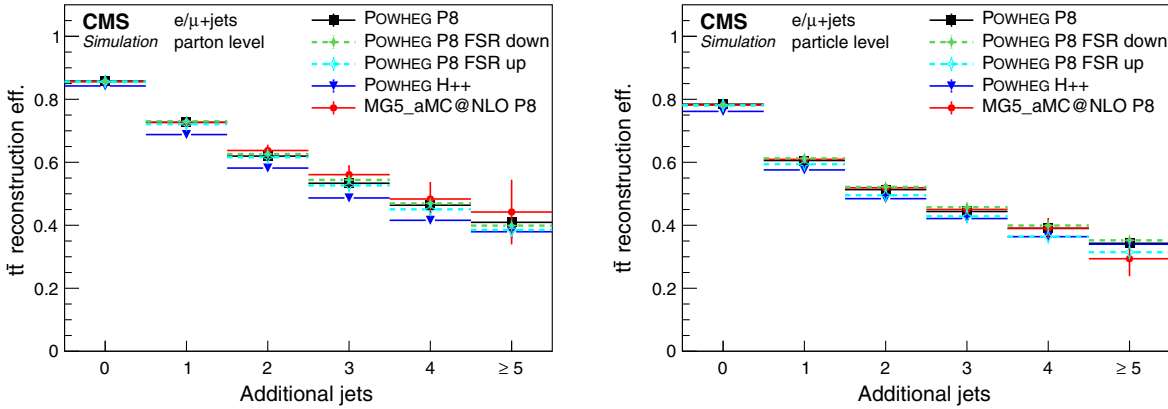


FIG. 3. Reconstruction efficiency of the $t\bar{t}$ system as a function of the number of additional jets for the (left) parton- and (right) particle-level measurements. The efficiencies are calculated based on the simulations with POWHEG+PYTHIA8 (P8) with scale variations up and down of the final-state PS, POWHEG+HERWIG++ (H++), and MG5_aMC@NLO+PYTHIA8. The vertical bars represent the statistical uncertainties in each simulation.

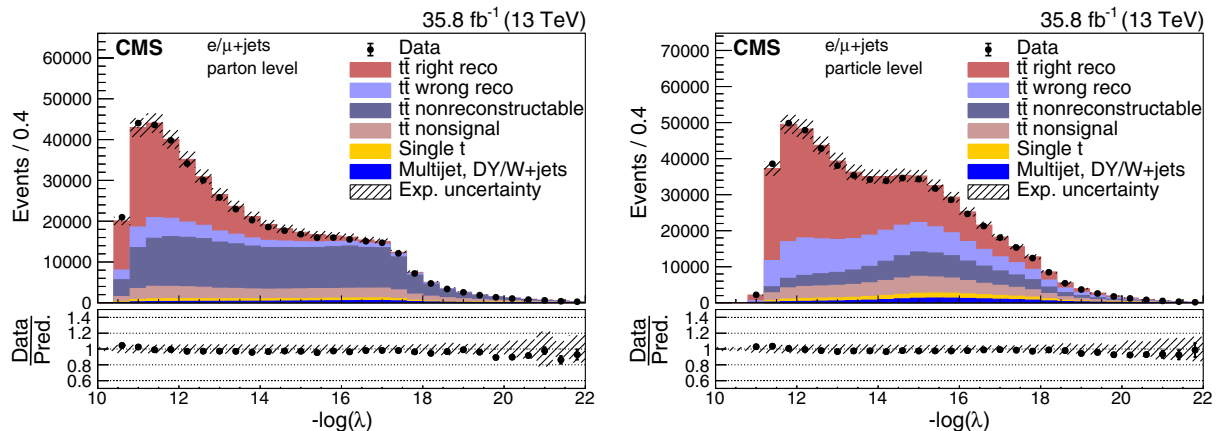


FIG. 4. Distribution of the negative log-likelihood for the selected best permutation in the (left) parton- and the (right) particle-level measurements in data and simulations. Events generated with POWHEG+PYTHIA8 are used to describe the $t\bar{t}$ production. The contribution of multijet, DY, and W boson plus jets background events is extracted from the data (cf. Sec. VII). Combined experimental (cf. Sec. IX) and statistical uncertainties (hatched area) are shown for the total predicted yields. The data points are shown with statistical uncertainties. The ratios of data to the sum of the predicted yields are provided at the bottom of each panel.

performance of the reconstruction as a function of jet multiplicity is shown for several $t\bar{t}$ simulations in Fig. 3, where we use the input distributions P_m and P_ν from the POWHEG+PYTHIA8 simulation. The reconstruction efficiency of the algorithm is defined as the probability that the most-likely permutation, as identified through the maximization of the likelihood λ , is the correct one, given that all $t\bar{t}$ decay products are reconstructed and selected. The performance deteriorates with the increase in the number of jets, since the number of permutations increases drastically and the probability of selecting a wrong permutation increases. The differences observed between the various simulations are taken into account in the estimation of the systematic uncertainties. We observe a lower reconstruction efficiency for the particle-level measurement. This is caused by the less powerful mass constraints for a particle-level top quark. This can be seen in the mass distributions of Fig. 2 and the likelihood distributions in Fig. 4, where the simulations are normalized to the measured integrated luminosity of the data sample, and the $t\bar{t}$ simulation is divided into the following categories: correctly reconstructed $t\bar{t}$ systems ($t\bar{t}$ right reco); events where all decay products are available, but the algorithm failed to identify the correct permutation ($t\bar{t}$ wrong reco); the nonreconstructable events ($t\bar{t}$ nonreconstructable); and events that are according to the parton- or particle-level definitions not $t\bar{t}$ signal events ($t\bar{t}$ nonsignal). Only the last category is treated as $t\bar{t}$ background, while the other categories are considered as signal. The lower reconstruction efficiency of the particle-level top quark is compensated by the higher number of reconstructable events.

In Fig. 5, the p_T of the jets from the $t\bar{t}$ system, as identified by the reconstruction algorithm, and of the additional jets are presented and compared to the simulation. In Fig. 6, the distributions of p_T and $|y|$ of the

reconstructed top quarks, and in Fig. 7, the distributions of $p_T(t\bar{t})$, $|y(t\bar{t})|$, and $M(t\bar{t})$ for the parton- and particle-level measurements are shown. The simulations are normalized according to the measured integrated luminosity of the data. In general, good agreement is observed between the data and the simulation, although all measured p_T spectra are softer than predicted by the simulation.

VII. BACKGROUND SUBTRACTION

After the event selection and $t\bar{t}$ reconstruction, we observe about 450 000 and 570 000 events at the parton and particle levels, respectively, where total background contributions of 4.5 and 6.0% from single top quark, DY, W boson, and multijet events are predicted. These backgrounds have to be estimated and subtracted from the selected data. In addition, a residual contamination from nonsignal $t\bar{t}$ events is expected and estimated from the simulation, as detailed below.

The predictions of the single top quark background are taken from simulations. Its overall contribution corresponds to about 2.7 and 3.3% of the selected data in the parton- and particle-level measurements, respectively.

Single top quark production cross sections are calculated with a precision of a few percent [35,36]. However, these calculations do not consider the production of additional jets as required by the $t\bar{t}$ selection. Therefore, we use an overall uncertainty of 50%, which represents a conservative estimate of the PS modeling, scale, and PDF uncertainties. Even with such a conservative estimate, its impact on the precision of the final results is negligible.

After the full $t\bar{t}$ selection, the numbers of events in the simulations of multijet, DY, and W boson production are not sufficient to obtain smooth background distributions. Therefore, we extract a common distribution for these

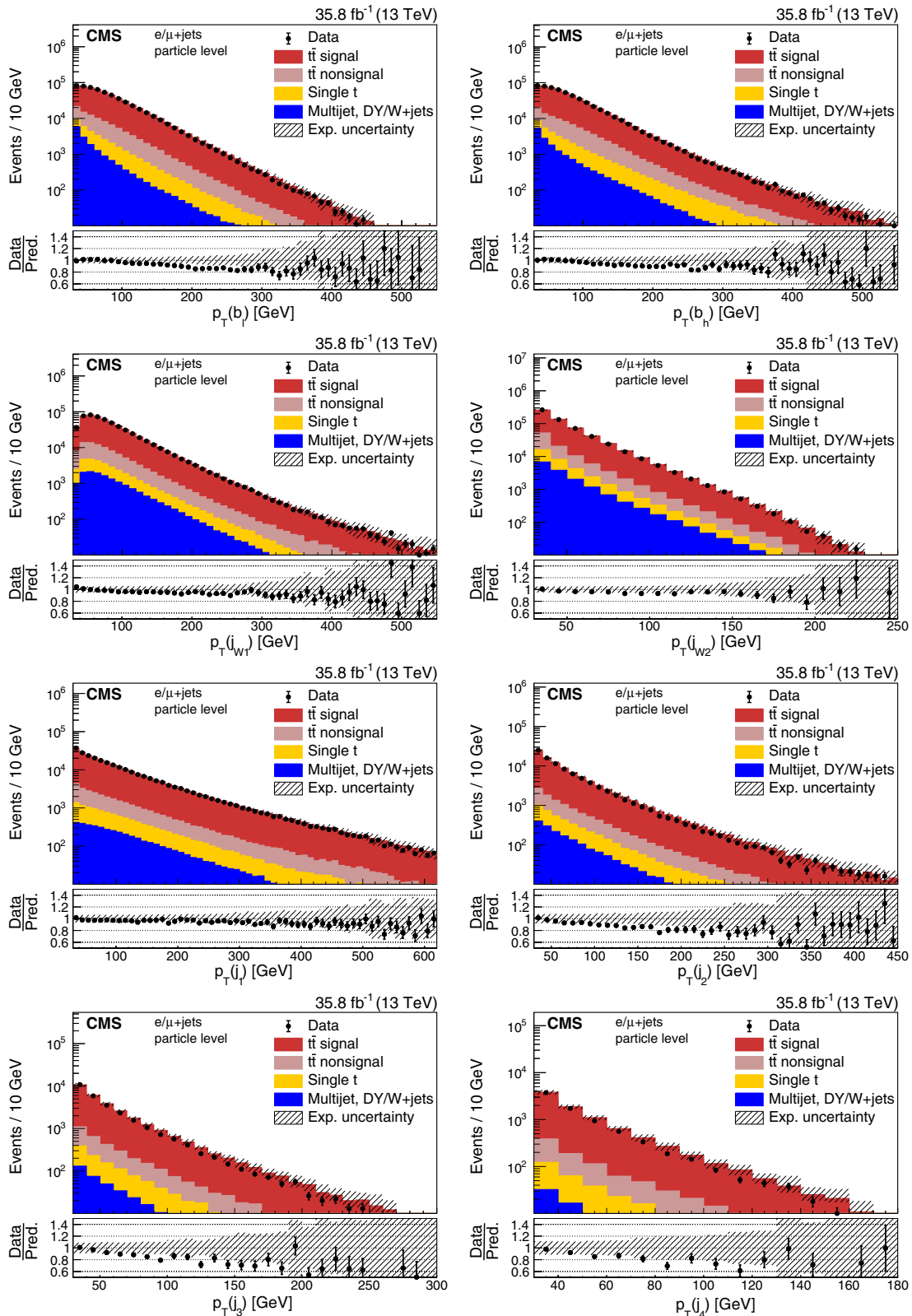


FIG. 5. Comparisons between data and simulation at the particle level of the reconstructed distributions of the p_T of jets as identified by the $t\bar{t}$ reconstruction algorithm. The simulation of POWHEG+PYTHIA8 is used to describe the $t\bar{t}$ production. The contribution of multijet, DY, and W boson plus jets background events is extracted from the data (cf. Sec. VII). Combined experimental (cf. Sec. IX) and statistical uncertainties (hatched area) are shown for the total predicted yields. The data points are shown with statistical uncertainties. The ratios of data to the predicted yields are given at the bottom of each panel.

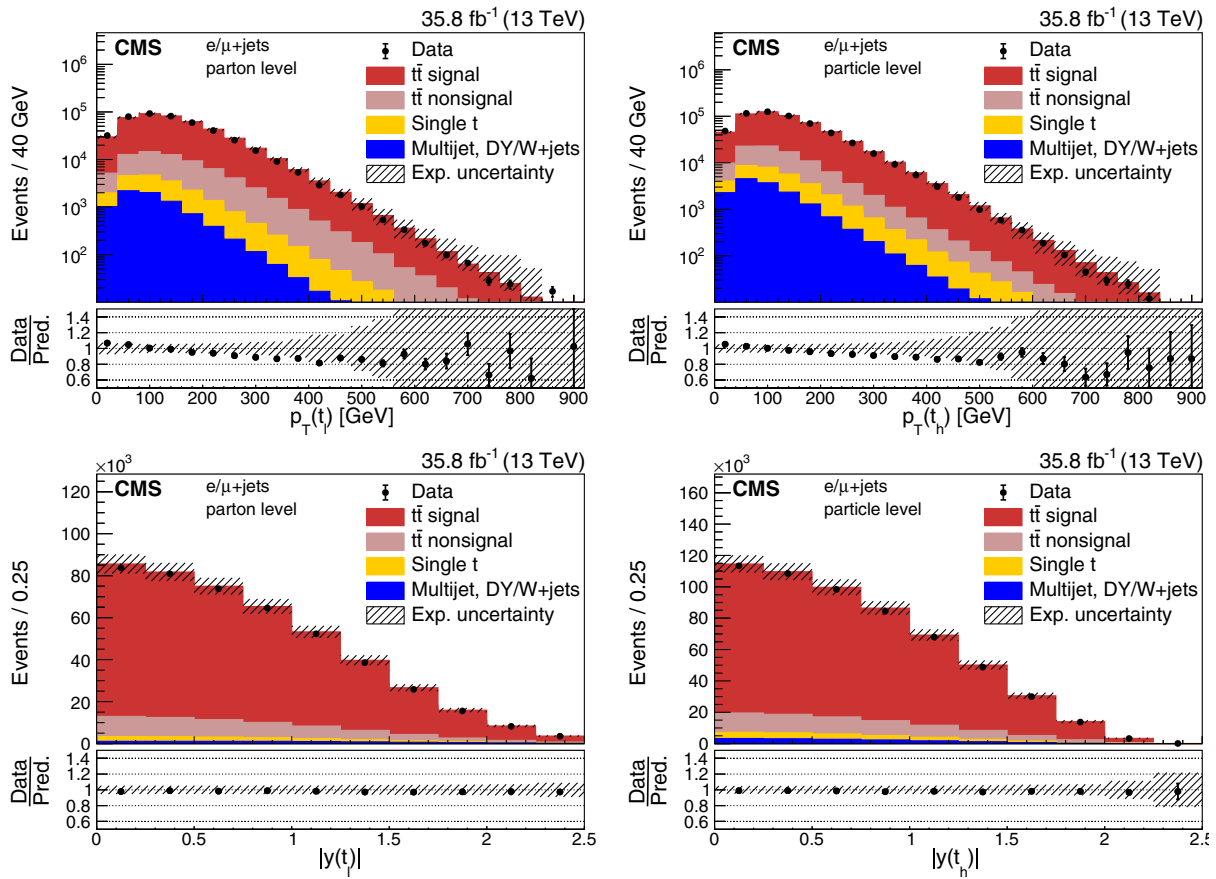


FIG. 6. Comparisons of the reconstructed p_T (upper) and $|y|$ (lower) in data and simulations for the t_ℓ (left) at the parton level and the t_h (right) at the particle level. The simulation of POWHEG+PYTHIA8 is used to describe the $t\bar{t}$ production. The contribution of multijet, DY, and W boson plus jets background events is extracted from the data (cf. Sec. VII). Combined experimental (cf. Sec. IX) and statistical uncertainties (hatched area) are shown for the total predicted yields. The data points are shown with statistical uncertainties. The ratios of data to the predicted yields are given at the bottom of each panel.

backgrounds from a control region in the data. Its selection differs from the signal selection by the requirement of having no b -tagged jet in the event. In this control region, the contribution of $t\bar{t}$ events is estimated to be about 15%, while the remaining fraction consists of multijet, DY, and W boson events. The background distributions are obtained after applying exactly the same $t\bar{t}$ reconstruction algorithm as in the signal region. The two b jet candidates still have the highest value of the b identification discriminant to maintain a similar number of allowed permutations of jets in the control and signal regions. To estimate the shape dependency on the selection of the control region, we vary the selection threshold of the b identification discriminant. This changes the $t\bar{t}$ signal contribution and the flavor composition. However, we find the observed shape variations to be small. In addition, we verify in the simulation that the shapes of the distributions obtained from the control region are compatible with the background distributions in the signal region. For the background subtraction the distributions extracted from the control region are normalized individually in each bin of jet multiplicity to the yield of multijet, DY, and W boson

events predicted by the simulation in the signal region. In the control region, the expected and measured event yields agree within their statistical uncertainties. Taking into account the statistical uncertainty in the normalization factor and the shape differences between the signal and control regions in the simulation, we derive an overall uncertainty of 20% in this background estimation.

Special care has to be taken with the contribution of nonsignal $t\bar{t}$ events. For the parton-level measurement these are dilepton, all-jets, and $\tau + \text{jets}$ events. For the particle-level measurement all $t\bar{t}$ events for which no pair of particle-level top quarks exists are considered as nonsignal $t\bar{t}$ events. The corresponding contributions are about 11.5% for both the parton- and the particle-level measurements. The behavior of these backgrounds depends on the $t\bar{t}$ cross section, and a subtraction according to the expected value can result in a bias of the measurement, especially if large differences between the simulation and the data are observed. However, the shapes of the distributions from data and simulation are consistent within their uncertainties, and we subtract the predicted relative fractions from the remaining event yields.

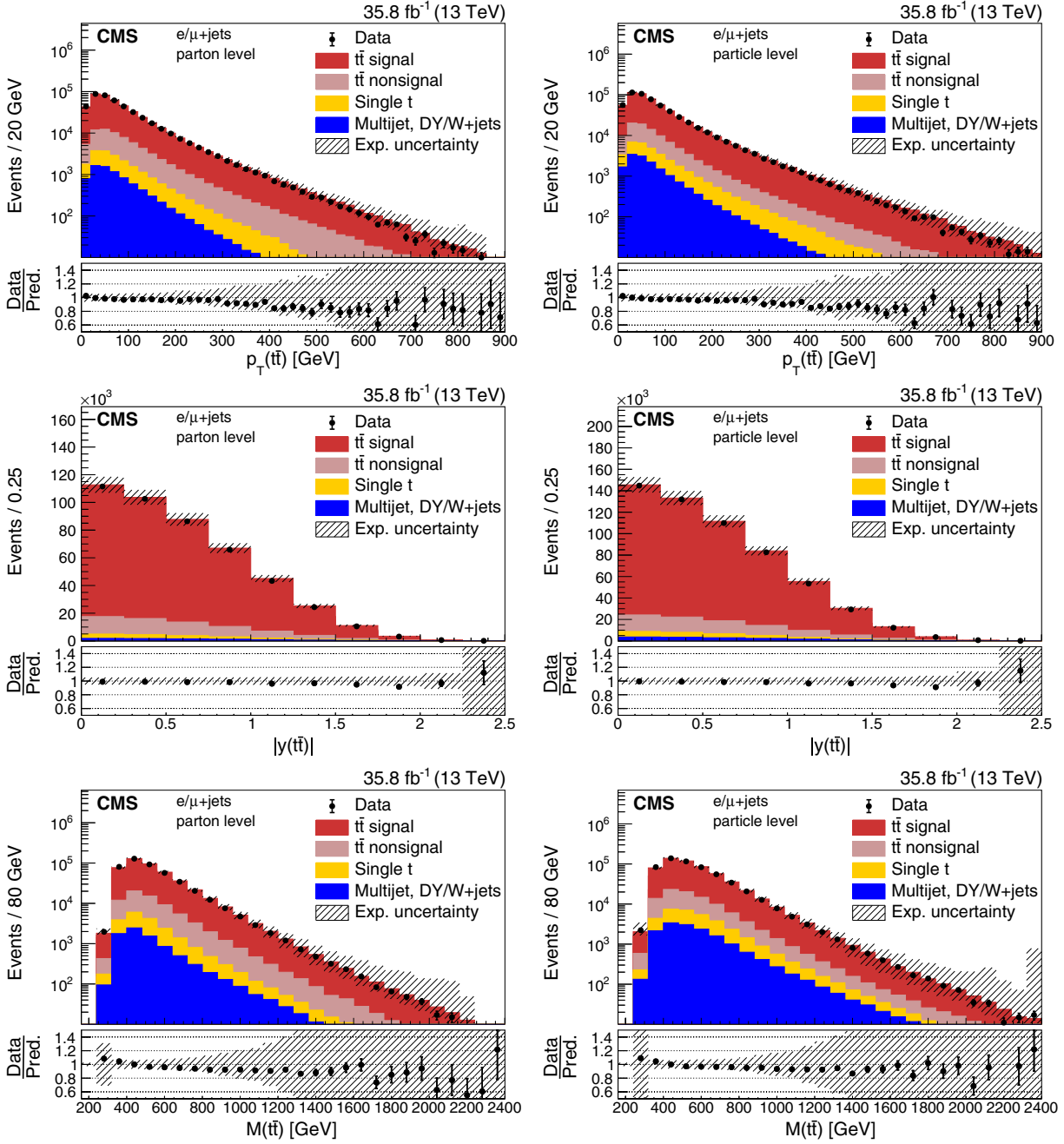


FIG. 7. Comparisons of the reconstructed distributions of $p_T(t\bar{t})$ (upper), $|y(t\bar{t})|$ (middle), and $M(t\bar{t})$ (lower) for the (left) parton- and the (right) particle-level measurements in data and simulation. The simulation of POWHEG+PYTHIA8 is used to describe the $t\bar{t}$ production. The contribution of multijet, DY, and W boson plus jets background events is extracted from the data (cf. Sec. VII). Combined experimental (cf. Sec. IX) and statistical uncertainties (hatched area) are shown for the total predicted yields. The data points are shown with statistical uncertainties. The ratios of data to the predicted yields are given at the bottom of each panel.

VIII. CORRECTIONS TO PARTICLE AND PARTON LEVELS

After the subtraction of the backgrounds, an unfolding procedure is used to correct the reconstructed distributions for detector-specific effects, e.g., efficiency and resolutions, and to extrapolate either to the parton or particle level. We do not subtract the fractions of wrongly reconstructed or

nonreconstructable events, since in many of these events a rather soft jet is misidentified, which has little impact on the resolution of the measured quantities. The iterative D'Agostini method [50] is used to unfold the data. The migration matrices, which relate the quantities at the parton or particle level and at detector level, and the acceptances are needed as the input. However, not only the detector simulation, but also the theoretical description of $t\bar{t}$ events

affects the migration matrix. This dependence is reduced in the particle-level measurement, where no extrapolation to parton-level top quarks is needed. For the central results the migration matrices and the acceptances are taken from the POWHEG+PYTHIA8 simulation, and other simulations are used to estimate the uncertainties. The binning of the distributions is optimized based on the resolution in the simulation. The minimal bin widths are selected such that, according to the resolution, at least 50% of the events are reconstructed in the correct bin. As an example, the migration matrices for the parton- and particle-level measurements of $p_T(t_h)$ are shown in the right-hand plots of Fig. 8. For the measured parton-level distributions of any quantity we define the purity as the fraction of parton-level top quarks in the same bin at the detector level, the stability as the fraction of detector-level top quarks in the same bin at the parton level, and the bin efficiency as the ratio of the number of detector- to parton-level top quarks in the same bin. Similar parameters are defined for the particle-level distributions. The purity, stability, and bin efficiency are shown for the $p_T(t_h)$ measurements in the left-hand plots of Fig. 8. These illustrate the improved agreement between the

reconstructed and the unfolded quantities, as well as the reduced extrapolation in the particle-level measurement.

To control the level of regularization, the iterative D'Agostini method takes the number of iterations as an input parameter. The initial distributions for the D'Agostini unfolding are taken from the POWHEG +PYTHIA8 simulation. The number of iterations is chosen such that the compatibility between a model and the unfolded data at either the parton or particle level is the same as the compatibility between the folded model and the data at detector level. The compatibilities are determined by χ^2 tests at each level that are based on all the available simulations and on several modified spectra obtained by reweighting the POWHEG+PYTHIA8 distributions of $p_T(t)$, $|y(t)|$, $p_T(t\bar{t})$, or $p_T(j_1)$ before the detector simulation. The modified spectra are chosen such that the effect of the reweighting corresponds roughly to the observed differences between the data and the unmodified simulation at detector level.

We have found that the number of iterations needed to fulfill the above criterion is such that a second χ^2 test between the detector-level spectrum with its statistical

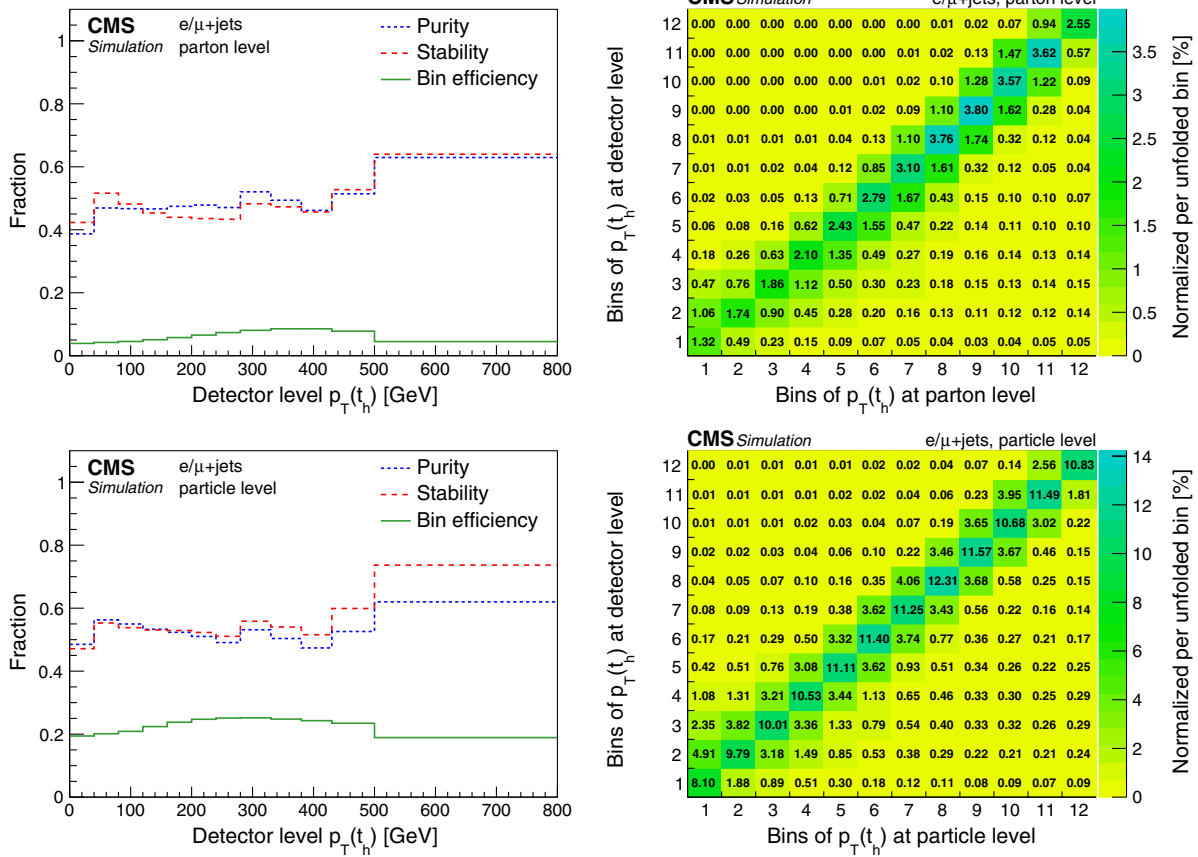


FIG. 8. Migration studies of the (upper) parton- and (lower) particle-level measurements of $p_T(t_h)$, extracted from the POWHEG +PYTHIA8 simulation. Left: purity, stability, and bin efficiency. Right: bin migrations between detector and parton (particle) level. The p_T range of the bins can be taken from the left panels. Each column is normalized such that the sum of its entries corresponds to the percentage of reconstructed events in this bin at the parton (particle) level.

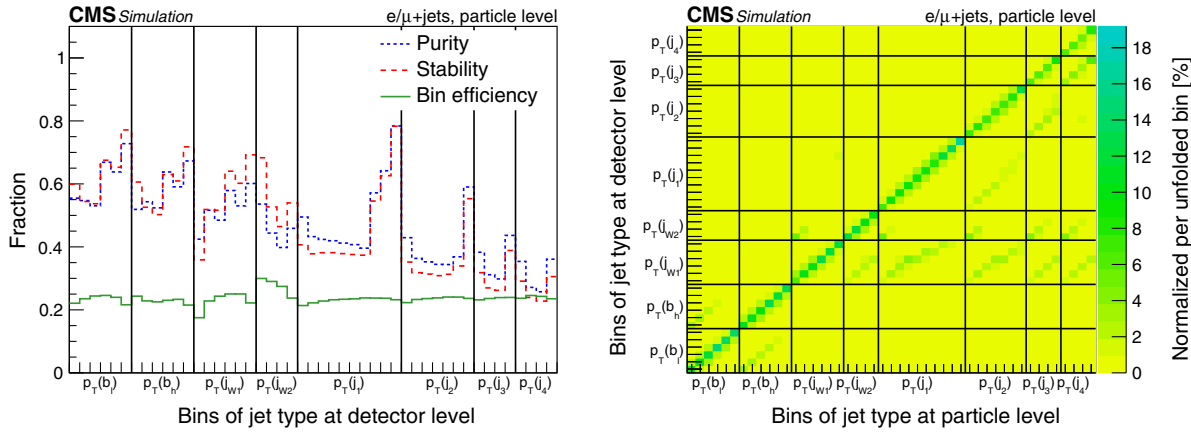


FIG. 9. Migration studies of the particle-level measurement of the jet p_T spectra, extracted from the POWHEG+PYTHIA8 simulation. Left: purity, stability, and bin efficiency. Right: bin migrations between detector and particle level. On the axes the p_T bins for each jet are shown. Each column is normalized in the way that the sum of its entries corresponds to the percentage of reconstructed events in this bin at the particle level.

uncertainty and the refolded spectrum with zero uncertainty exceeds a probability of 99.9%. The refolded spectrum is obtained by inverting the unfolding step. This consists of a multiplication with the response matrix and does not need any regularization. The algorithm needs between 4 and 56 iterations depending on the distribution. The numbers of iterations are higher for measurements with lower purities and stabilities of the migration matrices. This is the case for the measurements of $p_T(t_\ell)$ and $|y(t_\ell)|$, whose resolutions are significant worse than those of $p_T(t_h)$ and $|y(t_h)|$ due to the missing neutrino information.

For the two-dimensional measurements with n bins in one quantity and m_i , $i = 1 \dots n$ bins in the other the D'Agostini unfolding can be generalized using a vector of $B = \sum_i^n m_i$ entries of the form: $b_{1,1}, b_{2,1} \dots b_{n,1}, \dots b_{1,m_1}, b_{2,m_2} \dots b_{n,m_n}$, with a corresponding $B \times B$ migration matrix. The number of iterations is optimized in the same way.

In the measurements of jet kinematic properties, we do not unfold the measured spectra of each jet separately, but do correct for the effect of misidentified jets. The response matrix showing the migration among the identified jets is given in Fig. 9 for the measurements of the jet p_T spectra.

IX. SYSTEMATIC UNCERTAINTIES

Several sources of experimental and theoretical systematic uncertainty are considered. Uncertainties in the jet and \vec{p}_T^{miss} calibrations, pileup modeling, b identification and lepton selection efficiencies, and integrated luminosity fall into the first category.

The total uncertainty in the jet energy calibration is the combination of 19 different sources of uncertainty and the jet-flavor-specific uncertainties [47], where the uncertainty for b jets is evaluated separately. For each uncertainty source the energies of jets in the simulation are shifted up

and down. At the same time, \vec{p}_T^{miss} is recalculated accordingly to the rescaled jet energies. The recomputed backgrounds, response matrices, and acceptances are used to unfold the data. The observed differences between these and the original results are taken as an uncertainty in the unfolded event yields. The same technique is used to calculate the impact of the uncertainties in the jet energy resolution, the uncertainty in \vec{p}_T^{miss} not related to the jet energy calibration, the b identification, the pileup modeling, and the lepton reconstruction and selection.

The b identification efficiency in the simulation is corrected using scale factors determined from data [51]. These have an uncertainty of about 1–3% depending on the p_T of the b jet.

The effect on the measurement due to the uncertainty in the modeling of pileup in simulation is estimated by varying the average number of pileup events per bunch crossing by 4.6% [52] and reweighting the simulated events accordingly.

The trigger, reconstruction, and identification efficiencies of leptons are evaluated with tag-and-probe techniques using Z boson dilepton decays [45,46]. The uncertainties in the scale factors, which are used to correct the simulation to match the data, take into account the different lepton selection efficiencies in events with high jet multiplicities as in $t\bar{t}$ events. The uncertainty in the lepton reconstruction and selection efficiencies depends on p_T and η and is below 2% in the relevant phase-space region.

The relative uncertainty in the integrated luminosity measurement is 2.5% [2].

Uncertainties in the choice of μ_r and μ_f , the combination of the matrix-element calculation with the PS, the modeling of the PS and hadronization, the top quark mass, and the PDFs fall into the second category of uncertainties. The effects of these theoretical uncertainties are estimated either by using the event weights introduced in Sec. II, or by using a

$t\bar{t}$ signal simulation with varied settings. Again, the uncertainties are assessed using the recomputed backgrounds, response matrices, and acceptances to unfold the data.

The scales μ_r and μ_f are varied up and down by a factor of two individually and simultaneously in the same directions. Afterwards, the envelope of the observed variations is quoted as the uncertainty.

The uncertainty in the combination of the matrix-element calculation with the PS is estimated from an $\approx 40\%$ variation of the h_{damp} parameter in POWHEG, normally set to $h_{\text{damp}} = 1.58m_t$. This variation has been found to be compatible with the modeling of jet multiplicities in previous measurements at $\sqrt{s} = 8$ TeV [16].

To estimate the uncertainty in the PS, several effects have been studied and are assessed individually. The scale of the initial- (ISR) and final-state (FSR) radiation is varied up and down by a factor of 2 and $\sqrt{2}$, respectively. These variations are motivated by the uncertainties in the PS tuning [25]. The effect of multiple parton interactions and the parametrization of color reconnection have been studied in Ref. [26] and are varied accordingly. In addition, we use a simulation with activated color reconnection of resonant

decays. This enables the color reconnection of top quark decay products with other partons, which is not allowed in the default tune. The uncertainty in the b fragmentation function is taken from measurements at LEP experiments [53–55] and SLD [56], and the parametrization in PYTHIA8 is changed accordingly. Finally, the semileptonic branching fractions [41] of b hadrons are varied within their measured uncertainties.

The effect due to the uncertainty in the top quark mass is estimated using simulations with altered top quark masses. We quote as the uncertainty the cross section differences observed for a top quark mass variation of 1 GeV around the central value of 172.5 GeV used in the default simulation.

For the PDF uncertainty only the variation in the acceptance is taken into account, while variations due to migrations between bins can be neglected. It is calculated according to the uncertainties in the NNPDF30_nlo_as_0118 [31] parametrization. In addition, the uncertainties obtained using the PDF sets derived with the strong coupling strength set at $\alpha_s = 0.117$ and 0.119 are considered.

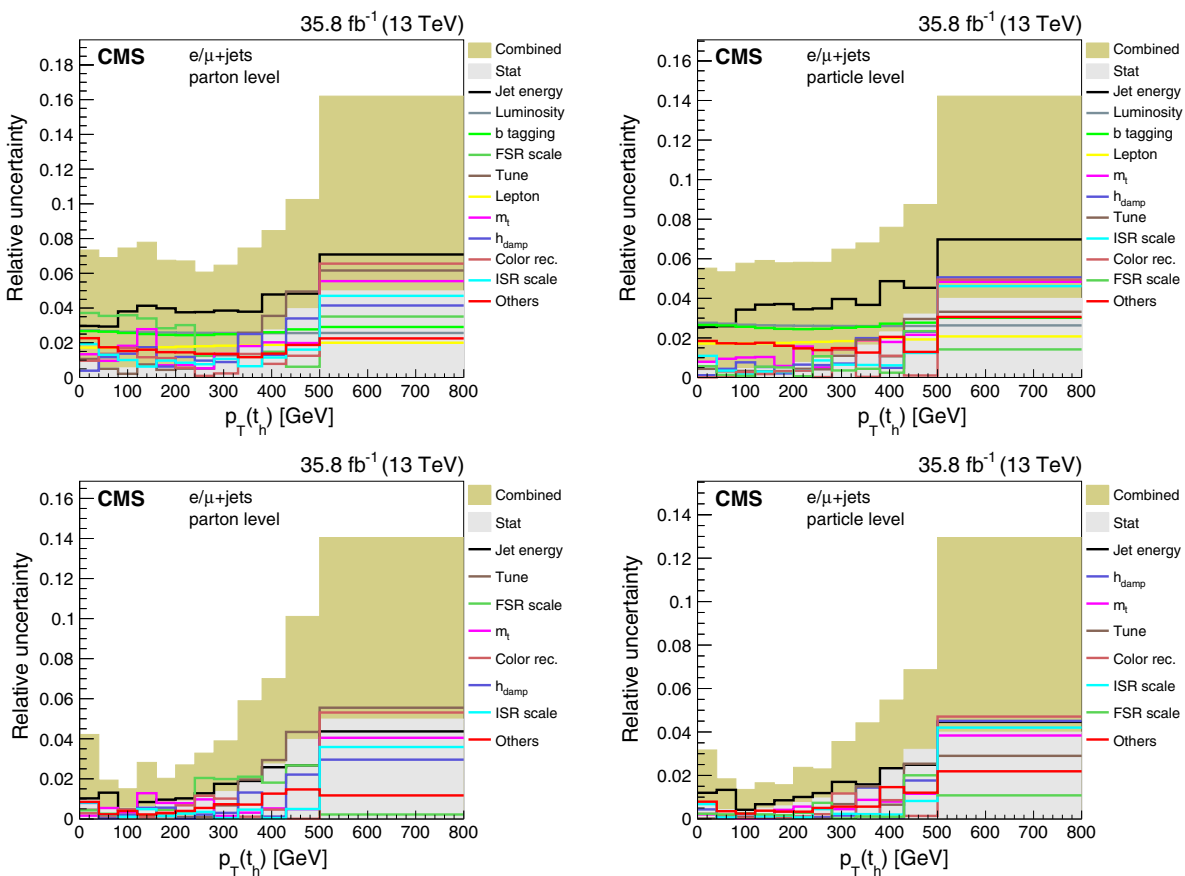


FIG. 10. Relative uncertainties due to the individual sources in the absolute (upper) and normalized (lower) measurement of $p_T(t_h)$ at the parton level (left) and particle level (right). Sources whose impact never exceeds 1% are summarized in the category “Others.” The combination of the individual sources of jet energy uncertainty is labeled “Jet energy.” The combined uncertainty is the sum in quadrature of the statistical and all the systematic uncertainties.

As an example, the sources of systematic uncertainty in the measurements of $p_T(t_h)$, as well as the statistical and total uncertainty, are shown in Fig. 10. Among the experimental uncertainties, the dominant sources are the jet energy scale; lepton triggering, reconstruction, and identification; and the b identification. In the parton-level measurement, the FSR scale is typically an important contribution to the systematic uncertainty.

As an additional consistency test, we subtract the $t\bar{t}$ background and unfold the data using the reweighted simulations that include all the differences in the measured distributions at detector level described in Sec. VIII. The differences between these unfolded distributions and the

one obtained with the unmodified simulation are small compared to the uncertainties evaluated by the variations described above.

X. DIFFERENTIAL CROSS SECTIONS AS FUNCTIONS OF OBSERVABLES OF THE TOP QUARK AND THE $t\bar{t}$ SYSTEM

The cross section σ in each bin is calculated as the ratio of the unfolded signal yield and the integrated luminosity. These are further divided by the bin width or the product of the two bin widths to obtain the single- or double-differential cross section results, respectively. To allow for a

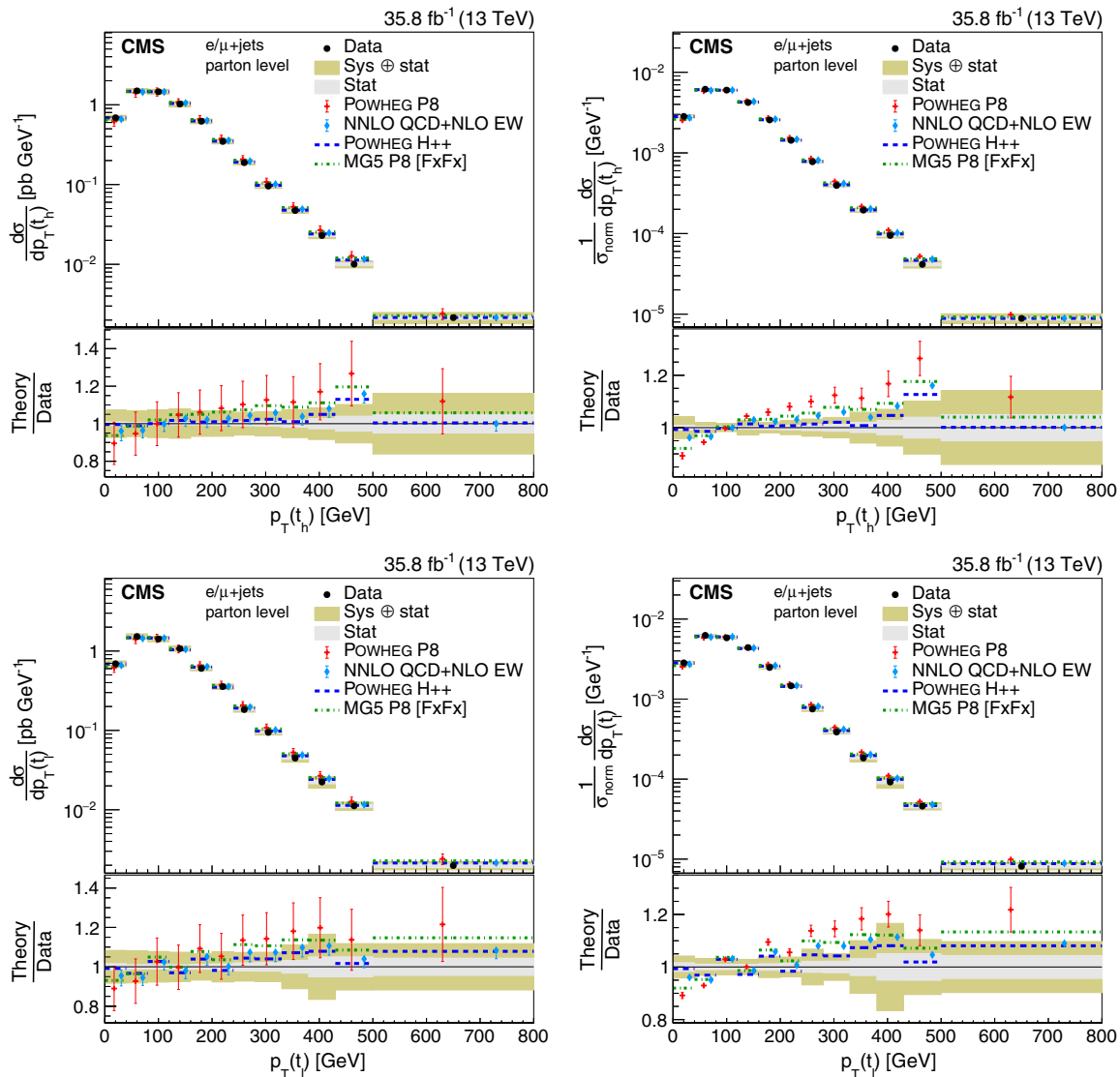


FIG. 11. Absolute (left) and normalized (right) differential cross sections at the parton level as a function of $p_T(t_h)$ (upper) and $p_T(t_\ell)$ (lower). The data are shown as points with light (dark) bands indicating the statistical (statistical and systematic) uncertainties. The cross sections are compared to the predictions of POWHEG combined with PYTHIA8 (P8) or HERWIG++ (H++), the multiparton simulation MG5_amc@NLO (MG5)+PYTHIA8 FxFx, and the NNLO QCD + NLO EW calculations. The ratios of the various predictions to the measured cross sections are shown at the bottom of each panel.

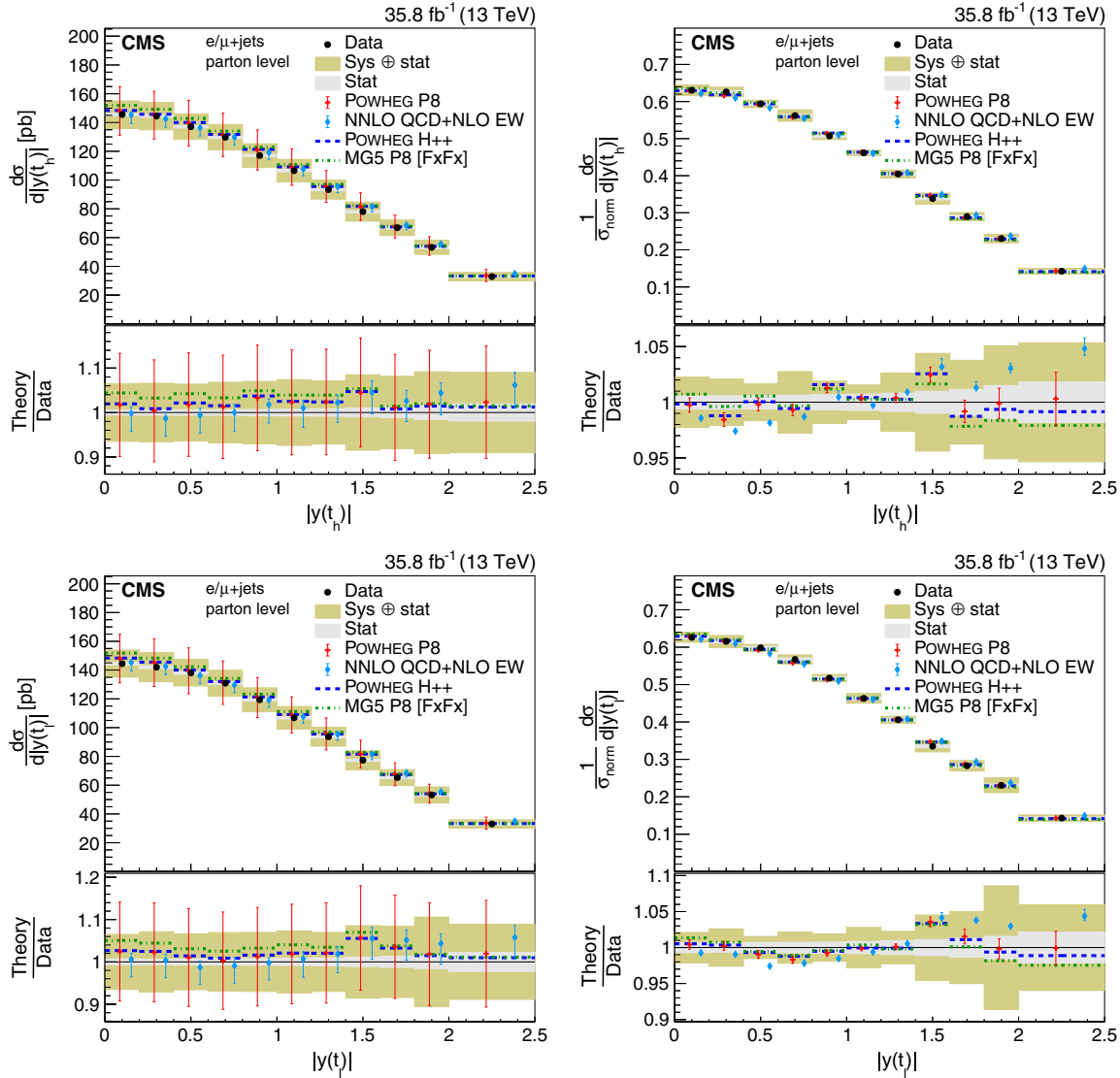


FIG. 12. Absolute (left) and normalized (right) differential cross sections at the parton level as a function of $|y(t_h)|$ (upper) and $|y(t_\ell)|$ (lower). The data are shown as points with light (dark) bands indicating the statistical (statistical and systematic) uncertainties. The cross sections are compared to the predictions of POWHEG combined with PYTHIA8 (P8) or HERWIG++ (H++), the multiparton simulation MG5_AMC@NLO (MG5)+PYTHIA8 FxFx, and the NNLO QCD + NLO EW calculations. The ratios of the various predictions to the measured cross sections are shown at the bottom of each panel.

precise comparison of the measured shapes with theoretical predictions, irrespective of the integrated cross section and its uncertainty, we also present normalized differential cross sections. For this purpose the absolute differential cross sections are divided by the normalizing cross sections σ_{norm} , which are obtained for each measurement from the integration of the cross section over the measured one- or two-dimensional range. The uncertainties in the normalized distributions are evaluated using error propagation and include the correlations between uncertainties in the individual measurements and σ_{norm} . For the statistical uncertainty the covariances are taken directly from the unfolding procedure. For each of the studied systematic uncertainties we assume a full correlation among all bins,

while the various sources are assumed to be uncorrelated. The same assumptions about correlations of uncertainty sources are made for the calculation of the normalized theoretical predictions.

The measured differential cross sections are compared to the predictions of POWHEG, combined with the PS simulations of PYTHIA8 and HERWIG++, and the $t\bar{t}$ multiparton simulation of MG5_AMC@NLO+PYTHIA8 FxFx. In addition, several parton-level results are compared to calculations of $t\bar{t}$ production with NNLO QCD + NLO EW [1] accuracy, where a top quark mass of 173.3 GeV [57] is used. For the calculations of the theoretical cross sections as functions of $M(t\bar{t})$ and rapidities the scales are set to $\mu_r = \mu_f = (1/4)(m_T(t) + m_T(\bar{t}))$ and the scales for the p_T

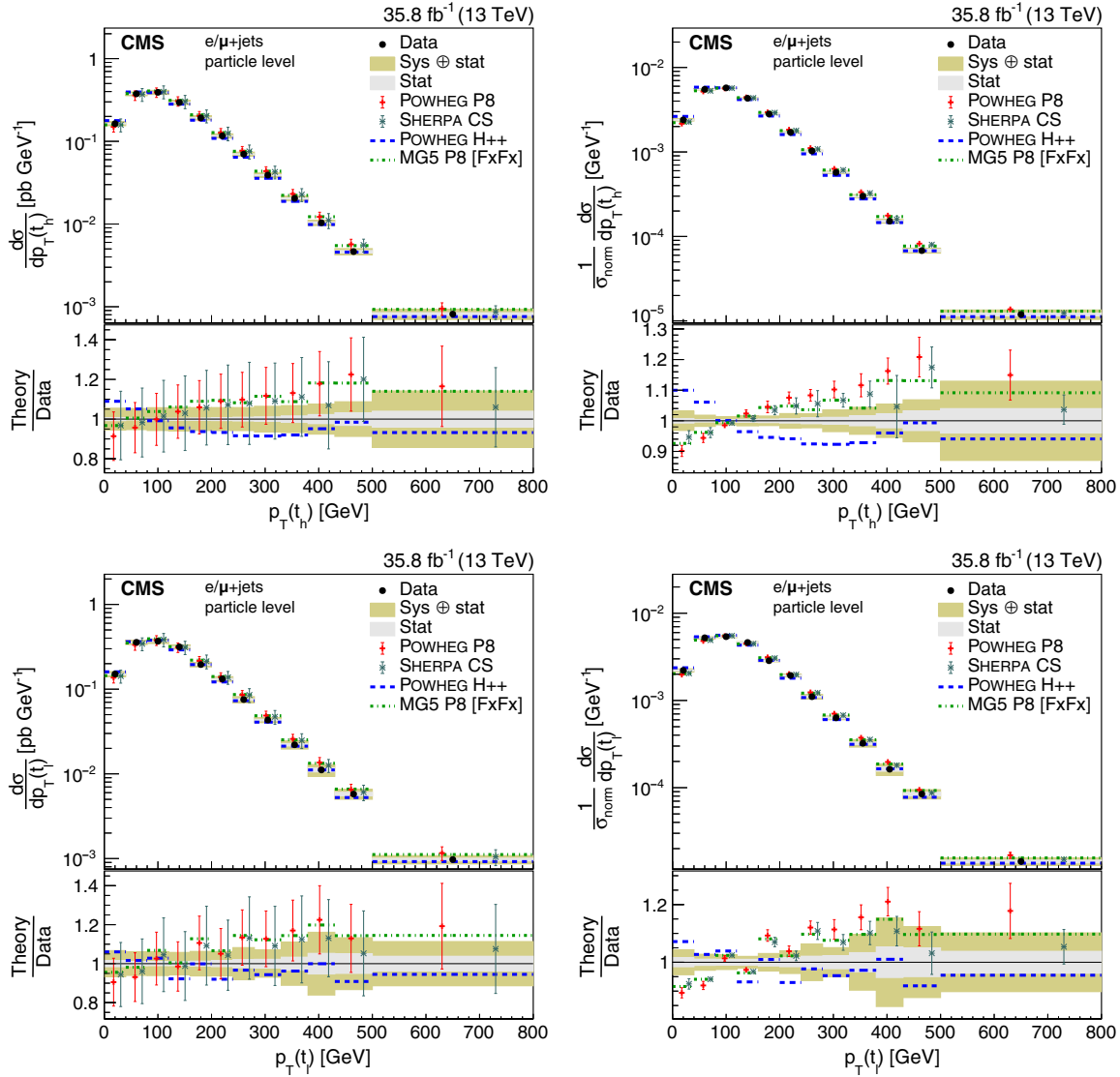


FIG. 13. Absolute (left) and normalized (right) differential cross sections at the particle level as a function of $p_T(t_h)$ (upper) and $p_T(t_\ell)$ (lower). The data are shown as points with light (dark) bands indicating the statistical (statistical and systematic) uncertainties. The cross sections are compared to the predictions of POWHEG combined with PYTHIA8 (P8) or HERWIG++ (H++) and the multiparton simulations MG5_amc@NLO (MG5)+PYTHIA8 FxFx and SHERPA. The ratios of the various predictions to the measured cross sections are shown at the bottom of each panel.

calculations are selected as $(1/2)m_T(t)$ or $(1/2)m_T(\bar{t})$ depending on the variable under consideration. The PDF parametrizations LUXqed_plus_PDF4LHC15_nnlo_100 [58] are used for these calculations. The uncertainties consider variations of the scales μ_r and μ_f . The particle-level results are compared to a prediction obtained with the Monte Carlo generator SHERPA [59] (v2.2.3) in combination with OPENLOOPs [60]. The processes of $t\bar{t}$ production with up to one additional parton are calculated at NLO QCD accuracy, and those with up to four additional partons are calculated at LO. These processes are merged and matched with the Catani–Seymour PS [61] based on the SHERPA default tune. For the scales we select

$$\mu_r = \mu_f = \frac{1}{2} \left(m_T(t) + m_T(\bar{t}) + \sum_{\text{partons}} p_T \right), \quad (3)$$

where the summation over partons includes the p_T of all partons obtained from the fixed-order calculation. The NNPDF30_nlo_as_0118 [31] PDF parametrizations are used. Uncertainties in the predictions of SHERPA are evaluated by halving and doubling the scales of renormalization, factorization, resummation, and the initial- and final-state PS. In addition, the PDF uncertainties are taken into account. For the predictions of POWHEG+PYTHIA8 we evaluate all the theoretical uncertainties described in Sec. IX. Although the

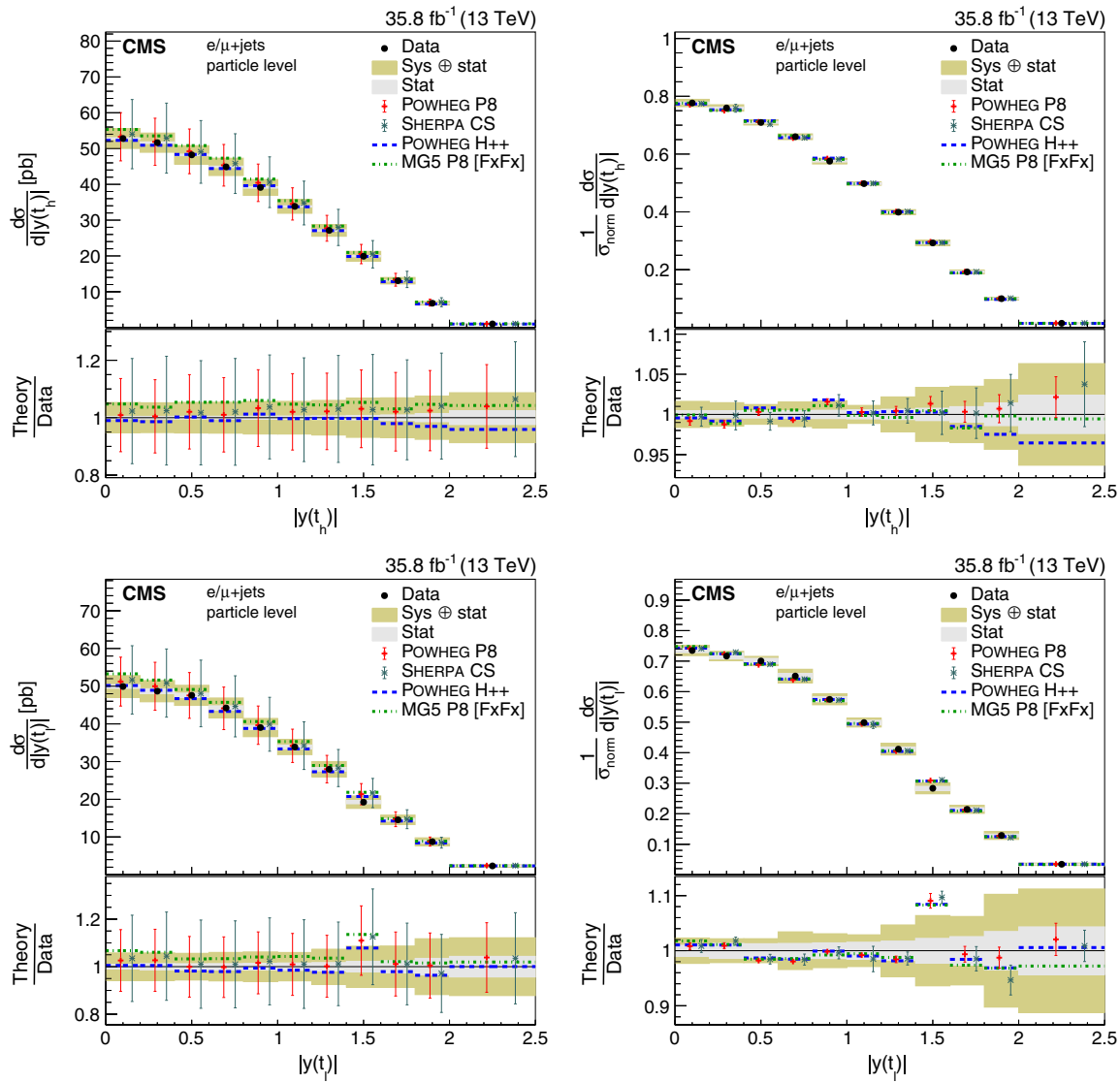


FIG. 14. Absolute (left) and normalized (right) differential cross sections at the particle level as a function of $|y(t_h)|$ (upper) and $|y(t_\ell)|$ (lower). The data are shown as points with light (dark) bands indicating the statistical (statistical and systematic) uncertainties. The cross sections are compared to the predictions of POWHEG combined with PYTHIA8 (P8) or HERWIG++ (H++) and the multiparton simulations MG5_amc@NLO (MG5)+PYTHIA8 FxFx and SHERPA. The ratios of the various predictions to the measured cross sections are shown at the bottom of each panel.

SHERPA and the POWHEG+PYTHIA8 simulations are normalized to the NNLO $t\bar{t}$ production cross section, we use their intrinsic scale uncertainties.

The comparisons between the measurements and the theoretical predictions as a function of the top quark p_T and $|y|$ are shown in Figs. 11–12 and 13–14 for the parton and particle level, respectively. At parton level, the kinematic properties of t_h and t_ℓ are identical, and we measure the differential cross section as a function of the top quark p_T using the higher- and lower- p_T values in the $t\bar{t}$ pair, as shown in Fig. 15. The measured p_T spectra of t_h and t_ℓ are consistently softer than predicted by all the simulations using the PYTHIA8 PS generator at both the parton and

particle levels. Also the NNLO QCD + NLO EW calculation predicts a slightly harder p_T spectrum than observed in the data. The POWHEG+HERWIG++ simulation describes the data well at the parton level. However, at the particle level, the $p_T(t_h)$ distribution is noticeably softer than in the data. In Figs. 16 and 17, the cross sections as a function of kinematic variables of the $t\bar{t}$ system are compared to the same theoretical predictions. In general, the predictions are in agreement with the measured distributions. The NNLO QCD + NLO EW calculation predicts a higher-average $M(t\bar{t})$ spectrum than observed in the data. For POWHEG +HERWIG++ a similar behavior as for the $p_T(t_h)$ distributions is observed—while the parton-level distribution is

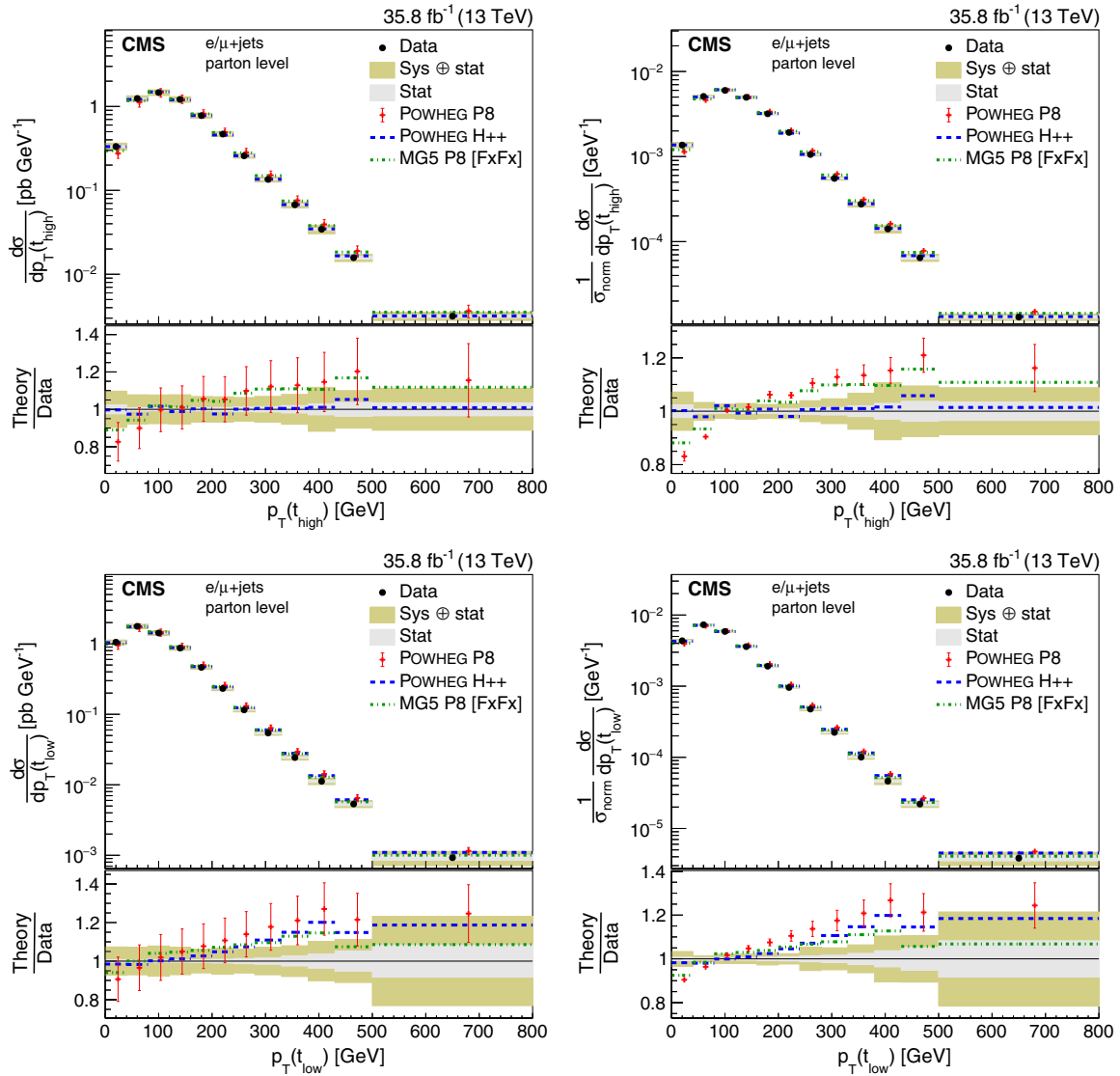


FIG. 15. Absolute (left) and normalized (right) differential cross sections at the parton level as a function of the transverse momentum of the top quark with the higher and lower p_T . The data are shown as points with light (dark) bands indicating the statistical (statistical and systematic) uncertainties. The data are shown as points with light (dark) bands indicating the statistical (statistical and systematic) uncertainties. The cross sections are compared to the predictions of POWHEG combined with PYTHIA8 (P8) or HERWIG++ (H++), and the multiparton simulation MG5_aMC@NLO (MG5)+PYTHIA8 FxFx. The ratios of the various predictions to the measured cross sections are shown at the bottom of each panel.

well described, a softer spectrum is observed at the particle level.

The measurement of double-differential cross sections allows for the study of correlations between kinematic properties of the top quarks and provides insights into extreme regions of the phase space. The most fundamental double-differential distribution is that of the top quark properties $|y(t_h)|$ vs. $p_T(t_h)$. The absolute double-differential cross sections are shown in Figs. 18 and 20, and the normalized in Figs. 19 and 21 at the parton and particle levels, respectively. The observation of a softer $p_T(t)$ spectrum is persistent in all rapidity regions. In Figs. 22–25, the corresponding measurements as a function of $M(t\bar{t})$ vs. $|y(t\bar{t})|$ are shown. This

distribution is sensitive to the PDFs [11]. As $M(t\bar{t})$ increases, the simulations overestimate the cross sections at high $|y(t\bar{t})|$. Finally, we measure $p_T(t_h)$ vs. $M(t\bar{t})$, as shown in Figs. 26–29. For these distributions the simulations of POWHEG+PYTHIA8, MG5_aMC@NLO+PYTHIA8 FxFx, and SHERPA predict similar shapes, which differ substantially from the data.

The precision of the differential cross section measurements is limited by the systematic uncertainty, dominated by jet energy scale uncertainties on the experimental side and PS modeling and scale uncertainties on the theoretical side. As expected, the theoretical uncertainties are reduced in the particle-level measurements since they are less dependent on theory-based extrapolations.

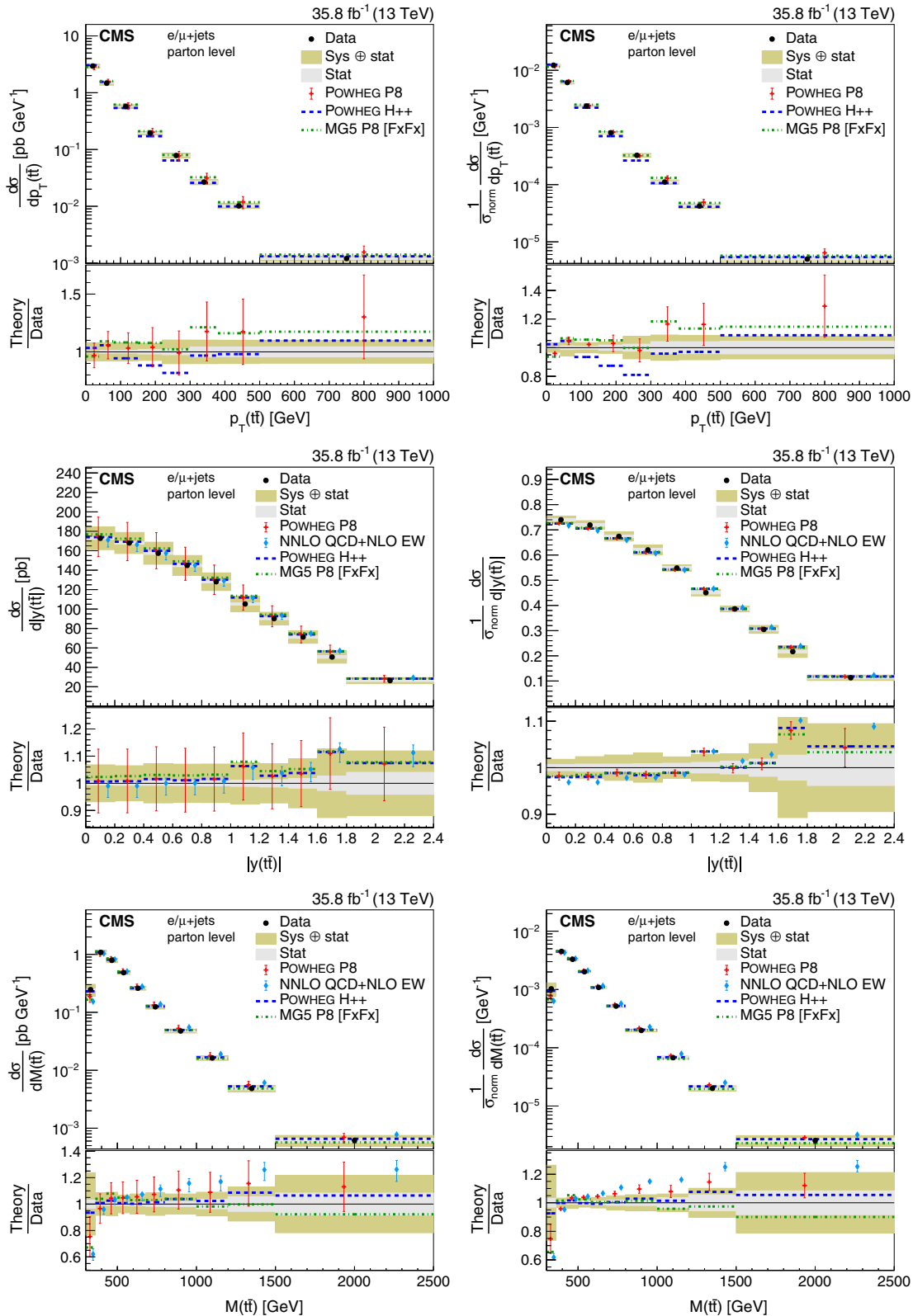


FIG. 16. Absolute (left) and normalized (right) differential cross sections at the parton level as a function of $p_T(t\bar{t})$ (upper), $|y(t\bar{t})|$ (middle), and $M(t\bar{t})$ (lower). The data are shown as points with light (dark) bands indicating the statistical (statistical and systematic) uncertainties. The cross sections are compared to the predictions of POWHEG combined with PYTHIA8 (P8) or HERWIG++ (H++), the multiparton simulation MG5_amc@NLO (MG5)+PYTHIA8 FxFx, and the NNLO QCD + NLO EW calculations. The ratios of the various predictions to the measured cross sections are shown at the bottom of each panel.

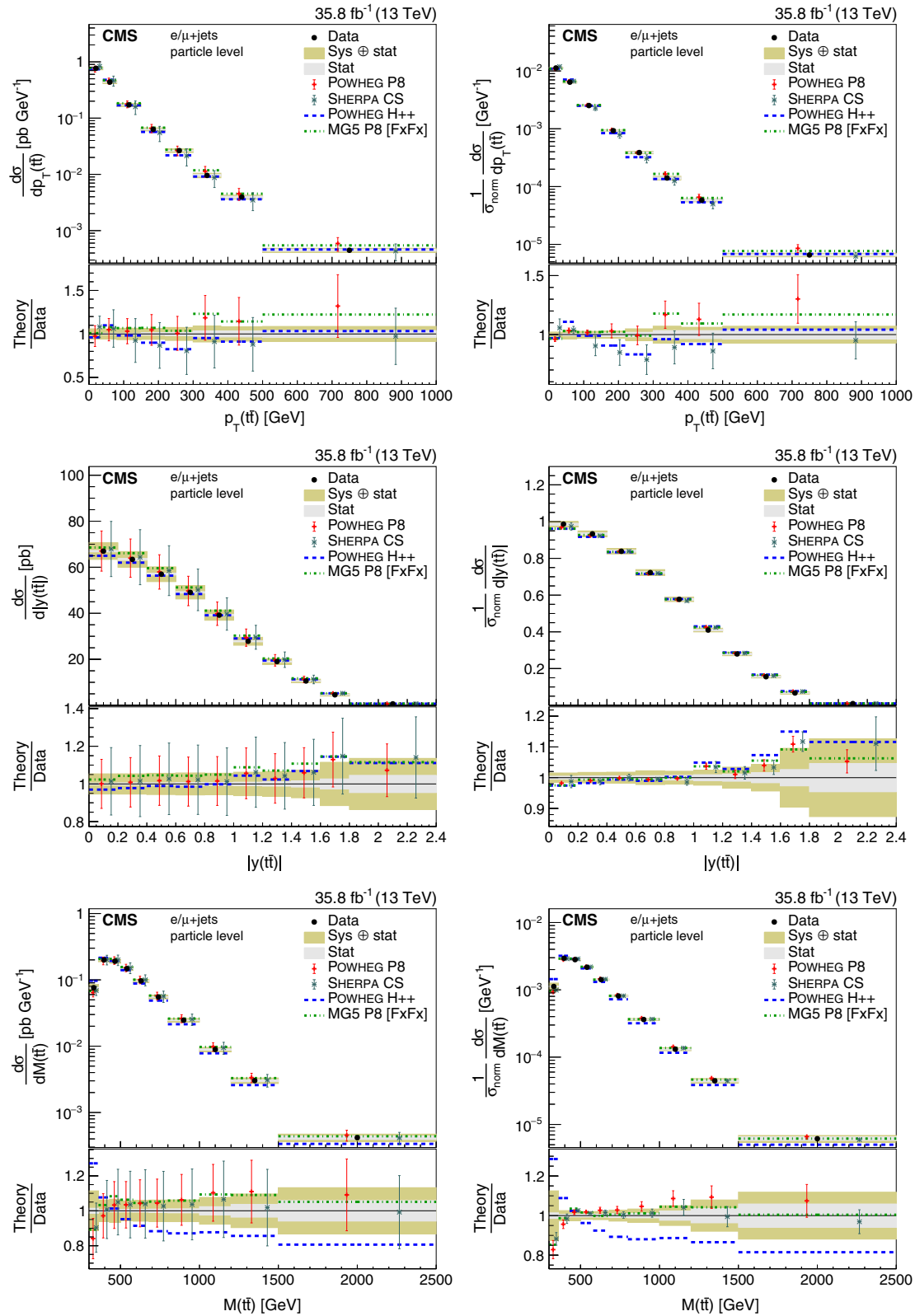


FIG. 17. Absolute (left) and normalized (right) differential cross sections at the particle level as a function of $p_T(t\bar{t})$ (upper), $|y(t\bar{t})|$ (middle), and $M(t\bar{t})$ (lower). The data are shown as points with light (dark) bands indicating the statistical (statistical and systematic) uncertainties. The cross sections are compared to the predictions of POWHEG combined with PYTHIA8 (P8) or HERWIG++ (H++) and the multiparton simulations MG5_amc@NLO (MG5)+PYTHIA8 FxFx and SHERPA. The ratios of the various predictions to the measured cross sections are shown at the bottom of each panel.

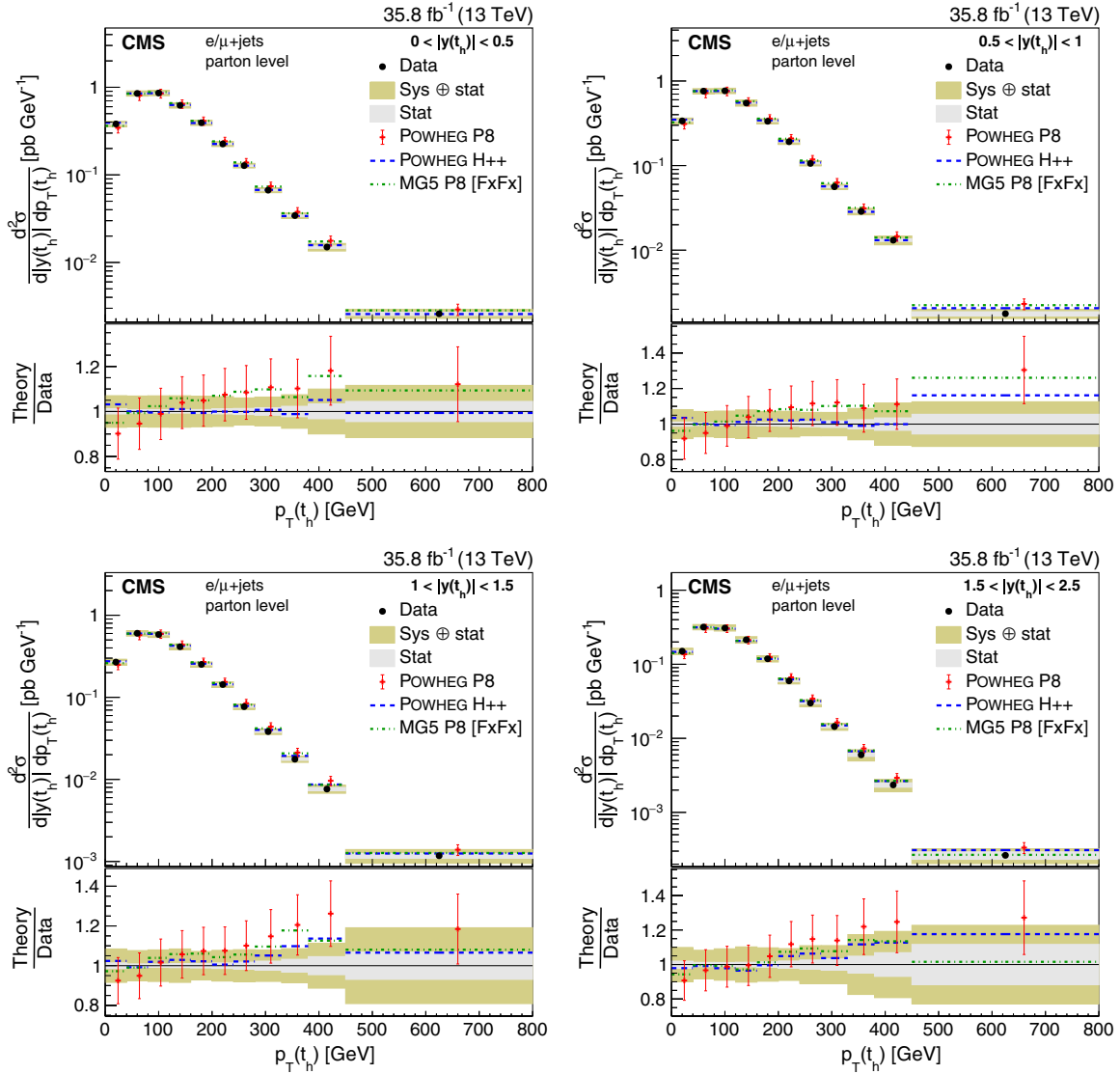


FIG. 18. Double-differential cross section at the parton level as a function of $|y(t_h)|$ vs. $p_T(t_h)$. The data are shown as points with light (dark) bands indicating the statistical (statistical and systematic) uncertainties. The cross sections are compared to the predictions of POWHEG combined with PYTHIA8 (P8) or HERWIG++ (H++), and the multiparton simulation MG5_amc@NLO (MG5)+PYTHIA8 FxFx. The ratios of the various predictions to the measured cross sections are shown at the bottom of each panel.

We evaluate the level of agreement between the measured differential cross sections and the various theoretical predictions using χ^2 tests. In these tests, we take into account the full covariance matrices of the measured differential cross sections. For the POWHEG+PYTHIA8 and the SHERPA predictions we consider the theoretical uncertainties and their correlation among the bins. In addition, we perform the χ^2 tests without any uncertainties in the theoretical models. We do this since the generation of simulated events does not include any of these theoretical uncertainties; the simulated distributions of the various kinematic quantities correspond exactly to the central predictions. Therefore, it is worthwhile to compare how well the central predictions agree with the data,

independent of the theoretical uncertainties. From the χ^2 values and the numbers of degrees of freedom, which correspond to the numbers of bins in the distributions, the p -values are calculated. The results are shown in Table I for the parton-level and in Table III for the particle-level absolute measurements. The corresponding χ^2 tests for the normalized distributions, for which the numbers of degrees of freedom are reduced by 1, are given in Tables II and IV for the parton- and particle-level measurements, respectively.

The χ^2 tests show that the measurements are largely compatible with the POWHEG+PYTHIA8 and SHERPA predictions if the uncertainties in the simulations are taken into account. Some tension is observed between the data and the

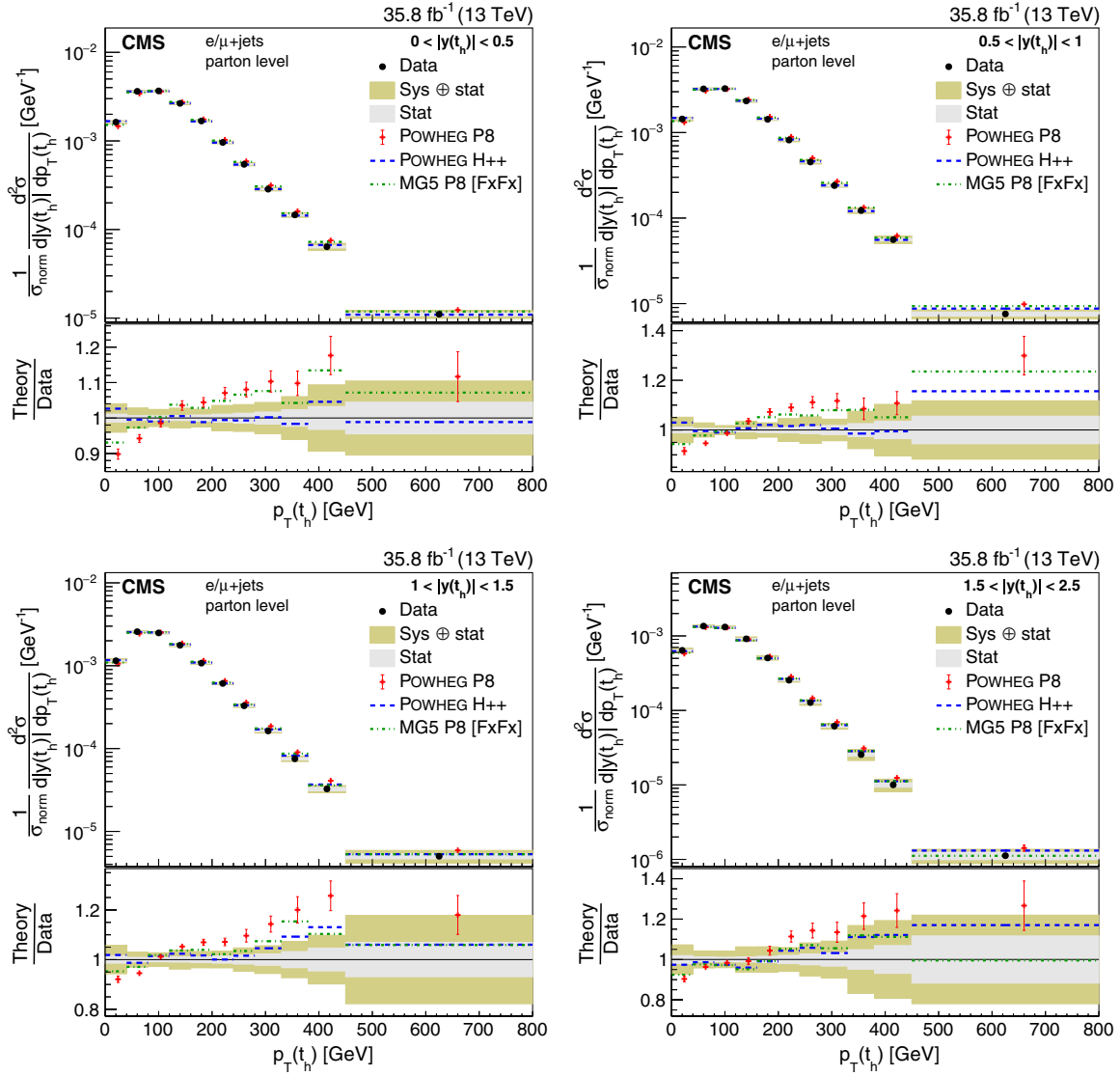


FIG. 19. Normalized double-differential cross section at the parton level as a function of $|y(t_h)|$ vs. $p_T(t_h)$. The data are shown as points with light (dark) bands indicating the statistical (statistical and systematic) uncertainties. The cross sections are compared to the predictions of POWHEG combined with PYTHIA8 (P8) or HERWIG++ (H++), and the multiparton simulation MG5_{AMC}@NLO (MG5) +PYTHIA8 FxFx. The ratios of the various predictions to the measured cross sections are shown at the bottom of each panel.

predictions of $p_T(t)$ and related distributions like $p_T(t_h)$ vs. $M(t\bar{t})$. Comparisons of the p -values at the parton and particle level obtained for the central predictions, ignoring their theoretical uncertainties, show a similar performance. For all tested models we obtain p -values below 1% for at least two distributions. These are typically distributions related to $p_T(t)$ and $p_T(t\bar{t})$.

XI. MEASUREMENTS OF MULTIPLICITIES AND KINEMATIC PROPERTIES OF JETS

In the following, we discuss the measurements involving the multiplicities and kinematic properties of jets in $t\bar{t}$ events. These are performed at the particle level only. In the

POWHEG simulations, all jets beyond one additional jet are described by the PS simulation and, hence, their description is subject to PS tuning. In the SHERPA simulation, the production of up to one additional jet is calculated at NLO accuracy, and up to four jets at LO. However, these LO calculations are very sensitive to the choice of the scales. Since in the MG5_{AMC}@NLO+PYTHIA8 FxFx simulation up to two additional jets are calculated at NLO, it is expected to be more accurate at high jet multiplicities.

The absolute and normalized differential cross sections as a function of $p_T(t_h)$, $M(t\bar{t})$, and $p_T(t\bar{t})$ for different numbers of additional jets are shown in Figs. 30–35. These distributions are helpful to estimate the $t\bar{t}$ background contribution in searches for physics beyond the standard

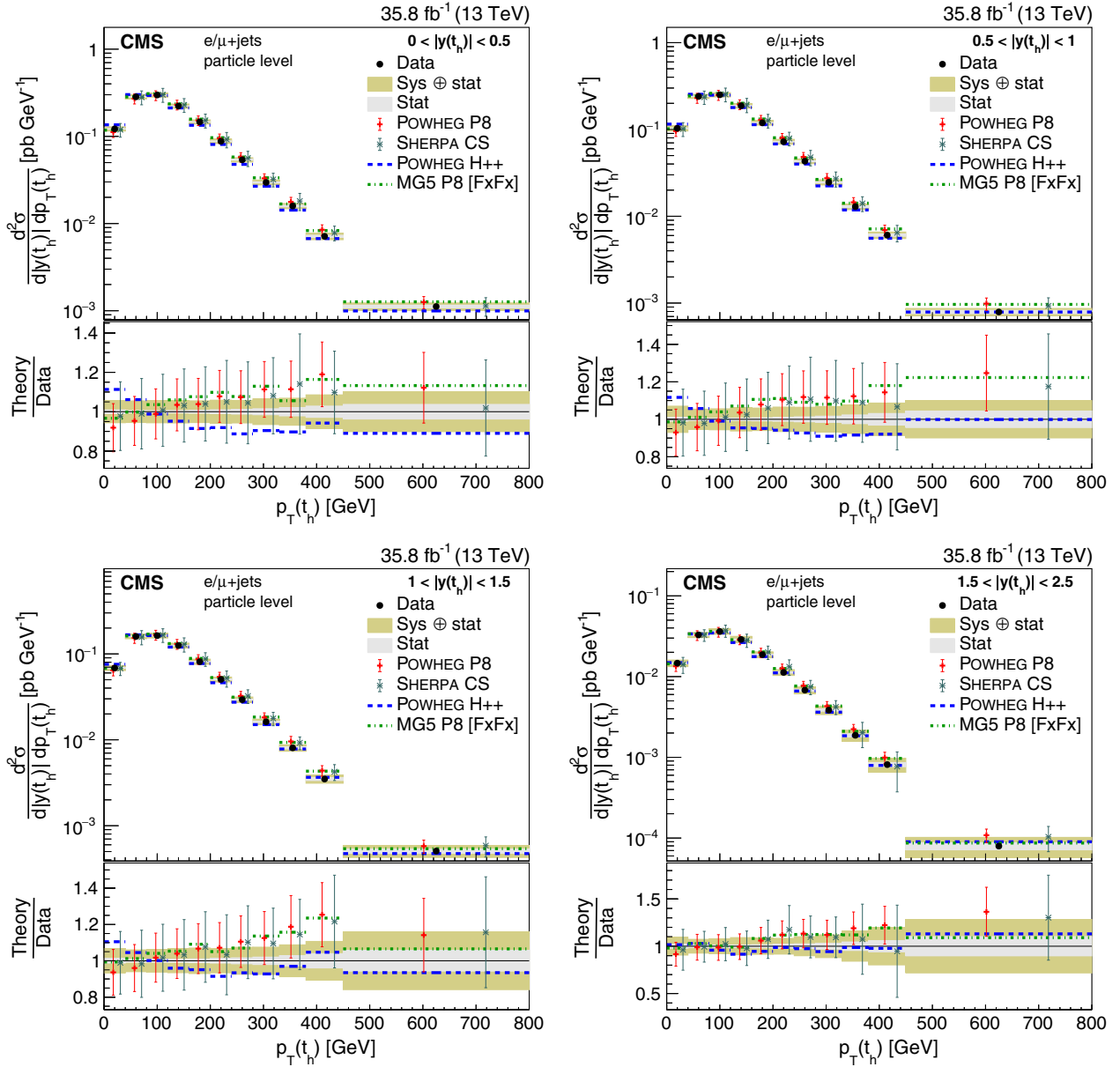


FIG. 20. Double-differential cross section at the particle level as a function of $|y(t_h)|$ vs. $p_T(t_h)$. The data are shown as points with light (dark) bands indicating the statistical (statistical and systematic) uncertainties. The cross sections are compared to the predictions of POWHEG combined with PYTHIA8 (P8) or HERWIG++ (H++) and the multiparton simulations MG5_amc@NLO (MG5)+PYTHIA8 FxFx and SHERPA. The ratios of the various predictions to the measured cross sections are shown at the bottom of each panel.

model that are looking for signatures with high jet multiplicities. The observation that the $p_T(t)$ distribution is softer in data than in the simulations is mainly true for events with zero or one additional jet.

We also measure the properties of the individual jets in $t\bar{t}$ events. The absolute and normalized differential cross sections as a function of the p_T of jets in the $t\bar{t}$ system and of the four leading additional jets are shown in Figs. 36 and 37, respectively. The trend of a softer p_T spectrum of

the top quark is also visible for all jets of the $t\bar{t}$ system. From these p_T distributions we calculate the jet multiplicities with minimum p_T thresholds of 30, 50, 75, and 100 GeV shown in Fig. 38, and gap fractions [16,17]. The gap fraction $f_n(p_T)$ is the fraction of unfolded events that contain less than n additional jets above the given p_T threshold. It is shown for $n = 1$ and 2 in Fig. 39. In the calculations of jet multiplicities and gap fractions, we take into account the small fraction of jets above the displayed

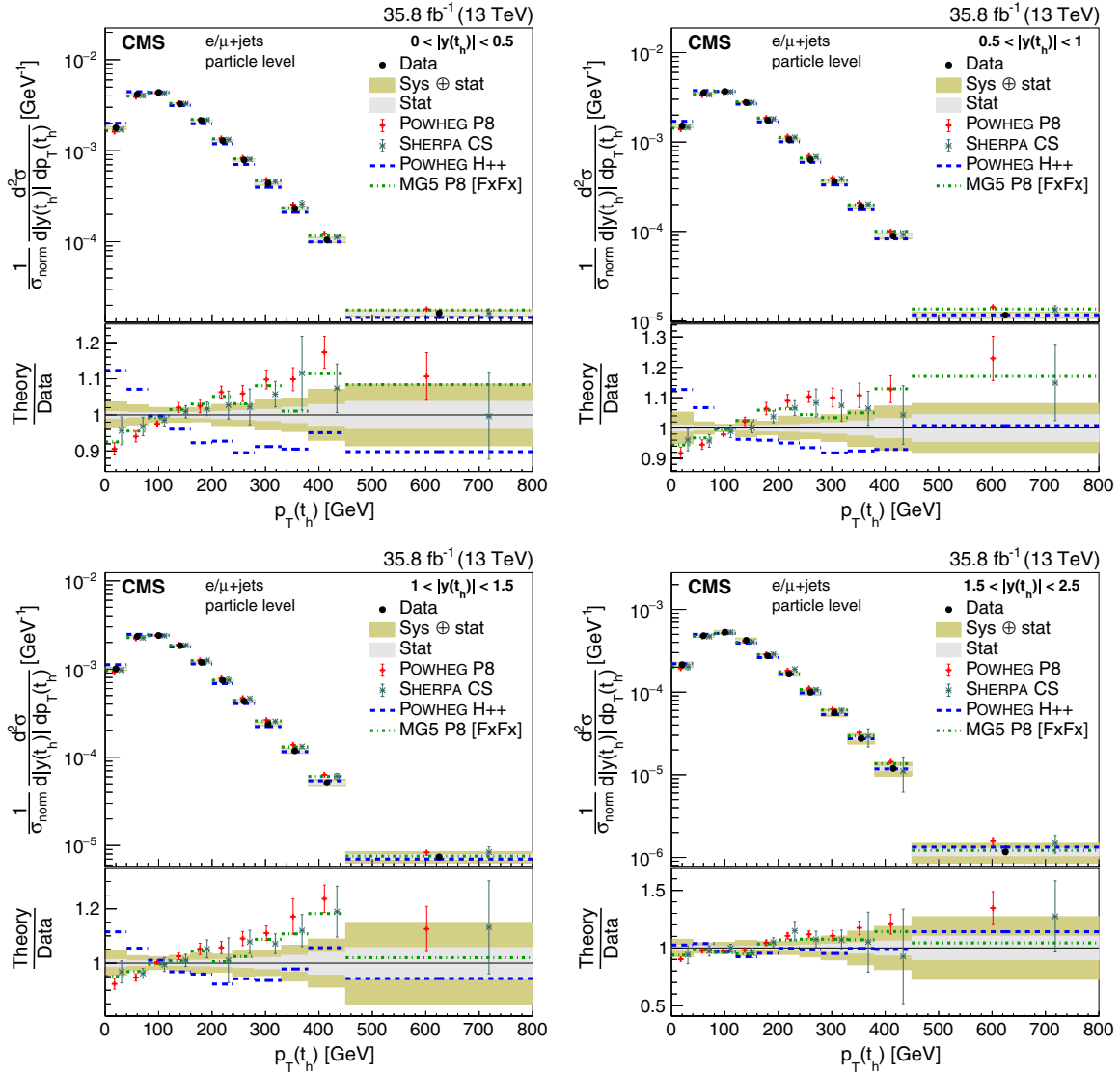


FIG. 21. Normalized double-differential cross section at the particle level as a function of $|y(t_h)|$ vs. $p_T(t_h)$. The data are shown as points with light (dark) bands indicating the statistical (statistical and systematic) uncertainties. The cross sections are compared to the predictions of POWHEG combined with PYTHIA8 (P8) or HERWIG++ (H++) and the multiparton simulations MG5_AMC@NLO (MG5)+PYTHIA8 FxFx and SHERPA. The ratios of the various predictions to the measured cross sections are shown at the bottom of each panel.

p_T ranges. The uncertainties are obtained by error propagation using the full covariance matrices. The jet multiplicities and gap fractions are reasonably described by most of the simulations. However, the central predictions of SHERPA and POWHEG+HERWIG++ show noticeable deviations in the gap fraction.

In Figs. 40–45, the absolute and normalized distributions of $|\eta|$, ΔR_j , and ΔR , are shown for the jets in the $t\bar{t}$ system and the additional jets. The differential cross section as a function of $|\eta|$ is well described by most of the simulations, while POWHEG+HERWIG++ overestimates the radiation of additional jets close to the jets in the $t\bar{t}$ system. In the predictions, such collinear radiation is mainly described by the PS model. Since the parton-level

prediction is not affected by the simulation of the final-state PS, this overestimation of radiation may explain the discrepancies between the parton- and particle-level predictions of POWHEG+HERWIG++ in the $p_T(t_h)$ and $M(t\bar{t})$ distributions.

Table V presents the results of the χ^2 tests comparing the absolute measurements involving multiplicities and kinematic properties of jets to the simulations. The corresponding results for the normalized measurements are shown in Table VI. Most of the kinematic distributions and multiplicities of the additional jets are reasonably well modeled by POWHEG+PYTHIA8. Inconsistencies with the data are observed for p_T and η of jets, and $p_T(t\bar{t})$ for different jet multiplicities. The POWHEG descriptions of

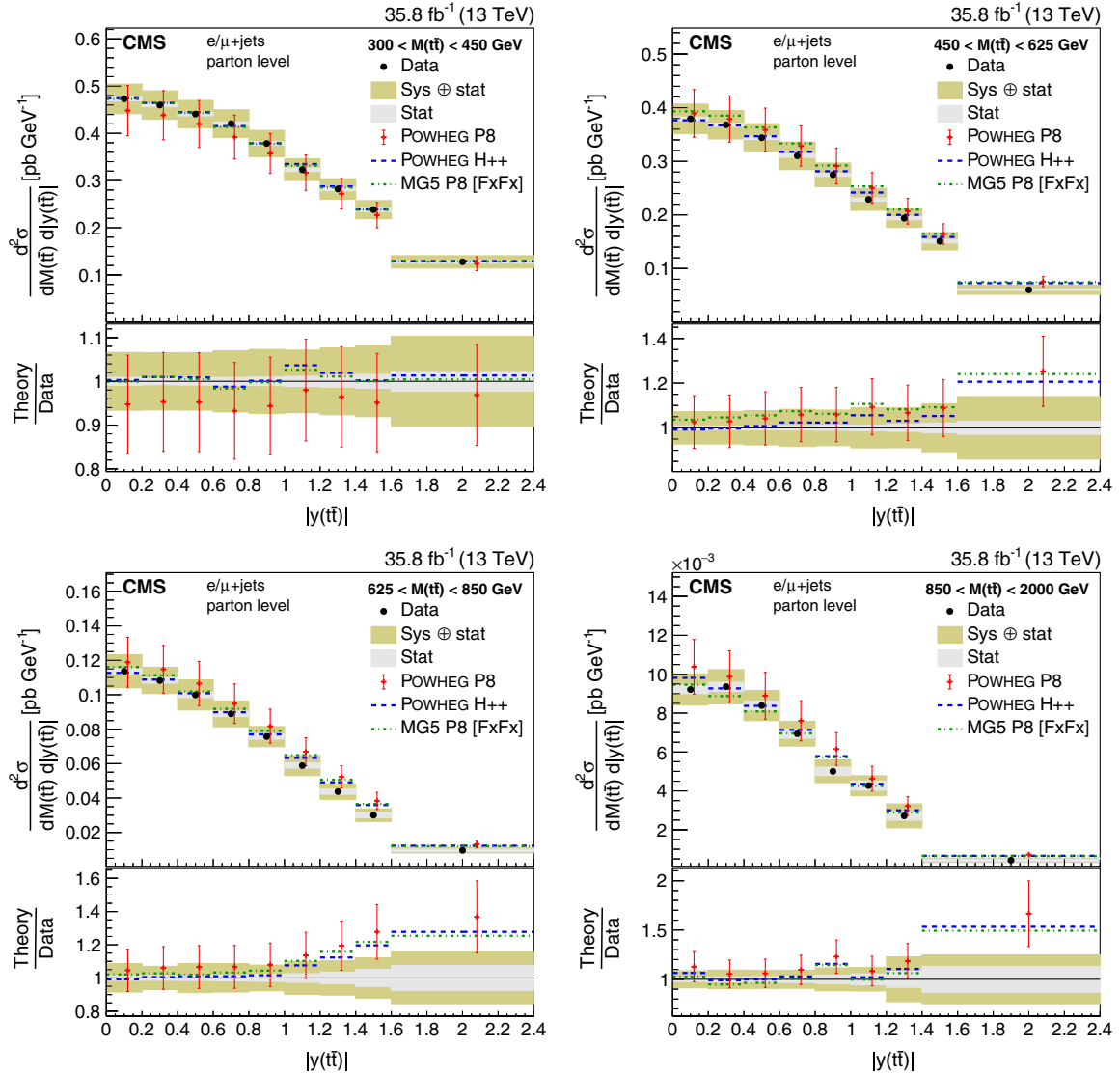


FIG. 22. Double-differential cross section at the parton level as a function of $M(t\bar{t})$ vs. $|y(t\bar{t})|$. The data are shown as points with light (dark) bands indicating the statistical (statistical and systematic) uncertainties. The cross sections are compared to the predictions of POWHEG combined with PYTHIA8 (P8) or HERWIG++ (H++), and the multiparton simulation MG5_AMC@NLO (MG5)+PYTHIA8 FxFx. The ratios of the various predictions to the measured cross sections are shown at the bottom of each panel.

additional jets rely on phenomenological models of the PS and are substantially different for PYTHIA8 and HERWIG++. With the selected settings SHERPA fails to describe most of the kinematic distributions and multiplicities of the jets. Comparisons of the measurements to the central predictions, ignoring their theoretical uncertainties, show that the p -values are typically below 1% for all models. Here the

multiparton simulation MG5_AMC@NLO+PYTHIA8 FxFx performs best.

All cross section values, together with their statistical and systematic uncertainties, are listed in Appendices A and B for the parton- and particle-level measurements, respectively. In addition, the corresponding normalized cross sections are provided in Appendices C and D.

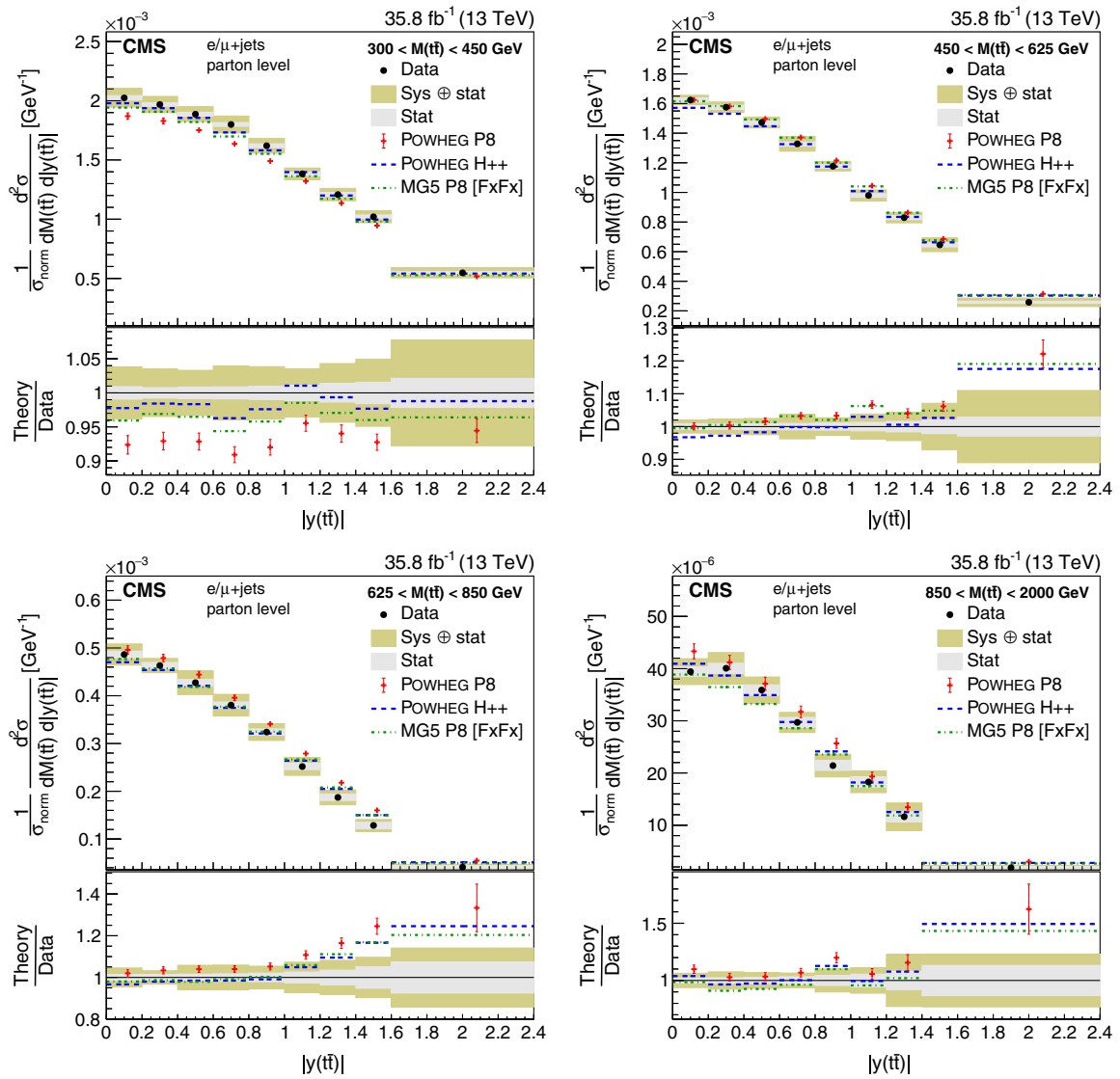


FIG. 23. Normalized double-differential cross section at the parton level as a function of $M(t\bar{t})$ vs. $|y(t\bar{t})|$. The data are shown as points with light (dark) bands indicating the statistical (statistical and systematic) uncertainties. The cross sections are compared to the predictions of POWHEG combined with PYTHIA8 (P8) or HERWIG++ (H++), and the multiparton simulation MG5_amc@NLO (MG5)+PYTHIA8 FxFx. The ratios of the various predictions to the measured cross sections are shown at the bottom of each panel.

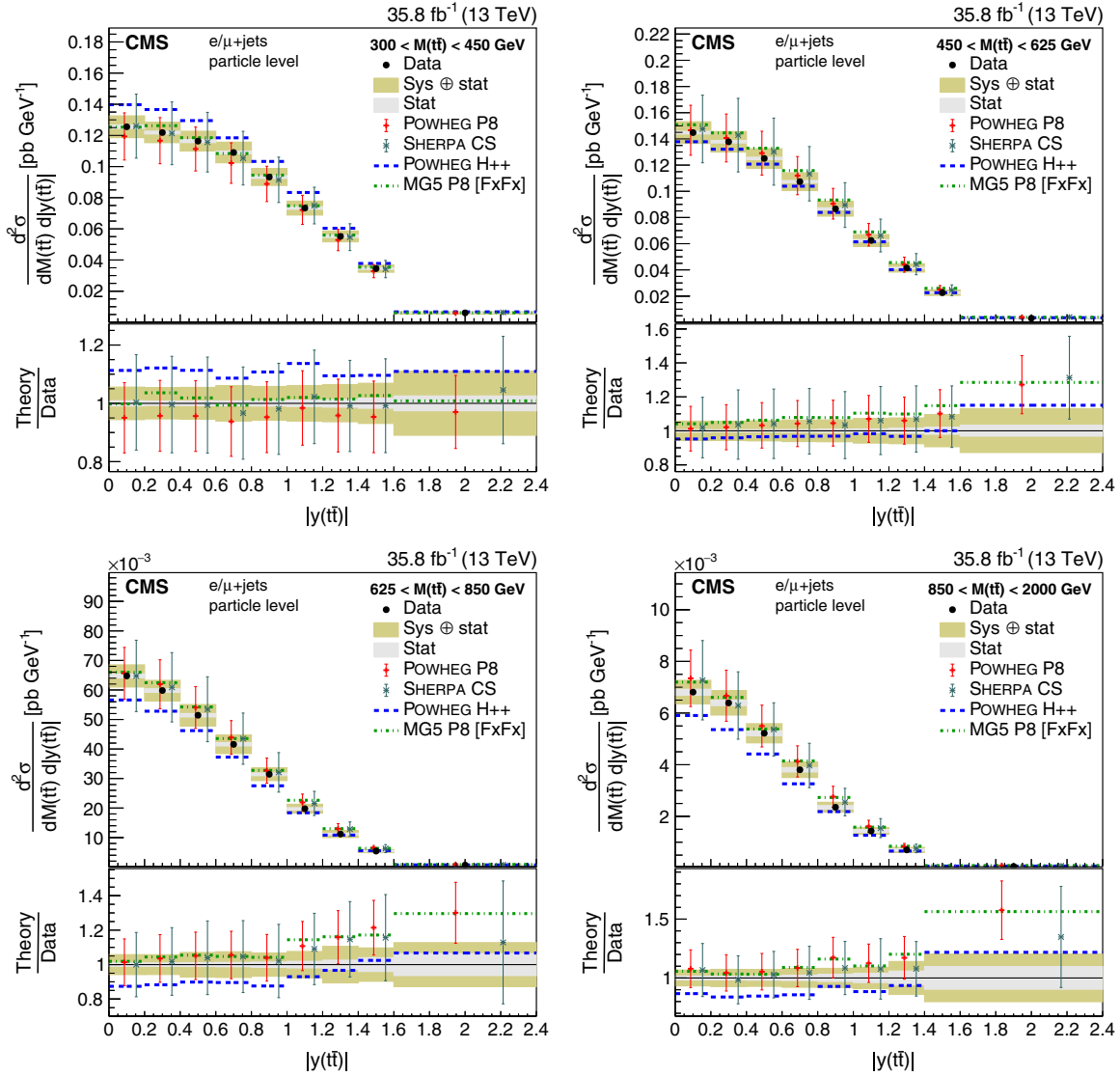


FIG. 24. Double-differential cross section at the particle level as a function of $M(t\bar{t})$ vs. $|y(t\bar{t})|$. The data are shown as points with light (dark) bands indicating the statistical (statistical and systematic) uncertainties. The cross sections are compared to the predictions of POWHEG combined with PYTHIA8 (P8) or HERWIG++ (H++) and the multiparton simulations MG5_amc@NLO (MG5)+PYTHIA8 FxFx and SHERPA. The ratios of the various predictions to the measured cross sections are shown at the bottom of each panel.

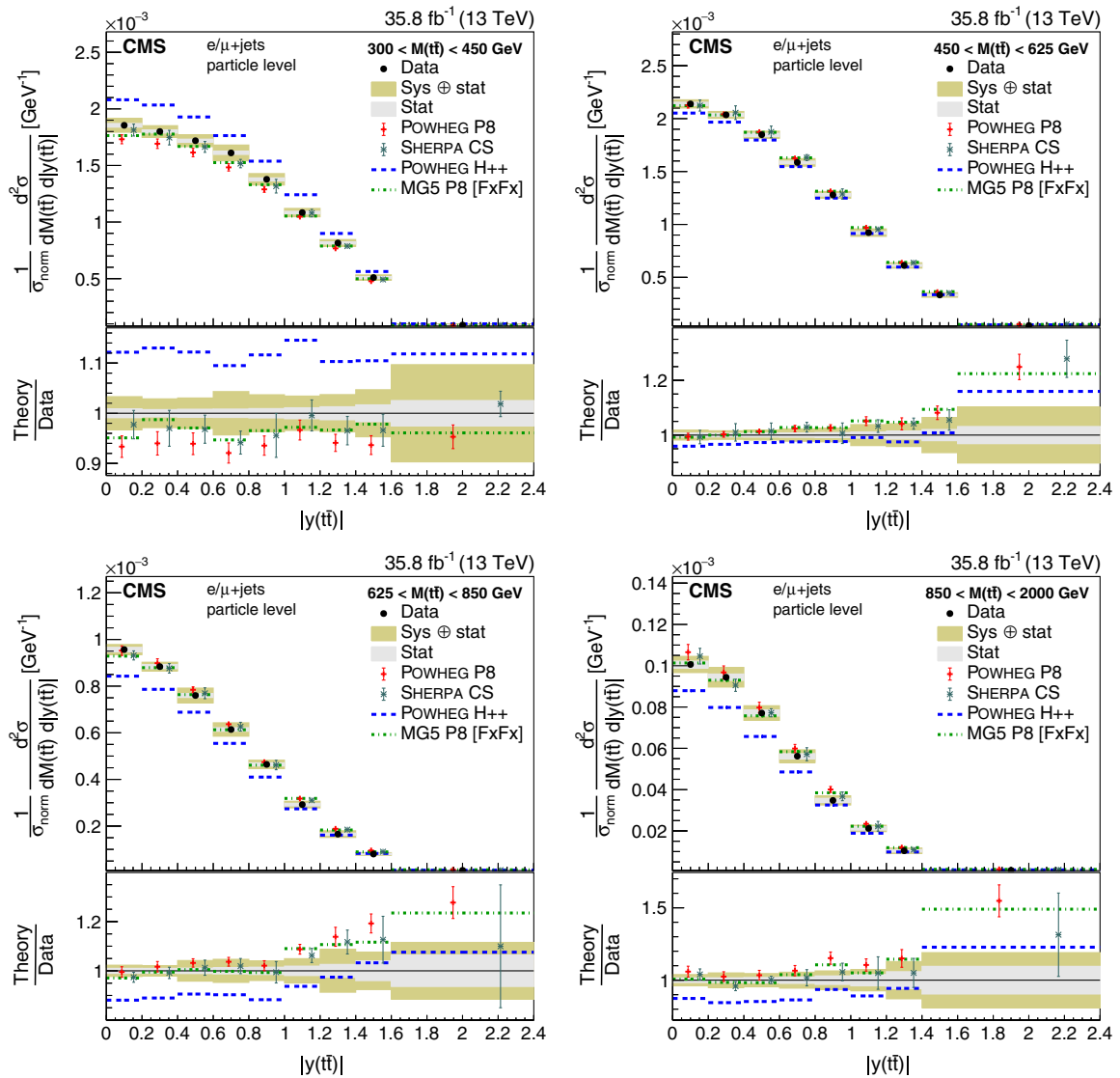


FIG. 25. Normalized double-differential cross section at the particle level as a function of $M(t\bar{t})$ vs. $|y(t\bar{t})|$. The data are shown as points with light (dark) bands indicating the statistical (statistical and systematic) uncertainties. The cross sections are compared to the predictions of POWHEG combined with PYTHIA8 (P8) or HERWIG++ (H++) and the multiparton simulations MG5_AMC@NLO (MG5) +PYTHIA8 FxFx and SHERPA. The ratios of the various predictions to the measured cross sections are shown at the bottom of each panel.

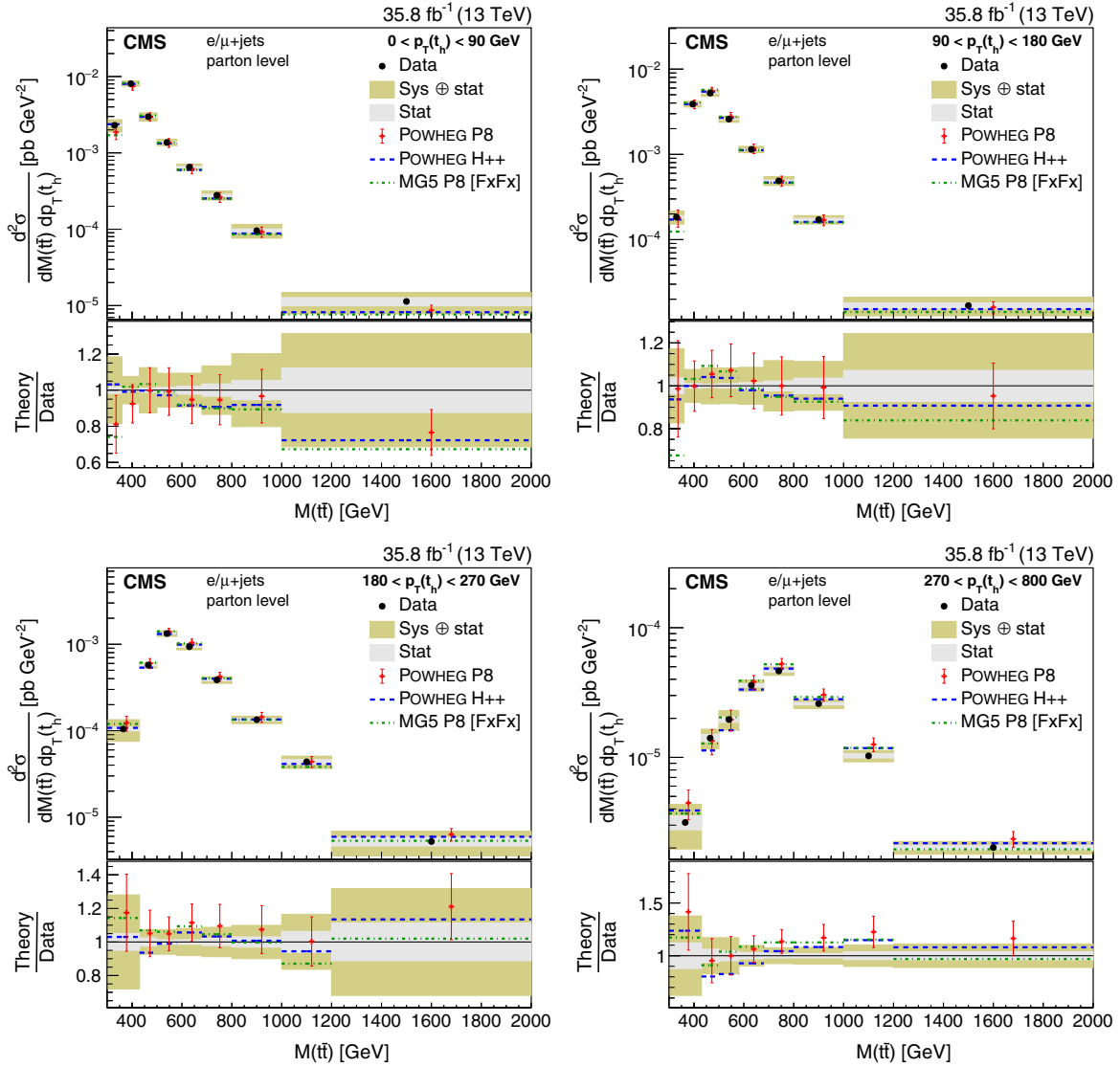


FIG. 26. Double-differential cross section at the parton level as a function of $p_T(t_h)$ vs. $M(t\bar{t})$. The data are shown as points with light (dark) bands indicating the statistical (statistical and systematic) uncertainties. The cross sections are compared to the predictions of POWHEG combined with PYTHIA8 (P8) or HERWIG++ (H++), and the multiparton simulation MG5_amc@NLO (MG5)+PYTHIA8 FxFx. The ratios of the various predictions to the measured cross sections are shown at the bottom of each panel.

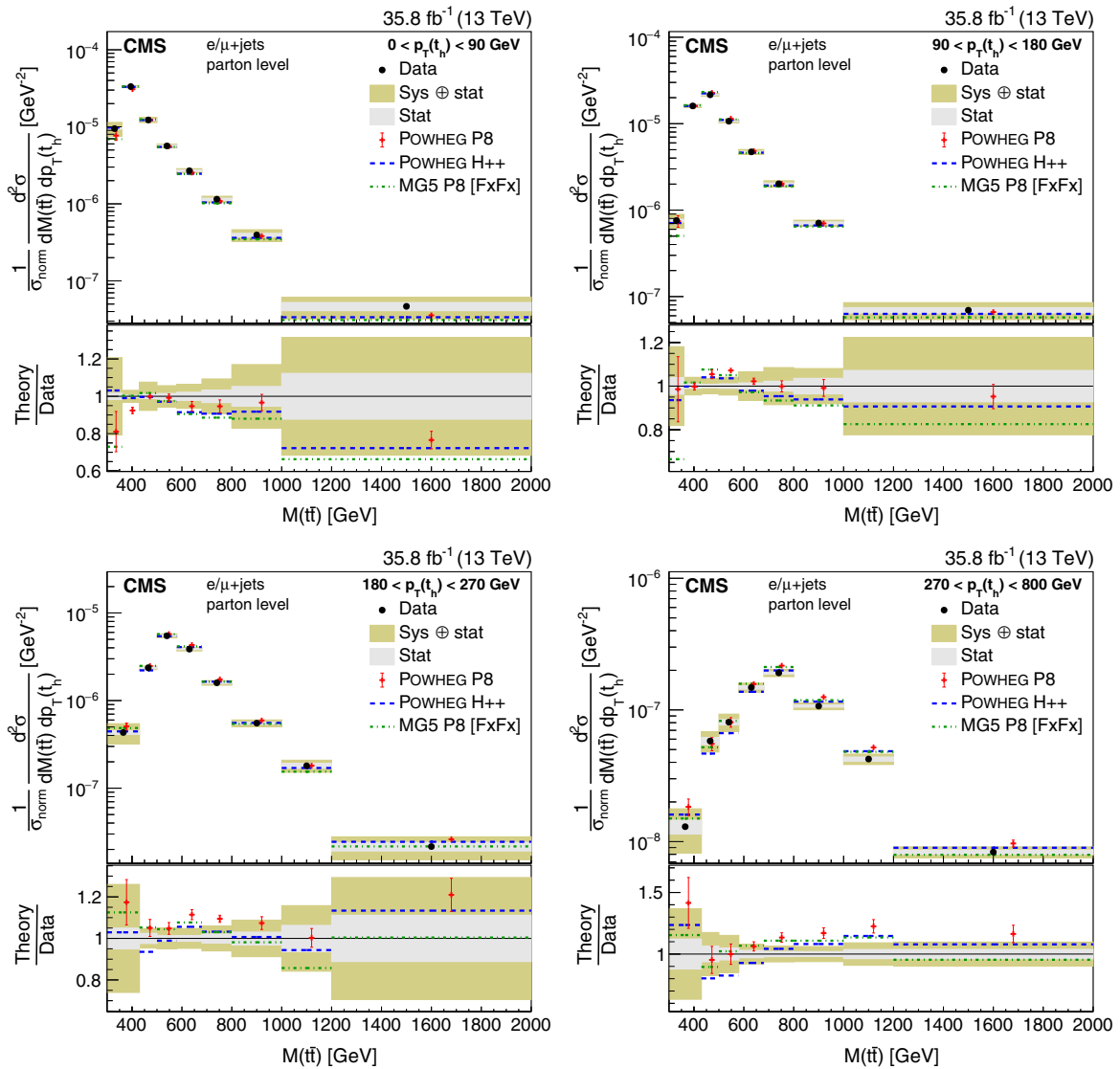


FIG. 27. Normalized double-differential cross section at the parton level as a function of $p_T(t_h)$ vs. $M(t\bar{t})$. The data are shown as points with light (dark) bands indicating the statistical (statistical and systematic) uncertainties. The cross sections are compared to the predictions of POWHEG combined with PYTHIA8 (P8) or HERWIG++ (H++), and the multiparton simulation MG5_{AMC@NLO} (MG5) +PYTHIA8 FxFx. The ratios of the various predictions to the measured cross sections are shown at the bottom of each panel.

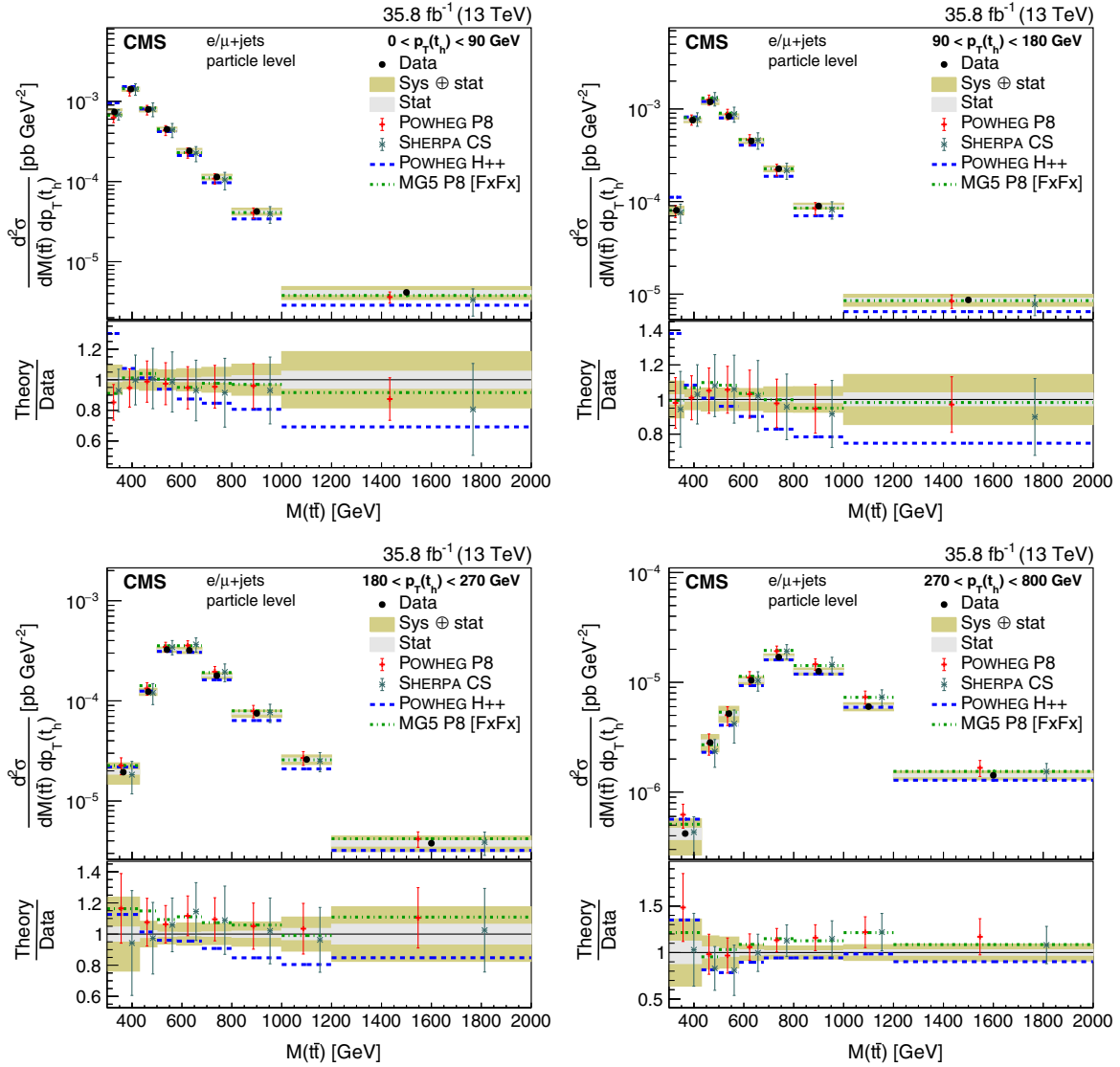


FIG. 28. Double-differential cross section at the particle level as a function of $p_T(t_h)$ vs. $M(t\bar{t})$. The data are shown as points with light (dark) bands indicating the statistical (statistical and systematic) uncertainties. The cross sections are compared to the predictions of POWHEG combined with PYTHIA8 (P8) or HERWIG++ (H++) and the multiparton simulations MG5_AMC@NLO (MG5)+PYTHIA8 FxFx and SHERPA. The ratios of the various predictions to the measured cross sections are shown at the bottom of each panel.

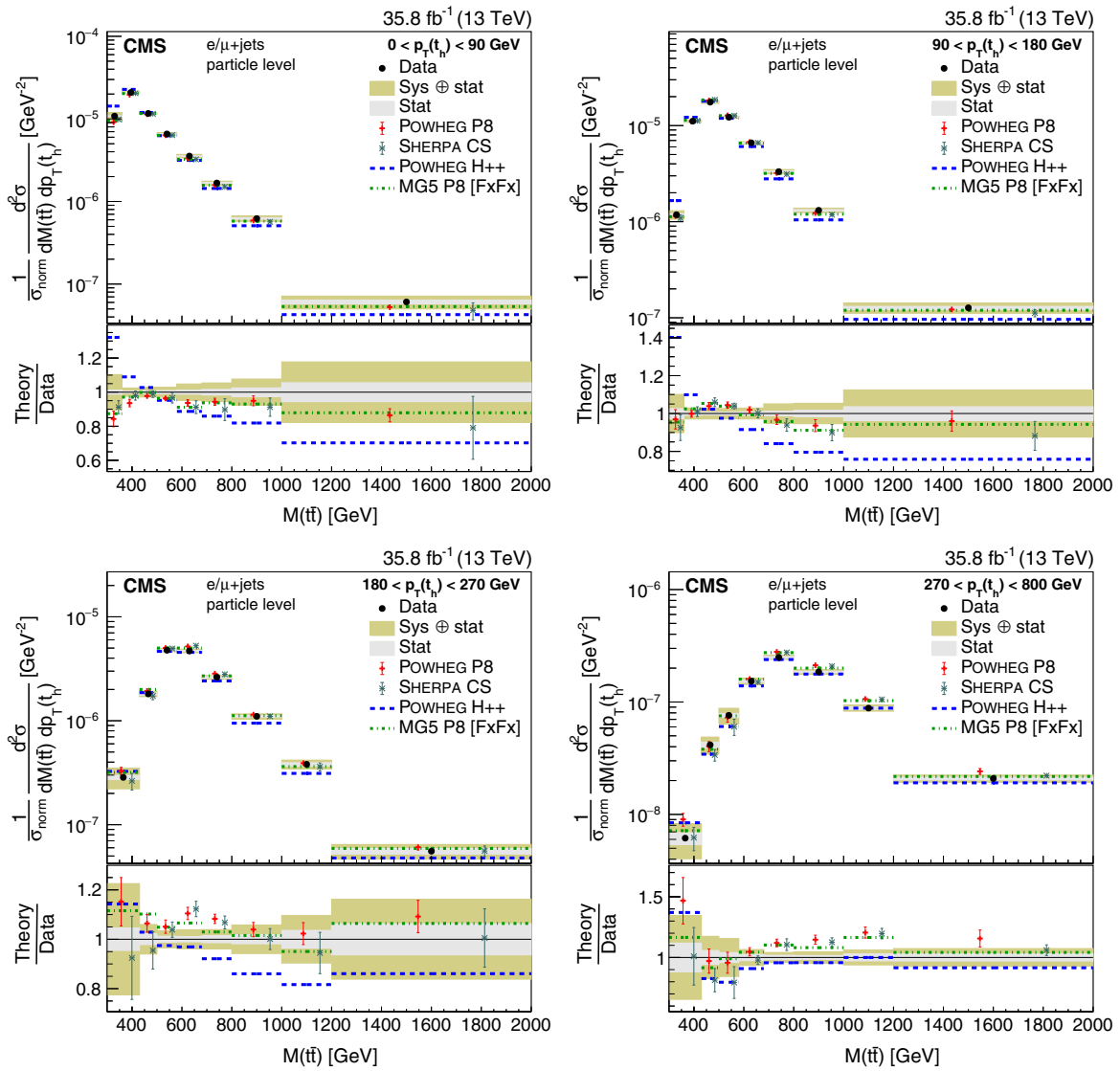


FIG. 29. Normalized double-differential cross section at the particle level as a function of $p_T(t_h)$ vs. $M(t\bar{t})$. The data are shown as points with light (dark) bands indicating the statistical (statistical and systematic) uncertainties. The cross sections are compared to the predictions of POWHEG combined with PYTHIA8 (P8) or HERWIG++ (H++) and the multiparton simulations MG5_amc@NLO (MG5)+PYTHIA8 FxFx and SHERPA. The ratios of the various predictions to the measured cross sections are shown at the bottom of each panel.

TABLE I. Comparison between the measured absolute differential cross sections at the parton level and the predictions of POWHEG combined with PYTHIA8 (P8) or HERWIG++ (H++), the multiparton simulation MG5_AMC@NLO FxFx, and the NNLO QCD + NLO EW calculations. The compatibility with the POWHEG+PYTHIA8 prediction is also calculated including its theoretical uncertainties (with unc.), while those are not taken into account for the other comparisons. The results of the χ^2 tests are listed, together with the numbers of degrees of freedom (dof) and the corresponding p -values.

Distribution	χ^2/dof	p -value	χ^2/dof	p -value	χ^2/dof	p -value
POWHEG+P8 with unc.						
$p_T(t_{\text{high}})$	16.4/12	0.173	27.4/12	<0.01		
$p_T(t_{\text{low}})$	22.4/12	0.033	42.7/12	<0.01		
$p_T(t_h)$	16.4/12	0.175	24.0/12	0.020	5.13/12	0.953
$ y(t_h) $	1.28/11	1.000	1.41/11	1.000	2.27/11	0.997
$p_T(t_\ell)$	22.2/12	0.035	38.3/12	<0.01	9.56/12	0.654
$ y(t_\ell) $	2.04/11	0.998	2.42/11	0.996	8.14/11	0.700
$M(t\bar{t})$	7.67/10	0.661	11.6/10	0.314	24.7/10	<0.01
$p_T(t\bar{t})$	5.38/8	0.717	46.5/8	<0.01		
$ y(t\bar{t}) $	3.98/10	0.948	5.66/10	0.843	9.26/10	0.507
$ y(t_h) $ vs. $p_T(t_h)$	23.6/44	0.995	41.6/44	0.577		
$M(t\bar{t})$ vs. $ y(t\bar{t}) $	20.6/35	0.975	35.0/35	0.469		
$p_T(t_h)$ vs. $M(t\bar{t})$	38.9/32	0.188	59.3/32	<0.01		
POWHEG+H++						
$p_T(t_{\text{high}})$	6.60/12	0.883	16.3/12	0.180		
$p_T(t_{\text{low}})$	28.5/12	<0.01	15.3/12	0.225		
$p_T(t_h)$	5.09/12	0.955	11.0/12	0.530		
$ y(t_h) $	2.39/11	0.997	2.21/11	0.998		
$p_T(t_\ell)$	6.55/12	0.886	17.4/12	0.136		
$ y(t_\ell) $	2.54/11	0.995	3.99/11	0.970		
$M(t\bar{t})$	4.16/10	0.940	12.1/10	0.275		
$p_T(t\bar{t})$	55.0/8	<0.01	26.8/8	<0.01		
$ y(t\bar{t}) $	11.9/10	0.292	8.92/10	0.540		
$ y(t_h) $ vs. $p_T(t_h)$	57.9/44	0.077	40.2/44	0.634		
$M(t\bar{t})$ vs. $ y(t\bar{t}) $	40.8/35	0.229	58.7/35	<0.01		
$p_T(t_h)$ vs. $M(t\bar{t})$	93.0/32	<0.01	166/32	<0.01		
MG5_AMC@NLO+FxFx						
					...	

TABLE II. Comparison between the measured normalized differential cross sections at the parton level and the predictions of POWHEG combined with PYTHIA8 (P8) or HERWIG++ (H++), the multiparton simulation MG5_AMC@NLO FxFx, and the NNLO QCD + NLO EW calculations. The compatibility with the POWHEG+PYTHIA8 prediction is also calculated including its theoretical uncertainties (with unc.), while those are not taken into account for the other comparisons. The results of the χ^2 tests are listed, together with the numbers of degrees of freedom (dof) and the corresponding p -values.

Distribution	χ^2/dof	p -value	χ^2/dof	p -value	χ^2/dof	p -value
POWHEG+P8 with unc.						
$p_T(t_{\text{high}})$	18.4/11	0.073	24.4/11	0.011		
$p_T(t_{\text{low}})$	16.6/11	0.120	40.0/11	<0.01		
$p_T(t_h)$	16.1/11	0.138	22.9/11	0.018	4.99/11	0.932
$ y(t_h) $	1.25/10	1.000	1.33/10	0.999	2.23/10	0.994
$p_T(t_\ell)$	23.6/11	0.014	33.0/11	<0.01	8.67/11	0.652
$ y(t_\ell) $	2.03/10	0.996	2.29/10	0.994	8.18/10	0.611
$M(t\bar{t})$	7.78/9	0.556	11.3/9	0.259	24.4/9	<0.01
$p_T(t\bar{t})$	5.52/7	0.597	40.9/7	<0.01		
$ y(t\bar{t}) $	3.89/9	0.919	5.36/9	0.802	9.29/9	0.411

(Table continued)

TABLE II. (*Continued*)

Distribution	χ^2/dof	<i>p</i> -value	χ^2/dof	<i>p</i> -value	χ^2/dof	<i>p</i> -value
$ y(t_h) $ vs. $p_T(t_h)$	22.7/43	0.995	38.8/43	0.654		
$M(t\bar{t})$ vs. $ y(t\bar{t}) $	20.2/34	0.970	33.2/34	0.507		
$p_T(t_h)$ vs. $M(t\bar{t})$	34.4/31	0.309	57.4/31	<0.01		
	POWHEG+H++		MG5_aMC@NLO+P8 FxFx		...	
$p_T(t_{\text{high}})$	4.10/11	0.967	13.2/11	0.283		
$p_T(t_{\text{low}})$	17.4/11	0.096	11.9/11	0.370		
$p_T(t_h)$	3.61/11	0.980	9.95/11	0.535		
$ y(t_h) $	1.63/10	0.998	1.11/10	1.000		
$p_T(t_\ell)$	8.36/11	0.680	16.4/11	0.128		
$ y(t_\ell) $	1.57/10	0.999	2.48/10	0.991		
$M(t\bar{t})$	3.57/9	0.937	7.61/9	0.574		
$p_T(t\bar{t})$	43.4/7	<0.01	20.5/7	<0.01		
$ y(t\bar{t}) $	5.94/9	0.746	4.65/9	0.864		
$ y(t_h) $ vs. $p_T(t_h)$	32.6/43	0.877	27.8/43	0.965		
$M(t\bar{t})$ vs. $ y(t\bar{t}) $	27.2/34	0.788	40.2/34	0.214		
$p_T(t_h)$ vs. $M(t\bar{t})$	67.9/31	<0.01	77.9/31	<0.01		

TABLE III. Comparison between the measured absolute differential cross sections at the particle level and the predictions of POWHEG combined with PYTHIA8 (P8) or HERWIG++ (H++) and the multiparton simulations of MG5_aMC@NLO FxFx and SHERPA. The compatibilities with the POWHEG+PYTHIA8 and the SHERPA predictions are also calculated including their theoretical uncertainties (with unc.), while those are not taken into account for the other comparisons. The results of the χ^2 tests are listed, together with the numbers of degrees of freedom (dof) and the corresponding *p*-values.

Distribution	χ^2/dof	<i>p</i> -value	χ^2/dof	<i>p</i> -value	χ^2/dof	<i>p</i> -value
	POWHEG+P8 with unc.		SHERPA with unc.		POWHEG+P8	
$p_T(t_h)$	15.9/12	0.197	7.21/12	0.844	29.5/12	<0.01
$ y(t_h) $	1.96/11	0.999	1.48/11	1.000	2.23/11	0.997
$p_T(t_\ell)$	27.0/12	<0.01	22.3/12	0.034	80.2/12	<0.01
$ y(t_\ell) $	4.55/11	0.951	5.07/11	0.928	4.99/11	0.932
$M(t\bar{t})$	5.83/10	0.829	2.40/10	0.992	9.07/10	0.525
$p_T(t\bar{t})$	4.96/8	0.761	28.9/8	<0.01	41.2/8	<0.01
$ y(t\bar{t}) $	5.93/10	0.821	6.63/10	0.760	8.61/10	0.570
$ y(t_h) $ vs. $p_T(t_h)$	35.7/44	0.810	29.6/44	0.953	64.1/44	0.025
$M(t\bar{t})$ vs. $ y(t\bar{t}) $	25.9/35	0.867	24.2/35	0.914	56.2/35	0.013
$p_T(t_h)$ vs. $M(t\bar{t})$	47.4/32	0.039	57.2/32	<0.01	73.2/32	<0.01
	SHERPA		POWHEG+H++		MG5_aMC@NLO+P8 FxFx	
$p_T(t_h)$	13.5/12	0.335	32.1/12	<0.01	17.4/12	0.137
$ y(t_h) $	2.32/11	0.997	4.89/11	0.936	3.16/11	0.988
$p_T(t_\ell)$	39.4/12	<0.01	21.8/12	0.040	47.7/12	<0.01
$ y(t_\ell) $	5.54/11	0.902	4.04/11	0.969	7.22/11	0.781
$M(t\bar{t})$	2.86/10	0.985	52.8/10	<0.01	5.45/10	0.859
$p_T(t\bar{t})$	68.7/8	<0.01	46.8/8	<0.01	21.3/8	<0.01
$ y(t\bar{t}) $	12.1/10	0.276	18.6/10	0.046	8.13/10	0.616
$ y(t_h) $ vs. $p_T(t_h)$	48.3/44	0.305	116/44	<0.01	44.9/44	0.434
$M(t\bar{t})$ vs. $ y(t\bar{t}) $	41.5/35	0.208	219/35	<0.01	55.7/35	0.014
$p_T(t_h)$ vs. $M(t\bar{t})$	66.5/32	<0.01	152/32	<0.01	48.9/32	0.028

TABLE IV. Comparison between the measured normalized differential cross sections at the particle level and the predictions of POWHEG combined with PYTHIA8 (P8) or HERWIG++ (H++) and the multiparton simulations of MG5_aMC@NLO FxFx and SHERPA. The compatibilities with the POWHEG+PYTHIA8 and the SHERPA predictions are also calculated including their theoretical uncertainties (with unc.), while those are not taken into account for the other comparisons. The results of the χ^2 tests are listed, together with the numbers of degrees of freedom (dof) and the corresponding p -values.

Distribution	χ^2/dof	p -value	χ^2/dof	p -value	χ^2/dof	p -value
POWHEG+P8 with unc.			SHERPA with unc.			POWHEG+P8
$p_T(t_h)$	14.9/11	0.186	6.99/11	0.800	29.4/11	<0.01
$ y(t_h) $	1.77/10	0.998	1.25/10	1.000	1.90/10	0.997
$p_T(t_\ell)$	25.3/11	<0.01	28.0/11	<0.01	74.0/11	<0.01
$ y(t_\ell) $	4.50/10	0.922	4.88/10	0.899	5.00/10	0.891
$M(t\bar{t})$	5.69/9	0.770	2.17/9	0.989	9.33/9	0.407
$p_T(t\bar{t})$	5.36/7	0.616	12.5/7	0.086	34.8/7	<0.01
$ y(t\bar{t}) $	5.79/9	0.761	6.68/9	0.671	8.48/9	0.486
$ y(t_h) $ vs. $p_T(t_h)$	27.6/43	0.967	32.7/43	0.872	53.8/43	0.126
$M(t\bar{t})$ vs. $ y(t\bar{t}) $	26.5/34	0.817	22.7/34	0.931	54.0/34	0.016
$p_T(t_h)$ vs. $M(t\bar{t})$	42.5/31	0.082	39.2/31	0.149	64.8/31	<0.01
SHERPA			POWHEG+H++			MG5_aMC@NLO+P8 FxFx
$p_T(t_h)$	13.9/11	0.238	34.1/11	<0.01	15.2/11	0.173
$ y(t_h) $	1.60/10	0.999	3.81/10	0.955	2.73/10	0.987
$p_T(t_\ell)$	37.3/11	<0.01	25.0/11	<0.01	40.5/11	<0.01
$ y(t_\ell) $	5.28/10	0.872	3.92/10	0.951	5.54/10	0.853
$M(t\bar{t})$	2.99/9	0.965	51.7/9	<0.01	4.98/9	0.836
$p_T(t\bar{t})$	59.4/7	<0.01	43.8/7	<0.01	17.9/7	0.013
$ y(t\bar{t}) $	11.3/9	0.253	18.2/9	0.033	8.37/9	0.498
$ y(t_h) $ vs. $p_T(t_h)$	47.7/43	0.287	108/43	<0.01	40.9/43	0.561
$M(t\bar{t})$ vs. $ y(t\bar{t}) $	37.6/34	0.308	234/34	<0.01	55.5/34	0.011
$p_T(t_h)$ vs. $M(t\bar{t})$	63.2/31	<0.01	126/31	<0.01	43.0/31	0.074

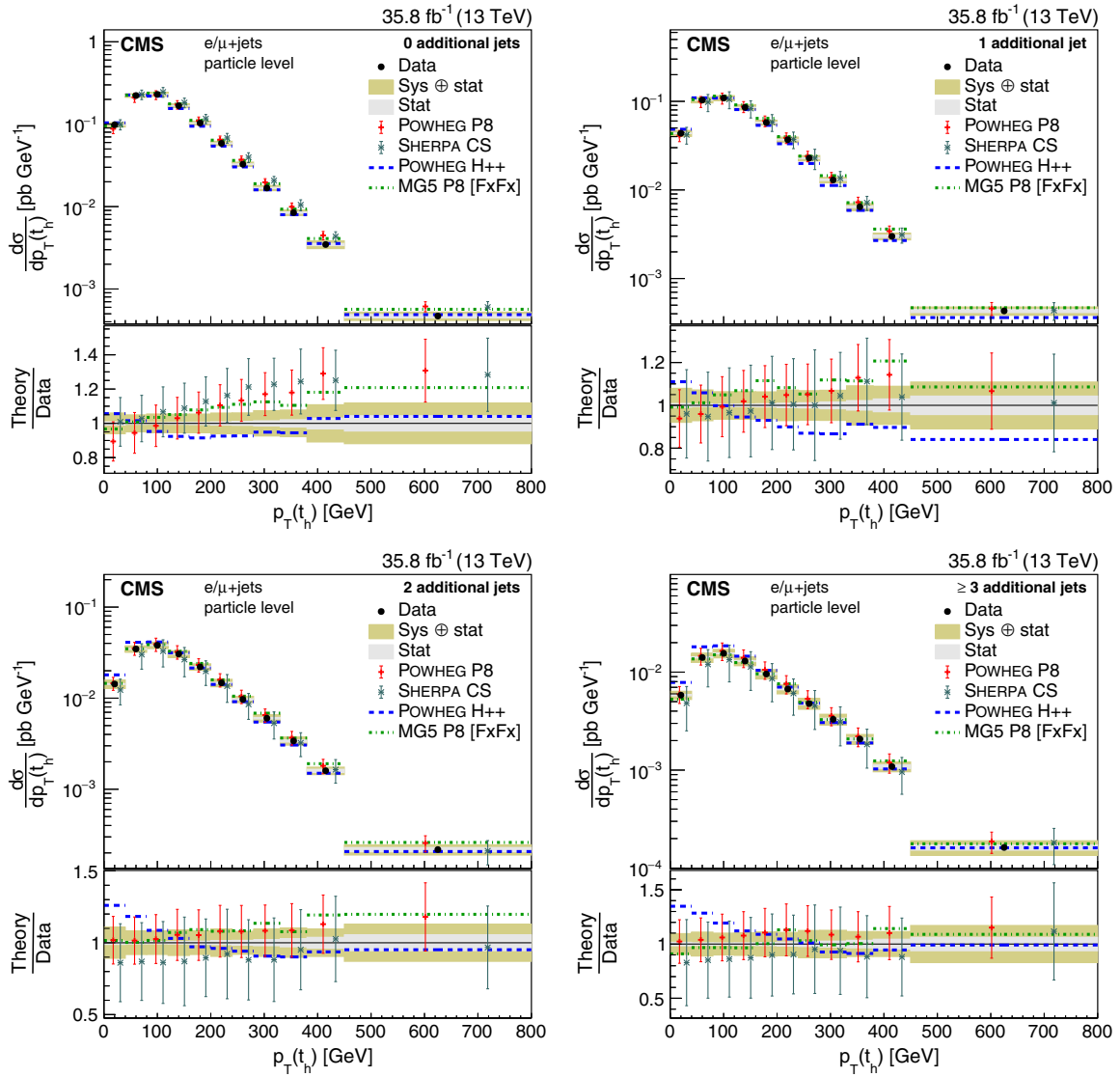


FIG. 30. Differential cross sections at the particle level as a function of $p_T(t_h)$ in bins of the number of additional jets. The data are shown as points with light (dark) bands indicating the statistical (statistical and systematic) uncertainties. The cross sections are compared to the predictions of POWHEG combined with PYTHIA8 (P8) or HERWIG++ (H++) and the multiparton simulations MG5_aMC@NLO (MG5)+PYTHIA8 FxFx and SHERPA. The ratios of the various predictions to the measured cross sections are shown at the bottom of each panel.

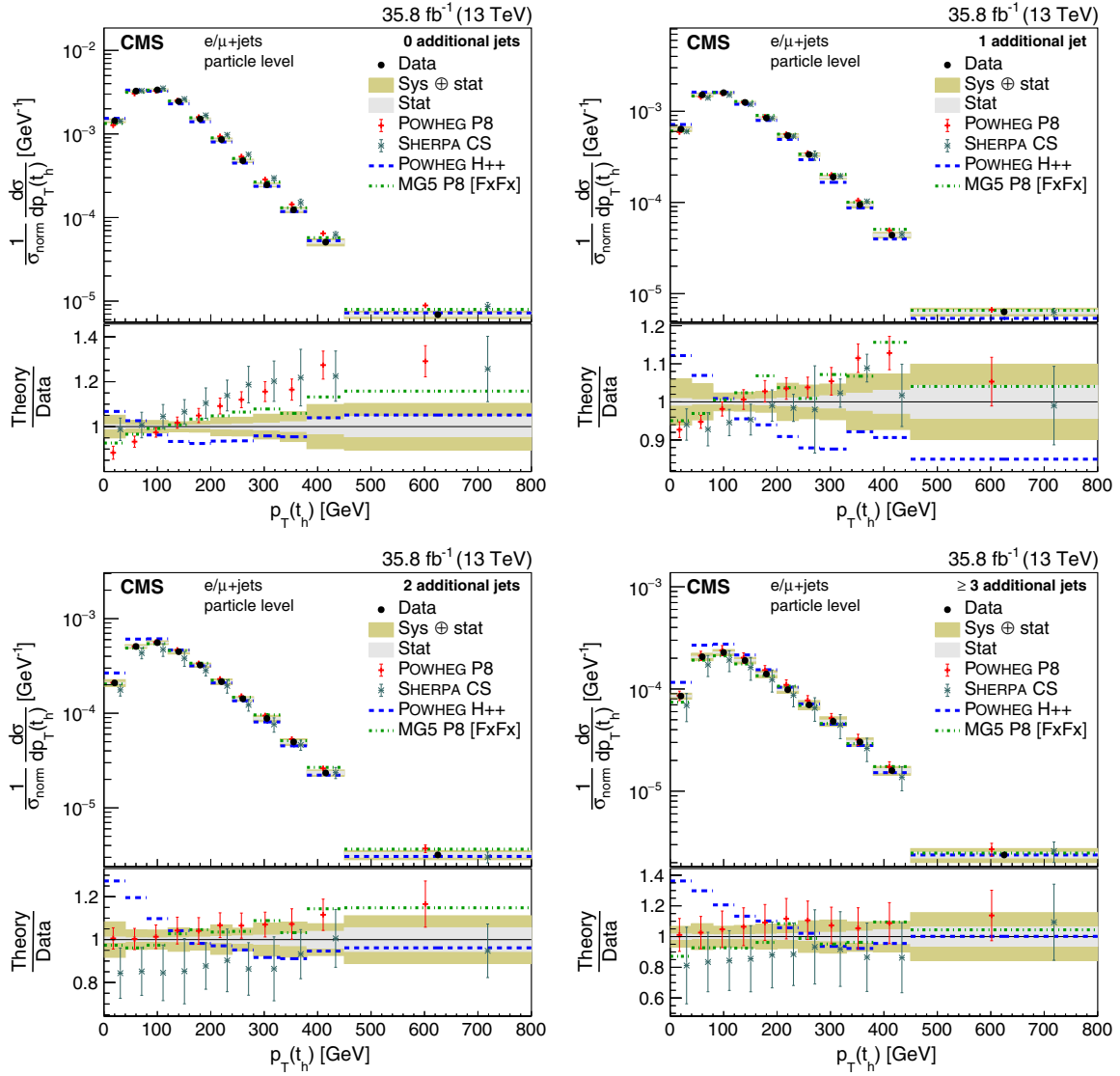


FIG. 31. Differential cross sections at the particle level normalized to the sum of the cross sections σ_{norm} in the measured ranges as a function of $p_T(t_h)$ in bins of the number of additional jets. The data are shown as points with light (dark) bands indicating the statistical (statistical and systematic) uncertainties. The cross sections are compared to the predictions of POWHEG combined with PYTHIA8 (P8) or HERWIG++ (H++) and the multiparton simulations MG5_AMC@NLO (MG5)+PYTHIA8 FxFx and SHERPA. The ratios of the various predictions to the measured cross sections are shown at the bottom of each panel.

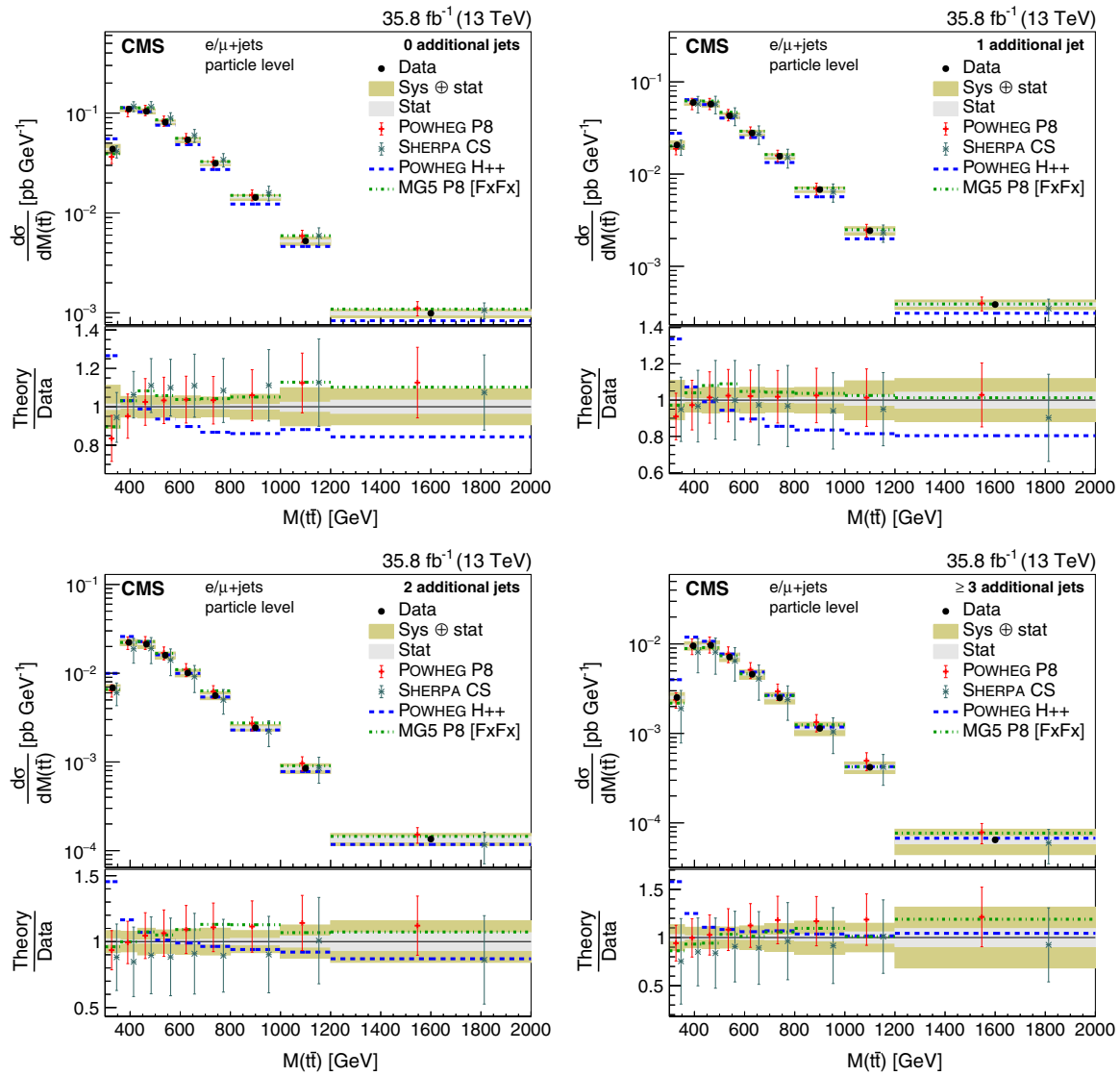


FIG. 32. Differential cross sections at the particle level as a function of $M(t\bar{t})$ in bins of the number of additional jets. The data are shown as points with light (dark) bands indicating the statistical (statistical and systematic) uncertainties. The cross sections are compared to the predictions of POWHEG combined with PYTHIA8 (P8) or HERWIG++ (H++) and the multiparton simulations MG5_amc@NLO (MG5)+PYTHIA8 FxFx and SHERPA. The ratios of the various predictions to the measured cross sections are shown at the bottom of each panel.

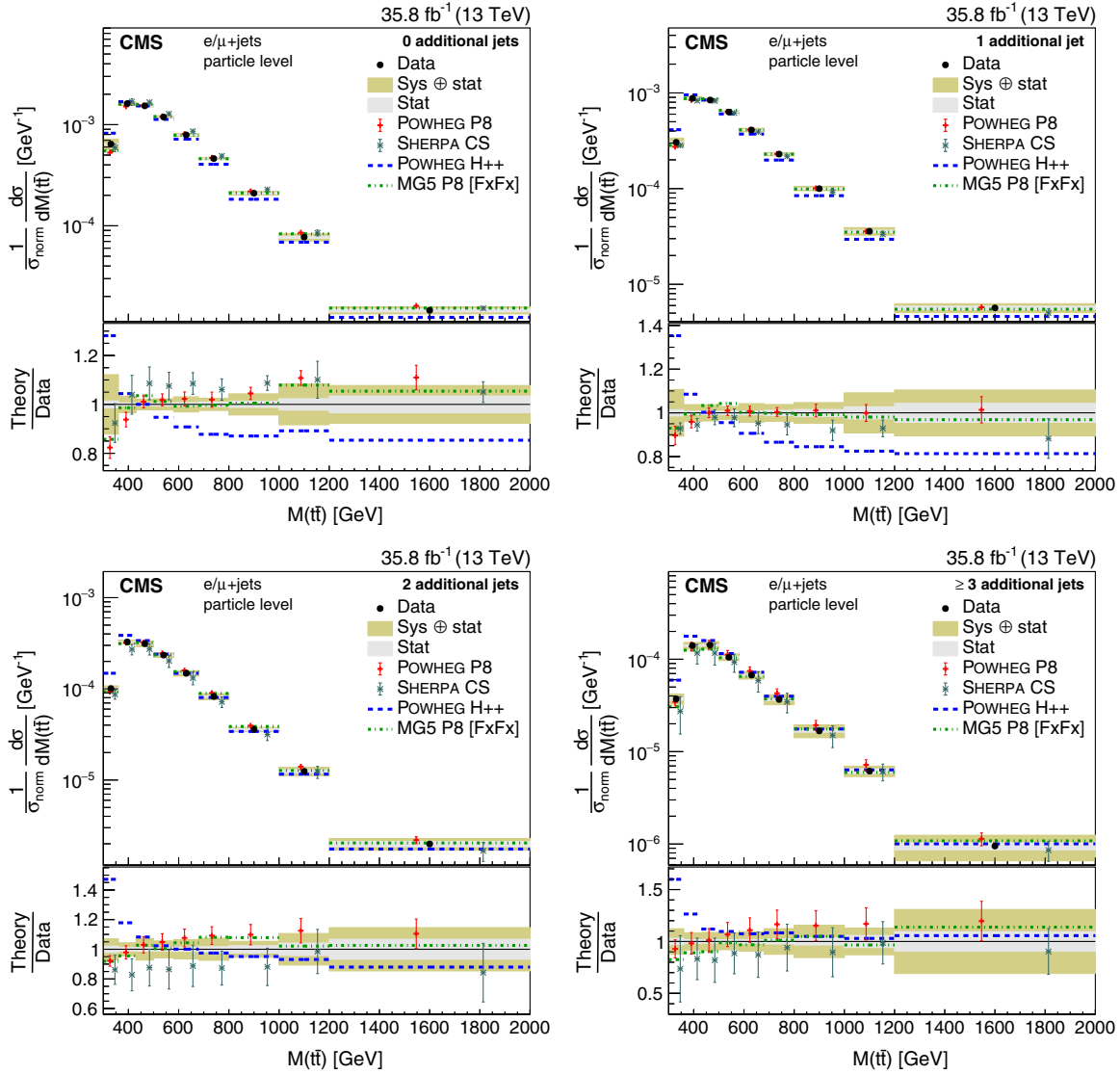


FIG. 33. Differential cross sections at the particle level normalized to the sum of the cross sections σ_{norm} in the measured ranges as a function of $M(t\bar{t})$ in bins of the number of additional jets. The data are shown as points with light (dark) bands indicating the statistical (statistical and systematic) uncertainties. The cross sections are compared to the predictions of POWHEG combined with PYTHIA8 (P8) or HERWIG++ (H++) and the multiparton simulations MG5_AMC@NLO (MG5)+PYTHIA8 FxFx and SHERPA. The ratios of the various predictions to the measured cross sections are shown at the bottom of each panel.

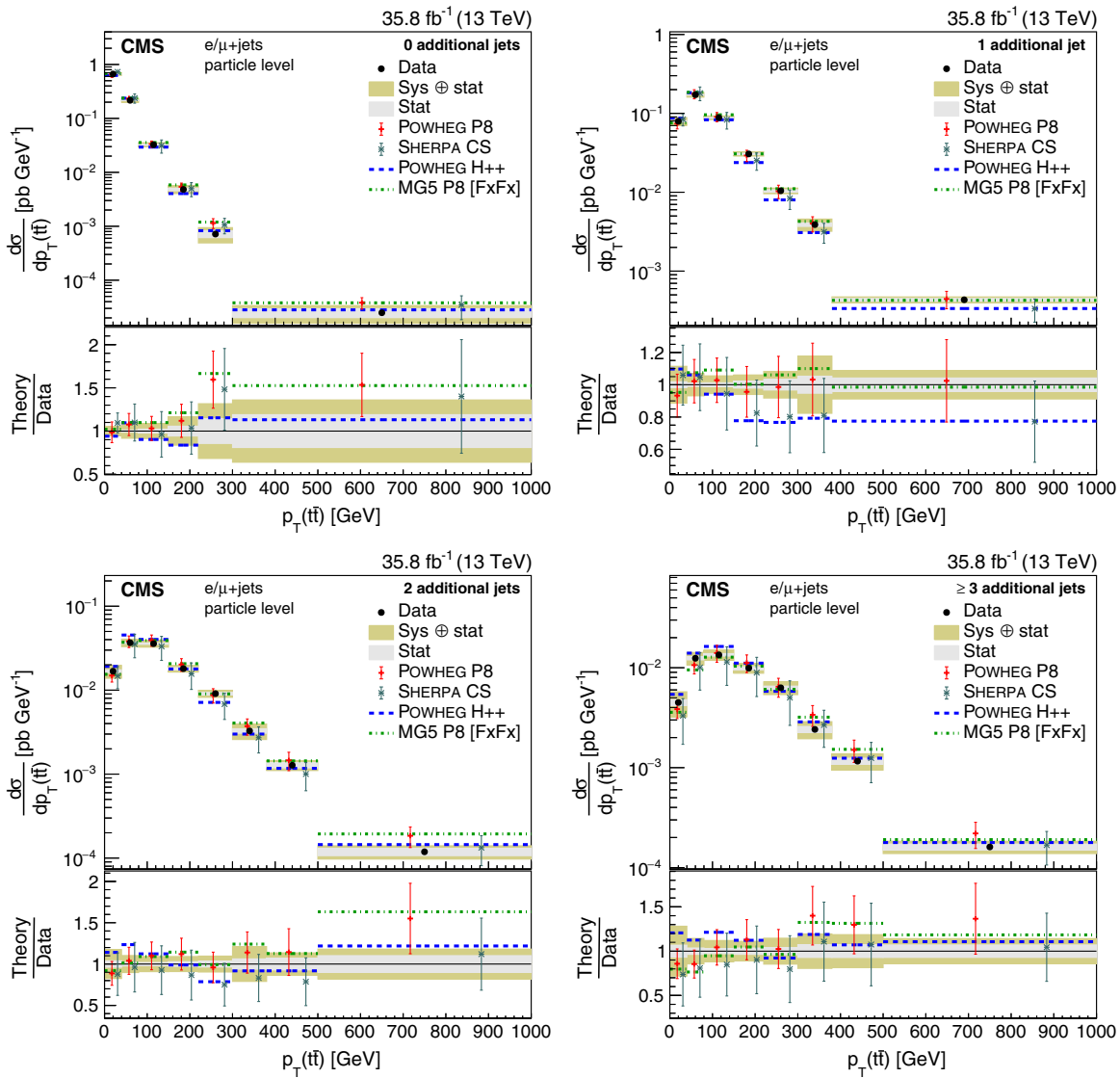


FIG. 34. Differential cross sections at the particle level as a function of $p_T(t\bar{t})$ in bins of the number of additional jets. The data are shown as points with light (dark) bands indicating the statistical (statistical and systematic) uncertainties. The cross sections are compared to the predictions of POWHEG combined with PYTHIA8 (P8) or HERWIG++ (H++) and the multiparton simulations MG5_amc@NLO (MG5)+PYTHIA8 FxFx and SHERPA. The ratios of the various predictions to the measured cross sections are shown at the bottom of each panel.

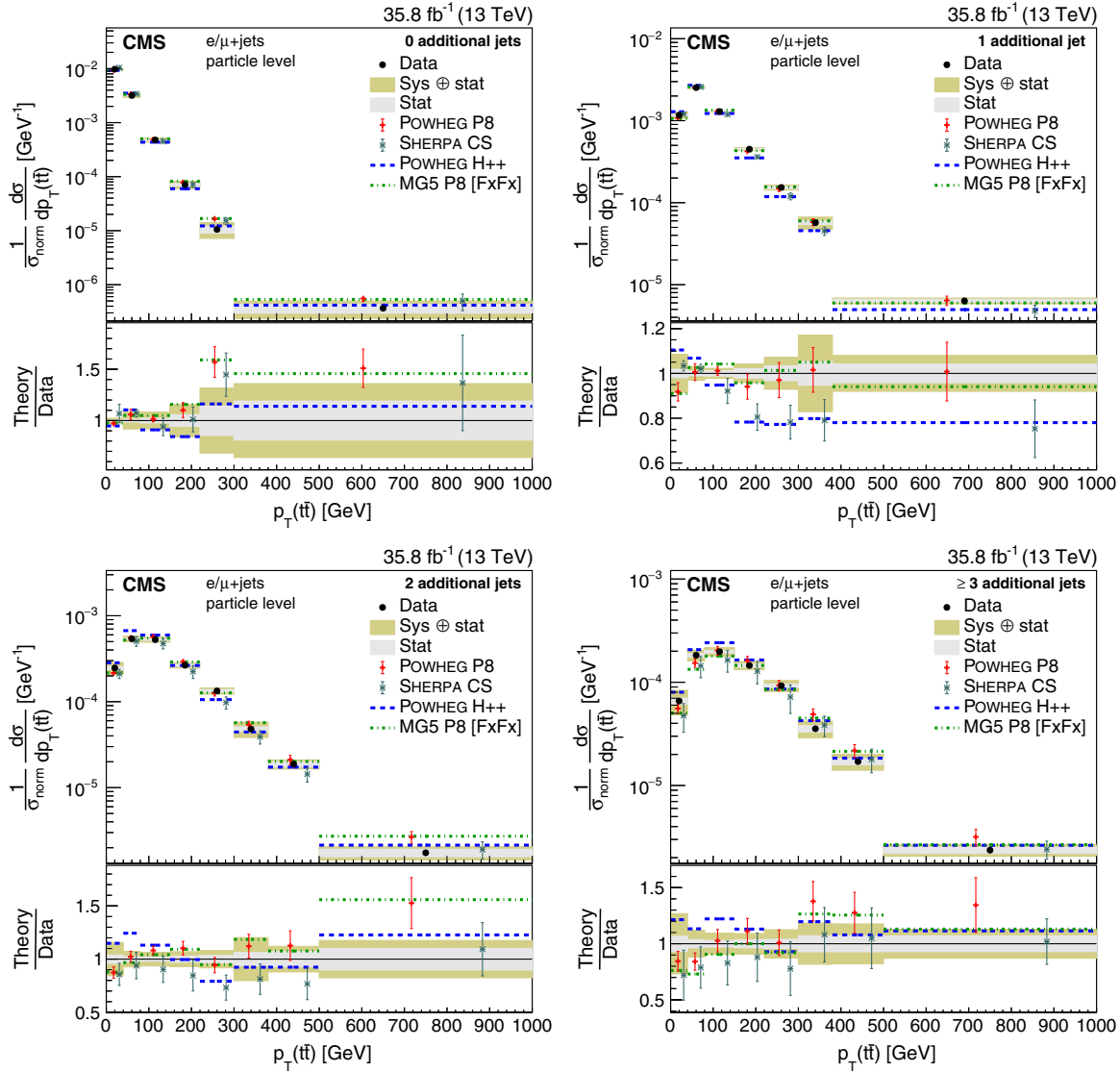


FIG. 35. Differential cross sections at the particle level normalized to the sum of the cross sections σ_{norm} in the measured ranges as a function of $p_T(t\bar{t})$ in bins of the number of additional jets. The data are shown as points with light (dark) bands indicating the statistical (statistical and systematic) uncertainties. The cross sections are compared to the predictions of POWHEG combined with PYTHIA8 (P8) or HERWIG++ (H++) and the multiparton simulations MG5_amc@NLO (MG5)+PYTHIA8 FxFx and SHERPA. The ratios of the various predictions to the measured cross sections are shown at the bottom of each panel.

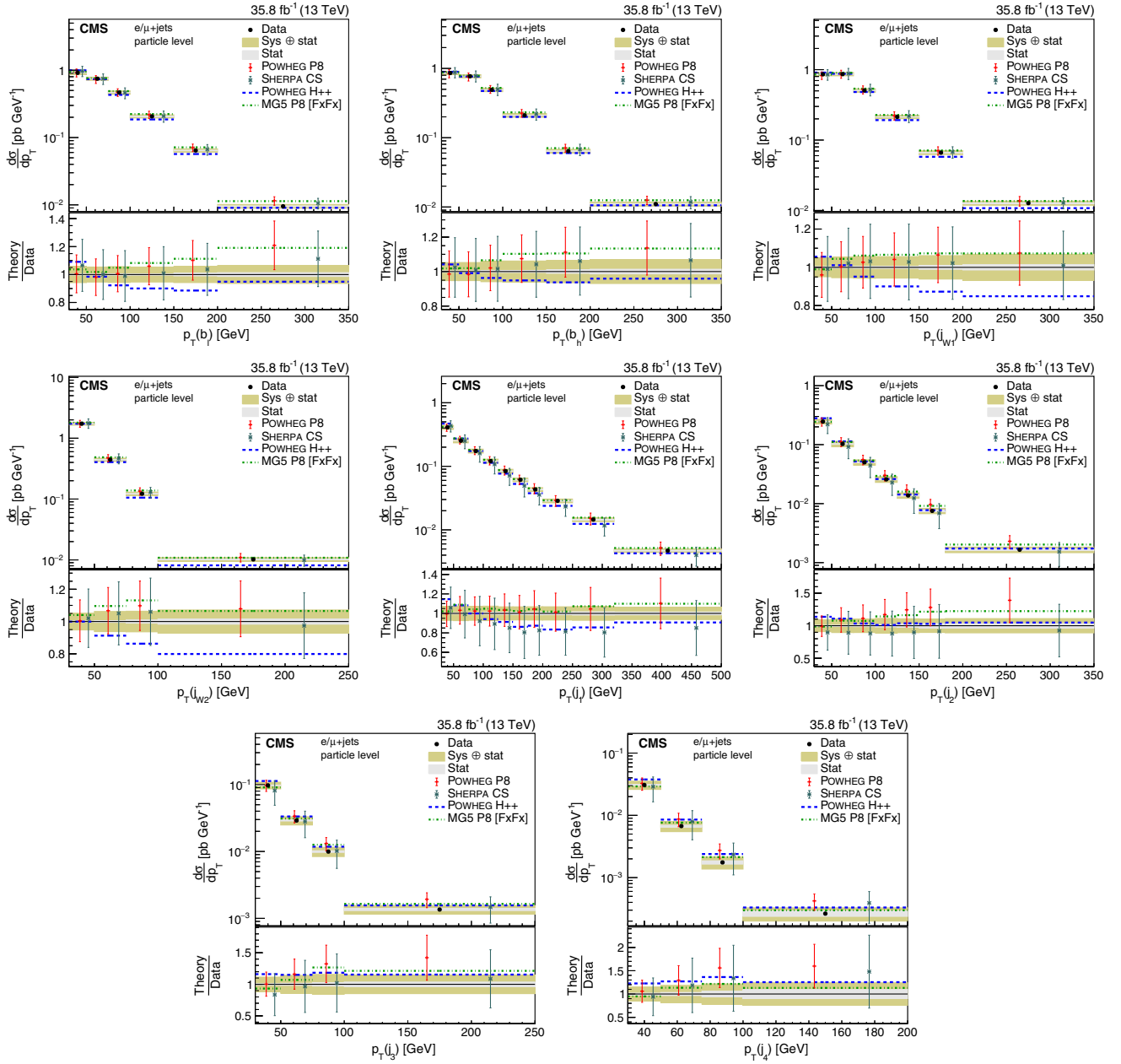


FIG. 36. Differential cross section at the particle level as a function of jet p_T . The upper two rows show the p_T distributions for the jets in the $t\bar{t}$ system, the lower two rows the distribution for additional jets. The data are shown as points with light (dark) bands indicating the statistical (statistical and systematic) uncertainties. The cross sections are compared to the predictions of POWHEG combined with PYTHIA8 (P8) or HERWIG++ (H++) and the multiparton simulations MG5_aMC@NLO (MG5)+PYTHIA8 FxFx and SHERPA. The ratios of the predictions to the measured cross sections are shown at the bottom of each panel.

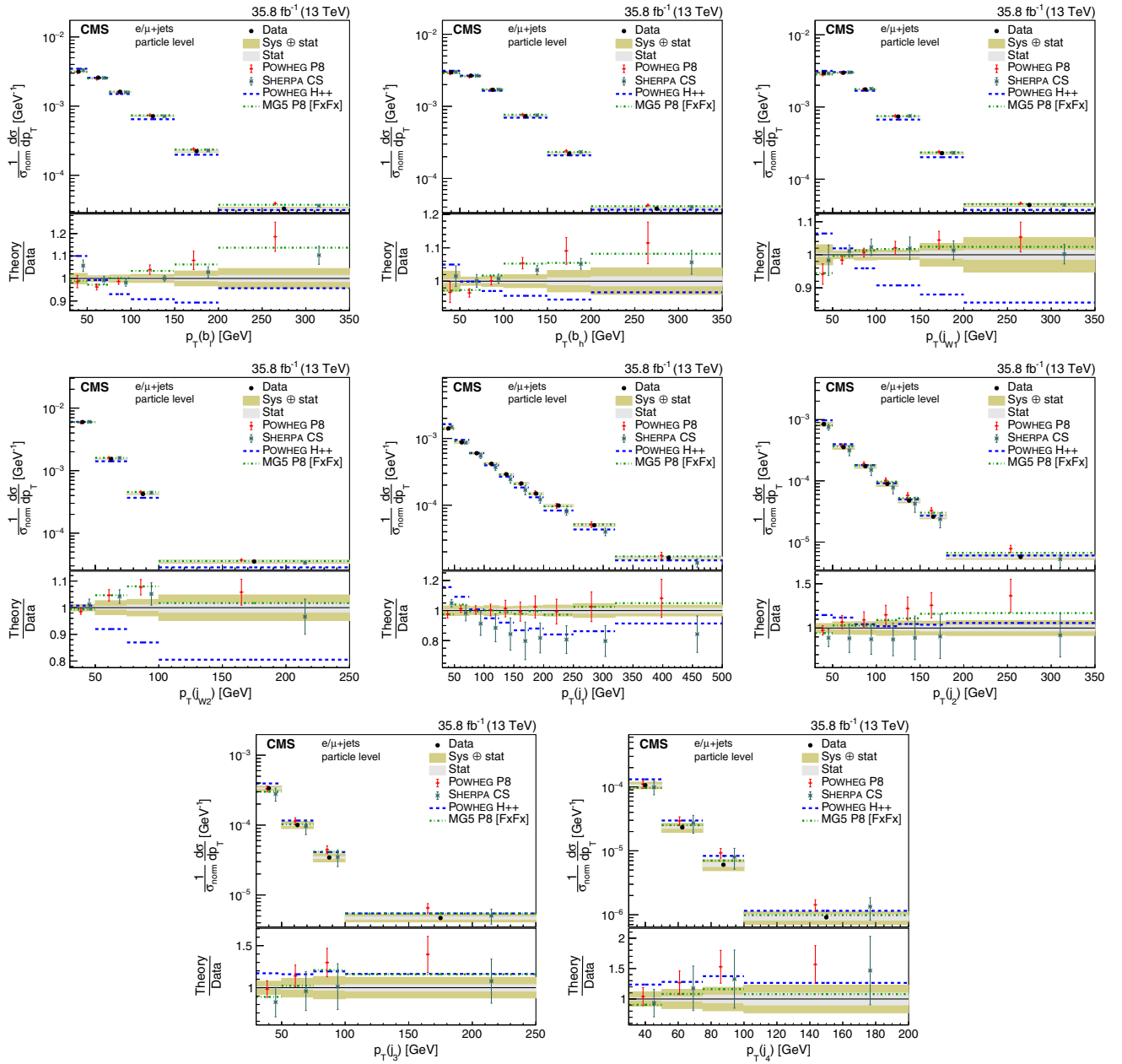


FIG. 37. Normalized differential cross section at the particle level as a function of jet p_T . The upper two rows show the p_T distributions for the jets in the $t\bar{t}$ system, the lower two rows the distribution for additional jets. The data are shown as points with light (dark) bands indicating the statistical (statistical and systematic) uncertainties. The cross sections are compared to the predictions of POWHEG combined with PYTHIA8 (P8) or HERWIG++ (H++) and the multiparton simulations MG5_aMC@NLO (MG5)+PYTHIA8 FxFx and SHERPA. The ratios of the predictions to the measured cross sections are shown at the bottom of each panel.

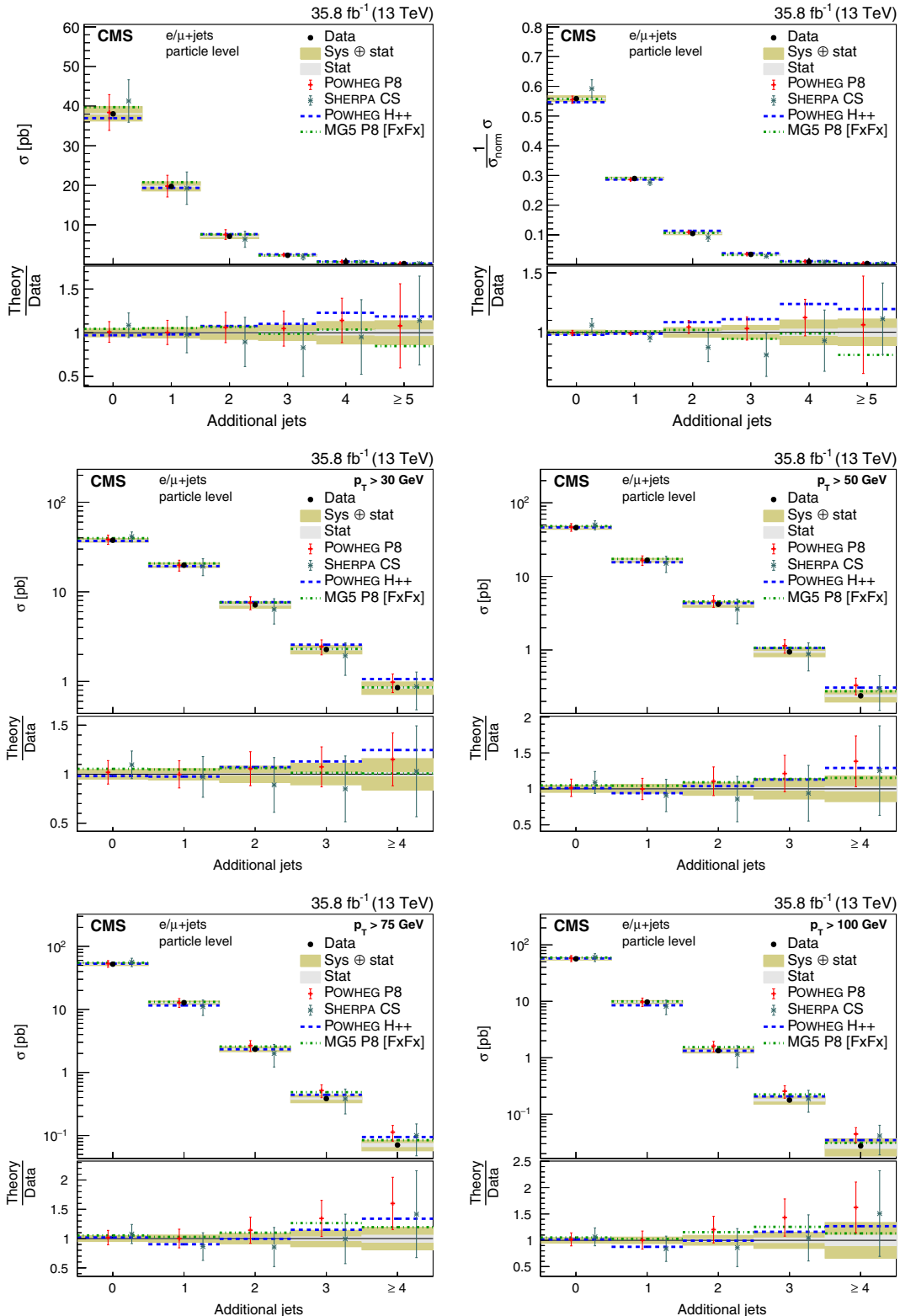


FIG. 38. Upper: absolute (left) and normalized (right) cross sections of jet multiplicities. Middle, lower: absolute cross sections of jet multiplicities for various thresholds of the jet p_T . The data are shown as points with light (dark) bands indicating the statistical (statistical and systematic) uncertainties. The cross sections are compared to the predictions of POWHEG combined with PYTHIA8 (P8) or HERWIG++ (H++) and the multiparton simulations MG5_aMC@NLO (MG5)+PYTHIA8 FxFx and SHERPA. The ratios of the predictions to the measured cross sections are shown at the bottom of each panel.

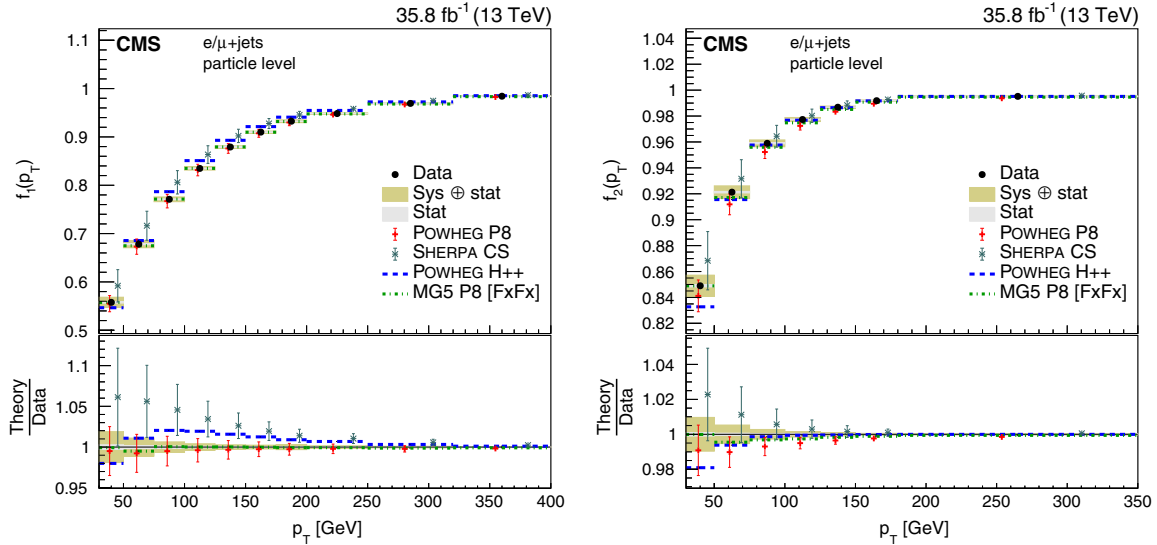


FIG. 39. Distributions of the gap fractions $f_1(p_T)$ and $f_2(p_T)$. The data are shown as points with light (dark) bands indicating the statistical (statistical and systematic) uncertainties. The measurements are compared to the predictions of POWHEG combined with PYTHIA8 (P8) or HERWIG++ (H++) and the multiparton simulations MG5_aMC@NLO (MG5)+PYTHIA8 FxFx and SHERPA. The ratios of the predictions to the measured cross sections are shown at the bottom of each panel.

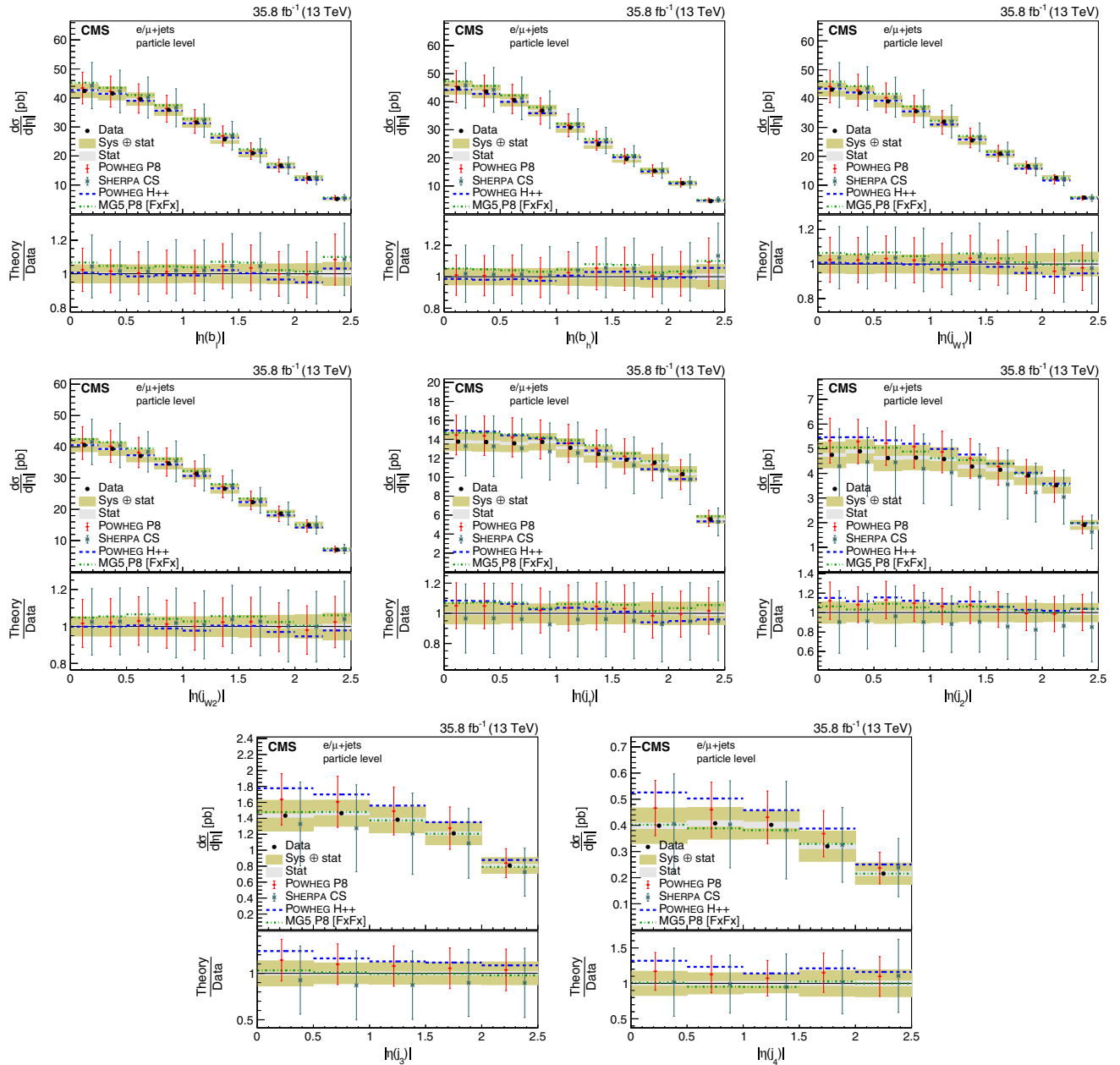


FIG. 40. Differential cross section at the particle level as a function of jet $|\eta|$. The upper two rows show the $|\eta|$ distributions for the jets in the $t\bar{t}$ system, the lower two rows the distributions for additional jets. The data are shown as points with light (dark) bands indicating the statistical (statistical and systematic) uncertainties. The cross sections are compared to the predictions of POWHEG combined with PYTHIA8 (P8) or HERWIG++ (H++) and the multiparton simulations MG5_amc@NLO (MG5)+PYTHIA8 FxFx and SHERPA. The ratios of the predictions to the measured cross sections are shown at the bottom of each panel.

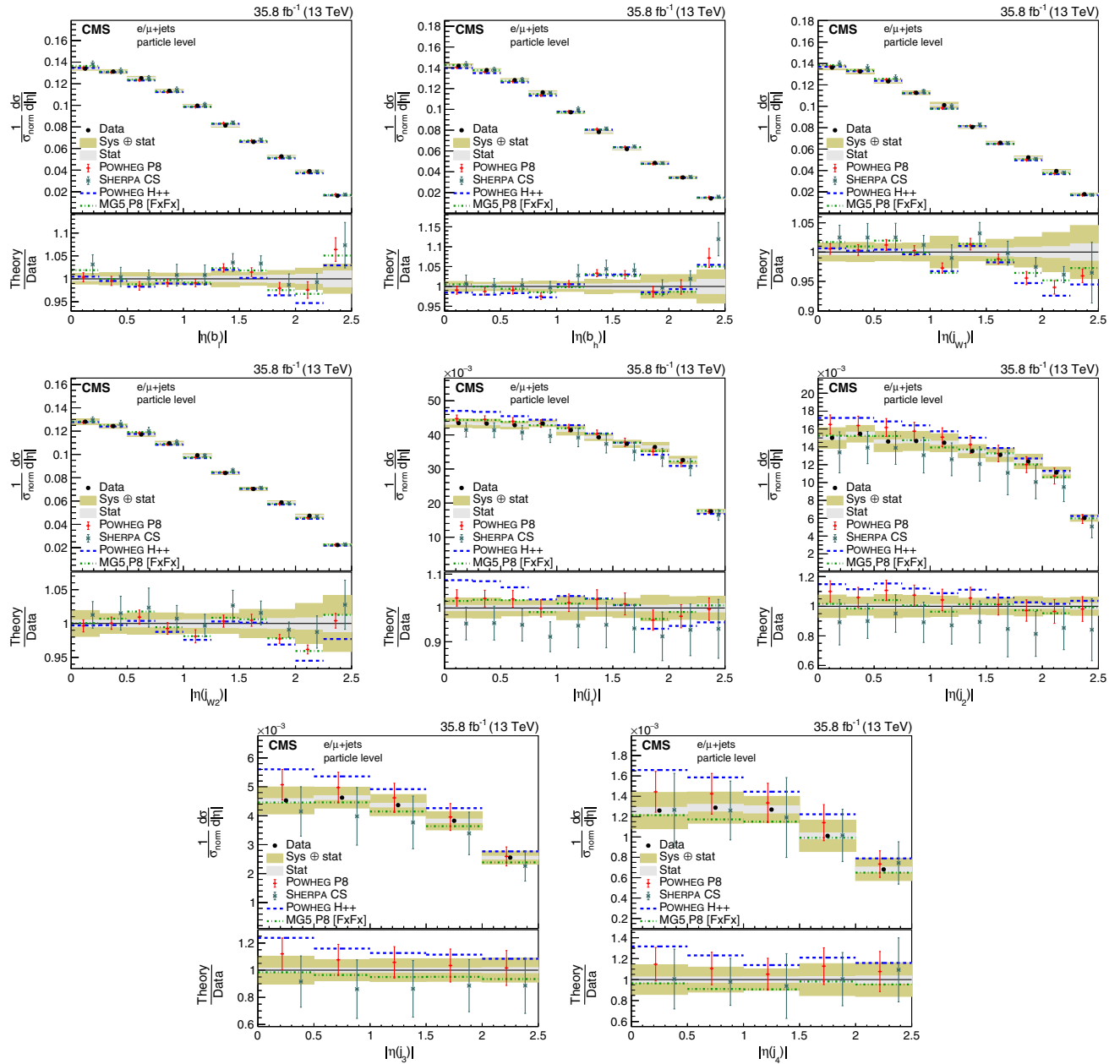


FIG. 41. Normalized differential cross section at the particle level as a function of jet $|\eta|$. The upper two rows show the $|\eta|$ distributions for the jets in the $t\bar{t}$ system, the lower two rows the distributions for additional jets. The data are shown as points with light (dark) bands indicating the statistical (statistical and systematic) uncertainties. The cross sections are compared to the predictions of POWHEG combined with PYTHIA8 (P8) or HERWIG++ (H++) and the multiparton simulations MG5_aMC@NLO (MG5)+PYTHIA8 FxFx and SHERPA. The ratios of the predictions to the measured cross sections are shown at the bottom of each panel.

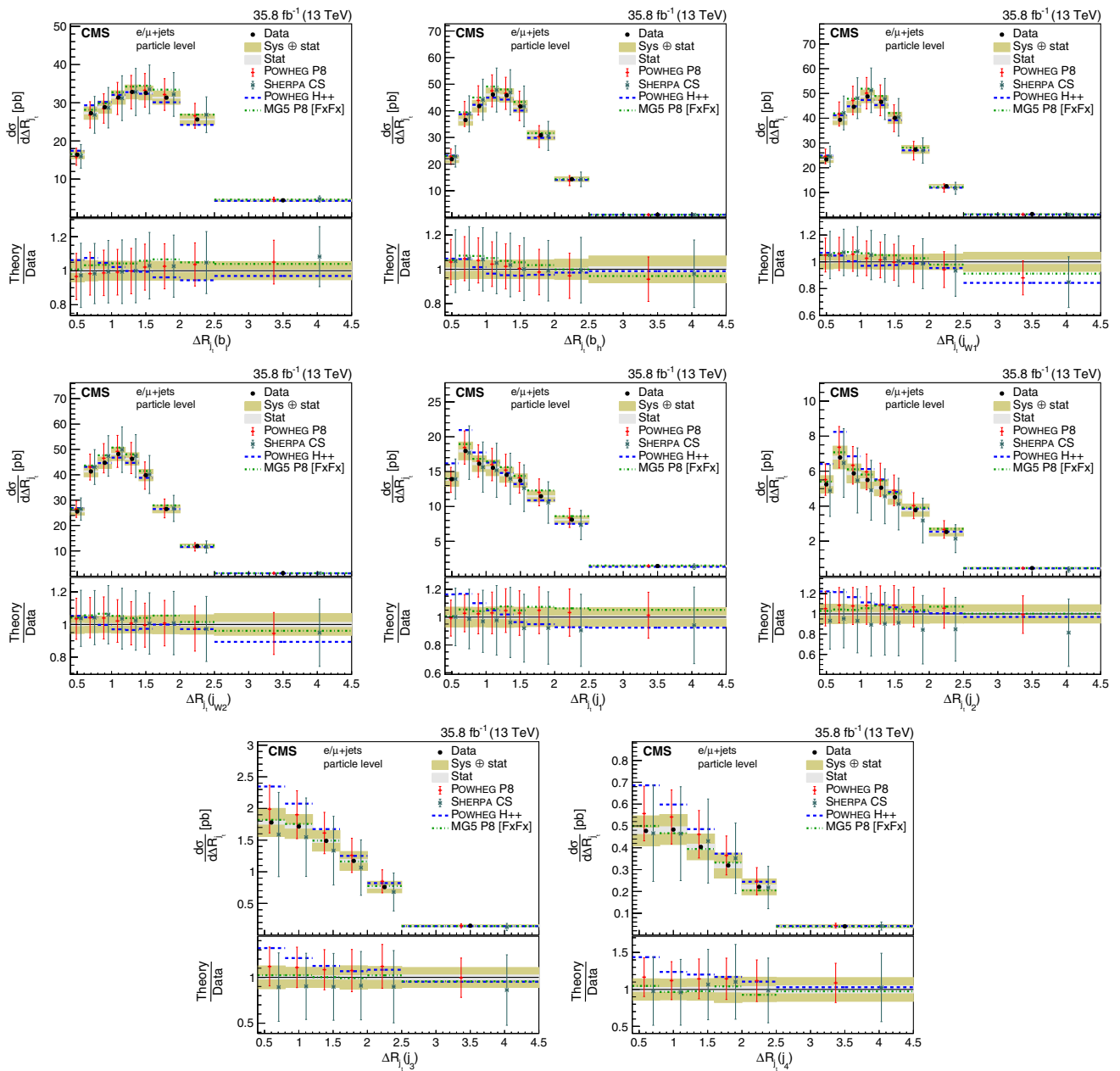


FIG. 42. Differential cross section at the particle level as a function of jet ΔR_{j_i} . The upper two rows show the ΔR_{j_i} distributions for the jets in the $t\bar{t}$ system, the lower two rows the distribution for additional jets. The data are shown as points with light (dark) bands indicating the statistical (statistical and systematic) uncertainties. The cross sections are compared to the predictions of POWHEG combined with PYTHIA8 (P8) or HERWIG++ (H++) and the multiparton simulations MG5_aMC@NLO (MG5)+PYTHIA8 FxFx and SHERPA. The ratios of the predictions to the measured cross sections are shown at the bottom of each panel.

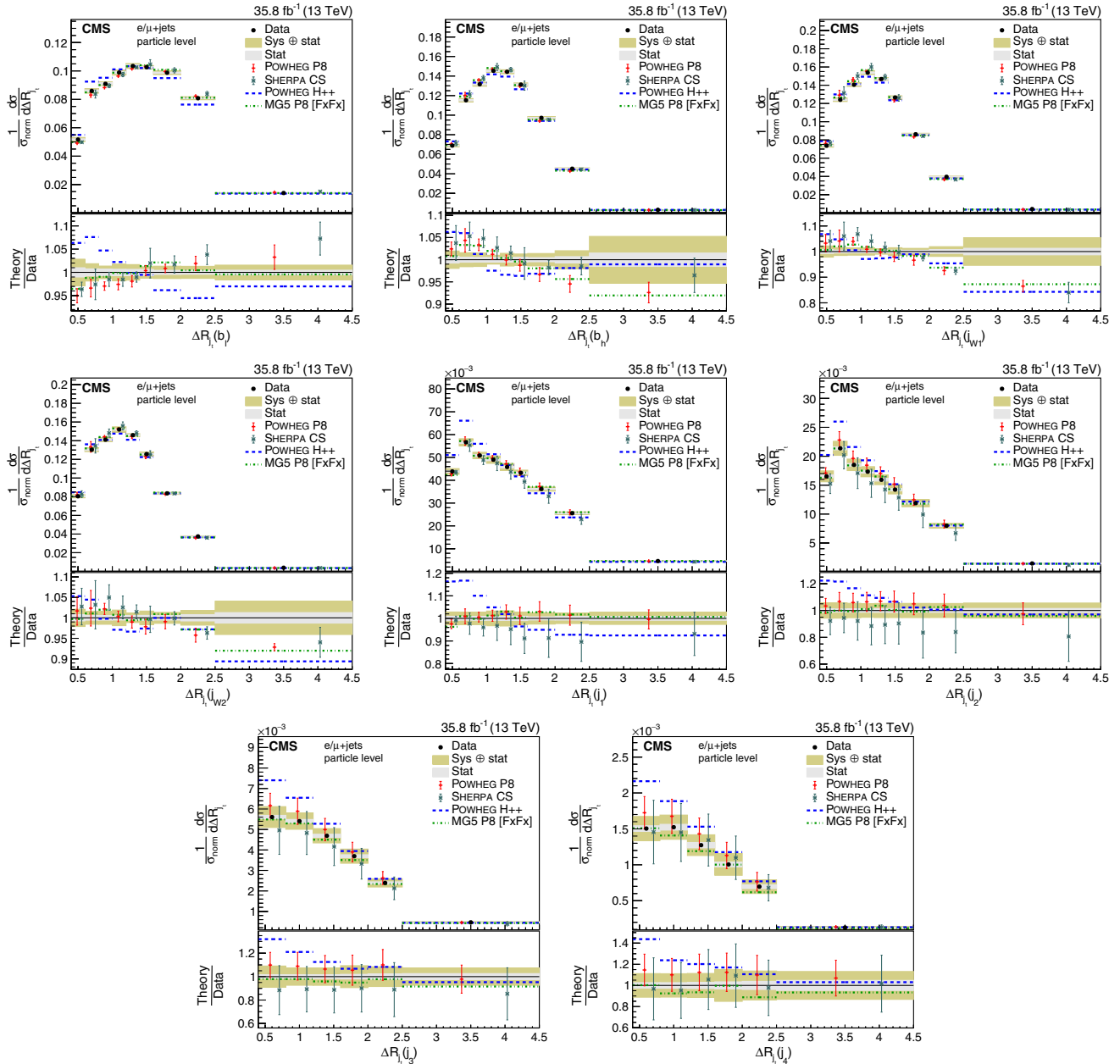


FIG. 43. Normalized differential cross section at the particle level as a function of jet ΔR_{j_i} . The upper two rows show the ΔR_{j_i} distributions for the jets in the $t\bar{t}$ system, the lower two rows the distribution for additional jets. The data are shown as points with light (dark) bands indicating the statistical (statistical and systematic) uncertainties. The cross sections are compared to the predictions of POWHEG combined with PYTHIA8 (P8) or HERWIG++ (H++) and the multiparton simulations MG5_AMC@NLO (MG5)+PYTHIA8 FxFx and SHERPA. The ratios of the predictions to the measured cross sections are shown at the bottom of each panel.

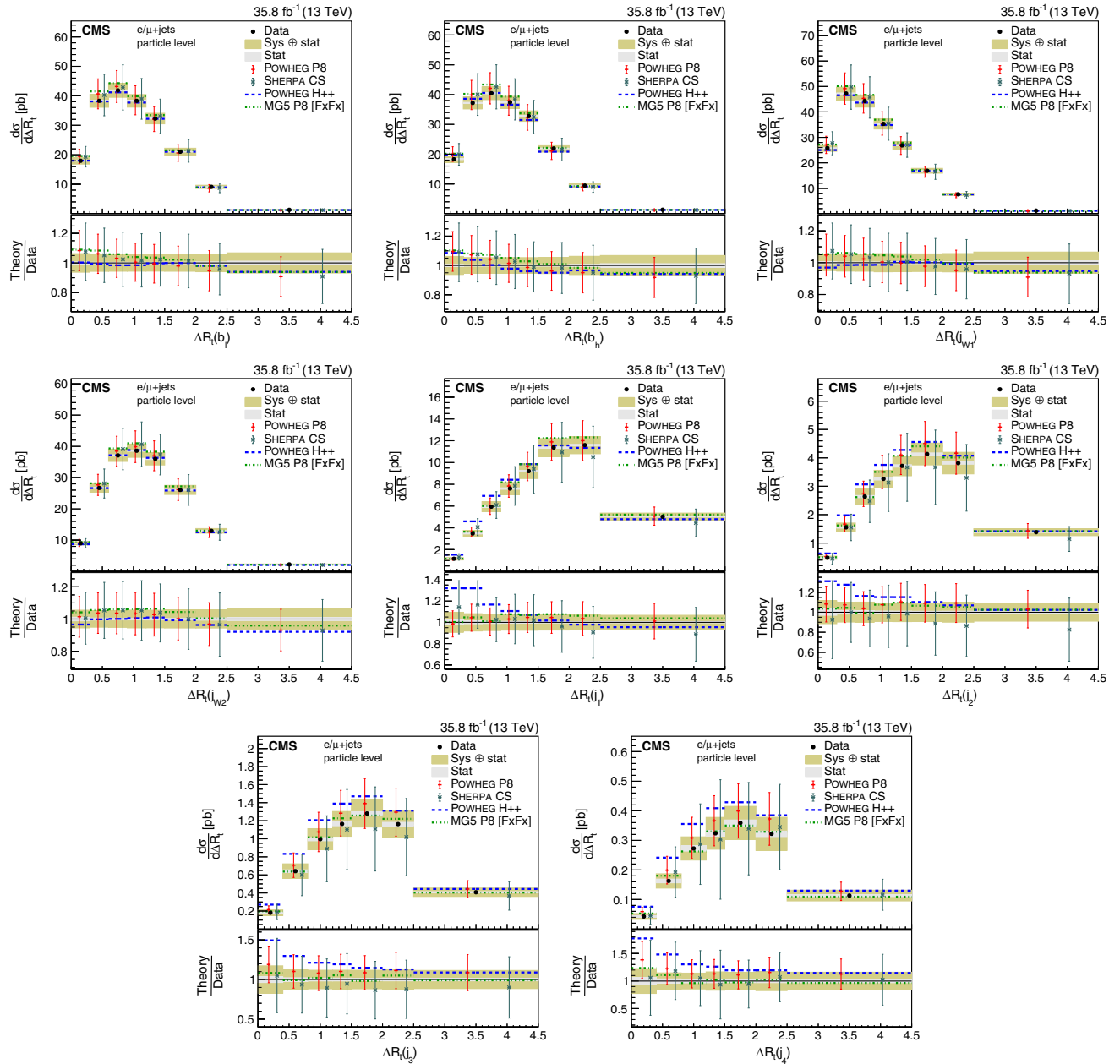


FIG. 44. Differential cross section at the particle level as a function of ΔR_t . The upper two rows show the ΔR_t distributions for the jets in the $t\bar{t}$ system, the lower two rows the distribution for additional jets. The data are shown as points with light (dark) bands indicating the statistical (statistical and systematic) uncertainties. The cross sections are compared to the predictions of POWHEG combined with PYTHIA8 (P8) or HERWIG++ (H++) and the multiparton simulations MG5_aMC@NLO (MG5)+PYTHIA8 FxFx and SHERPA. The ratios of the predictions to the measured cross sections are shown at the bottom of each panel.

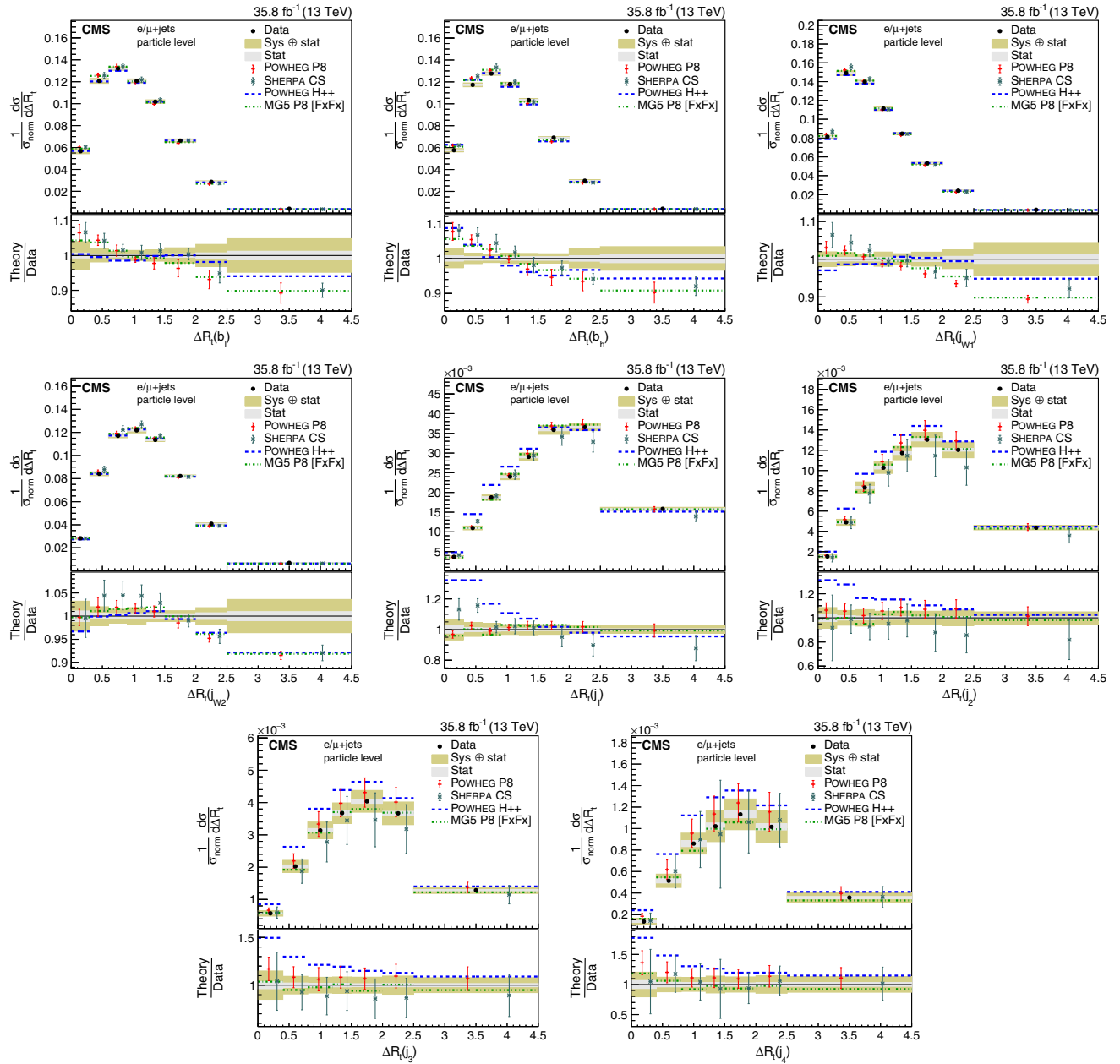


FIG. 45. Normalized differential cross section at the particle level as a function of ΔR_t . The upper two rows show the ΔR_t distributions for the jets in the $t\bar{t}$ system, the lower two rows the distribution for additional jets. The data are shown as points with light (dark) bands indicating the statistical (statistical and systematic) uncertainties. The cross sections are compared to the predictions of POWHEG combined with PYTHIA8 (P8) or HERWIG++ (H++) and the multiparton simulations MG5_aMC@NLO (MG5)+PYTHIA8 FxFx and SHERPA. The ratios of the predictions to the measured cross sections are shown at the bottom of each panel.

TABLE V. Comparison between the absolute measurements involving multiplicities and kinematic properties of jets and the predictions of POWHEG combined with PYTHIA8 (P8) or HERWIG++ (H++) and the multiparton simulations of MG5_AMC@NLO FxFx and SHERPA. The compatibilities with the POWHEG+PYTHIA8 and the SHERPA predictions are also calculated including their theoretical uncertainties (with unc.), while those are not taken into account for the other comparisons. The results of the χ^2 tests are listed, together with the numbers of degrees of freedom (dof) and the corresponding p -values. The rows labeled as “Additional jets” refer to the measurement of the cross section as a function of jet multiplicities for up to five additional jets with $p_T > 30$ GeV (Fig. 38 upper row).

Distribution	χ^2/dof	p -value	χ^2/dof	p -value	χ^2/dof	p -value
POWHEG+P8 with unc.						
Additional jets	1.52/6	0.958	27.3/6	<0.01	10.1/6	0.121
Additional jets vs. $p_T(t_h)$	35.1/44	0.830	64.6/44	0.023	71.6/44	<0.01
Additional jets vs. $M(t\bar{t})$	27.5/36	0.845	68.9/36	<0.01	38.8/36	0.345
Additional jets vs. $p_T(t\bar{t})$	64.6/29	<0.01	181/29	<0.01	175/29	<0.01
$p_T(\text{jet})$	70.2/47	0.016	374/47	<0.01	133/47	<0.01
$ \eta(\text{jet}) $	120/70	<0.01	174/70	<0.01	171/70	<0.01
ΔR_{j_i}	60.9/66	0.655	215/66	<0.01	168/66	<0.01
ΔR_t	64.0/62	0.405	229/62	<0.01	121/62	<0.01
SHERPA						
Additional jets	63.0/6	<0.01	34.1/6	<0.01	11.1/6	0.086
Additional jets vs. $p_T(t_h)$	88.5/44	<0.01	230/44	<0.01	53.4/44	0.156
Additional jets vs. $M(t\bar{t})$	112/36	<0.01	300/36	<0.01	55.1/36	0.022
Additional jets vs. $p_T(t\bar{t})$	285/29	<0.01	223/29	<0.01	122/29	<0.01
$p_T(\text{jet})$	768/47	<0.01	624/47	<0.01	111/47	<0.01
$ \eta(\text{jet}) $	214/70	<0.01	259/70	<0.01	133/70	<0.01
ΔR_{j_i}	334/66	<0.01	959/66	<0.01	67.0/66	0.441
ΔR_t	316/62	<0.01	483/62	<0.01	78.9/62	0.073
POWHEG+H++						
MG5_AMC@NLO+P8 FxFx						

TABLE VI. Comparison between the normalized measurements involving multiplicities and kinematic properties of jets and the predictions of POWHEG combined with PYTHIA8 (P8) or HERWIG++ (H++) and the multiparton simulations of MG5_AMC@NLO FxFx and SHERPA. The compatibilities with the POWHEG+PYTHIA8 and the SHERPA predictions are also calculated including their theoretical uncertainties (with unc.), while those are not taken into account for the other comparisons. The results of the χ^2 tests are listed, together with the numbers of degrees of freedom (dof) and the corresponding p -values. The rows labeled as “Additional jets” refer to the measurement of the cross section as a function of jet multiplicities for up to five additional jets with $p_T > 30$ GeV (Fig. 38 upper row).

Distribution	χ^2/dof	p -value	χ^2/dof	p -value	χ^2/dof	p -value
POWHEG+P8 with unc.						
Additional jets	2.20/5	0.820	26.4/5	<0.01	12.5/5	0.029
Additional jets vs. $p_T(t_h)$	28.6/43	0.955	35.8/43	0.773	69.7/43	<0.01
Additional jets vs. $M(t\bar{t})$	24.5/35	0.908	46.1/35	0.100	38.9/35	0.298
Additional jets vs. $p_T(t\bar{t})$	73.3/28	<0.01	122/28	<0.01	164/28	<0.01
$p_T(\text{jet})$	75.3/46	<0.01	184/46	<0.01	134/46	<0.01
$ \eta(\text{jet}) $	141/69	<0.01	162/69	<0.01	160/69	<0.01
ΔR_{j_i}	69.9/65	0.317	157/65	<0.01	173/65	<0.01
ΔR_t	82.2/61	0.036	163/61	<0.01	126/61	<0.01
SHERPA						
POWHEG+H++						
Additional jets	62.4/5	<0.01	35.4/5	<0.01	9.31/5	0.097
Additional jets vs. $p_T(t_h)$	79.8/43	<0.01	194/43	<0.01	51.4/43	0.178
Additional jets vs. $M(t\bar{t})$	86.3/35	<0.01	287/35	<0.01	48.2/35	0.068
Additional jets vs. $p_T(t\bar{t})$	282/28	<0.01	232/28	<0.01	112/28	<0.01
$p_T(\text{jet})$	692/46	<0.01	623/46	<0.01	112/46	<0.01
$ \eta(\text{jet}) $	213/69	<0.01	255/69	<0.01	121/69	<0.01
ΔR_{j_i}	301/65	<0.01	976/65	<0.01	65.2/65	0.469
ΔR_t	325/61	<0.01	506/61	<0.01	74.7/61	0.112
MG5_AMC@NLO+P8 FxFx						

XII. SUMMARY

Measurements of the absolute and normalized differential and double-differential cross sections for $t\bar{t}$ production in proton-proton collisions at $\sqrt{s} = 13$ TeV have been presented. The data correspond to an integrated luminosity of 35.8 fb^{-1} recorded by the CMS experiment. The $t\bar{t}$ production cross section is measured in the $\ell + \text{jets}$ channels at the parton and particle levels as a function of the transverse momentum p_T and absolute rapidity $|y|$ of the top quarks and p_T , $|y|$, and invariant mass of the $t\bar{t}$ system. In addition, at the particle level detailed studies of multiplicities and kinematic properties of the jets in $t\bar{t}$ events are performed. The dominant sources of uncertainty are the jet energy scale uncertainties on the experimental side and parton shower modeling on the theoretical side.

The results are compared to several standard model predictions that use different methods and approximations for their calculations. The simulations of POWHEG+PYTHIA8 and SHERPA, for which theoretical uncertainties are considered, describe most of the studied kinematic distributions of the top quark and the $t\bar{t}$ system reasonably well. The largest deviation is the measurement of a softer p_T spectrum of the top quarks compared to all the predictions. This has also been observed in other measurements [5–10,13,14,18]. Most of the kinematic distributions and multiplicities of additional jets are modeled reasonably well by POWHEG+PYTHIA8, however, this description of additional jets relies on the phenomenological model of the parton shower with tuned parameters. With the selected settings SHERPA fails to describe most of these distributions. Comparisons of the measurements to the central values of all tested models, ignoring their theoretical uncertainties, result in low p -values for many distributions related to the p_T of the top quarks or the $t\bar{t}$ system, and for the kinematic distributions and multiplicities of additional jets.

ACKNOWLEDGMENTS

We congratulate our colleagues in the CERN accelerator departments for the excellent performance of the LHC and thank the technical and administrative staffs at CERN and at other CMS institutes for their contributions to the success of the CMS effort. In addition, we gratefully acknowledge the computing centers and personnel of the Worldwide LHC Computing Grid for delivering so effectively the computing infrastructure essential to our analyses. Finally, we acknowledge the enduring support for the construction and operation of the LHC and the CMS detector provided by the following funding agencies: the Austrian Federal Ministry of Science, Research and Economy and the Austrian Science Fund; the Belgian Fonds de la Recherche Scientifique, and Fonds voor Wetenschappelijk Onderzoek; the Brazilian Funding Agencies (CNPq, CAPES, FAPERJ, and FAPESP); the

Bulgarian Ministry of Education and Science; CERN; the Chinese Academy of Sciences, Ministry of Science and Technology, and National Natural Science Foundation of China; the Colombian Funding Agency (COLCIENCIAS); the Croatian Ministry of Science, Education and Sport, and the Croatian Science Foundation; the Research Promotion Foundation, Cyprus; the Secretariat for Higher Education, Science, Technology and Innovation, Ecuador; the Ministry of Education and Research, Estonian Research Council via IUT23-4 and IUT23-6 and European Regional Development Fund, Estonia; the Academy of Finland, Finnish Ministry of Education and Culture, and Helsinki Institute of Physics; the Institut National de Physique Nucléaire et de Physique des Particules / CNRS, and Commissariat à l’Énergie Atomique et aux Énergies Alternatives / CEA, France; the Bundesministerium für Bildung und Forschung, Deutsche Forschungsgemeinschaft, and Helmholtz-Gemeinschaft Deutscher Forschungszentren, Germany; the General Secretariat for Research and Technology, Greece; the National Scientific Research Foundation, and National Innovation Office, Hungary; the Department of Atomic Energy and the Department of Science and Technology, India; the Institute for Studies in Theoretical Physics and Mathematics, Iran; the Science Foundation, Ireland; the Istituto Nazionale di Fisica Nucleare, Italy; the Ministry of Science, ICT and Future Planning, and National Research Foundation (NRF), Republic of Korea; the Lithuanian Academy of Sciences; the Ministry of Education, and University of Malaya (Malaysia); the Mexican Funding Agencies (BUAP, CINVESTAV, CONACYT, LNS, SEP, and UASLP-FAI); the Ministry of Business, Innovation and Employment, New Zealand; the Pakistan Atomic Energy Commission; the Ministry of Science and Higher Education and the National Science Centre, Poland; the Fundação para a Ciência e a Tecnologia, Portugal; JINR, Dubna; the Ministry of Education and Science of the Russian Federation, the Federal Agency of Atomic Energy of the Russian Federation, Russian Academy of Sciences, and the Russian Foundation for Basic Research; the Ministry of Education, Science and Technological Development of Serbia; the Secretaría de Estado de Investigación, Desarrollo e Innovación and Programa Consolider-Ingenio 2010, Spain; the Swiss Funding Agencies (ETH Board, ETH Zurich, PSI, SNF, UniZH, Canton Zurich, and SER); the Ministry of Science and Technology, Taipei; the Thailand Center of Excellence in Physics, the Institute for the Promotion of Teaching Science and Technology of Thailand, Special Task Force for Activating Research and the National Science and Technology Development Agency of Thailand; the Scientific and Technical Research Council of Turkey, and Turkish Atomic Energy Authority; the National Academy of Sciences of Ukraine, and State Fund for Fundamental Researches, Ukraine; the Science and

Technology Facilities Council, UK; the US Department of Energy, and the US National Science Foundation. Individuals have received support from the Marie-Curie program and the European Research Council and EPLANET (European Union); the Leventis Foundation; the A. P. Sloan Foundation; the Alexander von Humboldt Foundation; the Belgian Federal Science Policy Office; the Fonds pour la Formation à la Recherche dans l’Industrie et dans l’Agriculture (FRIA-Belgium); the Agentschap voor Innovatie door Wetenschap en Technologie (IWT-Belgium); the Ministry of Education, Youth and Sports (MEYS) of the Czech Republic; the Council of Science and Industrial Research, India; the HOMING PLUS program of the Foundation for Polish Science, cofinanced from

European Union, Regional Development Fund, the Mobility Plus program of the Ministry of Science and Higher Education, the National Science Center (Poland), Contracts Harmonia 2014/14/M/ST2/00428, Opus 2013/11/B/ST2/04202, 2014/13/B/ST2/02543 and 2014/15/B/ST2/03998, Sonata-bis 2012/07/E/ST2/01406; the Thalis and Aristeia programs cofinanced by EU-ESF and the Greek NSRF; the National Priorities Research Program by Qatar National Research Fund; the Programa Clarín-COFUND del Principado de Asturias; the Rachadapisek Sompot Fund for Postdoctoral Fellowship, Chulalongkorn University and the Chulalongkorn Academic into Its 2nd Century Project Advancement Project (Thailand); and the Welch Foundation, Contract No. C-1845.

APPENDIX A: TABLES OF PARTON-LEVEL CROSS SECTIONS

The measured differential cross sections at the parton level as a function of all the measured variables are listed in Tables VII–XVI. The results are shown together with their statistical and systematic uncertainties.

TABLE VII. Differential cross section at the parton level as a function of $p_T(t_{\text{high}})$. The values are shown together with their statistical and systematic uncertainties.

$p_T(t_{\text{high}})$ [GeV]	$\frac{d\sigma}{dp_T(t_{\text{high}})}$ [fb GeV $^{-1}$]	$p_T(t_{\text{high}})$ [GeV]	$\frac{d\sigma}{dp_T(t_{\text{high}})}$ [fb GeV $^{-1}$]
0–40	$333 \pm 8 \pm 31$	240–280	$258 \pm 3 \pm 16$
40–80	$1244 \pm 11 \pm 96$	280–330	$135.0 \pm 1.9 \pm 9.2$
80–120	$1460 \pm 10 \pm 110$	330–380	$67.3 \pm 1.3 \pm 5.2$
120–160	$1213 \pm 9 \pm 94$	380–430	$34.4 \pm 1.0 \pm 3.9$
160–200	$777 \pm 7 \pm 53$	430–500	$15.7 \pm 0.6 \pm 1.5$
200–240	$468 \pm 5 \pm 31$	500–800	$3.16 \pm 0.11 \pm 0.34$

TABLE VIII. Differential cross section at the parton level as a function of $p_T(t_{\text{low}})$. The values are shown together with their statistical and systematic uncertainties.

$p_T(t_{\text{low}})$ [GeV]	$\frac{d\sigma}{dp_T(t_{\text{low}})}$ [fb GeV $^{-1}$]	$p_T(t_{\text{low}})$ [GeV]	$\frac{d\sigma}{dp_T(t_{\text{low}})}$ [fb GeV $^{-1}$]
0–40	$1054 \pm 8 \pm 77$	240–280	$115.4 \pm 1.5 \pm 7.0$
40–80	$1770 \pm 9 \pm 130$	280–330	$54.3 \pm 0.9 \pm 3.7$
80–120	$1420 \pm 8 \pm 110$	330–380	$24.3 \pm 0.6 \pm 1.8$
120–160	$871 \pm 5 \pm 61$	380–430	$11.2 \pm 0.4 \pm 1.1$
160–200	$463 \pm 4 \pm 28$	430–500	$5.34 \pm 0.28 \pm 0.52$
200–240	$232 \pm 2 \pm 16$	500–800	$0.92 \pm 0.08 \pm 0.20$

TABLE IX. Differential cross section at the parton level as a function of $p_T(t_h)$. The values are shown together with their statistical and systematic uncertainties.

$p_T(t_h)$ [GeV]	$\frac{d\sigma}{dp_T(t_h)}$ [fb GeV $^{-1}$]	$p_T(t_h)$ [GeV]	$\frac{d\sigma}{dp_T(t_h)}$ [fb GeV $^{-1}$]
0–40	$687 \pm 7 \pm 50$	240–280	$188 \pm 2 \pm 11$
40–80	$1490 \pm 8 \pm 100$	280–330	$95.6 \pm 1.3 \pm 6.0$
80–120	$1460 \pm 8 \pm 110$	330–380	$47.2 \pm 0.9 \pm 3.4$
120–160	$1022 \pm 6 \pm 79$	380–430	$22.9 \pm 0.6 \pm 1.8$
160–200	$621 \pm 4 \pm 42$	430–500	$10.03 \pm 0.40 \pm 0.95$
200–240	$347 \pm 3 \pm 23$	500–800	$2.15 \pm 0.11 \pm 0.33$

TABLE X. Differential cross section at the parton level as a function of $|y(t_h)|$. The values are shown together with their statistical and systematic uncertainties.

$ y(t_h) $	$\frac{d\sigma}{d y(t_h) }$ [pb]	$ y(t_h) $	$\frac{d\sigma}{d y(t_h) }$ [pb]
0.0–0.2	$145.5 \pm 0.8 \pm 9.4$	1.2–1.4	$93.3 \pm 0.8 \pm 6.6$
0.2–0.4	$144.5 \pm 0.9 \pm 9.5$	1.4–1.6	$78.1 \pm 0.8 \pm 6.6$
0.4–0.6	$137.0 \pm 0.9 \pm 8.7$	1.6–1.8	$66.9 \pm 0.8 \pm 5.4$
0.6–0.8	$129.7 \pm 0.8 \pm 8.8$	1.8–2.0	$53.2 \pm 0.8 \pm 4.8$
0.8–1.0	$117.0 \pm 0.8 \pm 8.1$	2.0–2.5	$32.9 \pm 0.6 \pm 2.9$
1.0–1.2	$106.5 \pm 0.8 \pm 7.8$...

TABLE XI. Differential cross section at the parton level as a function of $p_T(\bar{t}\bar{t})$. The values are shown together with their statistical and systematic uncertainties.

$p_T(\bar{t}\bar{t})$ [GeV]	$\frac{d\sigma}{dp_T(\bar{t}\bar{t})}$ [fb GeV $^{-1}$]	$p_T(\bar{t}\bar{t})$ [GeV]	$\frac{d\sigma}{dp_T(\bar{t}\bar{t})}$ [fb GeV $^{-1}$]
0–40	$2950 \pm 20 \pm 230$	220–300	$78.4 \pm 1.9 \pm 7.8$
40–80	$1470 \pm 20 \pm 110$	300–380	$26.7 \pm 1.1 \pm 2.5$
80–150	$570 \pm 6 \pm 45$	380–500	$10.15 \pm 0.42 \pm 0.93$
150–220	$194 \pm 4 \pm 14$	500–1000	$1.20 \pm 0.05 \pm 0.11$

TABLE XII. Differential cross section at the parton level as a function of $|y(\bar{t}\bar{t})|$. The values are shown together with their statistical and systematic uncertainties.

$ y(\bar{t}\bar{t}) $	$\frac{d\sigma}{d y(\bar{t}\bar{t}) }$ [pb]	$ y(\bar{t}\bar{t}) $	$\frac{d\sigma}{d y(\bar{t}\bar{t}) }$ [pb]
0.0–0.2	$173 \pm 1 \pm 12$	1.0–1.2	$105.2 \pm 1.2 \pm 7.9$
0.2–0.4	$168 \pm 1 \pm 11$	1.2–1.4	$90.2 \pm 1.2 \pm 6.4$
0.4–0.6	$157 \pm 1 \pm 11$	1.4–1.6	$71.2 \pm 1.3 \pm 6.3$
0.6–0.8	$145 \pm 1 \pm 10$	1.6–1.8	$50.7 \pm 1.4 \pm 6.2$
0.8–1.0	$128.1 \pm 1.2 \pm 9.0$	1.8–2.4	$26.4 \pm 1.1 \pm 3.0$

TABLE XIII. Differential cross section at the parton level as a function of $M(\bar{t}\bar{t})$. The values are shown together with their statistical and systematic uncertainties.

$M(\bar{t}\bar{t})$ [GeV]	$\frac{d\sigma}{dM(\bar{t}\bar{t})}$ [fb GeV $^{-1}$]	$M(\bar{t}\bar{t})$ [GeV]	$\frac{d\sigma}{dM(\bar{t}\bar{t})}$ [fb GeV $^{-1}$]
300–360	$247 \pm 8 \pm 57$	680–800	$125 \pm 2 \pm 10$
360–430	$1081 \pm 9 \pm 92$	800–1000	$47.7 \pm 0.9 \pm 3.5$
430–500	$791 \pm 8 \pm 70$	1000–1200	$16.3 \pm 0.6 \pm 1.3$
500–580	$485 \pm 6 \pm 32$	1200–1500	$4.85 \pm 0.27 \pm 0.56$
580–680	$261 \pm 4 \pm 20$	1500–2500	$0.62 \pm 0.05 \pm 0.12$

TABLE XIV. Double-differential cross section at the parton level as a function of $|y(t_h)|$ vs. $p_T(t_h)$. The values are shown together with their statistical and systematic uncertainties.

$p_T(t_h)$ [GeV]	$\frac{d^2\sigma}{dp_T(t_h)dy(t_h)} [\text{pb GeV}^{-1}]$	$p_T(t_h)$ [GeV]	$\frac{d^2\sigma}{dp_T(t_h)dy(t_h)} [\text{pb GeV}^{-1}]$
$0 < y(t_h) < 0.5$			
0–40	$0.382 \pm 0.004 \pm 0.026$	240–280	$0.1276 \pm 0.0017 \pm 0.0075$
40–80	$0.850 \pm 0.006 \pm 0.058$	280–330	$0.0669 \pm 0.0011 \pm 0.0041$
80–120	$0.860 \pm 0.006 \pm 0.060$	330–380	$0.0343 \pm 0.0008 \pm 0.0024$
120–160	$0.622 \pm 0.005 \pm 0.043$	380–450	$0.0150 \pm 0.0005 \pm 0.0014$
160–200	$0.394 \pm 0.003 \pm 0.027$	450–800	$(2.59 \pm 0.12 \pm 0.28) \times 10^{-3}$
200–240	$0.225 \pm 0.002 \pm 0.015$...
$0.5 < y(t_h) < 1$			
0–40	$0.337 \pm 0.004 \pm 0.027$	240–280	$0.1060 \pm 0.0016 \pm 0.0068$
40–80	$0.759 \pm 0.006 \pm 0.054$	280–330	$0.0562 \pm 0.0010 \pm 0.0035$
80–120	$0.766 \pm 0.005 \pm 0.056$	330–380	$0.0287 \pm 0.0007 \pm 0.0024$
120–160	$0.548 \pm 0.004 \pm 0.044$	380–450	$0.0131 \pm 0.0005 \pm 0.0015$
160–200	$0.334 \pm 0.003 \pm 0.024$	450–800	$(1.77 \pm 0.10 \pm 0.20) \times 10^{-3}$
200–240	$0.191 \pm 0.002 \pm 0.014$...
$1 < y(t_h) < 1.5$			
0–40	$0.269 \pm 0.004 \pm 0.022$	240–280	$0.0770 \pm 0.0014 \pm 0.0061$
40–80	$0.603 \pm 0.006 \pm 0.046$	280–330	$0.0382 \pm 0.0009 \pm 0.0029$
80–120	$0.583 \pm 0.005 \pm 0.046$	330–380	$0.0176 \pm 0.0006 \pm 0.0014$
120–160	$0.414 \pm 0.004 \pm 0.035$	380–450	$(7.63 \pm 0.35 \pm 0.79) \times 10^{-3}$
160–200	$0.252 \pm 0.003 \pm 0.018$	450–800	$(1.17 \pm 0.08 \pm 0.21) \times 10^{-3}$
200–240	$0.143 \pm 0.002 \pm 0.011$...
$1.5 < y(t_h) < 2.5$			
0–40	$0.150 \pm 0.003 \pm 0.015$	240–280	$0.0299 \pm 0.0008 \pm 0.0032$
40–80	$0.318 \pm 0.004 \pm 0.026$	280–330	$0.0144 \pm 0.0005 \pm 0.0015$
80–120	$0.309 \pm 0.004 \pm 0.028$	330–380	$(5.99 \pm 0.29 \pm 1.00) \times 10^{-3}$
120–160	$0.214 \pm 0.003 \pm 0.022$	380–450	$(2.35 \pm 0.16 \pm 0.42) \times 10^{-3}$
160–200	$0.119 \pm 0.002 \pm 0.011$	450–800	$(2.63 \pm 0.31 \pm 0.51) \times 10^{-4}$
200–240	$0.0596 \pm 0.0012 \pm 0.0054$...

TABLE XV. Double-differential cross section at the parton level as a function of $M(t\bar{t})$ vs. $|y(t\bar{t})|$. The values are shown together with their statistical and systematic uncertainties.

$ y(t\bar{t}) $	$\frac{d^2\sigma}{dM(t\bar{t})dy(t\bar{t})} [\text{fb GeV}^{-1}]$	$ y(t\bar{t}) $	$\frac{d^2\sigma}{dM(t\bar{t})dy(t\bar{t})} [\text{fb GeV}^{-1}]$
$300 < M(t\bar{t}) < 450$			
0.0–0.2	$473 \pm 4 \pm 31$	1.0–1.2	$323 \pm 4 \pm 23$
0.2–0.4	$460 \pm 4 \pm 30$	1.2–1.4	$282 \pm 4 \pm 21$
0.4–0.6	$441 \pm 4 \pm 29$	1.4–1.6	$238 \pm 4 \pm 19$
0.6–0.8	$420 \pm 4 \pm 29$	1.6–2.4	$128 \pm 3 \pm 13$
0.8–1.0	$379 \pm 4 \pm 27$...
$450 < M(t\bar{t}) < 625$			
0.0–0.2	$379 \pm 3 \pm 27$	1.0–1.2	$229 \pm 3 \pm 20$
0.2–0.4	$368 \pm 3 \pm 26$	1.2–1.4	$194 \pm 3 \pm 17$
0.4–0.6	$344 \pm 3 \pm 26$	1.4–1.6	$151 \pm 3 \pm 16$
0.6–0.8	$310 \pm 3 \pm 26$	1.6–2.4	$60.3 \pm 1.8 \pm 8.3$
0.8–1.0	$275 \pm 3 \pm 22$...
$625 < M(t\bar{t}) < 850$			
0.0–0.2	$113.6 \pm 1.6 \pm 9.5$	1.0–1.2	$58.8 \pm 1.5 \pm 5.6$
0.2–0.4	$108.2 \pm 1.5 \pm 7.4$	1.2–1.4	$43.7 \pm 1.5 \pm 4.2$
0.4–0.6	$99.9 \pm 1.6 \pm 8.6$	1.4–1.6	$30.0 \pm 1.6 \pm 3.3$

(Table continued)

TABLE XV. (*Continued*)

$ y(t\bar{t}) $	$\frac{d^2\sigma}{dM(t\bar{t})dy(t\bar{t})}$ [fb GeV $^{-1}$]	$ y(t\bar{t}) $	$\frac{d^2\sigma}{dM(t\bar{t})dy(t\bar{t})}$ [fb GeV $^{-1}$]
0.6–0.8	$88.9 \pm 1.6 \pm 7.3$	1.6–2.4	$9.6 \pm 0.7 \pm 1.3$
0.8–1.0	$75.7 \pm 1.6 \pm 5.7$...	
$850 < M(t\bar{t}) < 2000$			
0.0–0.2	$9.21 \pm 0.21 \pm 0.77$	0.8–1.0	$5.00 \pm 0.22 \pm 0.54$
0.2–0.4	$9.36 \pm 0.23 \pm 0.85$	1.0–1.2	$4.27 \pm 0.24 \pm 0.45$
0.4–0.6	$8.39 \pm 0.23 \pm 0.74$	1.2–1.4	$2.71 \pm 0.22 \pm 0.58$
0.6–0.8	$6.94 \pm 0.23 \pm 0.59$	1.4–2.4	$0.433 \pm 0.057 \pm 0.091$

TABLE XVI. Double-differential cross section at the parton level as a function of $p_T(t_h)$ vs. $M(t\bar{t})$. The values are shown together with their statistical and systematic uncertainties.

$M(t\bar{t})$ [GeV]	$\frac{d^2\sigma}{dp_T(t_h)dM(t\bar{t})}$ [fb GeV $^{-2}$]	$M(t\bar{t})$ [GeV]	$\frac{d^2\sigma}{dp_T(t_h)dM(t\bar{t})}$ [fb GeV $^{-2}$]
$0 < p_T(t_h) < 90$			
300–360	$2.30 \pm 0.04 \pm 0.42$	580–680	$0.652 \pm 0.015 \pm 0.059$
360–430	$8.07 \pm 0.05 \pm 0.61$	680–800	$0.279 \pm 0.009 \pm 0.036$
430–500	$2.98 \pm 0.04 \pm 0.37$	800–1000	$0.096 \pm 0.005 \pm 0.019$
500–580	$1.37 \pm 0.02 \pm 0.13$	1000–2000	$0.0113 \pm 0.0014 \pm 0.0033$
$90 < p_T(t_h) < 180$			
300–360	$0.184 \pm 0.007 \pm 0.031$	580–680	$1.144 \pm 0.017 \pm 0.097$
360–430	$3.89 \pm 0.04 \pm 0.29$	680–800	$0.489 \pm 0.011 \pm 0.056$
430–500	$5.23 \pm 0.04 \pm 0.44$	800–1000	$0.172 \pm 0.006 \pm 0.019$
500–580	$2.59 \pm 0.03 \pm 0.21$	1000–2000	$0.0169 \pm 0.0012 \pm 0.0039$
$180 < p_T(t_h) < 270$			
300–430	$0.105 \pm 0.005 \pm 0.029$	680–800	$0.387 \pm 0.008 \pm 0.033$
430–500	$0.573 \pm 0.014 \pm 0.040$	800–1000	$0.134 \pm 0.004 \pm 0.013$
500–580	$1.330 \pm 0.018 \pm 0.096$	1000–1200	$0.0437 \pm 0.0027 \pm 0.0066$
580–680	$0.937 \pm 0.013 \pm 0.075$	1200–2000	$(5.2 \pm 0.6 \pm 1.6) \times 10^{-3}$
$270 < p_T(t_h) < 800$			
300–430	$(3.1 \pm 0.4 \pm 1.1) \times 10^{-3}$	680–800	$0.0464 \pm 0.0010 \pm 0.0033$
430–500	$0.0141 \pm 0.0009 \pm 0.0022$	800–1000	$0.0259 \pm 0.0005 \pm 0.0020$
500–580	$0.0196 \pm 0.0009 \pm 0.0032$	1000–1200	$0.01027 \pm 0.00038 \pm 0.00097$
580–680	$0.0359 \pm 0.0011 \pm 0.0034$	1200–2000	$(2.02 \pm 0.08 \pm 0.21) \times 10^{-3}$

APPENDIX B: TABLES OF PARTICLE-LEVEL CROSS SECTIONS

The measured differential cross sections at the particle level as a function of all the measured variables are listed in Tables XVII–XXXIV. The results are shown together with their statistical and systematic uncertainties.

TABLE XVII. Differential cross section at the particle level as a function of $p_T(t_h)$. The values are shown together with their statistical and systematic uncertainties.

$p_T(t_h)$ [GeV]	$\frac{d\sigma}{dp_T(t_h)}$ [fb GeV $^{-1}$]	$p_T(t_h)$ [GeV]	$\frac{d\sigma}{dp_T(t_h)}$ [fb GeV $^{-1}$]
0–40	$163.5 \pm 1.3 \pm 8.9$	240–280	$70.0 \pm 0.7 \pm 4.0$
40–80	$376 \pm 2 \pm 20$	280–330	$39.1 \pm 0.5 \pm 2.5$
80–120	$391 \pm 2 \pm 23$	330–380	$20.4 \pm 0.3 \pm 1.3$
120–160	$295 \pm 2 \pm 17$	380–430	$10.37 \pm 0.24 \pm 0.75$
160–200	$192 \pm 1 \pm 11$	430–500	$4.64 \pm 0.15 \pm 0.38$
200–240	$116.5 \pm 0.9 \pm 6.7$	500–800	$0.81 \pm 0.03 \pm 0.11$

TABLE XVIII. Differential cross section at the particle level as a function of $|y(t_h)|$. The values are shown together with their statistical and systematic uncertainties.

$ y(t_h) $	$\frac{d\sigma}{dy(t_h)} [\text{pb}]$	$ y(t_h) $	$\frac{d\sigma}{dy(t_h)} [\text{pb}]$
0.0–0.2	$52.8 \pm 0.2 \pm 2.8$	1.2–1.4	$27.1 \pm 0.2 \pm 1.6$
0.2–0.4	$51.6 \pm 0.2 \pm 2.7$	1.4–1.6	$19.9 \pm 0.2 \pm 1.4$
0.4–0.6	$48.2 \pm 0.2 \pm 2.6$	1.6–1.8	$13.08 \pm 0.13 \pm 0.90$
0.6–0.8	$44.9 \pm 0.2 \pm 2.4$	1.8–2.0	$6.79 \pm 0.10 \pm 0.50$
0.8–1.0	$39.1 \pm 0.2 \pm 2.2$	2.0–2.5	$1.009 \pm 0.024 \pm 0.084$
1.0–1.2	$33.8 \pm 0.2 \pm 1.9$...	

TABLE XIX. Differential cross section at the particle level as a function of $p_T(t_\ell)$. The values are shown together with their statistical and systematic uncertainties.

$p_T(t_\ell) [\text{GeV}]$	$\frac{d\sigma}{dp_T(t_\ell)} [\text{fb GeV}^{-1}]$	$p_T(t_\ell) [\text{GeV}]$	$\frac{d\sigma}{dp_T(t_\ell)} [\text{fb GeV}^{-1}]$
0–40	$151.1 \pm 2.4 \pm 9.9$	240–280	$75.5 \pm 1.6 \pm 6.0$
40–80	$357 \pm 4 \pm 21$	280–330	$43.2 \pm 1.0 \pm 2.8$
80–120	$368 \pm 4 \pm 22$	330–380	$22.1 \pm 0.7 \pm 2.3$
120–160	$316 \pm 3 \pm 18$	380–430	$11.1 \pm 0.6 \pm 1.7$
160–200	$195 \pm 3 \pm 12$	430–500	$5.78 \pm 0.29 \pm 0.71$
200–240	$132.1 \pm 2.0 \pm 8.1$	500–800	$0.97 \pm 0.04 \pm 0.10$

TABLE XX. Differential cross section at the particle level as a function of $|y(t_\ell)|$. The values are shown together with their statistical and systematic uncertainties.

$ y(t_\ell) $	$\frac{d\sigma}{dy(t_\ell)} [\text{pb}]$	$ y(t_\ell) $	$\frac{d\sigma}{dy(t_\ell)} [\text{pb}]$
0.0–0.2	$49.9 \pm 0.5 \pm 2.9$	1.2–1.4	$28.0 \pm 0.5 \pm 2.0$
0.2–0.4	$48.7 \pm 0.6 \pm 2.7$	1.4–1.6	$19.2 \pm 0.4 \pm 1.6$
0.4–0.6	$47.6 \pm 0.6 \pm 2.6$	1.6–1.8	$14.6 \pm 0.4 \pm 1.2$
0.6–0.8	$44.2 \pm 0.6 \pm 2.6$	1.8–2.0	$8.75 \pm 0.31 \pm 0.98$
0.8–1.0	$39.0 \pm 0.6 \pm 2.4$	2.0–2.5	$2.34 \pm 0.10 \pm 0.27$
1.0–1.2	$33.9 \pm 0.5 \pm 2.0$...	

TABLE XXI. Differential cross section at the particle level as a function of $p_T(t\bar{t})$. The values are shown together with their statistical and systematic uncertainties.

$p_T(t\bar{t}) [\text{GeV}]$	$\frac{d\sigma}{dp_T(t\bar{t})} [\text{fb GeV}^{-1}]$	$p_T(t\bar{t}) [\text{GeV}]$	$\frac{d\sigma}{dp_T(t\bar{t})} [\text{fb GeV}^{-1}]$
0–40	$768 \pm 3 \pm 45$	220–300	$26.4 \pm 0.5 \pm 1.9$
40–80	$436 \pm 4 \pm 25$	300–380	$9.59 \pm 0.33 \pm 0.82$
80–150	$172 \pm 1 \pm 11$	380–500	$3.96 \pm 0.14 \pm 0.30$
150–220	$63.1 \pm 0.9 \pm 3.9$	500–1000	$0.447 \pm 0.017 \pm 0.035$

TABLE XXII. Differential cross section at the particle level as a function of $|y(t\bar{t})|$. The values are shown together with their statistical and systematic uncertainties.

$ y(t\bar{t}) $	$\frac{d\sigma}{dy(t\bar{t})} [\text{pb}]$	$ y(t\bar{t}) $	$\frac{d\sigma}{dy(t\bar{t})} [\text{pb}]$
0.0–0.2	$67.0 \pm 0.3 \pm 3.6$	1.0–1.2	$27.8 \pm 0.3 \pm 1.7$
0.2–0.4	$63.4 \pm 0.4 \pm 3.4$	1.2–1.4	$19.0 \pm 0.2 \pm 1.2$
0.4–0.6	$57.0 \pm 0.4 \pm 3.2$	1.4–1.6	$10.59 \pm 0.18 \pm 0.76$
0.6–0.8	$49.1 \pm 0.3 \pm 2.8$	1.6–1.8	$4.57 \pm 0.12 \pm 0.51$
0.8–1.0	$39.2 \pm 0.3 \pm 2.2$	1.8–2.4	$0.643 \pm 0.030 \pm 0.082$

TABLE XXIII. Differential cross section at the particle level as a function of $M(t\bar{t})$. The values are shown together with their statistical and systematic uncertainties.

$M(t\bar{t})$ [GeV]	$\frac{d\sigma}{dM(t\bar{t})}$ [fb GeV $^{-1}$]	$M(t\bar{t})$ [GeV]	$\frac{d\sigma}{dM(t\bar{t})}$ [fb GeV $^{-1}$]
300–360	$76.2 \pm 1.1 \pm 8.6$	680–800	$55.1 \pm 0.6 \pm 3.3$
360–430	$200 \pm 1 \pm 12$	800–1000	$24.6 \pm 0.3 \pm 1.5$
430–500	$191 \pm 1 \pm 13$	1000–1200	$8.91 \pm 0.21 \pm 0.65$
500–580	$147.1 \pm 1.0 \pm 8.3$	1200–1500	$3.03 \pm 0.11 \pm 0.27$
580–680	$96.3 \pm 0.8 \pm 5.7$	1500–2500	$0.417 \pm 0.025 \pm 0.049$

TABLE XXIV. Cross sections at the particle level for different numbers of additional jets. The values are shown together with their statistical and systematic uncertainties.

Additional jets	σ [pb]	Additional jets	σ [pb]
0	$38.0 \pm 0.10 \pm 1.8$	3	$2.33 \pm 0.03 \pm 0.21$
1	$19.7 \pm 0.08 \pm 1.2$	4	$0.629 \pm 0.017 \pm 0.079$
2	$7.13 \pm 0.05 \pm 0.55$	≥ 5	$0.244 \pm 0.008 \pm 0.033$

TABLE XXV. Double-differential cross section at the particle level as a function of $|y(t_h)|$ vs. $p_T(t_h)$. The values are shown together with their statistical and systematic uncertainties.

$p_T(t_h)$ [GeV]	$\frac{d^2\sigma}{dp_T(t_h)d y(t_h) }$ [fb GeV $^{-1}$]	$p_T(t_h)$ [GeV]	$\frac{d^2\sigma}{dp_T(t_h)d y(t_h) }$ [fb GeV $^{-1}$]
$0 < y(t_h) < 0.5$			
0–40	$121.9 \pm 1.1 \pm 6.8$	240–280	$53.8 \pm 0.7 \pm 3.0$
40–80	$284 \pm 2 \pm 16$	280–330	$29.6 \pm 0.5 \pm 1.9$
80–120	$298 \pm 2 \pm 17$	330–380	$15.9 \pm 0.3 \pm 1.0$
120–160	$222 \pm 1 \pm 13$	380–450	$7.14 \pm 0.21 \pm 0.58$
160–200	$146.4 \pm 1.1 \pm 8.0$	450–800	$1.12 \pm 0.04 \pm 0.11$
200–240	$87.9 \pm 0.9 \pm 5.1$...	
$0.5 < y(t_h) < 1$			
0–40	$103.1 \pm 1.0 \pm 7.2$	240–280	$43.1 \pm 0.6 \pm 2.7$
40–80	$240 \pm 2 \pm 13$	280–330	$24.6 \pm 0.4 \pm 1.6$
80–120	$251 \pm 2 \pm 14$	330–380	$12.90 \pm 0.30 \pm 0.93$
120–160	$187 \pm 1 \pm 12$	380–450	$6.06 \pm 0.19 \pm 0.49$
160–200	$119.3 \pm 1.0 \pm 7.1$	450–800	$0.789 \pm 0.035 \pm 0.070$
200–240	$72.3 \pm 0.8 \pm 4.7$...	
$1 < y(t_h) < 1.5$			
0–40	$68.5 \pm 0.9 \pm 4.5$	240–280	$29.3 \pm 0.5 \pm 2.1$
40–80	$159.7 \pm 1.3 \pm 9.5$	280–330	$16.2 \pm 0.3 \pm 1.2$
80–120	$163 \pm 1 \pm 10$	330–380	$8.06 \pm 0.23 \pm 0.67$
120–160	$125.2 \pm 1.1 \pm 8.2$	380–450	$3.50 \pm 0.14 \pm 0.35$
160–200	$81.2 \pm 0.9 \pm 5.6$	450–800	$0.507 \pm 0.029 \pm 0.075$
200–240	$50.5 \pm 0.6 \pm 3.3$...	
$1.5 < y(t_h) < 2.5$			
0–40	$14.7 \pm 0.3 \pm 1.3$	240–280	$6.80 \pm 0.17 \pm 0.66$
40–80	$32.8 \pm 0.4 \pm 2.4$	280–330	$3.84 \pm 0.12 \pm 0.45$
80–120	$36.2 \pm 0.5 \pm 2.8$	330–380	$1.87 \pm 0.08 \pm 0.29$
120–160	$28.9 \pm 0.4 \pm 2.6$	380–450	$0.81 \pm 0.05 \pm 0.15$
160–200	$18.7 \pm 0.3 \pm 1.6$	450–800	$0.080 \pm 0.008 \pm 0.021$
200–240	$11.26 \pm 0.23 \pm 0.91$...	

TABLE XXVI. Double-differential cross section at the particle level as a function of $M(t\bar{t})$ vs. $|y(t\bar{t})|$. The values are shown together with their statistical and systematic uncertainties.

$ y(t\bar{t}) $	$\frac{d^2\sigma}{dM(t\bar{t})d y(t\bar{t}) }$ [fb GeV $^{-1}$]	$ y(t\bar{t}) $	$\frac{d^2\sigma}{dM(t\bar{t})d y(t\bar{t}) }$ [fb GeV $^{-1}$]
$300 < M(t\bar{t}) < 450$			
0.0–0.2	$125.5 \pm 1.1 \pm 6.9$	1.0–1.2	$73.3 \pm 0.8 \pm 4.4$
0.2–0.4	$121.8 \pm 0.9 \pm 6.5$	1.2–1.4	$55.2 \pm 0.7 \pm 3.4$
0.4–0.6	$116.3 \pm 1.0 \pm 6.3$	1.4–1.6	$34.5 \pm 0.6 \pm 2.3$
0.6–0.8	$109.0 \pm 0.9 \pm 6.6$	1.6–2.4	$6.05 \pm 0.15 \pm 0.64$
0.8–1.0	$93.2 \pm 0.9 \pm 5.3$...	
$450 < M(t\bar{t}) < 625$			
0.0–0.2	$144.8 \pm 1.1 \pm 8.2$	1.0–1.2	$62.5 \pm 0.7 \pm 4.5$
0.2–0.4	$137.8 \pm 1.0 \pm 7.8$	1.2–1.4	$41.5 \pm 0.6 \pm 3.1$
0.4–0.6	$125.1 \pm 0.9 \pm 7.4$	1.4–1.6	$22.6 \pm 0.5 \pm 2.1$
0.6–0.8	$107.4 \pm 0.9 \pm 6.8$	1.6–2.4	$3.03 \pm 0.10 \pm 0.38$
0.8–1.0	$86.6 \pm 0.8 \pm 5.5$...	
$625 < M(t\bar{t}) < 850$			
0.0–0.2	$64.8 \pm 0.7 \pm 3.7$	1.0–1.2	$19.8 \pm 0.4 \pm 1.5$
0.2–0.4	$59.8 \pm 0.6 \pm 3.4$	1.2–1.4	$11.2 \pm 0.3 \pm 1.2$
0.4–0.6	$51.4 \pm 0.6 \pm 3.6$	1.4–1.6	$5.41 \pm 0.22 \pm 0.48$
0.6–0.8	$41.6 \pm 0.5 \pm 3.1$	1.6–2.4	$0.686 \pm 0.044 \pm 0.076$
0.8–1.0	$31.4 \pm 0.5 \pm 2.1$...	
$850 < M(t\bar{t}) < 2000$			
0.0–0.2	$6.81 \pm 0.11 \pm 0.44$	0.8–1.0	$2.35 \pm 0.07 \pm 0.18$
0.2–0.4	$6.39 \pm 0.11 \pm 0.46$	1.0–1.2	$1.44 \pm 0.06 \pm 0.12$
0.4–0.6	$5.22 \pm 0.10 \pm 0.36$	1.2–1.4	$0.703 \pm 0.041 \pm 0.090$
0.6–0.8	$3.80 \pm 0.09 \pm 0.29$	1.4–2.4	$0.062 \pm 0.006 \pm 0.011$

TABLE XXVII. Double-differential cross section at the particle level as a function of $p_T(t_h)$ vs. $M(t\bar{t})$. The values are shown together with their statistical and systematic uncertainties.

$M(t\bar{t})$ [GeV]	$\frac{d^2\sigma}{dp_T(t_h)dM(t\bar{t})}$ [fb GeV $^{-2}$]	$M(t\bar{t})$ [GeV]	$\frac{d^2\sigma}{dp_T(t_h)dM(t\bar{t})}$ [fb GeV $^{-2}$]
$0 < p_T(t_h) < 90$			
300–360	$0.737 \pm 0.009 \pm 0.069$	580–680	$0.242 \pm 0.003 \pm 0.017$
360–430	$1.424 \pm 0.009 \pm 0.084$	680–800	$0.1141 \pm 0.0019 \pm 0.0091$
430–500	$0.794 \pm 0.007 \pm 0.054$	800–1000	$0.0423 \pm 0.0011 \pm 0.0041$
500–580	$0.448 \pm 0.004 \pm 0.029$	1000–2000	$(4.14 \pm 0.23 \pm 0.73) \times 10^{-3}$
$90 < p_T(t_h) < 180$			
300–360	$0.0805 \pm 0.0021 \pm 0.0083$	580–680	$0.451 \pm 0.004 \pm 0.028$
360–430	$0.757 \pm 0.007 \pm 0.044$	680–800	$0.226 \pm 0.003 \pm 0.016$
430–500	$1.195 \pm 0.008 \pm 0.079$	800–1000	$0.0895 \pm 0.0016 \pm 0.0064$
500–580	$0.832 \pm 0.006 \pm 0.053$	1000–2000	$(8.7 \pm 0.3 \pm 1.2) \times 10^{-3}$
$180 < p_T(t_h) < 270$			
300–430	$0.0194 \pm 0.0009 \pm 0.0045$	680–800	$0.179 \pm 0.003 \pm 0.012$
430–500	$0.1235 \pm 0.0027 \pm 0.0098$	800–1000	$0.0751 \pm 0.0014 \pm 0.0057$
500–580	$0.325 \pm 0.004 \pm 0.020$	1000–1200	$0.0260 \pm 0.0009 \pm 0.0027$
580–680	$0.320 \pm 0.004 \pm 0.022$	1200–2000	$(3.79 \pm 0.24 \pm 0.62) \times 10^{-3}$
$270 < p_T(t_h) < 800$			
300–430	$(4.2 \pm 0.5 \pm 1.4) \times 10^{-4}$	680–800	$0.0170 \pm 0.0003 \pm 0.0011$
430–500	$(2.83 \pm 0.16 \pm 0.48) \times 10^{-3}$	800–1000	$0.01261 \pm 0.00021 \pm 0.00086$
500–580	$(5.18 \pm 0.21 \pm 0.84) \times 10^{-3}$	1000–1200	$(6.01 \pm 0.17 \pm 0.48) \times 10^{-3}$
580–680	$0.01043 \pm 0.00027 \pm 0.00085$	1200–2000	$(1.42 \pm 0.04 \pm 0.12) \times 10^{-3}$

TABLE XXVIII. Differential cross sections at the particle level as a function of $p_T(t_h)$ for different numbers of additional jets. The values are shown together with their statistical and systematic uncertainties.

$p_T(t_h)$ [GeV]	$\frac{d\sigma}{dp_T(t_h)}$ [fb GeV $^{-1}$]	$p_T(t_h)$ [GeV]	$\frac{d\sigma}{dp_T(t_h)}$ [fb GeV $^{-1}$]
Additional jets: 0			
0–40	$98.4 \pm 0.9 \pm 5.9$	240–280	$32.7 \pm 0.4 \pm 2.0$
40–80	$223 \pm 1 \pm 11$	280–330	$16.8 \pm 0.3 \pm 1.2$
80–120	$230 \pm 1 \pm 13$	330–380	$8.44 \pm 0.18 \pm 0.63$
120–160	$167.7 \pm 1.0 \pm 8.9$	380–450	$3.47 \pm 0.11 \pm 0.36$
160–200	$103.3 \pm 0.7 \pm 5.6$	450–800	$0.470 \pm 0.021 \pm 0.052$
200–240	$58.6 \pm 0.5 \pm 3.5$...	
Additional jets: 1			
0–40	$43.6 \pm 0.4 \pm 3.4$	240–280	$22.9 \pm 0.3 \pm 1.5$
40–80	$103.5 \pm 0.6 \pm 7.4$	280–330	$12.96 \pm 0.21 \pm 0.89$
80–120	$109.1 \pm 0.6 \pm 6.9$	330–380	$6.44 \pm 0.14 \pm 0.57$
120–160	$85.4 \pm 0.5 \pm 5.4$	380–450	$2.99 \pm 0.09 \pm 0.25$
160–200	$57.7 \pm 0.5 \pm 3.6$	450–800	$0.431 \pm 0.019 \pm 0.043$
200–240	$36.9 \pm 0.4 \pm 2.6$...	
Additional jets: 2			
0–40	$14.3 \pm 0.2 \pm 1.5$	240–280	$9.71 \pm 0.17 \pm 0.76$
40–80	$34.7 \pm 0.3 \pm 2.8$	280–330	$6.02 \pm 0.12 \pm 0.56$
80–120	$38.1 \pm 0.3 \pm 3.1$	330–380	$3.39 \pm 0.10 \pm 0.33$
120–160	$30.5 \pm 0.3 \pm 2.7$	380–450	$1.60 \pm 0.06 \pm 0.14$
160–200	$22.0 \pm 0.2 \pm 1.8$	450–800	$0.217 \pm 0.012 \pm 0.025$
200–240	$14.7 \pm 0.2 \pm 1.4$...	
Additional jets: ≥ 3			
0–40	$5.82 \pm 0.10 \pm 0.55$	240–280	$4.77 \pm 0.11 \pm 0.59$
40–80	$14.1 \pm 0.2 \pm 1.5$	280–330	$3.30 \pm 0.09 \pm 0.41$
80–120	$15.5 \pm 0.2 \pm 1.6$	330–380	$2.07 \pm 0.07 \pm 0.23$
120–160	$13.0 \pm 0.2 \pm 1.3$	380–450	$1.09 \pm 0.05 \pm 0.12$
160–200	$9.6 \pm 0.1 \pm 1.1$	450–800	$0.162 \pm 0.010 \pm 0.026$
200–240	$6.72 \pm 0.13 \pm 0.71$...	

TABLE XXIX. Differential cross sections at the particle level as a function of $p_T(t\bar{t})$ for different numbers of additional jets. The values are shown together with their statistical and systematic uncertainties.

$p_T(t\bar{t})$ [GeV]	$\frac{d\sigma}{dp_T(t\bar{t})}$ [pb GeV $^{-1}$]	$p_T(t\bar{t})$ [GeV]	$\frac{d\sigma}{dp_T(t\bar{t})}$ [pb GeV $^{-1}$]
Additional jets: 0			
0–40	$0.665 \pm 0.003 \pm 0.037$	150–220	$(4.82 \pm 0.27 \pm 0.74) \times 10^{-3}$
40–80	$0.216 \pm 0.003 \pm 0.018$	220–300	$(7.2 \pm 1.0 \pm 2.0) \times 10^{-4}$
80–150	$0.0325 \pm 0.0007 \pm 0.0027$	300–1000	$(2.49 \pm 0.47 \pm 0.76) \times 10^{-5}$
Additional jets: 1			
0–40	$0.0794 \pm 0.0015 \pm 0.0089$	220–300	$0.01043 \pm 0.00034 \pm 0.00079$
40–80	$0.172 \pm 0.002 \pm 0.012$	300–380	$(3.89 \pm 0.21 \pm 0.66) \times 10^{-3}$
80–150	$0.0879 \pm 0.0011 \pm 0.0047$	380–1000	$(4.33 \pm 0.18 \pm 0.34) \times 10^{-4}$
150–220	$0.0306 \pm 0.0006 \pm 0.0017$...	
Additional jets: 2			
0–40	$0.0168 \pm 0.0007 \pm 0.0029$	220–300	$(9.09 \pm 0.33 \pm 0.82) \times 10^{-3}$
40–80	$0.0367 \pm 0.0008 \pm 0.0037$	300–380	$(3.27 \pm 0.20 \pm 0.66) \times 10^{-3}$
80–150	$0.0358 \pm 0.0007 \pm 0.0032$	380–500	$(1.28 \pm 0.09 \pm 0.15) \times 10^{-3}$
150–220	$0.0181 \pm 0.0005 \pm 0.0016$	500–1000	$(1.19 \pm 0.12 \pm 0.18) \times 10^{-4}$
Additional jets: ≥ 3			
0–40	$(4.5 \pm 0.3 \pm 1.2) \times 10^{-3}$	220–300	$(6.30 \pm 0.25 \pm 0.89) \times 10^{-3}$
40–80	$0.0124 \pm 0.0005 \pm 0.0017$	300–380	$(2.42 \pm 0.17 \pm 0.44) \times 10^{-3}$
80–150	$0.0135 \pm 0.0004 \pm 0.0016$	380–500	$(1.16 \pm 0.08 \pm 0.20) \times 10^{-3}$
150–220	$(9.9 \pm 0.4 \pm 1.0) \times 10^{-3}$	500–1000	$(1.61 \pm 0.11 \pm 0.20) \times 10^{-4}$

TABLE XXX. Differential cross sections at the particle level as a function of $M(t\bar{t})$ for different numbers of additional jets. The values are shown together with their statistical and systematic uncertainties.

$M(t\bar{t})$ [GeV]	$\frac{d\sigma}{dM(t\bar{t})}$ [fb GeV $^{-1}$]	$M(t\bar{t})$ [GeV]	$\frac{d\sigma}{dM(t\bar{t})}$ [fb GeV $^{-1}$]
Additional jets: 0			
300–360	$43.7 \pm 0.6 \pm 4.9$	680–800	$31.4 \pm 0.3 \pm 1.6$
360–430	$109.8 \pm 0.7 \pm 5.8$	800–1000	$14.27 \pm 0.17 \pm 0.91$
430–500	$104.2 \pm 0.7 \pm 6.0$	1000–1200	$5.24 \pm 0.12 \pm 0.50$
500–580	$80.9 \pm 0.5 \pm 4.4$	1200–2000	$0.989 \pm 0.034 \pm 0.086$
580–680	$53.8 \pm 0.4 \pm 3.0$...	
Additional jets: 1			
300–360	$20.7 \pm 0.3 \pm 2.2$	680–800	$15.6 \pm 0.2 \pm 1.0$
360–430	$59.7 \pm 0.5 \pm 3.9$	800–1000	$6.79 \pm 0.11 \pm 0.46$
430–500	$57.3 \pm 0.4 \pm 4.1$	1000–1200	$2.43 \pm 0.07 \pm 0.25$
500–580	$42.9 \pm 0.3 \pm 2.8$	1200–2000	$0.385 \pm 0.017 \pm 0.043$
580–680	$27.9 \pm 0.3 \pm 2.0$...	
Additional jets: 2			
300–360	$6.85 \pm 0.14 \pm 0.55$	680–800	$5.60 \pm 0.10 \pm 0.56$
360–430	$22.3 \pm 0.3 \pm 1.7$	800–1000	$2.44 \pm 0.06 \pm 0.20$
430–500	$21.2 \pm 0.2 \pm 2.1$	1000–1200	$0.85 \pm 0.04 \pm 0.10$
500–580	$15.9 \pm 0.2 \pm 1.4$	1200–2000	$0.135 \pm 0.009 \pm 0.019$
580–680	$10.06 \pm 0.14 \pm 0.95$...	
Additional jets: ≥ 3			
300–360	$2.52 \pm 0.08 \pm 0.33$	680–800	$2.49 \pm 0.06 \pm 0.36$
360–430	$9.5 \pm 0.2 \pm 1.0$	800–1000	$1.14 \pm 0.04 \pm 0.19$
430–500	$9.7 \pm 0.1 \pm 1.1$	1000–1200	$0.418 \pm 0.025 \pm 0.057$
500–580	$7.14 \pm 0.12 \pm 0.77$	1200–2000	$0.065 \pm 0.006 \pm 0.019$
580–680	$4.58 \pm 0.09 \pm 0.54$...	

TABLE XXXI. Differential cross sections at the particle level as a function of $p_T(\text{jet})$ for jets. The values are shown together with their statistical and systematic uncertainties.

$p_T(\text{jet})$ [GeV]	$\frac{d\sigma}{dp_T(\text{jet})}$ [pb GeV $^{-1}$]	$p_T(\text{jet})$ [GeV]	$\frac{d\sigma}{dp_T(\text{jet})}$ [pb GeV $^{-1}$]
$p_T(b_\ell)$			
30–50	$0.913 \pm 0.004 \pm 0.052$	100–150	$0.206 \pm 0.001 \pm 0.011$
50–75	$0.748 \pm 0.003 \pm 0.040$	150–200	$0.0643 \pm 0.0006 \pm 0.0036$
75–100	$0.466 \pm 0.002 \pm 0.026$	200–350	$(9.53 \pm 0.13 \pm 0.59) \times 10^{-3}$
$p_T(b_h)$			
30–50	$0.858 \pm 0.004 \pm 0.045$	100–150	$0.211 \pm 0.001 \pm 0.013$
50–75	$0.771 \pm 0.003 \pm 0.040$	150–200	$0.0640 \pm 0.0006 \pm 0.0041$
75–100	$0.491 \pm 0.002 \pm 0.029$	200–350	$0.01103 \pm 0.00015 \pm 0.00075$
$p_T(j_{W1})$			
30–50	$0.861 \pm 0.004 \pm 0.042$	100–150	$0.213 \pm 0.001 \pm 0.012$
50–75	$0.864 \pm 0.003 \pm 0.047$	150–200	$0.0663 \pm 0.0007 \pm 0.0040$
75–100	$0.506 \pm 0.003 \pm 0.029$	200–350	$0.01270 \pm 0.00018 \pm 0.00085$
$p_T(j_{W2})$			
30–50	$1.730 \pm 0.004 \pm 0.090$	75–100	$0.1223 \pm 0.0012 \pm 0.0077$
50–75	$0.443 \pm 0.002 \pm 0.028$	100–250	$0.01019 \pm 0.00017 \pm 0.00071$
$p_T(j_1)$			
30–50	$0.410 \pm 0.002 \pm 0.029$	150–175	$0.0613 \pm 0.0007 \pm 0.0041$
50–75	$0.253 \pm 0.002 \pm 0.019$	175–200	$0.0432 \pm 0.0006 \pm 0.0029$
75–100	$0.174 \pm 0.001 \pm 0.012$	200–250	$0.0286 \pm 0.0004 \pm 0.0019$

(Table continued)

TABLE XXXI. (*Continued*)

$p_T(\text{jet})$ [GeV]	$\frac{d\sigma}{dp_T(\text{jet})}$ [pb GeV $^{-1}$]	$p_T(\text{jet})$ [GeV]	$\frac{d\sigma}{dp_T(\text{jet})}$ [pb GeV $^{-1}$]
100–125	$0.1207 \pm 0.0011 \pm 0.0089$	250–320	$0.0145 \pm 0.0002 \pm 0.0010$
125–150	$0.0840 \pm 0.0009 \pm 0.0056$	320–500	$(4.71 \pm 0.07 \pm 0.29) \times 10^{-3}$
		$p_T(j_2)$	
30–50	$0.246 \pm 0.002 \pm 0.022$	125–150	$0.0138 \pm 0.0003 \pm 0.0014$
50–75	$0.103 \pm 0.001 \pm 0.011$	150–180	$(7.54 \pm 0.26 \pm 0.74) \times 10^{-3}$
75–100	$0.0501 \pm 0.0007 \pm 0.0052$	180–350	$(1.65 \pm 0.05 \pm 0.17) \times 10^{-3}$
100–125	$0.0258 \pm 0.0005 \pm 0.0029$...
		$p_T(j_3)$	
30–50	$0.097 \pm 0.001 \pm 0.011$	75–100	$(10.0 \pm 0.3 \pm 1.6) \times 10^{-3}$
50–75	$0.0290 \pm 0.0005 \pm 0.0041$	100–250	$(1.35 \pm 0.05 \pm 0.19) \times 10^{-3}$
		$p_T(j_4)$	
30–50	$0.0307 \pm 0.0006 \pm 0.0046$	75–100	$(1.75 \pm 0.11 \pm 0.37) \times 10^{-3}$
50–75	$(6.7 \pm 0.2 \pm 1.2) \times 10^{-3}$	100–200	$(2.64 \pm 0.26 \pm 0.58) \times 10^{-4}$

TABLE XXXII. Differential cross sections at the particle level as a function of $|\eta(\text{jet})|$ for jets. The values are shown together with their statistical and systematic uncertainties.

$ \eta(\text{jet}) $	$\frac{d\sigma}{d\eta(\text{jet})}$ [pb]	$ \eta(\text{jet}) $	$\frac{d\sigma}{d\eta(\text{jet})}$ [pb]
		$ \eta(b_e) $	
0.00–0.25	$42.4 \pm 0.2 \pm 2.3$	1.25–1.50	$25.7 \pm 0.2 \pm 1.4$
0.25–0.50	$41.6 \pm 0.2 \pm 2.3$	1.50–1.75	$20.9 \pm 0.1 \pm 1.2$
0.50–0.75	$39.6 \pm 0.2 \pm 2.1$	1.75–2.00	$16.69 \pm 0.13 \pm 0.97$
0.75–1.00	$35.9 \pm 0.2 \pm 1.9$	2.00–2.25	$12.37 \pm 0.12 \pm 0.74$
1.00–1.25	$31.6 \pm 0.2 \pm 1.7$	2.25–2.50	$5.14 \pm 0.09 \pm 0.34$
		$ \eta(b_h) $	
0.00–0.25	$44.9 \pm 0.2 \pm 2.3$	1.25–1.50	$24.8 \pm 0.2 \pm 1.4$
0.25–0.50	$43.6 \pm 0.2 \pm 2.3$	1.50–1.75	$19.6 \pm 0.1 \pm 1.1$
0.50–0.75	$40.6 \pm 0.2 \pm 2.1$	1.75–2.00	$15.3 \pm 0.1 \pm 1.0$
0.75–1.00	$36.8 \pm 0.2 \pm 1.9$	2.00–2.25	$10.93 \pm 0.12 \pm 0.73$
1.00–1.25	$30.8 \pm 0.2 \pm 1.7$	2.25–2.50	$4.54 \pm 0.08 \pm 0.34$
		$ \eta(j_{W1}) $	
0.00–0.25	$43.1 \pm 0.2 \pm 2.3$	1.25–1.50	$25.5 \pm 0.2 \pm 1.4$
0.25–0.50	$42.0 \pm 0.2 \pm 2.3$	1.50–1.75	$20.9 \pm 0.1 \pm 1.2$
0.50–0.75	$39.1 \pm 0.2 \pm 2.0$	1.75–2.00	$16.6 \pm 0.1 \pm 1.0$
0.75–1.00	$35.7 \pm 0.2 \pm 1.9$	2.00–2.25	$12.52 \pm 0.12 \pm 0.77$
1.00–1.25	$32.0 \pm 0.2 \pm 1.8$	2.25–2.50	$5.66 \pm 0.08 \pm 0.38$
		$ \eta(j_{W2}) $	
0.00–0.25	$40.6 \pm 0.2 \pm 2.1$	1.25–1.50	$26.6 \pm 0.2 \pm 1.4$
0.25–0.50	$39.4 \pm 0.2 \pm 2.0$	1.50–1.75	$22.3 \pm 0.2 \pm 1.3$
0.50–0.75	$37.1 \pm 0.2 \pm 1.9$	1.75–2.00	$18.6 \pm 0.1 \pm 1.1$
0.75–1.00	$34.7 \pm 0.2 \pm 1.8$	2.00–2.25	$15.00 \pm 0.12 \pm 0.94$
1.00–1.25	$31.4 \pm 0.2 \pm 1.6$	2.25–2.50	$7.07 \pm 0.09 \pm 0.50$
		$ \eta(j_1) $	
0.00–0.25	$13.76 \pm 0.11 \pm 0.95$	1.25–1.50	$12.45 \pm 0.10 \pm 0.84$
0.25–0.50	$13.72 \pm 0.11 \pm 0.97$	1.50–1.75	$11.84 \pm 0.10 \pm 0.83$
0.50–0.75	$13.57 \pm 0.11 \pm 0.88$	1.75–2.00	$11.54 \pm 0.10 \pm 0.86$
0.75–1.00	$13.73 \pm 0.11 \pm 0.85$	2.00–2.25	$10.33 \pm 0.09 \pm 0.76$
1.00–1.25	$13.11 \pm 0.10 \pm 0.96$	2.25–2.50	$5.57 \pm 0.06 \pm 0.41$

(Table continued)

TABLE XXXII. (*Continued*)

$ \eta(\text{jet}) $	$\frac{d\sigma}{d\eta(\text{jet})}$ [pb]	$ \eta(\text{j}_2) $	$\frac{d\sigma}{d\eta(\text{j}_2)}$ [pb]
0.00–0.25	$4.75 \pm 0.06 \pm 0.52$	1.25–1.50	$4.28 \pm 0.06 \pm 0.39$
0.25–0.50	$4.90 \pm 0.06 \pm 0.46$	1.50–1.75	$4.15 \pm 0.05 \pm 0.39$
0.50–0.75	$4.62 \pm 0.06 \pm 0.51$	1.75–2.00	$3.92 \pm 0.05 \pm 0.37$
0.75–1.00	$4.64 \pm 0.06 \pm 0.49$	2.00–2.25	$3.52 \pm 0.05 \pm 0.32$
1.00–1.25	$4.58 \pm 0.06 \pm 0.46$	2.25–2.50	$1.91 \pm 0.04 \pm 0.18$
		$ \eta(\text{j}_3) $	
0.0–0.5	$1.43 \pm 0.02 \pm 0.19$	1.5–2.0	$1.21 \pm 0.02 \pm 0.14$
0.5–1.0	$1.46 \pm 0.02 \pm 0.16$	2.0–2.5	$0.808 \pm 0.015 \pm 0.098$
1.0–1.5	$1.38 \pm 0.02 \pm 0.16$...	
		$ \eta(\text{j}_4) $	
0.0–0.5	$0.399 \pm 0.010 \pm 0.067$	1.5–2.0	$0.320 \pm 0.009 \pm 0.057$
0.5–1.0	$0.408 \pm 0.010 \pm 0.060$	2.0–2.5	$0.216 \pm 0.008 \pm 0.040$
1.0–1.5	$0.402 \pm 0.011 \pm 0.053$...	

TABLE XXXIII. Differential cross sections at the particle level as a function of ΔR_{j_i} for jets. The values are shown together with their statistical and systematic uncertainties.

ΔR_{j_i}	$\frac{d\sigma}{d\Delta R_{j_i}}$ [fb]	ΔR_{j_i}	$\frac{d\sigma}{d\Delta R_{j_i}}$ [fb]
		$\Delta R_{j_i}(b_e)$	
0.4–0.6	$16400 \pm 200 \pm 1100$	1.4–1.6	$32600 \pm 200 \pm 1800$
0.6–0.8	$27300 \pm 200 \pm 1600$	1.6–2.0	$31300 \pm 100 \pm 1700$
0.8–1.0	$28800 \pm 200 \pm 1600$	2.0–2.5	$25600 \pm 100 \pm 1400$
1.0–1.2	$31400 \pm 200 \pm 1700$	2.5–4.5	$4450 \pm 20 \pm 230$
1.2–1.4	$32800 \pm 200 \pm 1800$...	
		$\Delta R_{j_i}(b_h)$	
0.4–0.6	$21800 \pm 200 \pm 1300$	1.4–1.6	$41600 \pm 200 \pm 2200$
0.6–0.8	$36500 \pm 200 \pm 2000$	1.6–2.0	$30800 \pm 100 \pm 1700$
0.8–1.0	$41800 \pm 200 \pm 2200$	2.0–2.5	$14340 \pm 100 \pm 840$
1.0–1.2	$46100 \pm 200 \pm 2400$	2.5–4.5	$980 \pm 15 \pm 75$
1.2–1.4	$45800 \pm 200 \pm 2500$...	
		$\Delta R_{j_i}(j_{W1})$	
0.4–0.6	$23400 \pm 200 \pm 1200$	1.4–1.6	$40100 \pm 200 \pm 2300$
0.6–0.8	$39300 \pm 200 \pm 1900$	1.6–2.0	$27400 \pm 100 \pm 1500$
0.8–1.0	$44600 \pm 200 \pm 2300$	2.0–2.5	$12550 \pm 90 \pm 710$
1.0–1.2	$48800 \pm 300 \pm 2500$	2.5–4.5	$1330 \pm 17 \pm 93$
1.2–1.4	$46600 \pm 200 \pm 2500$...	
		$\Delta R_{j_i}(j_{W2})$	
0.4–0.6	$25500 \pm 200 \pm 1400$	1.4–1.6	$39900 \pm 200 \pm 2200$
0.6–0.8	$41300 \pm 200 \pm 2100$	1.6–2.0	$26500 \pm 100 \pm 1500$
0.8–1.0	$44800 \pm 300 \pm 2200$	2.0–2.5	$11890 \pm 90 \pm 700$
1.0–1.2	$48200 \pm 300 \pm 2600$	2.5–4.5	$1250 \pm 16 \pm 81$
1.2–1.4	$46300 \pm 300 \pm 2400$...	
		$\Delta R_{j_i}(j_1)$	
0.4–0.6	$13920 \pm 130 \pm 980$	1.4–1.6	$13720 \pm 130 \pm 950$
0.6–0.8	$18000 \pm 100 \pm 1300$	1.6–2.0	$11460 \pm 80 \pm 780$
0.8–1.0	$16100 \pm 100 \pm 1100$	2.0–2.5	$8110 \pm 60 \pm 520$
1.0–1.2	$15500 \pm 100 \pm 1100$	2.5–4.5	$1459 \pm 12 \pm 97$
1.2–1.4	$14500 \pm 100 \pm 1100$...	

(Table continued)

TABLE XXXIII. (*Continued*)

ΔR_{j_t}	$\frac{d\sigma}{d\Delta R_{j_t}}$ [fb]	ΔR_{j_t}	$\frac{d\sigma}{d\Delta R_{j_t}}$ [fb]
$\Delta R_{j_t}(j_2)$			
0.4–0.6	$5240 \pm 70 \pm 490$	1.4–1.6	$4510 \pm 70 \pm 400$
0.6–0.8	$6780 \pm 80 \pm 640$	1.6–2.0	$3770 \pm 50 \pm 350$
0.8–1.0	$5870 \pm 80 \pm 530$	2.0–2.5	$2530 \pm 30 \pm 230$
1.0–1.2	$5500 \pm 70 \pm 490$	2.5–4.5	$463 \pm 7 \pm 41$
1.2–1.4	$5050 \pm 70 \pm 450$...	
$\Delta R_{j_t}(j_3)$			
0.4–0.8	$1780 \pm 30 \pm 220$	1.6–2.0	$1170 \pm 20 \pm 150$
0.8–1.2	$1720 \pm 30 \pm 190$	2.0–2.5	$759 \pm 17 \pm 89$
1.2–1.6	$1490 \pm 30 \pm 160$	2.5–4.5	$148 \pm 4 \pm 15$
$\Delta R_{j_t}(j_4)$			
0.4–0.8	$477 \pm 13 \pm 68$	1.6–2.0	$319 \pm 11 \pm 56$
0.8–1.2	$483 \pm 13 \pm 67$	2.0–2.5	$221 \pm 9 \pm 35$
1.2–1.6	$404 \pm 12 \pm 58$	2.5–4.5	$40.3 \pm 1.9 \pm 6.2$

TABLE XXXIV. Differential cross sections at the particle level as a function of ΔR_t for jets. The values are shown together with their statistical and systematic uncertainties.

ΔR_t	$\frac{d\sigma}{d\Delta R_t}$ [fb]	ΔR_t	$\frac{d\sigma}{d\Delta R_t}$ [fb]
$\Delta R_t(b_\ell)$			
0.0–0.3	$18000 \pm 100 \pm 1100$	1.2–1.5	$32300 \pm 100 \pm 1800$
0.3–0.6	$38300 \pm 200 \pm 2200$	1.5–2.0	$21000 \pm 100 \pm 1200$
0.6–0.9	$41800 \pm 200 \pm 2300$	2.0–2.5	$9110 \pm 70 \pm 540$
0.9–1.2	$38300 \pm 200 \pm 2100$	2.5–4.5	$1318 \pm 16 \pm 88$
$\Delta R_t(b_h)$			
0.0–0.3	$18300 \pm 100 \pm 1100$	1.2–1.5	$32800 \pm 200 \pm 1700$
0.3–0.6	$37200 \pm 200 \pm 2000$	1.5–2.0	$21900 \pm 100 \pm 1200$
0.6–0.9	$40500 \pm 200 \pm 2100$	2.0–2.5	$9440 \pm 80 \pm 580$
0.9–1.2	$37400 \pm 200 \pm 2000$	2.5–4.5	$1334 \pm 16 \pm 89$
$\Delta R_t(j_{W1})$			
0.0–0.3	$25800 \pm 200 \pm 1300$	1.2–1.5	$26800 \pm 100 \pm 1500$
0.3–0.6	$47200 \pm 200 \pm 2500$	1.5–2.0	$16860 \pm 90 \pm 930$
0.6–0.9	$44300 \pm 200 \pm 2400$	2.0–2.5	$7630 \pm 60 \pm 430$
0.9–1.2	$35300 \pm 200 \pm 2000$	2.5–4.5	$1187 \pm 14 \pm 78$
$\Delta R_t(j_{W2})$			
0.0–0.3	$8980 \pm 100 \pm 480$	1.2–1.5	$36000 \pm 200 \pm 2000$
0.3–0.6	$26700 \pm 200 \pm 1300$	1.5–2.0	$26100 \pm 100 \pm 1400$
0.6–0.9	$37100 \pm 200 \pm 1900$	2.0–2.5	$12970 \pm 90 \pm 720$
0.9–1.2	$38600 \pm 200 \pm 2100$	2.5–4.5	$2230 \pm 20 \pm 140$
$\Delta R_t(j_1)$			
0.0–0.3	$1160 \pm 30 \pm 110$	1.2–1.5	$9210 \pm 80 \pm 680$
0.3–0.6	$3480 \pm 50 \pm 280$	1.5–2.0	$11380 \pm 70 \pm 820$
0.6–0.9	$5950 \pm 60 \pm 460$	2.0–2.5	$11600 \pm 80 \pm 790$
0.9–1.2	$7610 \pm 70 \pm 550$	2.5–4.5	$5020 \pm 30 \pm 330$
$\Delta R_t(j_2)$			
0.0–0.3	$482 \pm 15 \pm 53$	1.2–1.5	$3720 \pm 40 \pm 350$
0.3–0.6	$1550 \pm 30 \pm 150$	1.5–2.0	$4140 \pm 40 \pm 380$
0.6–0.9	$2640 \pm 40 \pm 260$	2.0–2.5	$3820 \pm 40 \pm 380$
0.9–1.2	$3260 \pm 40 \pm 300$	2.5–4.5	$1380 \pm 10 \pm 120$

(Table continued)

TABLE XXXIV. (*Continued*)

ΔR_t	$\frac{d\sigma}{d\Delta R_t}$ [fb]	ΔR_t	$\frac{d\sigma}{d\Delta R_t}$ [fb]
$\Delta R_t(j_3)$			
0.0–0.4	$181 \pm 7 \pm 31$	1.5–2.0	$1280 \pm 20 \pm 150$
0.4–0.8	$642 \pm 14 \pm 79$	2.0–2.5	$1160 \pm 20 \pm 150$
0.8–1.2	$1000 \pm 20 \pm 120$	2.5–4.5	$408 \pm 7 \pm 46$
1.2–1.5	$1160 \pm 20 \pm 140$...	
$\Delta R_t(j_4)$			
0.0–0.4	$42.7 \pm 2.9 \pm 9.2$	1.5–2.0	$359 \pm 10 \pm 55$
0.4–0.8	$163 \pm 6 \pm 23$	2.0–2.5	$322 \pm 9 \pm 55$
0.8–1.2	$273 \pm 9 \pm 38$	2.5–4.5	$113 \pm 3 \pm 18$
1.2–1.5	$324 \pm 10 \pm 53$...	

APPENDIX C: TABLES OF NORMALIZED PARTON-LEVEL CROSS SECTIONS

The measured normalized differential cross sections at the parton level as a function of all the measured variables are listed in Tables XXXV–XLIV. The results are shown together with their statistical and systematic uncertainties.

TABLE XXXV. Differential cross section at the parton level as a function of $p_T(t_{\text{high}})$ normalized to the cross section σ_{norm} in the measured range. The values are shown together with their statistical and systematic uncertainties.

$p_T(t_{\text{high}})$ [GeV]	$\frac{1}{\sigma_{\text{norm}}} \frac{d\sigma}{dp_T(t_{\text{high}})}$ [GeV $^{-1}$]	$p_T(t_{\text{high}})$ [GeV]	$\frac{1}{\sigma_{\text{norm}}} \frac{d\sigma}{dp_T(t_{\text{high}})}$ [GeV $^{-1}$]
0–40	$(1.364 \pm 0.032 \pm 0.092) \times 10^{-3}$	240–280	$(1.056 \pm 0.013 \pm 0.039) \times 10^{-3}$
40–80	$(5.10 \pm 0.04 \pm 0.16) \times 10^{-3}$	280–330	$(5.53 \pm 0.08 \pm 0.24) \times 10^{-4}$
80–120	$(6.00 \pm 0.05 \pm 0.15) \times 10^{-3}$	330–380	$(2.75 \pm 0.05 \pm 0.18) \times 10^{-4}$
120–160	$(4.97 \pm 0.04 \pm 0.14) \times 10^{-3}$	380–430	$(1.41 \pm 0.04 \pm 0.14) \times 10^{-4}$
160–200	$(3.183 \pm 0.027 \pm 0.076) \times 10^{-3}$	430–500	$(6.45 \pm 0.24 \pm 0.56) \times 10^{-5}$
200–240	$(1.918 \pm 0.019 \pm 0.051) \times 10^{-3}$	500–800	$(1.30 \pm 0.04 \pm 0.11) \times 10^{-5}$

TABLE XXXVI. Differential cross section at the parton level as a function of $p_T(t_{\text{low}})$ normalized to the cross section σ_{norm} in the measured range. The values are shown together with their statistical and systematic uncertainties.

$p_T(t_{\text{low}})$ [GeV]	$\frac{1}{\sigma_{\text{norm}}} \frac{d\sigma}{dp_T(t_{\text{low}})}$ [GeV $^{-1}$]	$p_T(t_{\text{low}})$ [GeV]	$\frac{1}{\sigma_{\text{norm}}} \frac{d\sigma}{dp_T(t_{\text{low}})}$ [GeV $^{-1}$]
0–40	$(4.35 \pm 0.03 \pm 0.14) \times 10^{-3}$	240–280	$(4.76 \pm 0.06 \pm 0.25) \times 10^{-4}$
40–80	$(7.307 \pm 0.032 \pm 0.095) \times 10^{-3}$	280–330	$(2.24 \pm 0.04 \pm 0.11) \times 10^{-4}$
80–120	$(5.88 \pm 0.03 \pm 0.12) \times 10^{-3}$	330–380	$(1.004 \pm 0.025 \pm 0.059) \times 10^{-4}$
120–160	$(3.593 \pm 0.022 \pm 0.075) \times 10^{-3}$	380–430	$(4.62 \pm 0.17 \pm 0.45) \times 10^{-5}$
160–200	$(1.909 \pm 0.015 \pm 0.051) \times 10^{-3}$	430–500	$(2.20 \pm 0.12 \pm 0.20) \times 10^{-5}$
200–240	$(9.58 \pm 0.10 \pm 0.20) \times 10^{-4}$	500–800	$(3.81 \pm 0.32 \pm 0.75) \times 10^{-6}$

TABLE XXXVII. Differential cross section at the parton level as a function of $p_T(t_h)$ normalized to the cross section σ_{norm} in the measured range. The values are shown together with their statistical and systematic uncertainties.

$p_T(t_h)$ [GeV]	$\frac{1}{\sigma_{\text{norm}}} \frac{d\sigma}{dp_T(t_h)}$ [GeV $^{-1}$]	$p_T(t_h)$ [GeV]	$\frac{1}{\sigma_{\text{norm}}} \frac{d\sigma}{dp_T(t_h)}$ [GeV $^{-1}$]
0–40	$(2.84 \pm 0.03 \pm 0.12) \times 10^{-3}$	240–280	$(7.76 \pm 0.09 \pm 0.24) \times 10^{-4}$
40–80	$(6.17 \pm 0.03 \pm 0.12) \times 10^{-3}$	280–330	$(3.95 \pm 0.05 \pm 0.14) \times 10^{-4}$
80–120	$(6.011 \pm 0.032 \pm 0.085) \times 10^{-3}$	330–380	$(1.95 \pm 0.04 \pm 0.11) \times 10^{-4}$
120–160	$(4.22 \pm 0.03 \pm 0.12) \times 10^{-3}$	380–430	$(9.46 \pm 0.26 \pm 0.61) \times 10^{-5}$
160–200	$(2.565 \pm 0.018 \pm 0.049) \times 10^{-3}$	430–500	$(4.14 \pm 0.16 \pm 0.39) \times 10^{-5}$
200–240	$(1.431 \pm 0.013 \pm 0.036) \times 10^{-3}$	500–800	$(8.9 \pm 0.4 \pm 1.2) \times 10^{-6}$

TABLE XXXVIII. Differential cross section at the parton level as a function of $|y(t_h)|$ normalized to the cross section σ_{norm} in the measured range. The values are shown together with their statistical and systematic uncertainties.

$ y(t_h) $	$\frac{1}{\sigma_{\text{norm}}} \frac{d\sigma}{d y(t_h) }$	$ y(t_h) $	$\frac{1}{\sigma_{\text{norm}}} \frac{d\sigma}{d y(t_h) }$
0.0–0.2	$0.631 \pm 0.004 \pm 0.014$	1.2–1.4	$0.404 \pm 0.003 \pm 0.010$
0.2–0.4	$0.626 \pm 0.004 \pm 0.013$	1.4–1.6	$0.338 \pm 0.003 \pm 0.014$
0.4–0.6	$0.5938 \pm 0.0037 \pm 0.0091$	1.6–1.8	$0.290 \pm 0.003 \pm 0.010$
0.6–0.8	$0.562 \pm 0.004 \pm 0.015$	1.8–2.0	$0.230 \pm 0.003 \pm 0.011$
0.8–1.0	$0.5072 \pm 0.0035 \pm 0.0090$	2.0–2.5	$0.1424 \pm 0.0026 \pm 0.0072$
1.0–1.2	$0.4615 \pm 0.0034 \pm 0.0064$...	

TABLE XXXIX. Differential cross section at the parton level as a function of $p_T(t\bar{t})$ normalized to the cross section σ_{norm} in the measured range. The values are shown together with their statistical and systematic uncertainties.

$p_T(t\bar{t})$ [GeV]	$\frac{1}{\sigma_{\text{norm}}} \frac{d\sigma}{dp_T(t\bar{t})}$ [GeV $^{-1}$]	$p_T(t\bar{t})$ [GeV]	$\frac{1}{\sigma_{\text{norm}}} \frac{d\sigma}{dp_T(t\bar{t})}$ [GeV $^{-1}$]
0–40	$0.01227 \pm 0.00007 \pm 0.00039$	220–300	$(3.26 \pm 0.08 \pm 0.24) \times 10^{-4}$
40–80	$(6.11 \pm 0.08 \pm 0.35) \times 10^{-3}$	300–380	$(1.111 \pm 0.047 \pm 0.086) \times 10^{-4}$
80–150	$(2.371 \pm 0.026 \pm 0.082) \times 10^{-3}$	380–500	$(4.22 \pm 0.18 \pm 0.31) \times 10^{-5}$
150–220	$(8.07 \pm 0.15 \pm 0.29) \times 10^{-4}$	500–1000	$(4.99 \pm 0.22 \pm 0.33) \times 10^{-6}$

TABLE XL. Differential cross section at the parton level as a function of $|y(t\bar{t})|$ normalized to the cross section σ_{norm} in the measured range. The values are shown together with their statistical and systematic uncertainties.

$ y(t\bar{t}) $	$\frac{1}{\sigma_{\text{norm}}} \frac{d\sigma}{d y(t\bar{t}) }$	$ y(t\bar{t}) $	$\frac{1}{\sigma_{\text{norm}}} \frac{d\sigma}{d y(t\bar{t}) }$
0.0–0.2	$0.740 \pm 0.005 \pm 0.012$	1.0–1.2	$0.451 \pm 0.005 \pm 0.012$
0.2–0.4	$0.719 \pm 0.006 \pm 0.016$	1.2–1.4	$0.386 \pm 0.005 \pm 0.010$
0.4–0.6	$0.674 \pm 0.005 \pm 0.018$	1.4–1.6	$0.305 \pm 0.006 \pm 0.015$
0.6–0.8	$0.620 \pm 0.005 \pm 0.019$	1.6–1.8	$0.217 \pm 0.006 \pm 0.023$
0.8–1.0	$0.549 \pm 0.005 \pm 0.012$	1.8–2.4	$0.1129 \pm 0.0043 \pm 0.0098$

TABLE XLI. Differential cross section at the parton level as a function of $M(t\bar{t})$ normalized to the cross section σ_{norm} in the measured range. The values are shown together with their statistical and systematic uncertainties.

$M(t\bar{t})$ [GeV]	$\frac{1}{\sigma_{\text{norm}}} \frac{d\sigma}{dM(t\bar{t})}$ [GeV $^{-1}$]	$M(t\bar{t})$ [GeV]	$\frac{1}{\sigma_{\text{norm}}} \frac{d\sigma}{dM(t\bar{t})}$ [GeV $^{-1}$]
300–360	$(1.03 \pm 0.03 \pm 0.27) \times 10^{-3}$	680–800	$(5.18 \pm 0.09 \pm 0.24) \times 10^{-4}$
360–430	$(4.50 \pm 0.04 \pm 0.14) \times 10^{-3}$	800–1000	$(1.98 \pm 0.04 \pm 0.11) \times 10^{-4}$
430–500	$(3.29 \pm 0.03 \pm 0.13) \times 10^{-3}$	1000–1200	$(6.77 \pm 0.24 \pm 0.34) \times 10^{-5}$
500–580	$(2.016 \pm 0.025 \pm 0.056) \times 10^{-3}$	1200–1500	$(2.02 \pm 0.11 \pm 0.17) \times 10^{-5}$
580–680	$(1.084 \pm 0.015 \pm 0.037) \times 10^{-3}$	1500–2500	$(2.56 \pm 0.21 \pm 0.50) \times 10^{-6}$

TABLE XLII. Double-differential cross section at the parton level as a function of $|y(t_h)|$ vs. $p_T(t_h)$ normalized to the cross section σ_{norm} in the measured in the two-dimensional range. The values are shown together with their statistical and systematic uncertainties.

$p_T(t_h)$ [GeV]	$\frac{1}{\sigma_{\text{norm}}} \frac{d^2\sigma}{d y(t_h) dp_T(t_h)}$ [GeV $^{-1}$]	$0 < y(t_h) < 0.5$	
		$p_T(t_h)$ [GeV]	$\frac{1}{\sigma_{\text{norm}}} \frac{d^2\sigma}{d y(t_h) dp_T(t_h)}$ [GeV $^{-1}$]
0–40	$(1.628 \pm 0.018 \pm 0.063) \times 10^{-3}$	240–280	$(5.44 \pm 0.07 \pm 0.19) \times 10^{-4}$
40–80	$(3.63 \pm 0.02 \pm 0.10) \times 10^{-3}$	280–330	$(2.85 \pm 0.05 \pm 0.12) \times 10^{-4}$
80–120	$(3.669 \pm 0.024 \pm 0.085) \times 10^{-3}$	330–380	$(1.462 \pm 0.034 \pm 0.081) \times 10^{-4}$
120–160	$(2.653 \pm 0.019 \pm 0.071) \times 10^{-3}$	380–450	$(6.40 \pm 0.21 \pm 0.56) \times 10^{-5}$
160–200	$(1.679 \pm 0.015 \pm 0.038) \times 10^{-3}$	450–800	$(1.11 \pm 0.05 \pm 0.10) \times 10^{-5}$
200–240	$(9.62 \pm 0.10 \pm 0.33) \times 10^{-4}$...	

(Table continued)

TABLE XLII. (*Continued*)

$p_T(t_h)$ [GeV]	$\frac{1}{\sigma_{\text{norm}}} \frac{d^2\sigma}{dy(t_h)dp_T(t_h)}$ [GeV $^{-1}$]	$p_T(t_h)$ [GeV]	$\frac{1}{\sigma_{\text{norm}}} \frac{d^2\sigma}{dy(t_h)dp_T(t_h)}$ [GeV $^{-1}$]
$0.5 < y(t_h) < 1$			
0–40	$(1.440 \pm 0.017 \pm 0.072) \times 10^{-3}$	240–280	$(4.52 \pm 0.07 \pm 0.23) \times 10^{-4}$
40–80	$(3.239 \pm 0.024 \pm 0.089) \times 10^{-3}$	280–330	$(2.397 \pm 0.044 \pm 0.094) \times 10^{-4}$
80–120	$(3.266 \pm 0.023 \pm 0.054) \times 10^{-3}$	330–380	$(1.224 \pm 0.031 \pm 0.086) \times 10^{-4}$
120–160	$(2.339 \pm 0.019 \pm 0.081) \times 10^{-3}$	380–450	$(5.60 \pm 0.20 \pm 0.54) \times 10^{-5}$
160–200	$(1.426 \pm 0.014 \pm 0.039) \times 10^{-3}$	450–800	$(7.57 \pm 0.42 \pm 0.78) \times 10^{-6}$
200–240	$(8.17 \pm 0.10 \pm 0.36) \times 10^{-4}$...
$1 < y(t_h) < 1.5$			
0–40	$(1.147 \pm 0.016 \pm 0.064) \times 10^{-3}$	240–280	$(3.28 \pm 0.06 \pm 0.14) \times 10^{-4}$
40–80	$(2.574 \pm 0.023 \pm 0.074) \times 10^{-3}$	280–330	$(1.631 \pm 0.037 \pm 0.083) \times 10^{-4}$
80–120	$(2.487 \pm 0.022 \pm 0.065) \times 10^{-3}$	330–380	$(7.52 \pm 0.24 \pm 0.49) \times 10^{-5}$
120–160	$(1.765 \pm 0.017 \pm 0.065) \times 10^{-3}$	380–450	$(3.26 \pm 0.15 \pm 0.28) \times 10^{-5}$
160–200	$(1.074 \pm 0.012 \pm 0.033) \times 10^{-3}$	450–800	$(5.01 \pm 0.35 \pm 0.82) \times 10^{-6}$
200–240	$(6.11 \pm 0.09 \pm 0.18) \times 10^{-4}$...
$1.5 < y(t_h) < 2.5$			
0–40	$(6.41 \pm 0.12 \pm 0.45) \times 10^{-4}$	240–280	$(1.276 \pm 0.034 \pm 0.099) \times 10^{-4}$
40–80	$(1.356 \pm 0.016 \pm 0.055) \times 10^{-3}$	280–330	$(6.15 \pm 0.20 \pm 0.52) \times 10^{-5}$
80–120	$(1.317 \pm 0.015 \pm 0.051) \times 10^{-3}$	330–380	$(2.55 \pm 0.12 \pm 0.41) \times 10^{-5}$
120–160	$(9.14 \pm 0.12 \pm 0.56) \times 10^{-4}$	380–450	$(1.00 \pm 0.07 \pm 0.18) \times 10^{-5}$
160–200	$(5.06 \pm 0.08 \pm 0.31) \times 10^{-4}$	450–800	$(1.12 \pm 0.13 \pm 0.21) \times 10^{-6}$
200–240	$(2.54 \pm 0.05 \pm 0.14) \times 10^{-4}$...

TABLE XLIII. Double-differential cross section at the parton level as a function of $M(t\bar{t})$ vs. $|y(t\bar{t})|$ normalized to the cross section σ_{norm} in the measured in the two-dimensional range. The values are shown together with their statistical and systematic uncertainties.

$ y(t\bar{t}) $	$\frac{1}{\sigma_{\text{norm}}} \frac{d^2\sigma}{dM(t\bar{t})dy(t\bar{t})}$ [GeV $^{-1}$]	$ y(t\bar{t}) $	$\frac{1}{\sigma_{\text{norm}}} \frac{d^2\sigma}{dM(t\bar{t})dy(t\bar{t})}$ [GeV $^{-1}$]
$300 < M(t\bar{t}) < 450$			
0.0–0.2	$(2.024 \pm 0.019 \pm 0.075) \times 10^{-3}$	1.0–1.2	$(1.383 \pm 0.016 \pm 0.047) \times 10^{-3}$
0.2–0.4	$(1.968 \pm 0.015 \pm 0.067) \times 10^{-3}$	1.2–1.4	$(1.208 \pm 0.016 \pm 0.049) \times 10^{-3}$
0.4–0.6	$(1.886 \pm 0.016 \pm 0.060) \times 10^{-3}$	1.4–1.6	$(1.020 \pm 0.016 \pm 0.048) \times 10^{-3}$
0.6–0.8	$(1.799 \pm 0.016 \pm 0.070) \times 10^{-3}$	1.6–2.4	$(5.47 \pm 0.12 \pm 0.41) \times 10^{-4}$
0.8–1.0	$(1.620 \pm 0.016 \pm 0.060) \times 10^{-3}$...
$450 < M(t\bar{t}) < 625$			
0.0–0.2	$(1.624 \pm 0.015 \pm 0.029) \times 10^{-3}$	1.0–1.2	$(9.80 \pm 0.13 \pm 0.35) \times 10^{-4}$
0.2–0.4	$(1.575 \pm 0.013 \pm 0.033) \times 10^{-3}$	1.2–1.4	$(8.30 \pm 0.13 \pm 0.33) \times 10^{-4}$
0.4–0.6	$(1.472 \pm 0.013 \pm 0.034) \times 10^{-3}$	1.4–1.6	$(6.46 \pm 0.14 \pm 0.44) \times 10^{-4}$
0.6–0.8	$(1.328 \pm 0.013 \pm 0.048) \times 10^{-3}$	1.6–2.4	$(2.58 \pm 0.07 \pm 0.27) \times 10^{-4}$
0.8–1.0	$(1.177 \pm 0.013 \pm 0.029) \times 10^{-3}$...
$625 < M(t\bar{t}) < 850$			
0.0–0.2	$(4.86 \pm 0.07 \pm 0.21) \times 10^{-4}$	1.0–1.2	$(2.52 \pm 0.07 \pm 0.17) \times 10^{-4}$
0.2–0.4	$(4.63 \pm 0.07 \pm 0.13) \times 10^{-4}$	1.2–1.4	$(1.87 \pm 0.07 \pm 0.14) \times 10^{-4}$
0.4–0.6	$(4.27 \pm 0.07 \pm 0.24) \times 10^{-4}$	1.4–1.6	$(1.29 \pm 0.07 \pm 0.11) \times 10^{-4}$
0.6–0.8	$(3.80 \pm 0.07 \pm 0.22) \times 10^{-4}$	1.6–2.4	$(4.11 \pm 0.31 \pm 0.49) \times 10^{-5}$
0.8–1.0	$(3.24 \pm 0.07 \pm 0.16) \times 10^{-4}$...
$850 < M(t\bar{t}) < 2000$			
0.0–0.2	$(3.94 \pm 0.09 \pm 0.23) \times 10^{-5}$	0.8–1.0	$(2.14 \pm 0.09 \pm 0.20) \times 10^{-5}$
0.2–0.4	$(4.01 \pm 0.10 \pm 0.29) \times 10^{-5}$	1.0–1.2	$(1.83 \pm 0.10 \pm 0.18) \times 10^{-5}$
0.4–0.6	$(3.59 \pm 0.10 \pm 0.23) \times 10^{-5}$	1.2–1.4	$(1.16 \pm 0.10 \pm 0.25) \times 10^{-5}$
0.6–0.8	$(2.97 \pm 0.10 \pm 0.17) \times 10^{-5}$	1.4–2.4	$(1.85 \pm 0.24 \pm 0.35) \times 10^{-6}$

TABLE XLIV. Double-differential cross section at the parton level as a function of $p_T(t_h)$ vs. $M(t\bar{t})$ normalized to the cross section σ_{norm} in the measured in the two-dimensional range. The values are shown together with their statistical and systematic uncertainties.

$M(t\bar{t})$ [GeV]	$\frac{1}{\sigma_{\text{norm}}} \frac{d^2\sigma}{dy(t_h) dM(t\bar{t})}$ [GeV $^{-2}$]	$M(t\bar{t})$ [GeV]	$\frac{1}{\sigma_{\text{norm}}} \frac{d^2\sigma}{dy(t_h) dM(t\bar{t})}$ [GeV $^{-2}$]
$0 < p_T(t_h) < 90$			
300–360	$(9.5 \pm 0.2 \pm 2.0) \times 10^{-6}$	580–680	$(2.69 \pm 0.06 \pm 0.16) \times 10^{-6}$
360–430	$(3.33 \pm 0.02 \pm 0.11) \times 10^{-5}$	680–800	$(1.149 \pm 0.039 \pm 0.100) \times 10^{-6}$
430–500	$(1.228 \pm 0.015 \pm 0.092) \times 10^{-5}$	800–1000	$(3.95 \pm 0.21 \pm 0.64) \times 10^{-7}$
500–580	$(5.65 \pm 0.09 \pm 0.31) \times 10^{-6}$	1000–2000	$(4.7 \pm 0.6 \pm 1.4) \times 10^{-8}$
$90 < p_T(t_h) < 180$			
300–360	$(7.6 \pm 0.3 \pm 1.3) \times 10^{-7}$	580–680	$(4.72 \pm 0.07 \pm 0.30) \times 10^{-6}$
360–430	$(1.604 \pm 0.017 \pm 0.063) \times 10^{-5}$	680–800	$(2.02 \pm 0.05 \pm 0.17) \times 10^{-6}$
430–500	$(2.157 \pm 0.018 \pm 0.074) \times 10^{-5}$	800–1000	$(7.08 \pm 0.25 \pm 0.51) \times 10^{-7}$
500–580	$(1.068 \pm 0.011 \pm 0.042) \times 10^{-5}$	1000–2000	$(7.0 \pm 0.5 \pm 1.5) \times 10^{-8}$
$180 < p_T(t_h) < 270$			
300–430	$(4.3 \pm 0.2 \pm 1.1) \times 10^{-7}$	680–800	$(1.595 \pm 0.035 \pm 0.090) \times 10^{-6}$
430–500	$(2.364 \pm 0.058 \pm 0.094) \times 10^{-6}$	800–1000	$(5.53 \pm 0.17 \pm 0.46) \times 10^{-7}$
500–580	$(5.48 \pm 0.07 \pm 0.27) \times 10^{-6}$	1000–1200	$(1.80 \pm 0.11 \pm 0.26) \times 10^{-7}$
580–680	$(3.86 \pm 0.05 \pm 0.18) \times 10^{-6}$	1200–2000	$(2.16 \pm 0.24 \pm 0.59) \times 10^{-8}$
$270 < p_T(t_h) < 800$			
300–430	$(1.30 \pm 0.16 \pm 0.45) \times 10^{-8}$	680–800	$(1.91 \pm 0.04 \pm 0.12) \times 10^{-7}$
430–500	$(5.81 \pm 0.36 \pm 0.95) \times 10^{-8}$	800–1000	$(1.070 \pm 0.022 \pm 0.062) \times 10^{-7}$
500–580	$(8.1 \pm 0.4 \pm 1.2) \times 10^{-8}$	1000–1200	$(4.24 \pm 0.16 \pm 0.35) \times 10^{-8}$
580–680	$(1.48 \pm 0.04 \pm 0.11) \times 10^{-7}$	1200–2000	$(8.32 \pm 0.32 \pm 0.75) \times 10^{-9}$

APPENDIX D: TABLES OF NORMALIZED PARTICLE-LEVEL CROSS SECTIONS

The measured normalized differential cross sections at the particle level as a function of all the measured variables are listed in Tables XLV–LXII. The results are shown together with their statistical and systematic uncertainties.

TABLE XLV. Differential cross section at the particle level as a function of $p_T(t_h)$ normalized to the cross section σ_{norm} in the measured range. The values are shown together with their statistical and systematic uncertainties.

$p_T(t_h)$ [GeV]	$\frac{1}{\sigma_{\text{norm}}} \frac{d\sigma}{dp_T(t_h)}$ [GeV $^{-1}$]	$p_T(t_h)$ [GeV]	$\frac{1}{\sigma_{\text{norm}}} \frac{d\sigma}{dp_T(t_h)}$ [GeV $^{-1}$]
0–40	$(2.397 \pm 0.018 \pm 0.074) \times 10^{-3}$	240–280	$(1.027 \pm 0.010 \pm 0.021) \times 10^{-3}$
40–80	$(5.508 \pm 0.024 \pm 0.099) \times 10^{-3}$	280–330	$(5.73 \pm 0.07 \pm 0.19) \times 10^{-4}$
80–120	$(5.735 \pm 0.025 \pm 0.074) \times 10^{-3}$	330–380	$(3.00 \pm 0.05 \pm 0.12) \times 10^{-4}$
120–160	$(4.322 \pm 0.022 \pm 0.069) \times 10^{-3}$	380–430	$(1.520 \pm 0.035 \pm 0.075) \times 10^{-4}$
160–200	$(2.816 \pm 0.017 \pm 0.041) \times 10^{-3}$	430–500	$(6.80 \pm 0.22 \pm 0.41) \times 10^{-5}$
200–240	$(1.707 \pm 0.013 \pm 0.038) \times 10^{-3}$	500–800	$(1.19 \pm 0.05 \pm 0.15) \times 10^{-5}$

TABLE XLVI. Differential cross section at the particle level as a function of $|y(t_h)|$ normalized to the cross section σ_{norm} in the measured range. The values are shown together with their statistical and systematic uncertainties.

$ y(t_h) $	$\frac{1}{\sigma_{\text{norm}}} \frac{d\sigma}{d y(t_h) }$	$ y(t_h) $	$\frac{1}{\sigma_{\text{norm}}} \frac{d\sigma}{d y(t_h) }$
0.0–0.2	$0.777 \pm 0.003 \pm 0.012$	1.2–1.4	$0.3990 \pm 0.0026 \pm 0.0083$
0.2–0.4	$0.759 \pm 0.003 \pm 0.011$	1.4–1.6	$0.2928 \pm 0.0023 \pm 0.0096$
0.4–0.6	$0.7093 \pm 0.0033 \pm 0.0081$	1.6–1.8	$0.1924 \pm 0.0019 \pm 0.0065$
0.6–0.8	$0.6600 \pm 0.0032 \pm 0.0095$	1.8–2.0	$0.0999 \pm 0.0014 \pm 0.0041$
0.8–1.0	$0.5755 \pm 0.0030 \pm 0.0093$	2.0–2.5	$0.01485 \pm 0.00035 \pm 0.00087$
1.0–1.2	$0.4977 \pm 0.0028 \pm 0.0048$...

TABLE XLVII. Differential cross section at the particle level as a function of $p_T(t_\ell)$ normalized to the cross section σ_{norm} in the measured range. The values are shown together with their statistical and systematic uncertainties.

$p_T(t_\ell)$ [GeV]	$\frac{1}{\sigma_{\text{norm}}} \frac{d\sigma}{dp_T(t_\ell)}$ [GeV $^{-1}$]	$p_T(t_\ell)$ [GeV]	$\frac{1}{\sigma_{\text{norm}}} \frac{d\sigma}{dp_T(t_\ell)}$ [GeV $^{-1}$]
0–40	$(2.212 \pm 0.035 \pm 0.090) \times 10^{-3}$	240–280	$(1.105 \pm 0.023 \pm 0.066) \times 10^{-3}$
40–80	$(5.23 \pm 0.06 \pm 0.13) \times 10^{-3}$	280–330	$(6.33 \pm 0.14 \pm 0.29) \times 10^{-4}$
80–120	$(5.39 \pm 0.06 \pm 0.12) \times 10^{-3}$	330–380	$(3.23 \pm 0.11 \pm 0.29) \times 10^{-4}$
120–160	$(4.619 \pm 0.048 \pm 0.082) \times 10^{-3}$	380–430	$(1.63 \pm 0.09 \pm 0.23) \times 10^{-4}$
160–200	$(2.857 \pm 0.037 \pm 0.079) \times 10^{-3}$	430–500	$(8.46 \pm 0.42 \pm 0.95) \times 10^{-5}$
200–240	$(1.935 \pm 0.030 \pm 0.070) \times 10^{-3}$	500–800	$(1.43 \pm 0.05 \pm 0.13) \times 10^{-5}$

TABLE XLVIII. Differential cross section at the particle level as a function of $|y(t_\ell)|$ normalized to the cross section σ_{norm} in the measured range. The values are shown together with their statistical and systematic uncertainties.

$ y(t_\ell) $	$\frac{1}{\sigma_{\text{norm}}} \frac{d\sigma}{dy(t_\ell)}$	$ y(t_\ell) $	$\frac{1}{\sigma_{\text{norm}}} \frac{d\sigma}{dy(t_\ell)}$
0.0–0.2	$0.735 \pm 0.007 \pm 0.015$	1.2–1.4	$0.412 \pm 0.007 \pm 0.018$
0.2–0.4	$0.717 \pm 0.009 \pm 0.012$	1.4–1.6	$0.283 \pm 0.006 \pm 0.017$
0.4–0.6	$0.700 \pm 0.009 \pm 0.012$	1.6–1.8	$0.214 \pm 0.005 \pm 0.012$
0.6–0.8	$0.651 \pm 0.009 \pm 0.021$	1.8–2.0	$0.129 \pm 0.005 \pm 0.012$
0.8–1.0	$0.575 \pm 0.008 \pm 0.016$	2.0–2.5	$0.0344 \pm 0.0015 \pm 0.0036$
1.0–1.2	$0.499 \pm 0.008 \pm 0.012$...	

TABLE XLIX. Differential cross section at the particle level as a function of $p_T(t\bar{t})$ normalized to the cross section σ_{norm} in the measured range. The values are shown together with their statistical and systematic uncertainties.

$p_T(t\bar{t})$ [GeV]	$\frac{1}{\sigma_{\text{norm}}} \frac{d\sigma}{dp_T(t\bar{t})}$ [GeV $^{-1}$]	$p_T(t\bar{t})$ [GeV]	$\frac{1}{\sigma_{\text{norm}}} \frac{d\sigma}{dp_T(t\bar{t})}$ [GeV $^{-1}$]
0–40	$0.01126 \pm 0.00004 \pm 0.00024$	220–300	$(3.87 \pm 0.08 \pm 0.17) \times 10^{-4}$
40–80	$(6.40 \pm 0.06 \pm 0.22) \times 10^{-3}$	300–380	$(1.407 \pm 0.049 \pm 0.088) \times 10^{-4}$
80–150	$(2.520 \pm 0.022 \pm 0.068) \times 10^{-3}$	380–500	$(5.81 \pm 0.20 \pm 0.30) \times 10^{-5}$
150–220	$(9.26 \pm 0.13 \pm 0.25) \times 10^{-4}$	500–1000	$(6.56 \pm 0.25 \pm 0.39) \times 10^{-6}$

TABLE L. Differential cross section at the particle level as a function of $|y(t\bar{t})|$ normalized to the cross section σ_{norm} in the measured range. The values are shown together with their statistical and systematic uncertainties.

$ y(t\bar{t}) $	$\frac{1}{\sigma_{\text{norm}}} \frac{d\sigma}{dy(t\bar{t})}$	$ y(t\bar{t}) $	$\frac{1}{\sigma_{\text{norm}}} \frac{d\sigma}{dy(t\bar{t})}$
0.0–0.2	$0.987 \pm 0.005 \pm 0.014$	1.0–1.2	$0.4099 \pm 0.0039 \pm 0.0092$
0.2–0.4	$0.933 \pm 0.006 \pm 0.015$	1.2–1.4	$0.2799 \pm 0.0033 \pm 0.0090$
0.4–0.6	$0.839 \pm 0.005 \pm 0.014$	1.4–1.6	$0.1559 \pm 0.0026 \pm 0.0062$
0.6–0.8	$0.723 \pm 0.005 \pm 0.015$	1.6–1.8	$0.0673 \pm 0.0018 \pm 0.0062$
0.8–1.0	$0.577 \pm 0.005 \pm 0.011$	1.8–2.4	$(9.5 \pm 0.4 \pm 1.1) \times 10^{-3}$

TABLE LI. Differential cross section at the particle level as a function of $M(t\bar{t})$ normalized to the cross section σ_{norm} in the measured range. The values are shown together with their statistical and systematic uncertainties.

$M(t\bar{t})$ [GeV]	$\frac{1}{\sigma_{\text{norm}}} \frac{d\sigma}{dM(t\bar{t})}$ [GeV $^{-1}$]	$M(t\bar{t})$ [GeV]	$\frac{1}{\sigma_{\text{norm}}} \frac{d\sigma}{dM(t\bar{t})}$ [GeV $^{-1}$]
300–360	$(1.12 \pm 0.02 \pm 0.14) \times 10^{-3}$	680–800	$(8.11 \pm 0.08 \pm 0.21) \times 10^{-4}$
360–430	$(2.941 \pm 0.018 \pm 0.072) \times 10^{-3}$	800–1000	$(3.62 \pm 0.04 \pm 0.11) \times 10^{-4}$
430–500	$(2.807 \pm 0.019 \pm 0.071) \times 10^{-3}$	1000–1200	$(1.311 \pm 0.031 \pm 0.058) \times 10^{-4}$
500–580	$(2.165 \pm 0.015 \pm 0.038) \times 10^{-3}$	1200–1500	$(4.45 \pm 0.16 \pm 0.31) \times 10^{-5}$
580–680	$(1.417 \pm 0.011 \pm 0.027) \times 10^{-3}$	1500–2500	$(6.14 \pm 0.36 \pm 0.63) \times 10^{-6}$

TABLE LII. Cross sections at the particle level for different numbers of additional jets normalized to the cross section σ_{norm} in the measured range. The values are shown together with their statistical and systematic uncertainties.

Additional jets	$\frac{1}{\sigma_{\text{norm}}} \sigma$	Additional jets	$\frac{1}{\sigma_{\text{norm}}} \sigma$
0	$0.5586 \pm 0.0010 \pm 0.0099$	3	$0.0343 \pm 0.0005 \pm 0.0019$
1	$0.2897 \pm 0.0012 \pm 0.0043$	4	$(9.24 \pm 0.25 \pm 0.92) \times 10^{-3}$
2	$0.1046 \pm 0.0008 \pm 0.0041$	≥ 5	$(3.58 \pm 0.12 \pm 0.38) \times 10^{-3}$

TABLE LIII. Double-differential cross section at the particle level as a function of $|y(t_h)|$ vs. $p_T(t_h)$ normalized to the cross section σ_{norm} in the measured in the two-dimensional range. The values are shown together with their statistical and systematic uncertainties.

$p_T(t_h)$ [GeV]	$\frac{1}{\sigma_{\text{norm}}} \frac{d^2\sigma}{d y(t_h) dp_T(t_h)}$ [GeV $^{-1}$]	$p_T(t_h)$ [GeV]	$\frac{1}{\sigma_{\text{norm}}} \frac{d^2\sigma}{d y(t_h) dp_T(t_h)}$ [GeV $^{-1}$]
$0 < y(t_h) < 0.5$			
0–40	$(1.787 \pm 0.016 \pm 0.062) \times 10^{-3}$	240–280	$(7.89 \pm 0.10 \pm 0.21) \times 10^{-4}$
40–80	$(4.16 \pm 0.02 \pm 0.11) \times 10^{-3}$	280–330	$(4.35 \pm 0.07 \pm 0.17) \times 10^{-4}$
80–120	$(4.371 \pm 0.024 \pm 0.087) \times 10^{-3}$	330–380	$(2.330 \pm 0.050 \pm 0.095) \times 10^{-4}$
120–160	$(3.261 \pm 0.021 \pm 0.063) \times 10^{-3}$	380–450	$(1.046 \pm 0.030 \pm 0.067) \times 10^{-4}$
160–200	$(2.147 \pm 0.017 \pm 0.037) \times 10^{-3}$	450–800	$(1.64 \pm 0.06 \pm 0.13) \times 10^{-5}$
200–240	$(1.288 \pm 0.013 \pm 0.036) \times 10^{-3}$...
$0.5 < y(t_h) < 1$			
0–40	$(1.512 \pm 0.015 \pm 0.078) \times 10^{-3}$	240–280	$(6.32 \pm 0.09 \pm 0.21) \times 10^{-4}$
40–80	$(3.525 \pm 0.022 \pm 0.068) \times 10^{-3}$	280–330	$(3.61 \pm 0.06 \pm 0.15) \times 10^{-4}$
80–120	$(3.680 \pm 0.022 \pm 0.039) \times 10^{-3}$	330–380	$(1.89 \pm 0.04 \pm 0.10) \times 10^{-4}$
120–160	$(2.748 \pm 0.019 \pm 0.076) \times 10^{-3}$	380–450	$(8.88 \pm 0.28 \pm 0.58) \times 10^{-5}$
160–200	$(1.749 \pm 0.015 \pm 0.036) \times 10^{-3}$	450–800	$(1.157 \pm 0.051 \pm 0.078) \times 10^{-5}$
200–240	$(1.059 \pm 0.011 \pm 0.040) \times 10^{-3}$...
$1 < y(t_h) < 1.5$			
0–40	$(1.005 \pm 0.013 \pm 0.043) \times 10^{-3}$	240–280	$(4.30 \pm 0.07 \pm 0.19) \times 10^{-4}$
40–80	$(2.341 \pm 0.019 \pm 0.061) \times 10^{-3}$	280–330	$(2.375 \pm 0.048 \pm 0.098) \times 10^{-4}$
80–120	$(2.395 \pm 0.019 \pm 0.053) \times 10^{-3}$	330–380	$(1.182 \pm 0.034 \pm 0.070) \times 10^{-4}$
120–160	$(1.836 \pm 0.016 \pm 0.050) \times 10^{-3}$	380–450	$(5.12 \pm 0.20 \pm 0.41) \times 10^{-5}$
160–200	$(1.191 \pm 0.013 \pm 0.043) \times 10^{-3}$	450–800	$(7.4 \pm 0.4 \pm 1.0) \times 10^{-6}$
200–240	$(7.40 \pm 0.09 \pm 0.23) \times 10^{-4}$...
$1.5 < y(t_h) < 2.5$			
0–40	$(2.15 \pm 0.05 \pm 0.16) \times 10^{-4}$	240–280	$(9.96 \pm 0.25 \pm 0.74) \times 10^{-5}$
40–80	$(4.81 \pm 0.06 \pm 0.21) \times 10^{-4}$	280–330	$(5.63 \pm 0.18 \pm 0.55) \times 10^{-5}$
80–120	$(5.31 \pm 0.07 \pm 0.25) \times 10^{-4}$	330–380	$(2.75 \pm 0.12 \pm 0.38) \times 10^{-5}$
120–160	$(4.23 \pm 0.06 \pm 0.27) \times 10^{-4}$	380–450	$(1.19 \pm 0.07 \pm 0.21) \times 10^{-5}$
160–200	$(2.74 \pm 0.04 \pm 0.15) \times 10^{-4}$	450–800	$(1.17 \pm 0.12 \pm 0.29) \times 10^{-6}$
200–240	$(1.651 \pm 0.033 \pm 0.089) \times 10^{-4}$...

TABLE LIV. Double-differential cross section at the particle level as a function of $M(t\bar{t})$ vs. $|y(t\bar{t})|$ normalized to the cross section σ_{norm} in the measured in the two-dimensional range. The values are shown together with their statistical and systematic uncertainties.

$ y(t\bar{t}) $	$\frac{1}{\sigma_{\text{norm}}} \frac{d^2\sigma}{dM(t\bar{t})d y(t\bar{t}) }$ [GeV $^{-1}$]	$ y(t\bar{t}) $	$\frac{1}{\sigma_{\text{norm}}} \frac{d^2\sigma}{dM(t\bar{t})d y(t\bar{t}) }$ [GeV $^{-1}$]
$300 < M(t\bar{t}) < 450$			
0.0–0.2	$(1.855 \pm 0.017 \pm 0.059) \times 10^{-3}$	1.0–1.2	$(1.083 \pm 0.012 \pm 0.035) \times 10^{-3}$
0.2–0.4	$(1.800 \pm 0.013 \pm 0.050) \times 10^{-3}$	1.2–1.4	$(8.15 \pm 0.11 \pm 0.28) \times 10^{-4}$
0.4–0.6	$(1.719 \pm 0.014 \pm 0.051) \times 10^{-3}$	1.4–1.6	$(5.09 \pm 0.09 \pm 0.22) \times 10^{-4}$
0.6–0.8	$(1.611 \pm 0.014 \pm 0.068) \times 10^{-3}$	1.6–2.4	$(8.94 \pm 0.23 \pm 0.84) \times 10^{-5}$
0.8–1.0	$(1.378 \pm 0.013 \pm 0.049) \times 10^{-3}$...

(Table continued)

TABLE LIV. (*Continued*)

$ y(t\bar{t}) $	$\frac{1}{\sigma_{\text{norm}}} \frac{d^2\sigma}{dM(t\bar{t})dy(t\bar{t})}$ [GeV $^{-1}$]	$ y(t\bar{t}) $	$\frac{1}{\sigma_{\text{norm}}} \frac{d^2\sigma}{dM(t\bar{t})dy(t\bar{t})}$ [GeV $^{-1}$]
$450 < M(t\bar{t}) < 625$			
0.0–0.2	$(2.139 \pm 0.016 \pm 0.035) \times 10^{-3}$	1.0–1.2	$(9.23 \pm 0.11 \pm 0.34) \times 10^{-4}$
0.2–0.4	$(2.036 \pm 0.014 \pm 0.029) \times 10^{-3}$	1.2–1.4	$(6.13 \pm 0.09 \pm 0.24) \times 10^{-4}$
0.4–0.6	$(1.848 \pm 0.014 \pm 0.031) \times 10^{-3}$	1.4–1.6	$(3.33 \pm 0.07 \pm 0.20) \times 10^{-4}$
0.6–0.8	$(1.586 \pm 0.013 \pm 0.034) \times 10^{-3}$	1.6–2.4	$(4.47 \pm 0.14 \pm 0.44) \times 10^{-5}$
0.8–1.0	$(1.279 \pm 0.012 \pm 0.029) \times 10^{-3}$...
$625 < M(t\bar{t}) < 850$			
0.0–0.2	$(9.57 \pm 0.10 \pm 0.20) \times 10^{-4}$	1.0–1.2	$(2.92 \pm 0.06 \pm 0.13) \times 10^{-4}$
0.2–0.4	$(8.84 \pm 0.09 \pm 0.17) \times 10^{-4}$	1.2–1.4	$(1.65 \pm 0.04 \pm 0.14) \times 10^{-4}$
0.4–0.6	$(7.60 \pm 0.08 \pm 0.31) \times 10^{-4}$	1.4–1.6	$(8.00 \pm 0.32 \pm 0.52) \times 10^{-5}$
0.6–0.8	$(6.14 \pm 0.08 \pm 0.28) \times 10^{-4}$	1.6–2.4	$(1.013 \pm 0.065 \pm 0.098) \times 10^{-5}$
0.8–1.0	$(4.64 \pm 0.07 \pm 0.17) \times 10^{-4}$...
$850 < M(t\bar{t}) < 2000$			
0.0–0.2	$(1.006 \pm 0.017 \pm 0.036) \times 10^{-4}$	0.8–1.0	$(3.48 \pm 0.10 \pm 0.20) \times 10^{-5}$
0.2–0.4	$(9.44 \pm 0.16 \pm 0.45) \times 10^{-5}$	1.0–1.2	$(2.12 \pm 0.08 \pm 0.13) \times 10^{-5}$
0.4–0.6	$(7.71 \pm 0.15 \pm 0.32) \times 10^{-5}$	1.2–1.4	$(1.04 \pm 0.06 \pm 0.12) \times 10^{-5}$
0.6–0.8	$(5.62 \pm 0.13 \pm 0.28) \times 10^{-5}$	1.4–2.4	$(9.2 \pm 0.9 \pm 1.5) \times 10^{-7}$

TABLE LV. Double-differential cross section at the particle level as a function of $p_T(t_h)$ vs. $M(t\bar{t})$ normalized to the cross section σ_{norm} in the measured in the two-dimensional range. The values are shown together with their statistical and systematic uncertainties.

$M(t\bar{t})$ [GeV]	$\frac{1}{\sigma_{\text{norm}}} \frac{d^2\sigma}{d y(t_h) dM(t\bar{t})}$ [GeV $^{-2}$]	$M(t\bar{t})$ [GeV]	$\frac{1}{\sigma_{\text{norm}}} \frac{d^2\sigma}{d y(t_h) dM(t\bar{t})}$ [GeV $^{-2}$]
$0 < p_T(t_h) < 90$			
300–360	$(1.08 \pm 0.01 \pm 0.11) \times 10^{-5}$	580–680	$(3.55 \pm 0.04 \pm 0.17) \times 10^{-6}$
360–430	$(2.090 \pm 0.012 \pm 0.050) \times 10^{-5}$	680–800	$(1.675 \pm 0.028 \pm 0.086) \times 10^{-6}$
430–500	$(1.165 \pm 0.010 \pm 0.032) \times 10^{-5}$	800–1000	$(6.21 \pm 0.16 \pm 0.45) \times 10^{-7}$
500–580	$(6.58 \pm 0.06 \pm 0.18) \times 10^{-6}$	1000–2000	$(6.1 \pm 0.3 \pm 1.0) \times 10^{-8}$
$90 < p_T(t_h) < 180$			
300–360	$(1.18 \pm 0.03 \pm 0.12) \times 10^{-6}$	580–680	$(6.61 \pm 0.06 \pm 0.18) \times 10^{-6}$
360–430	$(1.111 \pm 0.010 \pm 0.031) \times 10^{-5}$	680–800	$(3.32 \pm 0.04 \pm 0.17) \times 10^{-6}$
430–500	$(1.753 \pm 0.012 \pm 0.049) \times 10^{-5}$	800–1000	$(1.313 \pm 0.023 \pm 0.067) \times 10^{-6}$
500–580	$(1.221 \pm 0.009 \pm 0.031) \times 10^{-5}$	1000–2000	$(1.27 \pm 0.05 \pm 0.15) \times 10^{-7}$
$180 < p_T(t_h) < 270$			
300–430	$(2.85 \pm 0.13 \pm 0.63) \times 10^{-7}$	680–800	$(2.622 \pm 0.037 \pm 0.097) \times 10^{-6}$
430–500	$(1.81 \pm 0.04 \pm 0.10) \times 10^{-6}$	800–1000	$(1.102 \pm 0.021 \pm 0.061) \times 10^{-6}$
500–580	$(4.77 \pm 0.06 \pm 0.16) \times 10^{-6}$	1000–1200	$(3.82 \pm 0.14 \pm 0.34) \times 10^{-7}$
580–680	$(4.69 \pm 0.05 \pm 0.17) \times 10^{-6}$	1200–2000	$(5.56 \pm 0.35 \pm 0.83) \times 10^{-8}$
$270 < p_T(t_h) < 800$			
300–430	$(6.2 \pm 0.7 \pm 2.0) \times 10^{-9}$	680–800	$(2.492 \pm 0.046 \pm 0.093) \times 10^{-7}$
430–500	$(4.15 \pm 0.24 \pm 0.68) \times 10^{-8}$	800–1000	$(1.850 \pm 0.030 \pm 0.083) \times 10^{-7}$
500–580	$(7.6 \pm 0.3 \pm 1.2) \times 10^{-8}$	1000–1200	$(8.82 \pm 0.25 \pm 0.49) \times 10^{-8}$
580–680	$(1.530 \pm 0.040 \pm 0.092) \times 10^{-7}$	1200–2000	$(2.09 \pm 0.06 \pm 0.14) \times 10^{-8}$

TABLE LVI. Differential cross sections at the particle level as a function of $p_T(t_h)$ for different numbers of additional jets normalized to the sum of the cross sections σ_{norm} in the measured ranges. The values are shown together with their statistical and systematic uncertainties.

$p_T(t_h)$ [GeV]	$\frac{1}{\sigma_{\text{norm}}} \frac{d\sigma}{dp_T(t_h)}$ [GeV $^{-1}$]	$p_T(t_h)$ [GeV]	$\frac{1}{\sigma_{\text{norm}}} \frac{d\sigma}{dp_T(t_h)}$ [GeV $^{-1}$]
Additional jets: 0			
0–40	$(1.440 \pm 0.012 \pm 0.072) \times 10^{-3}$	240–280	$(4.78 \pm 0.06 \pm 0.19) \times 10^{-4}$
40–80	$(3.261 \pm 0.016 \pm 0.090) \times 10^{-3}$	280–330	$(2.46 \pm 0.04 \pm 0.13) \times 10^{-4}$
80–120	$(3.367 \pm 0.016 \pm 0.091) \times 10^{-3}$	330–380	$(1.235 \pm 0.027 \pm 0.078) \times 10^{-4}$
120–160	$(2.455 \pm 0.014 \pm 0.051) \times 10^{-3}$	380–450	$(5.08 \pm 0.16 \pm 0.47) \times 10^{-5}$
160–200	$(1.512 \pm 0.010 \pm 0.036) \times 10^{-3}$	450–800	$(6.88 \pm 0.31 \pm 0.64) \times 10^{-6}$
200–240	$(8.57 \pm 0.08 \pm 0.34) \times 10^{-4}$...
Additional jets: 1			
0–40	$(6.38 \pm 0.06 \pm 0.38) \times 10^{-4}$	240–280	$(3.35 \pm 0.04 \pm 0.14) \times 10^{-4}$
40–80	$(1.515 \pm 0.009 \pm 0.071) \times 10^{-3}$	280–330	$(1.897 \pm 0.030 \pm 0.083) \times 10^{-4}$
80–120	$(1.598 \pm 0.009 \pm 0.036) \times 10^{-3}$	330–380	$(9.43 \pm 0.21 \pm 0.66) \times 10^{-5}$
120–160	$(1.251 \pm 0.008 \pm 0.029) \times 10^{-3}$	380–450	$(4.38 \pm 0.13 \pm 0.29) \times 10^{-5}$
160–200	$(8.44 \pm 0.07 \pm 0.22) \times 10^{-4}$	450–800	$(6.31 \pm 0.27 \pm 0.56) \times 10^{-6}$
200–240	$(5.41 \pm 0.05 \pm 0.26) \times 10^{-4}$...
Additional jets: 2			
0–40	$(2.09 \pm 0.02 \pm 0.17) \times 10^{-4}$	240–280	$(1.421 \pm 0.025 \pm 0.072) \times 10^{-4}$
40–80	$(5.08 \pm 0.04 \pm 0.23) \times 10^{-4}$	280–330	$(8.82 \pm 0.18 \pm 0.65) \times 10^{-5}$
80–120	$(5.58 \pm 0.04 \pm 0.25) \times 10^{-4}$	330–380	$(4.96 \pm 0.14 \pm 0.38) \times 10^{-5}$
120–160	$(4.47 \pm 0.04 \pm 0.24) \times 10^{-4}$	380–450	$(2.34 \pm 0.09 \pm 0.15) \times 10^{-5}$
160–200	$(3.23 \pm 0.04 \pm 0.15) \times 10^{-4}$	450–800	$(3.18 \pm 0.18 \pm 0.31) \times 10^{-6}$
200–240	$(2.16 \pm 0.03 \pm 0.15) \times 10^{-4}$...
Additional jets: ≥ 3			
0–40	$(8.52 \pm 0.14 \pm 0.55) \times 10^{-5}$	240–280	$(6.99 \pm 0.16 \pm 0.70) \times 10^{-5}$
40–80	$(2.07 \pm 0.03 \pm 0.17) \times 10^{-4}$	280–330	$(4.83 \pm 0.13 \pm 0.50) \times 10^{-5}$
80–120	$(2.28 \pm 0.03 \pm 0.15) \times 10^{-4}$	330–380	$(3.03 \pm 0.11 \pm 0.27) \times 10^{-5}$
120–160	$(1.90 \pm 0.02 \pm 0.14) \times 10^{-4}$	380–450	$(1.59 \pm 0.07 \pm 0.14) \times 10^{-5}$
160–200	$(1.40 \pm 0.02 \pm 0.11) \times 10^{-4}$	450–800	$(2.38 \pm 0.15 \pm 0.34) \times 10^{-6}$
200–240	$(9.84 \pm 0.19 \pm 0.73) \times 10^{-5}$...

TABLE LVII. Differential cross sections at the particle level as a function of $p_T(t\bar{t})$ for different numbers of additional jets normalized to the sum of the cross sections σ_{norm} in the measured ranges. The values are shown together with their statistical and systematic uncertainties.

$p_T(t\bar{t})$ [GeV]	$\frac{1}{\sigma_{\text{norm}}} \frac{d\sigma}{dp_T(t\bar{t})}$ [GeV $^{-1}$]	$p_T(t\bar{t})$ [GeV]	$\frac{1}{\sigma_{\text{norm}}} \frac{d\sigma}{dp_T(t\bar{t})}$ [GeV $^{-1}$]
Additional jets: 0			
0–40	$(9.77 \pm 0.04 \pm 0.22) \times 10^{-3}$	150–220	$(7.1 \pm 0.4 \pm 1.0) \times 10^{-5}$
40–80	$(3.18 \pm 0.04 \pm 0.26) \times 10^{-3}$	220–300	$(1.05 \pm 0.15 \pm 0.30) \times 10^{-5}$
80–150	$(4.77 \pm 0.11 \pm 0.37) \times 10^{-4}$	300–1000	$(3.7 \pm 0.7 \pm 1.1) \times 10^{-7}$
Additional jets: 1			
0–40	$(1.166 \pm 0.022 \pm 0.097) \times 10^{-3}$	220–300	$(1.533 \pm 0.050 \pm 0.097) \times 10^{-4}$
40–80	$(2.531 \pm 0.027 \pm 0.074) \times 10^{-3}$	300–380	$(5.71 \pm 0.30 \pm 0.93) \times 10^{-5}$
80–150	$(1.292 \pm 0.016 \pm 0.024) \times 10^{-3}$	380–1000	$(6.36 \pm 0.27 \pm 0.44) \times 10^{-6}$
150–220	$(4.50 \pm 0.09 \pm 0.16) \times 10^{-4}$...
Additional jets: 2			
0–40	$(2.47 \pm 0.10 \pm 0.37) \times 10^{-4}$	220–300	$(1.336 \pm 0.048 \pm 0.098) \times 10^{-4}$
40–80	$(5.39 \pm 0.12 \pm 0.37) \times 10^{-4}$	300–380	$(4.80 \pm 0.30 \pm 0.92) \times 10^{-5}$
80–150	$(5.26 \pm 0.10 \pm 0.32) \times 10^{-4}$	380–500	$(1.87 \pm 0.13 \pm 0.18) \times 10^{-5}$
150–220	$(2.65 \pm 0.08 \pm 0.17) \times 10^{-4}$	500–1000	$(1.75 \pm 0.18 \pm 0.25) \times 10^{-6}$

(Table continued)

TABLE LVII. (*Continued*)

$p_T(t\bar{t})$ [GeV]	$\frac{1}{\sigma_{\text{norm}}} \frac{d\sigma}{dp_T(t\bar{t})}$ [GeV $^{-1}$]	$p_T(t\bar{t})$ [GeV]	$\frac{1}{\sigma_{\text{norm}}} \frac{d\sigma}{dp_T(t\bar{t})}$ [GeV $^{-1}$]
Additional jets: ≥ 3			
0–40	$(6.6 \pm 0.4 \pm 1.7) \times 10^{-5}$	220–300	$(9.3 \pm 0.4 \pm 1.1) \times 10^{-5}$
40–80	$(1.83 \pm 0.07 \pm 0.21) \times 10^{-4}$	300–380	$(3.55 \pm 0.25 \pm 0.60) \times 10^{-5}$
80–150	$(1.98 \pm 0.06 \pm 0.18) \times 10^{-4}$	380–500	$(1.71 \pm 0.12 \pm 0.28) \times 10^{-5}$
150–220	$(1.45 \pm 0.05 \pm 0.12) \times 10^{-4}$	500–1000	$(2.36 \pm 0.17 \pm 0.26) \times 10^{-6}$

TABLE LVIII. Differential cross sections at the particle level as a function of $M(t\bar{t})$ for different numbers of additional jets normalized to the sum of the cross sections σ_{norm} in the measured ranges. The values are shown together with their statistical and systematic uncertainties.

$M(t\bar{t})$ [GeV]	$\frac{1}{\sigma_{\text{norm}}} \frac{d\sigma}{dM(t\bar{t})}$ [GeV $^{-1}$]	$M(t\bar{t})$ [GeV]	$\frac{1}{\sigma_{\text{norm}}} \frac{d\sigma}{dM(t\bar{t})}$ [GeV $^{-1}$]
Additional jets: 0			
300–360	$(6.43 \pm 0.09 \pm 0.78) \times 10^{-4}$	680–800	$(4.62 \pm 0.04 \pm 0.11) \times 10^{-4}$
360–430	$(1.615 \pm 0.010 \pm 0.053) \times 10^{-3}$	800–1000	$(2.101 \pm 0.025 \pm 0.087) \times 10^{-4}$
430–500	$(1.534 \pm 0.010 \pm 0.032) \times 10^{-3}$	1000–1200	$(7.72 \pm 0.18 \pm 0.62) \times 10^{-5}$
500–580	$(1.190 \pm 0.008 \pm 0.026) \times 10^{-3}$	1200–2000	$(1.46 \pm 0.05 \pm 0.10) \times 10^{-5}$
580–680	$(7.92 \pm 0.06 \pm 0.24) \times 10^{-4}$
Additional jets: 1			
300–360	$(3.05 \pm 0.04 \pm 0.32) \times 10^{-4}$	680–800	$(2.296 \pm 0.027 \pm 0.083) \times 10^{-4}$
360–430	$(8.79 \pm 0.07 \pm 0.32) \times 10^{-4}$	800–1000	$(9.99 \pm 0.15 \pm 0.44) \times 10^{-5}$
430–500	$(8.43 \pm 0.06 \pm 0.31) \times 10^{-4}$	1000–1200	$(3.58 \pm 0.10 \pm 0.31) \times 10^{-5}$
500–580	$(6.31 \pm 0.05 \pm 0.18) \times 10^{-4}$	1200–2000	$(5.67 \pm 0.25 \pm 0.54) \times 10^{-6}$
580–680	$(4.10 \pm 0.04 \pm 0.17) \times 10^{-4}$
Additional jets: 2			
300–360	$(1.008 \pm 0.021 \pm 0.068) \times 10^{-4}$	680–800	$(8.24 \pm 0.15 \pm 0.59) \times 10^{-5}$
360–430	$(3.27 \pm 0.04 \pm 0.14) \times 10^{-4}$	800–1000	$(3.59 \pm 0.09 \pm 0.17) \times 10^{-5}$
430–500	$(3.12 \pm 0.03 \pm 0.22) \times 10^{-4}$	1000–1200	$(1.25 \pm 0.05 \pm 0.12) \times 10^{-5}$
500–580	$(2.34 \pm 0.03 \pm 0.13) \times 10^{-4}$	1200–2000	$(1.99 \pm 0.13 \pm 0.26) \times 10^{-6}$
580–680	$(1.481 \pm 0.021 \pm 0.094) \times 10^{-4}$
Additional jets: ≥ 3			
300–360	$(3.72 \pm 0.11 \pm 0.44) \times 10^{-5}$	680–800	$(3.67 \pm 0.09 \pm 0.44) \times 10^{-5}$
360–430	$(1.40 \pm 0.02 \pm 0.11) \times 10^{-4}$	800–1000	$(1.68 \pm 0.06 \pm 0.25) \times 10^{-5}$
430–500	$(1.42 \pm 0.02 \pm 0.12) \times 10^{-4}$	1000–1200	$(6.16 \pm 0.36 \pm 0.71) \times 10^{-6}$
500–580	$(1.050 \pm 0.017 \pm 0.082) \times 10^{-4}$	1200–2000	$(9.5 \pm 0.9 \pm 2.8) \times 10^{-7}$
580–680	$(6.73 \pm 0.13 \pm 0.62) \times 10^{-5}$

TABLE LIX. Differential cross sections at the particle level as a function of $p_T(\text{jet})$ of jets normalized to the sum of the cross sections σ_{norm} of all jets in the measured ranges. The values are shown together with their statistical and systematic uncertainties.

$p_T(\text{jet})$ [GeV]	$\frac{1}{\sigma_{\text{norm}}} \frac{d\sigma}{dp_T(\text{jet})}$ [GeV $^{-1}$]	$p_T(\text{jet})$ [GeV]	$\frac{1}{\sigma_{\text{norm}}} \frac{d\sigma}{dp_T(\text{jet})}$ [GeV $^{-1}$]
$p_T(b_\ell)$			
30–50	$(3.155 \pm 0.013 \pm 0.070) \times 10^{-3}$	100–150	$(7.13 \pm 0.03 \pm 0.12) \times 10^{-4}$
50–75	$(2.583 \pm 0.010 \pm 0.029) \times 10^{-3}$	150–200	$(2.221 \pm 0.021 \pm 0.070) \times 10^{-4}$
75–100	$(1.611 \pm 0.008 \pm 0.023) \times 10^{-3}$	200–350	$(3.29 \pm 0.04 \pm 0.14) \times 10^{-5}$
$p_T(b_h)$			
30–50	$(2.966 \pm 0.013 \pm 0.088) \times 10^{-3}$	100–150	$(7.28 \pm 0.04 \pm 0.13) \times 10^{-4}$
50–75	$(2.665 \pm 0.010 \pm 0.031) \times 10^{-3}$	150–200	$(2.211 \pm 0.022 \pm 0.067) \times 10^{-4}$
75–100	$(1.698 \pm 0.009 \pm 0.025) \times 10^{-3}$	200–350	$(3.81 \pm 0.05 \pm 0.14) \times 10^{-5}$

(Table continued)

TABLE LIX. (*Continued*)

$p_T(\text{jet})$ [GeV]	$\frac{1}{\sigma_{\text{norm}}} \frac{d\sigma}{dp_T(\text{jet})}$ [GeV $^{-1}$]	$p_T(j_{W1})$	$\frac{1}{\sigma_{\text{norm}}} \frac{d\sigma}{dp_T(\text{jet})}$ [GeV $^{-1}$]
30–50	$(2.974 \pm 0.013 \pm 0.090) \times 10^{-3}$	100–150	$(7.369 \pm 0.039 \pm 0.097) \times 10^{-4}$
50–75	$(2.987 \pm 0.011 \pm 0.034) \times 10^{-3}$	150–200	$(2.290 \pm 0.024 \pm 0.075) \times 10^{-4}$
75–100	$(1.748 \pm 0.009 \pm 0.026) \times 10^{-3}$	200–350	$(4.39 \pm 0.06 \pm 0.22) \times 10^{-5}$
		$p_T(j_{W2})$	
30–50	$(5.977 \pm 0.015 \pm 0.070) \times 10^{-3}$	75–100	$(4.23 \pm 0.04 \pm 0.12) \times 10^{-4}$
50–75	$(1.531 \pm 0.008 \pm 0.039) \times 10^{-3}$	100–250	$(3.52 \pm 0.06 \pm 0.16) \times 10^{-5}$
		$p_T(j_1)$	
30–50	$(1.417 \pm 0.008 \pm 0.043) \times 10^{-3}$	150–175	$(2.118 \pm 0.026 \pm 0.056) \times 10^{-4}$
50–75	$(8.73 \pm 0.06 \pm 0.27) \times 10^{-4}$	175–200	$(1.491 \pm 0.021 \pm 0.042) \times 10^{-4}$
75–100	$(6.01 \pm 0.05 \pm 0.15) \times 10^{-4}$	200–250	$(9.88 \pm 0.14 \pm 0.33) \times 10^{-5}$
100–125	$(4.17 \pm 0.04 \pm 0.13) \times 10^{-4}$	250–320	$(5.01 \pm 0.08 \pm 0.21) \times 10^{-5}$
125–150	$(2.903 \pm 0.032 \pm 0.070) \times 10^{-4}$	320–500	$(1.629 \pm 0.024 \pm 0.053) \times 10^{-5}$
		$p_T(j_2)$	
30–50	$(8.50 \pm 0.06 \pm 0.42) \times 10^{-4}$	125–150	$(4.75 \pm 0.12 \pm 0.36) \times 10^{-5}$
50–75	$(3.55 \pm 0.03 \pm 0.24) \times 10^{-4}$	150–180	$(2.60 \pm 0.09 \pm 0.18) \times 10^{-5}$
75–100	$(1.73 \pm 0.02 \pm 0.12) \times 10^{-4}$	180–350	$(5.72 \pm 0.19 \pm 0.44) \times 10^{-6}$
100–125	$(8.92 \pm 0.17 \pm 0.71) \times 10^{-5}$...
		$p_T(j_3)$	
30–50	$(3.37 \pm 0.04 \pm 0.26) \times 10^{-4}$	75–100	$(3.44 \pm 0.10 \pm 0.44) \times 10^{-5}$
50–75	$(1.00 \pm 0.02 \pm 0.11) \times 10^{-4}$	100–250	$(4.68 \pm 0.17 \pm 0.55) \times 10^{-6}$
		$p_T(j_4)$	
30–50	$(1.06 \pm 0.02 \pm 0.12) \times 10^{-4}$	75–100	$(6.1 \pm 0.4 \pm 1.1) \times 10^{-6}$
50–75	$(2.32 \pm 0.08 \pm 0.36) \times 10^{-5}$	100–200	$(9.1 \pm 0.9 \pm 1.9) \times 10^{-7}$

TABLE LX. Differential cross sections at the particle level as a function of $|\eta(\text{jet})|$ of jets normalized to the sum of the cross sections σ_{norm} of all jets in the measured ranges. The values are shown together with their statistical and systematic uncertainties.

$ \eta(\text{jet}) $	$\frac{1}{\sigma_{\text{norm}}} \frac{d\sigma}{d\eta(\text{jet})}$	$ \eta(\text{jet}) $	$\frac{1}{\sigma_{\text{norm}}} \frac{d\sigma}{d\eta(\text{jet})}$
		$ \eta(b_\ell) $	
0.00–0.25	$0.1340 \pm 0.0006 \pm 0.0014$	1.25–1.50	$0.0813 \pm 0.0005 \pm 0.0013$
0.25–0.50	$0.1313 \pm 0.0006 \pm 0.0016$	1.50–1.75	$0.06614 \pm 0.00045 \pm 0.00081$
0.50–0.75	$0.1252 \pm 0.0006 \pm 0.0016$	1.75–2.00	$0.05272 \pm 0.00042 \pm 0.00086$
0.75–1.00	$0.1134 \pm 0.0005 \pm 0.0013$	2.00–2.25	$0.03908 \pm 0.00038 \pm 0.00082$
1.00–1.25	$0.0997 \pm 0.0005 \pm 0.0011$	2.25–2.50	$0.01624 \pm 0.00028 \pm 0.00043$
		$ \eta(b_h) $	
0.00–0.25	$0.1419 \pm 0.0006 \pm 0.0017$	1.25–1.50	$0.0782 \pm 0.0005 \pm 0.0013$
0.25–0.50	$0.1378 \pm 0.0006 \pm 0.0013$	1.50–1.75	$0.06182 \pm 0.00044 \pm 0.00085$
0.50–0.75	$0.1281 \pm 0.0006 \pm 0.0014$	1.75–2.00	$0.0484 \pm 0.0004 \pm 0.0014$
0.75–1.00	$0.1164 \pm 0.0006 \pm 0.0014$	2.00–2.25	$0.03451 \pm 0.00037 \pm 0.00096$
1.00–1.25	$0.0973 \pm 0.0005 \pm 0.0011$	2.25–2.50	$0.01433 \pm 0.00026 \pm 0.00054$
		$ \eta(j_{W1}) $	
0.00–0.25	$0.1362 \pm 0.0006 \pm 0.0020$	1.25–1.50	$0.0806 \pm 0.0005 \pm 0.0011$
0.25–0.50	$0.1325 \pm 0.0006 \pm 0.0021$	1.50–1.75	$0.0659 \pm 0.0004 \pm 0.0014$
0.50–0.75	$0.1233 \pm 0.0006 \pm 0.0017$	1.75–2.00	$0.0523 \pm 0.0004 \pm 0.0013$
0.75–1.00	$0.1126 \pm 0.0006 \pm 0.0016$	2.00–2.25	$0.0395 \pm 0.0004 \pm 0.0013$
1.00–1.25	$0.1011 \pm 0.0005 \pm 0.0027$	2.25–2.50	$0.01786 \pm 0.00025 \pm 0.00077$

(Table continued)

TABLE LX. (*Continued*)

$ \eta(\text{jet}) $	$\frac{1}{\sigma_{\text{norm}}} \frac{d\sigma}{d\eta(\text{jet})}$	$ \eta(j_{W2}) $	$\frac{1}{\sigma_{\text{norm}}} \frac{d\sigma}{d\eta(j_{W2})}$
0.00–0.25	$0.1281 \pm 0.0006 \pm 0.0024$	1.25–1.50	$0.0840 \pm 0.0005 \pm 0.0011$
0.25–0.50	$0.1243 \pm 0.0006 \pm 0.0017$	1.50–1.75	$0.0704 \pm 0.0005 \pm 0.0014$
0.50–0.75	$0.1172 \pm 0.0006 \pm 0.0017$	1.75–2.00	$0.0589 \pm 0.0004 \pm 0.0011$
0.75–1.00	$0.1097 \pm 0.0006 \pm 0.0016$	2.00–2.25	$0.0474 \pm 0.0004 \pm 0.0013$
1.00–1.25	$0.0993 \pm 0.0006 \pm 0.0013$	2.25–2.50	$0.02233 \pm 0.00027 \pm 0.00088$
		$ \eta(j_1) $	
0.00–0.25	$0.0435 \pm 0.0003 \pm 0.0012$	1.25–1.50	$0.03931 \pm 0.00032 \pm 0.00090$
0.25–0.50	$0.0433 \pm 0.0003 \pm 0.0012$	1.50–1.75	$0.0374 \pm 0.0003 \pm 0.0010$
0.50–0.75	$0.04287 \pm 0.00033 \pm 0.00094$	1.75–2.00	$0.0364 \pm 0.0003 \pm 0.0013$
0.75–1.00	$0.04337 \pm 0.00034 \pm 0.00088$	2.00–2.25	$0.0326 \pm 0.0003 \pm 0.0010$
1.00–1.25	$0.0414 \pm 0.0003 \pm 0.0014$	2.25–2.50	$0.01758 \pm 0.00020 \pm 0.00057$
		$ \eta(j_2) $	
0.00–0.25	$0.0150 \pm 0.0002 \pm 0.0011$	1.25–1.50	$0.01351 \pm 0.00017 \pm 0.00071$
0.25–0.50	$0.01547 \pm 0.00019 \pm 0.00091$	1.50–1.75	$0.01310 \pm 0.00017 \pm 0.00072$
0.50–0.75	$0.0146 \pm 0.0002 \pm 0.0011$	1.75–2.00	$0.01237 \pm 0.00017 \pm 0.00079$
0.75–1.00	$0.0147 \pm 0.0002 \pm 0.0011$	2.00–2.25	$0.01112 \pm 0.00016 \pm 0.00059$
1.00–1.25	$0.01446 \pm 0.00018 \pm 0.00098$	2.25–2.50	$(6.03 \pm 0.12 \pm 0.35) \times 10^{-3}$
		$ \eta(j_3) $	
0.0–0.5	$(4.53 \pm 0.06 \pm 0.46) \times 10^{-3}$	1.5–2.0	$(3.83 \pm 0.06 \pm 0.31) \times 10^{-3}$
0.5–1.0	$(4.63 \pm 0.06 \pm 0.35) \times 10^{-3}$	2.0–2.5	$(2.55 \pm 0.05 \pm 0.22) \times 10^{-3}$
1.0–1.5	$(4.37 \pm 0.06 \pm 0.36) \times 10^{-3}$...
		$ \eta(j_4) $	
0.0–0.5	$(1.26 \pm 0.03 \pm 0.18) \times 10^{-3}$	1.5–2.0	$(1.01 \pm 0.03 \pm 0.15) \times 10^{-3}$
0.5–1.0	$(1.29 \pm 0.03 \pm 0.15) \times 10^{-3}$	2.0–2.5	$(6.8 \pm 0.2 \pm 1.1) \times 10^{-4}$
1.0–1.5	$(1.27 \pm 0.03 \pm 0.13) \times 10^{-3}$...

TABLE LXI. Differential cross sections at the particle level as a function of ΔR_{j_t} of jets normalized to the sum of the cross sections σ_{norm} of all jets in the measured ranges. The values are shown together with their statistical and systematic uncertainties.

ΔR_{j_t}	$\frac{1}{\sigma_{\text{norm}}} \frac{d\sigma}{d\Delta R_{j_t}}$	ΔR_{j_t}	$\frac{1}{\sigma_{\text{norm}}} \frac{d\sigma}{d\Delta R_{j_t}}$
		$\Delta R_{j_t}(b_\ell)$	
0.4–0.6	$0.0517 \pm 0.0005 \pm 0.0014$	1.4–1.6	$0.1026 \pm 0.0007 \pm 0.0010$
0.6–0.8	$0.0860 \pm 0.0007 \pm 0.0015$	1.6–2.0	$0.0988 \pm 0.0004 \pm 0.0012$
0.8–1.0	$0.0909 \pm 0.0007 \pm 0.0010$	2.0–2.5	$0.08080 \pm 0.00033 \pm 0.00099$
1.0–1.2	$0.0989 \pm 0.0007 \pm 0.0016$	2.5–4.5	$0.01403 \pm 0.00007 \pm 0.00021$
1.2–1.4	$0.1035 \pm 0.0007 \pm 0.0016$...
		$\Delta R_{j_t}(b_h)$	
0.4–0.6	$0.0688 \pm 0.0005 \pm 0.0012$	1.4–1.6	$0.1313 \pm 0.0007 \pm 0.0015$
0.6–0.8	$0.1152 \pm 0.0007 \pm 0.0017$	1.6–2.0	$0.0972 \pm 0.0005 \pm 0.0013$
0.8–1.0	$0.1316 \pm 0.0007 \pm 0.0019$	2.0–2.5	$0.04520 \pm 0.00031 \pm 0.00086$
1.0–1.2	$0.1454 \pm 0.0008 \pm 0.0012$	2.5–4.5	$(3.09 \pm 0.05 \pm 0.16) \times 10^{-3}$
1.2–1.4	$0.1444 \pm 0.0008 \pm 0.0019$...
		$\Delta R_{j_t}(j_{W1})$	
0.4–0.6	$0.0737 \pm 0.0006 \pm 0.0015$	1.4–1.6	$0.1265 \pm 0.0007 \pm 0.0017$
0.6–0.8	$0.1241 \pm 0.0007 \pm 0.0018$	1.6–2.0	$0.08623 \pm 0.00044 \pm 0.00098$
0.8–1.0	$0.1406 \pm 0.0007 \pm 0.0019$	2.0–2.5	$0.03957 \pm 0.00029 \pm 0.00070$
1.0–1.2	$0.1538 \pm 0.0008 \pm 0.0020$	2.5–4.5	$(4.19 \pm 0.05 \pm 0.22) \times 10^{-3}$
1.2–1.4	$0.1468 \pm 0.0008 \pm 0.0013$...

(Table continued)

TABLE LXI. (*Continued*)

ΔR_{j_t}	$\frac{1}{\sigma_{\text{norm}}} \frac{d\sigma}{d\Delta R_{j_t}}$	ΔR_{j_t}	$\frac{1}{\sigma_{\text{norm}}} \frac{d\sigma}{d\Delta R_{j_t}}$
		$\Delta R_{j_t}(j_{W2})$	
0.4–0.6	$0.0805 \pm 0.0006 \pm 0.0016$	1.4–1.6	$0.1257 \pm 0.0008 \pm 0.0019$
0.6–0.8	$0.1303 \pm 0.0008 \pm 0.0019$	1.6–2.0	$0.0836 \pm 0.0005 \pm 0.0010$
0.8–1.0	$0.1411 \pm 0.0008 \pm 0.0021$	2.0–2.5	$0.03747 \pm 0.00028 \pm 0.00060$
1.0–1.2	$0.1520 \pm 0.0008 \pm 0.0028$	2.5–4.5	$(3.94 \pm 0.05 \pm 0.15) \times 10^{-3}$
1.2–1.4	$0.1459 \pm 0.0008 \pm 0.0015$...
		$\Delta R_{j_t}(j_1)$	
0.4–0.6	$0.0439 \pm 0.0004 \pm 0.0012$	1.4–1.6	$0.0432 \pm 0.0004 \pm 0.0011$
0.6–0.8	$0.0566 \pm 0.0005 \pm 0.0015$	1.6–2.0	$0.03614 \pm 0.00026 \pm 0.00087$
0.8–1.0	$0.0509 \pm 0.0004 \pm 0.0013$	2.0–2.5	$0.02556 \pm 0.00019 \pm 0.00055$
1.0–1.2	$0.0490 \pm 0.0004 \pm 0.0015$	2.5–4.5	$(4.60 \pm 0.04 \pm 0.12) \times 10^{-3}$
1.2–1.4	$0.0458 \pm 0.0004 \pm 0.0015$...
		$\Delta R_{j_t}(j_2)$	
0.4–0.6	$0.01653 \pm 0.00023 \pm 0.00092$	1.4–1.6	$0.01423 \pm 0.00021 \pm 0.00072$
0.6–0.8	$0.0214 \pm 0.0003 \pm 0.0012$	1.6–2.0	$0.01189 \pm 0.00015 \pm 0.00061$
0.8–1.0	$0.01852 \pm 0.00024 \pm 0.00097$	2.0–2.5	$(7.97 \pm 0.11 \pm 0.41) \times 10^{-3}$
1.0–1.2	$0.01733 \pm 0.00023 \pm 0.00085$	2.5–4.5	$(1.459 \pm 0.023 \pm 0.079) \times 10^{-3}$
1.2–1.4	$0.01593 \pm 0.00022 \pm 0.00081$...
		$\Delta R_{j_t}(j_3)$	
0.4–0.8	$(5.61 \pm 0.08 \pm 0.50) \times 10^{-3}$	1.6–2.0	$(3.70 \pm 0.07 \pm 0.34) \times 10^{-3}$
0.8–1.2	$(5.41 \pm 0.08 \pm 0.39) \times 10^{-3}$	2.0–2.5	$(2.39 \pm 0.05 \pm 0.19) \times 10^{-3}$
1.2–1.6	$(4.69 \pm 0.08 \pm 0.34) \times 10^{-3}$	2.5–4.5	$(4.67 \pm 0.12 \pm 0.32) \times 10^{-4}$
		$\Delta R_{j_t}(j_4)$	
0.4–0.8	$(1.50 \pm 0.04 \pm 0.16) \times 10^{-3}$	1.6–2.0	$(1.01 \pm 0.03 \pm 0.15) \times 10^{-3}$
0.8–1.2	$(1.52 \pm 0.04 \pm 0.16) \times 10^{-3}$	2.0–2.5	$(6.96 \pm 0.27 \pm 0.91) \times 10^{-4}$
1.2–1.6	$(1.27 \pm 0.04 \pm 0.14) \times 10^{-3}$	2.5–4.5	$(1.27 \pm 0.06 \pm 0.16) \times 10^{-4}$

TABLE LXII. Differential cross sections at the particle level as a function of ΔR_t of jets normalized to the sum of the cross sections σ_{norm} of all jets in the measured ranges. The values are shown together with their statistical and systematic uncertainties.

ΔR_t	$\frac{1}{\sigma_{\text{norm}}} \frac{d\sigma}{d\Delta R_t}$	ΔR_t	$\frac{1}{\sigma_{\text{norm}}} \frac{d\sigma}{d\Delta R_t}$
		$\Delta R_t(b_\ell)$	
0.0–0.3	$0.0566 \pm 0.0004 \pm 0.0022$	1.2–1.5	$0.1018 \pm 0.0005 \pm 0.0016$
0.3–0.6	$0.1208 \pm 0.0005 \pm 0.0022$	1.5–2.0	$0.0663 \pm 0.0003 \pm 0.0014$
0.6–0.9	$0.1319 \pm 0.0006 \pm 0.0014$	2.0–2.5	$0.02873 \pm 0.00022 \pm 0.00089$
0.9–1.2	$0.1208 \pm 0.0005 \pm 0.0017$	2.5–4.5	$(4.16 \pm 0.05 \pm 0.19) \times 10^{-3}$
		$\Delta R_t(b_h)$	
0.0–0.3	$0.0576 \pm 0.0004 \pm 0.0015$	1.2–1.5	$0.1034 \pm 0.0006 \pm 0.0014$
0.3–0.6	$0.1173 \pm 0.0006 \pm 0.0016$	1.5–2.0	$0.06910 \pm 0.00037 \pm 0.00084$
0.6–0.9	$0.1276 \pm 0.0006 \pm 0.0013$	2.0–2.5	$0.02976 \pm 0.00024 \pm 0.00077$
0.9–1.2	$0.1179 \pm 0.0006 \pm 0.0016$	2.5–4.5	$(4.21 \pm 0.05 \pm 0.13) \times 10^{-3}$
		$\Delta R_t(j_{W1})$	
0.0–0.3	$0.0813 \pm 0.0005 \pm 0.0015$	1.2–1.5	$0.0847 \pm 0.0005 \pm 0.0011$
0.3–0.6	$0.1490 \pm 0.0007 \pm 0.0025$	1.5–2.0	$0.05319 \pm 0.00030 \pm 0.00094$
0.6–0.9	$0.1396 \pm 0.0007 \pm 0.0016$	2.0–2.5	$0.02405 \pm 0.00018 \pm 0.00057$
0.9–1.2	$0.1113 \pm 0.0006 \pm 0.0020$	2.5–4.5	$(3.74 \pm 0.04 \pm 0.16) \times 10^{-3}$
		$\Delta R_t(j_{W2})$	
0.0–0.3	$0.02833 \pm 0.00031 \pm 0.00085$	1.2–1.5	$0.1135 \pm 0.0006 \pm 0.0012$
0.3–0.6	$0.0842 \pm 0.0005 \pm 0.0016$	1.5–2.0	$0.08220 \pm 0.00041 \pm 0.00086$

(Table continued)

TABLE LXII. (*Continued*)

ΔR_t	$\frac{1}{\sigma_{\text{norm}}} \frac{d\sigma}{d\Delta R_t}$	ΔR_t	$\frac{1}{\sigma_{\text{norm}}} \frac{d\sigma}{d\Delta R_t}$
0.6–0.9	$0.1171 \pm 0.0006 \pm 0.0016$	2.0–2.5	$0.04091 \pm 0.00029 \pm 0.00068$
0.9–1.2	$0.1218 \pm 0.0006 \pm 0.0021$	2.5–4.5	$(7.04 \pm 0.07 \pm 0.24) \times 10^{-3}$
		$\Delta R_t(j_1)$	
0.0–0.3	$(3.66 \pm 0.09 \pm 0.23) \times 10^{-3}$	1.2–1.5	$0.02904 \pm 0.00025 \pm 0.00097$
0.3–0.6	$0.01099 \pm 0.00015 \pm 0.00047$	1.5–2.0	$0.0359 \pm 0.0002 \pm 0.0011$
0.6–0.9	$0.01875 \pm 0.00020 \pm 0.00071$	2.0–2.5	$0.03657 \pm 0.00024 \pm 0.00084$
0.9–1.2	$0.02400 \pm 0.00022 \pm 0.00073$	2.5–4.5	$0.01584 \pm 0.00008 \pm 0.00038$
		$\Delta R_t(j_2)$	
0.0–0.3	$(1.52 \pm 0.05 \pm 0.12) \times 10^{-3}$	1.2–1.5	$0.01172 \pm 0.00014 \pm 0.00065$
0.3–0.6	$(4.89 \pm 0.09 \pm 0.28) \times 10^{-3}$	1.5–2.0	$0.01304 \pm 0.00013 \pm 0.00070$
0.6–0.9	$(8.31 \pm 0.12 \pm 0.55) \times 10^{-3}$	2.0–2.5	$0.01203 \pm 0.00013 \pm 0.00076$
0.9–1.2	$0.01028 \pm 0.00013 \pm 0.00055$	2.5–4.5	$(4.36 \pm 0.04 \pm 0.21) \times 10^{-3}$
		$\Delta R_t(j_3)$	
0.0–0.4	$(5.71 \pm 0.22 \pm 0.82) \times 10^{-4}$	1.5–2.0	$(4.04 \pm 0.06 \pm 0.33) \times 10^{-3}$
0.4–0.8	$(2.02 \pm 0.05 \pm 0.18) \times 10^{-3}$	2.0–2.5	$(3.67 \pm 0.06 \pm 0.34) \times 10^{-3}$
0.8–1.2	$(3.14 \pm 0.06 \pm 0.25) \times 10^{-3}$	2.5–4.5	$(1.288 \pm 0.021 \pm 0.099) \times 10^{-3}$
1.2–1.5	$(3.67 \pm 0.07 \pm 0.31) \times 10^{-3}$...
		$\Delta R_t(j_4)$	
0.0–0.4	$(1.35 \pm 0.09 \pm 0.26) \times 10^{-4}$	1.5–2.0	$(1.13 \pm 0.03 \pm 0.14) \times 10^{-3}$
0.4–0.8	$(5.14 \pm 0.20 \pm 0.59) \times 10^{-4}$	2.0–2.5	$(1.02 \pm 0.03 \pm 0.14) \times 10^{-3}$
0.8–1.2	$(8.60 \pm 0.28 \pm 0.93) \times 10^{-4}$	2.5–4.5	$(3.58 \pm 0.11 \pm 0.45) \times 10^{-4}$
1.2–1.5	$(1.02 \pm 0.03 \pm 0.14) \times 10^{-3}$...

- [1] M. Czakon, D. Heymes, A. Mitov, D. Pagani, I. Tsinikos, and M. Zaro, Top-pair production at the LHC through NNLO QCD and NLO EW, *J. High Energy Phys.* **10** (2017) 186.
- [2] CMS Collaboration, CMS Luminosity measurement for the 2016 data taking period, CMS Physics Analysis Summary Report No. CMS-PAS-LUM-17-001, 2017, <https://cds.cern.ch/record/2257069>.
- [3] CMS Collaboration, Measurement of differential top-quark pair production cross sections in pp collisions at $\sqrt{s} = 7$ TeV, *Eur. Phys. J. C* **73**, 2339 (2013).
- [4] ATLAS Collaboration, Differential top-antitop cross-section measurements as a function of observables constructed from final-state particles using pp collisions at $\sqrt{s} = 7$ TeV in the ATLAS detector, *J. High Energy Phys.* **06** (2015) 100.
- [5] CMS Collaboration, Measurement of the differential cross section for top quark pair production in pp collisions at $\sqrt{s} = 8$ TeV, *Eur. Phys. J. C* **75**, 542 (2015).
- [6] ATLAS Collaboration, Measurements of top-quark pair differential cross-sections in the lepton + jets channel in pp collisions at $\sqrt{s} = 8$ TeV using the ATLAS detector, *Eur. Phys. J. C* **76**, 538 (2016).
- [7] ATLAS Collaboration, Measurement of the differential cross-section of highly boosted top quarks as a function of

their transverse momentum in $\sqrt{s} = 8$ TeV proton-proton collisions using the ATLAS detector, *Phys. Rev. D* **93**, 032009 (2016).

- [8] CMS Collaboration, Measurement of the $t\bar{t}$ production cross section in the all-jets final state in pp collisions at $\sqrt{s} = 8$ TeV, *Eur. Phys. J. C* **76**, 128 (2016).
- [9] CMS Collaboration, Measurement of the integrated and differential $t\bar{t}$ production cross sections for high- p_T top quarks in pp collisions at $\sqrt{s} = 8$ TeV, *Phys. Rev. D* **94**, 072002 (2016).
- [10] ATLAS Collaboration, Measurement of top quark pair differential cross-sections in the dilepton channel in pp collisions at $\sqrt{s} = 7$ and 8 TeV with ATLAS, *Phys. Rev. D* **94**, 092003 (2016).
- [11] CMS Collaboration, Measurement of double-differential cross sections for top quark pair production in pp collisions at $\sqrt{s} = 8$ TeV and impact on parton distribution functions, *Eur. Phys. J. C* **77**, 459 (2017).
- [12] ATLAS Collaboration, Measurement of jet activity produced in top-quark events with an electron, a muon and two b-tagged jets in the final state in pp collisions at $\sqrt{s} = 13$ TeV with the ATLAS detector, *Eur. Phys. J. C* **77**, 220 (2017).
- [13] ATLAS Collaboration, Measurements of top-quark pair differential cross-sections in the $e\mu$ channel in pp collisions

- at $\sqrt{s} = 13$ TeV using the ATLAS detector, *Eur. Phys. J. C* **77**, 292 (2017).
- [14] CMS Collaboration, Measurement of normalized differential $t\bar{t}$ cross sections in the dilepton channel from pp collisions at $\sqrt{s} = 13$ TeV, *J. High Energy Phys.* **04** (2018) 060.
- [15] CMS Collaboration, Measurement of the differential cross sections for top quark pair production as a function of kinematic event variables in pp collisions at $\sqrt{s} = 7$ and 8 TeV, *Phys. Rev. D* **94**, 052006 (2016).
- [16] CMS Collaboration, Measurement of $t\bar{t}$ production with additional jet activity, including b quark jets, in the dilepton decay channel using pp collisions at $\sqrt{s} = 8$ TeV, *Eur. Phys. J. C* **76**, 379 (2016).
- [17] ATLAS Collaboration, Measurement of jet activity in top quark events using the $e\mu$ final state with two b-tagged jets in pp collisions at $\sqrt{s} = 8$ TeV with the ATLAS detector, *J. High Energy Phys.* **09** (2016) 074.
- [18] CMS Collaboration, Measurement of differential cross sections for top quark pair production using the lepton + jets final state in proton-proton collisions at 13 TeV, *Phys. Rev. D* **95**, 092001 (2017).
- [19] P. Nason, A new method for combining NLO QCD with shower Monte Carlo algorithms, *J. High Energy Phys.* **11** (2004) 040.
- [20] S. Frixione, P. Nason, and C. Oleari, Matching NLO QCD computations with parton shower simulations: the POWHEG method, *J. High Energy Phys.* **11** (2007) 070.
- [21] S. Alioli, P. Nason, C. Oleari, and E. Re, A general framework for implementing NLO calculations in shower Monte Carlo programs: the POWHEG BOX, *J. High Energy Phys.* **06** (2010) 043.
- [22] J. M. Campbell, R. K. Ellis, P. Nason, and E. Re, Top-pair production and decay at NLO matched with parton showers, *J. High Energy Phys.* **04** (2015) 114.
- [23] T. Sjöstrand, S. Mrenna, and P. Skands, PYTHIA 6.4 physics and manual, *J. High Energy Phys.* **05** (2006) 026.
- [24] T. Sjöstrand, S. Mrenna, and P. Skands, A brief introduction to PYTHIA 8.1, *Comput. Phys. Commun.* **178**, 852 (2008).
- [25] P. Skands, S. Carrazza, and J. Rojo, Tuning PYTHIA 8.1: the Monash 2013 tune, *Eur. Phys. J. C* **74**, 3024 (2014).
- [26] CMS Collaboration, Investigations of the impact of the parton shower tuning in PYTHIA 8 in the modelling of $t\bar{t}$ at $\sqrt{s} = 8$ and 13 TeV, CMS Physics Analysis Summary Report No. CMS-PAS-TOP-16-021, 2016, <https://cds.cern.ch/record/2235192>.
- [27] M. Bähr, S. Gieseke, M. A. Gigg, D. Grellscheid, K. Hamilton, O. Latunde-Dada, S. Plätzer, P. Richardson, M. H. Seymour, A. Sherstnev, and B. R. Webber, HERWIG++ physics and manual, *Eur. Phys. J. C* **58**, 639 (2008).
- [28] M. H. Seymour and A. Siomok, Constraining MPI models using σ_{eff} and recent Tevatron and LHC underlying event data, *J. High Energy Phys.* **10** (2013) 113.
- [29] J. Alwall, R. Frederix, S. Frixione, V. Hirschi, F. Maltoni, O. Mattelaer, H. S. Shao, T. Stelzer, P. Torrielli, and M. Zaro, The automated computation of tree-level and next-to-leading order differential cross sections, and their matching to parton shower simulations, *J. High Energy Phys.* **07** (2014) 079.
- [30] R. Frederix and S. Frixione, Merging meets matching in MC@NLO, *J. High Energy Phys.* **12** (2012) 061.
- [31] R. D. Ball *et al.* (NNPDF Collaboration), Parton distributions for the LHC Run II, *J. High Energy Phys.* **04** (2015) 040.
- [32] M. Czakon and A. Mitov, Top++: A program for the calculation of the top-pair cross-section at hadron colliders, *Comput. Phys. Commun.* **185**, 2930 (2014).
- [33] E. Re, Single-top Wt-channel production matched with parton showers using the POWHEG method, *Eur. Phys. J. C* **71**, 1547 (2011).
- [34] Y. Li and F. Petriello, Combining QCD and electroweak corrections to dilepton production in FEWZ, *Phys. Rev. D* **86**, 094034 (2012).
- [35] P. Kant, O. M. Kind, T. Kintscher, T. Lohse, T. Martini, S. Mölitz, P. Rieck, and P. Uwer, HatHor for single top-quark production: Updated predictions and uncertainty estimates for single top-quark production in hadronic collisions, *Comput. Phys. Commun.* **191**, 74 (2015).
- [36] N. Kidonakis, NNLL threshold resummation for top-pair and single-top production, *Phys. Part. Nucl.* **45**, 714 (2014).
- [37] S. Agostinelli *et al.* (GEANT4 Collaboration), GEANT4—a simulation toolkit, *Nucl. Instrum. Methods Phys. Res., Sect. A* **506**, 250 (2003).
- [38] CMS Collaboration, Object definitions for top quark analyses at the particle level, CMS Note Report No. CERN-CMS-NOTE-2017-004, 2017, <https://cds.cern.ch/record/2267573>.
- [39] M. Cacciari, G. P. Salam, and G. Soyez, The anti- k_t jet clustering algorithm, *J. High Energy Phys.* **04** (2008) 063.
- [40] M. Cacciari, G. P. Salam, and G. Soyez, FastJet user manual, *Eur. Phys. J. C* **72**, 1896 (2012).
- [41] C. Patrignani *et al.* (Particle Data Group), Review of particle physics, *Chin. Phys. C* **40**, 100001 (2016).
- [42] CMS Collaboration, The CMS experiment at the CERN LHC, *J. Instrum.* **3**, S08004 (2008).
- [43] CMS Collaboration, Particle-flow reconstruction and global event description with the CMS detector, *J. Instrum.* **12**, P10003 (2017).
- [44] CMS Collaboration, Measurements of inclusive W and Z cross sections in pp collisions at $\sqrt{s} = 7$ TeV, *J. High Energy Phys.* **01** (2011) 080.
- [45] CMS Collaboration, Performance of CMS muon reconstruction in pp collision events at $\sqrt{s} = 7$ TeV, *J. Instrum.* **7**, P10002 (2012).
- [46] CMS Collaboration, Performance of electron reconstruction and selection with the CMS detector in proton-proton collisions at $\sqrt{s} = 8$ TeV, *J. Instrum.* **10**, P06005 (2015).
- [47] CMS Collaboration, Jet energy scale and resolution in the CMS experiment in pp collisions at 8 TeV, *J. Instrum.* **12**, P02014 (2017).
- [48] CMS Collaboration, Identification of heavy-flavour jets with the CMS detector in pp collisions at 13 TeV, *J. Instrum.* **13**, P05011 (2018).
- [49] B. A. Betchart, R. Demina, and A. Harel, Analytic solutions for neutrino momenta in decay of top quarks, *Nucl. Instrum. Methods Phys. Res., Sect. A* **736**, 169 (2014).
- [50] G. D'Agostini, A multidimensional unfolding method based on Bayes' theorem, *Nucl. Instrum. Methods Phys. Res., Sect. A* **362**, 487 (1995).
- [51] CMS Collaboration, Identification of b quark jets at the CMS experiment in the LHC Run 2, CMS Physics Analysis Summary Report No. CMS-PAS-BTV-15-001, 2016, <https://cds.cern.ch/record/2138504>.

- [52] ATLAS Collaboration, Measurement of the Inelastic Proton-Proton Cross Section at $\sqrt{s} = 13$ TeV with the ATLAS Detector at the LHC, *Phys. Rev. Lett.* **117**, 182002 (2016).
- [53] A. Heister *et al.* (ALEPH Collaboration), Study of the fragmentation of b quarks into B mesons at the Z peak, *Phys. Lett. B* **512**, 30 (2001).
- [54] G. Abbiendi *et al.* (OPAL Collaboration), Inclusive analysis of the b quark fragmentation function in Z decays at LEP, *Eur. Phys. J. C* **29**, 463 (2003).
- [55] J. Abdallah *et al.* (DELPHI Collaboration), A study of the b-quark fragmentation function with the DELPHI detector at LEP I and an averaged distribution obtained at the Z pole, *Eur. Phys. J. C* **71**, 1557 (2011).
- [56] K. Abe *et al.* (SLD Collaboration), Measurement of the b quark fragmentation function in Z^0 decays, *Phys. Rev. D* **65**, 092006 (2002); Erratum, *Phys. Rev. D* **66**, 079905(E) (2002).
- [57] ATLAS, CDF, CMS and D0 Collaborations, First combination of Tevatron and LHC measurements of the top-quark mass, [arXiv:1403.4427](https://arxiv.org/abs/1403.4427).
- [58] A. Manohar, P. Nason, G. P. Salam, and G. Zanderighi, How Bright is the Proton? A Precise Determination of the Photon Parton Distribution Function, *Phys. Rev. Lett.* **117**, 242002 (2016).
- [59] T. Gleisberg, S. Hoeche, F. Krauss, M. Schonherr, S. Schumann, F. Siegert, and J. Winter, Event generation with SHERPA 1.1, *J. High Energy Phys.* **02** (2009) 007.
- [60] F. Cascioli, P. Maierhöfer, and S. Pozzorini, Scattering Amplitudes with Open Loops, *Phys. Rev. Lett.* **108**, 111601 (2012).
- [61] S. Schumann and F. Krauss, A parton shower algorithm based on Catani-Seymour dipole factorisation, *J. High Energy Phys.* **03** (2008) 038.

A. M. Sirunyan,¹ A. Tumasyan,¹ W. Adam,² F. Ambrogi,² E. Asilar,² T. Bergauer,² J. Brandstetter,² E. Brondolin,² M. Dragicevic,² J. Erö,² A. Escalante Del Valle,² M. Flechl,² M. Friedl,² R. Frühwirth,^{2,b} V. M. Ghete,² J. Hrubec,² M. Jeitler,^{2,b} N. Krammer,² I. Krätschmer,² D. Liko,² T. Madlener,² I. Mikulec,² N. Rad,² H. Rohringer,² J. Schieck,^{2,b} R. Schöfbeck,² M. Spanring,² D. Spitzbart,² A. Taurok,² W. Waltenberger,² J. Wittmann,² C.-E. Wulz,^{2,b} M. Zarucki,² V. Chekhovsky,³ V. Mossolov,³ J. Suarez Gonzalez,³ E. A. De Wolf,⁴ D. Di Croce,⁴ X. Janssen,⁴ J. Lauwers,⁴ M. Pieters,⁴ M. Van De Klundert,⁴ H. Van Haevermaet,⁴ P. Van Mechelen,⁴ N. Van Remortel,⁴ S. Abu Zeid,⁵ F. Blekman,⁵ J. D'Hondt,⁵ I. De Bruyn,⁵ J. De Clercq,⁵ K. Deroover,⁵ G. Flouris,⁵ D. Lontkovskyi,⁵ S. Lowette,⁵ I. Marchesini,⁵ S. Moortgat,⁵ L. Moreels,⁵ Q. Python,⁵ K. Skovpen,⁵ S. Tavernier,⁵ W. Van Doninck,⁵ P. Van Mulders,⁵ I. Van Parijs,⁵ D. Beghin,⁶ B. Bilin,⁶ H. Brun,⁶ B. Clerbaux,⁶ G. De Lentdecker,⁶ H. Delannoy,⁶ B. Dorney,⁶ G. Fasanella,⁶ L. Favart,⁶ R. Goldouzian,⁶ A. Grebenyuk,⁶ A. K. Kalsi,⁶ T. Lenzi,⁶ J. Luetic,⁶ T. Seva,⁶ E. Starling,⁶ C. Vander Velde,⁶ P. Vanlaer,⁶ D. Vannerom,⁶ R. Yonamine,⁶ T. Cornelis,⁷ D. Dobur,⁷ A. Fagot,⁷ M. Gul,⁷ I. Khvastunov,^{7,c} D. Poyraz,⁷ C. Roskas,⁷ D. Trocino,⁷ M. Tytgat,⁷ W. Verbeke,⁷ B. Vermassen,⁷ M. Vit,⁷ N. Zaganidis,⁷ H. Bakhshiansohi,⁸ O. Bondu,⁸ S. Brochet,⁸ G. Bruno,⁸ C. Caputo,⁸ A. Caudron,⁸ P. David,⁸ S. De Visscher,⁸ C. Delaere,⁸ M. Delcourt,⁸ B. Francois,⁸ A. Giannmanco,⁸ G. Krintiras,⁸ V. Lemaitre,⁸ A. Magitteri,⁸ A. Mertens,⁸ M. Musich,⁸ K. Piotrkowski,⁸ L. Quertenmont,⁸ A. Saggio,⁸ M. Vidal Marono,⁸ S. Wertz,⁸ J. Zobec,⁸ W. L. Aldá Júnior,⁹ F. L. Alves,⁹ G. A. Alves,⁹ L. Brito,⁹ G. Correia Silva,⁹ C. Hensel,⁹ A. Moraes,⁹ M. E. Pol,⁹ P. Rebello Teles,⁹ E. Belchior Batista Das Chagas,¹⁰ W. Carvalho,¹⁰ J. Chinellato,^{10,d} E. Coelho,¹⁰ E. M. Da Costa,¹⁰ G. G. Da Silveira,^{10,e} D. De Jesus Damiao,¹⁰ S. Fonseca De Souza,¹⁰ H. Malbouisson,¹⁰ M. Medina Jaime,^{10,f} M. Melo De Almeida,¹⁰ C. Mora Herrera,¹⁰ L. Mundim,¹⁰ H. Nogima,¹⁰ L. J. Sanchez Rosas,¹⁰ A. Santoro,¹⁰ A. Sznajder,¹⁰ M. Thiel,¹⁰ E. J. Tonelli Manganote,^{10,d} F. Torres Da Silva De Araujo,¹⁰ A. Vilela Pereira,¹⁰ S. Ahuja,^{11a} C. A. Bernardes,^{11a} L. Calligaris,^{11a} T. R. Fernandez Perez Tomei,^{11a} E. M. Gregores,^{11b} P. G. Mercadante,^{11b} S. F. Novaes,^{11a} Sandra S. Padula,^{11a} D. Romero Abad,^{11b} J. C. Ruiz Vargas,^{11a} A. Aleksandrov,¹² R. Hadjiiska,¹² P. Iaydjiev,¹² A. Marinov,¹² M. Misheva,¹² M. Rodozov,¹² M. Shopova,¹² G. Sultanov,¹² A. Dimitrov,¹³ L. Litov,¹³ B. Pavlov,¹³ P. Petkov,¹³ W. Fang,^{14,g} X. Gao,^{14,g} L. Yuan,¹⁴ M. Ahmad,¹⁵ J. G. Bian,¹⁵ G. M. Chen,¹⁵ H. S. Chen,¹⁵ M. Chen,¹⁵ Y. Chen,¹⁵ C. H. Jiang,¹⁵ D. Leggat,¹⁵ H. Liao,¹⁵ Z. Liu,¹⁵ F. Romeo,¹⁵ S. M. Shaheen,¹⁵ A. Spiezka,¹⁵ J. Tao,¹⁵ C. Wang,¹⁵ Z. Wang,¹⁵ E. Yazgan,¹⁵ H. Zhang,¹⁵ J. Zhao,¹⁵ Y. Ban,¹⁶ G. Chen,¹⁶ J. Li,¹⁶ Q. Li,¹⁶ S. Liu,¹⁶ Y. Mao,¹⁶ S. J. Qian,¹⁶ D. Wang,¹⁶ Z. Xu,¹⁶ Y. Wang,¹⁷ C. Avila,¹⁸ A. Cabrera,¹⁸ C. A. Carrillo Montoya,¹⁸ L. F. Chaparro Sierra,¹⁸ C. Florez,¹⁸ C. F. González Hernández,¹⁸ M. A. Segura Delgado,¹⁸ B. Courbon,¹⁹ N. Godinovic,¹⁹ D. Lelas,¹⁹ I. Puljak,¹⁹ T. Sculac,¹⁹ Z. Antunovic,²⁰ M. Kovac,²⁰ V. Brigljevic,²¹ D. Ferencek,²¹ K. Kadija,²¹ B. Mesic,²¹ A. Starodumov,^{21,h} T. Susa,²¹ M. W. Ather,²² A. Attikis,²² G. Mavromanolakis,²² J. Mousa,²² C. Nicolaou,²² F. Ptochos,²² P. A. Razis,²² H. Rykaczewski,²² M. Finger,^{23,i} M. Finger Jr.,^{23,i} E. Carrera Jarrin,²⁴ H. Abdalla,^{25,j} S. Khalil,^{25,k} Y. Mohammed,^{25,l} S. Bhowmik,²⁶ R. K. Dewanjee,²⁶ M. Kadastik,²⁶ L. Perrini,²⁶ M. Raidal,²⁶ C. Veelken,²⁶ P. Eerola,²⁷ H. Kirschenmann,²⁷ J. Pekkanen,²⁷ M. Voutilainen,²⁷ J. Havukainen,²⁸ J. K. Heikkilä,²⁸ T. Järvinen,²⁸ V. Karimäki,²⁸ R. Kinnunen,²⁸

- T. Lampén,²⁸ K. Lassila-Perini,²⁸ S. Laurila,²⁸ S. Lehti,²⁸ T. Lindén,²⁸ P. Luukka,²⁸ T. Mäenpää,²⁸ H. Siikonen,²⁸
 E. Tuominen,²⁸ J. Tuominiemi,²⁸ T. Tuuva,²⁹ M. Besancon,³⁰ F. Couderc,³⁰ M. Dejardin,³⁰ D. Denegri,³⁰ J. L. Faure,³⁰
 F. Ferri,³⁰ S. Ganjour,³⁰ S. Ghosh,³⁰ A. Givernaud,³⁰ P. Gras,³⁰ G. Hamel de Monchenault,³⁰ P. Jarry,³⁰ C. Leloup,³⁰
 E. Locci,³⁰ M. Machet,³⁰ J. Malcles,³⁰ G. Negro,³⁰ J. Rander,³⁰ A. Rosowsky,³⁰ M. Ö. Sahin,³⁰ M. Titov,³⁰
 A. Abdulsalam,^{31,m} C. Amendola,³¹ I. Antropov,³¹ S. Baffioni,³¹ F. Beaudette,³¹ P. Busson,³¹ L. Cadamuro,³¹ C. Charlöt,³¹
 R. Granier de Cassagnac,³¹ M. Jo,³¹ I. Kucher,³¹ S. Lisniak,³¹ A. Lobanov,³¹ J. Martin Blanco,³¹ M. Nguyen,³¹
 C. Ochando,³¹ G. Ortona,³¹ P. Paganini,³¹ P. Pigard,³¹ R. Salerno,³¹ J. B. Sauvan,³¹ Y. Sirois,³¹ A. G. Stahl Leiton,³¹
 Y. Yilmaz,³¹ A. Zabi,³¹ A. Zghiche,³¹ J.-L. Agram,^{32,n} J. Andrea,³² D. Bloch,³² J.-M. Brom,³² E. C. Chabert,³² C. Collard,³²
 E. Conte,^{32,n} X. Coubez,³² F. Drouhin,^{32,n} J.-C. Fontaine,^{32,n} D. Gelé,³² U. Goerlach,³² M. Jansová,³² P. Juillot,³²
 A.-C. Le Bihan,³² N. Tonon,³² P. Van Hove,³² S. Gadrat,³³ S. Beauceron,³⁴ C. Bernet,³⁴ G. Boudoul,³⁴ N. Chanon,³⁴
 R. Chierici,³⁴ D. Contardo,³⁴ P. Depasse,³⁴ H. El Mamouni,³⁴ J. Fay,³⁴ L. Finco,³⁴ S. Gascon,³⁴ M. Gouzevitch,³⁴
 G. Grenier,³⁴ B. Ille,³⁴ F. Lagarde,³⁴ I. B. Laktineh,³⁴ H. Lattaud,³⁴ M. Lethuillier,³⁴ L. Mirabito,³⁴ A. L. Pequegnot,³⁴
 S. Perries,³⁴ A. Popov,^{34,o} V. Sordini,³⁴ M. Vander Donckt,³⁴ S. Viret,³⁴ S. Zhang,³⁴ T. Toriashvili,^{35,p} Z. Tsamalaidze,^{36,i}
 C. Autermann,³⁷ L. Feld,³⁷ M. K. Kiesel,³⁷ K. Klein,³⁷ M. Lipinski,³⁷ M. Preuten,³⁷ M. P. Rauch,³⁷ C. Schomakers,³⁷
 J. Schulz,³⁷ M. Teroerde,³⁷ B. Wittmer,³⁷ V. Zhukov,^{37,o} A. Albert,³⁸ D. Duchardt,³⁸ M. Endres,³⁸ M. Erdmann,³⁸
 S. Erdweg,³⁸ T. Esch,³⁸ R. Fischer,³⁸ A. Güth,³⁸ T. Hebbeker,³⁸ C. Heidemann,³⁸ K. Hoepfner,³⁸ S. Knutzen,³⁸
 M. Merschmeyer,³⁸ A. Meyer,³⁸ P. Millet,³⁸ S. Mukherjee,³⁸ T. Pook,³⁸ M. Radziej,³⁸ H. Reithler,³⁸ M. Rieger,³⁸
 F. Scheuch,³⁸ D. Teyssier,³⁸ S. Thüer,³⁸ G. Flügge,³⁹ B. Kargoll,³⁹ T. Kress,³⁹ A. Künsken,³⁹ T. Müller,³⁹ A. Nehrkorn,³⁹
 A. Nowack,³⁹ C. Pistone,³⁹ O. Pooth,³⁹ A. Stahl,^{39,q} M. Aldaya Martin,⁴⁰ T. Arndt,⁴⁰ C. Asawatangtrakuldee,⁴⁰
 K. Beernaert,⁴⁰ O. Behnke,⁴⁰ U. Behrens,⁴⁰ A. Bermúdez Martínez,⁴⁰ A. A. Bin Anuar,⁴⁰ K. Borras,^{40,r} V. Botta,⁴⁰
 A. Campbell,⁴⁰ P. Connor,⁴⁰ C. Contreras-Campana,⁴⁰ F. Costanza,⁴⁰ V. Danilov,⁴⁰ A. De Wit,⁴⁰ C. Diez Pardos,⁴⁰
 D. Domínguez Damiani,⁴⁰ G. Eckerlin,⁴⁰ D. Eckstein,⁴⁰ T. Eichhorn,⁴⁰ A. Elwood,⁴⁰ E. Eren,⁴⁰ E. Gallo,^{40,s}
 J. Garay Garcia,⁴⁰ A. Geiser,⁴⁰ J. M. Grados Luyando,⁴⁰ A. Grohsjean,⁴⁰ P. Gunnellini,⁴⁰ M. Guthoff,⁴⁰ A. Harb,⁴⁰ J. Hauk,⁴⁰
 H. Jung,⁴⁰ M. Kasemann,⁴⁰ J. Keaveney,⁴⁰ C. Kleinwort,⁴⁰ J. Knolle,⁴⁰ I. Korol,⁴⁰ D. Krücker,⁴⁰ W. Lange,⁴⁰ A. Lelek,⁴⁰
 T. Lenz,⁴⁰ K. Lipka,⁴⁰ W. Lohmann,^{40,t} R. Mankel,⁴⁰ I.-A. Melzer-Pellmann,⁴⁰ A. B. Meyer,⁴⁰ M. Meyer,⁴⁰ M. Missiroli,⁴⁰
 G. Mittag,⁴⁰ J. Mnich,⁴⁰ A. Mussgiller,⁴⁰ D. Pitzl,⁴⁰ A. Raspereza,⁴⁰ M. Savitskyi,⁴⁰ P. Saxena,⁴⁰ R. Shevchenko,⁴⁰
 N. Stefaniuk,⁴⁰ H. Tholen,⁴⁰ G. P. Van Onsem,⁴⁰ R. Walsh,⁴⁰ Y. Wen,⁴⁰ K. Wichmann,⁴⁰ C. Wissing,⁴⁰ O. Zenaiev,⁴⁰
 R. Aggleton,⁴¹ S. Bein,⁴¹ V. Blobel,⁴¹ M. Centis Vignali,⁴¹ T. Dreyer,⁴¹ E. Garutti,⁴¹ D. Gonzalez,⁴¹ J. Haller,⁴¹
 A. Hinzmann,⁴¹ M. Hoffmann,⁴¹ A. Karavdina,⁴¹ G. Kasieczka,⁴¹ R. Klanner,⁴¹ R. Kogler,⁴¹ N. Kovalchuk,⁴¹ S. Kurz,⁴¹
 V. Kutzner,⁴¹ J. Lange,⁴¹ D. Marconi,⁴¹ J. Multhaup,⁴¹ M. Niedziela,⁴¹ D. Nowatschin,⁴¹ T. Peiffer,⁴¹ A. Perieanu,⁴¹
 A. Reimers,⁴¹ C. Scharf,⁴¹ P. Schleper,⁴¹ A. Schmidt,⁴¹ S. Schumann,⁴¹ J. Schwandt,⁴¹ J. Sonneveld,⁴¹ H. Stadie,⁴¹
 G. Steinbrück,⁴¹ F. M. Stober,⁴¹ M. Stöver,⁴¹ D. Troendle,⁴¹ E. Usai,⁴¹ A. Vanhoefer,⁴¹ B. Vormwald,⁴¹ M. Akbiyik,⁴²
 C. Barth,⁴² M. Baselga,⁴² S. Baur,⁴² E. Butz,⁴² R. Caspart,⁴² T. Chwalek,⁴² F. Colombo,⁴² W. De Boer,⁴² A. Dierlamm,⁴²
 N. Faltermann,⁴² B. Freund,⁴² R. Friese,⁴² M. Giffels,⁴² M. A. Harrendorf,⁴² F. Hartmann,^{42,q} S. M. Heindl,⁴²
 U. Husemann,⁴² F. Kassel,^{42,q} S. Kudella,⁴² H. Mildner,⁴² M. U. Mozer,⁴² Th. Müller,⁴² M. Plagge,⁴² G. Quast,⁴²
 K. Rabbertz,⁴² M. Schröder,⁴² I. Shvetsov,⁴² G. Sieber,⁴² H. J. Simonis,⁴² R. Ulrich,⁴² S. Wayand,⁴² M. Weber,⁴² T. Weiler,⁴²
 S. Williamson,⁴² C. Wöhrmann,⁴² R. Wolf,⁴² G. Anagnostou,⁴³ G. Daskalakis,⁴³ T. Geralis,⁴³ A. Kyriakis,⁴³ D. Loukas,⁴³
 I. Topsis-Giotis,⁴³ G. Karathanasis,⁴⁴ S. Kesisoglou,⁴⁴ A. Panagiotou,⁴⁴ N. Saoulidou,⁴⁴ E. Tziaferi,⁴⁴ K. Kousouris,⁴⁵
 I. Papakrivopoulos,⁴⁵ I. Evangelou,⁴⁶ C. Foudas,⁴⁶ P. Gianneios,⁴⁶ P. Katsoulis,⁴⁶ P. Kokkas,⁴⁶ S. Mallios,⁴⁶ N. Manthos,⁴⁶
 I. Papadopoulos,⁴⁶ E. Paradas,⁴⁶ J. Strologas,⁴⁶ F. A. Triantis,⁴⁶ D. Tsitsonis,⁴⁶ M. Csanad,⁴⁷ N. Filipovic,⁴⁷ G. Pasztor,⁴⁷
 O. Surányi,⁴⁷ G. I. Veres,⁴⁷ G. Bencze,⁴⁸ C. Hajdu,⁴⁸ D. Horvath,^{48,u} Á. Hunyadi,⁴⁸ F. Sikler,⁴⁸ V. Veszpremi,⁴⁸
 G. Vesztergombi,^{48,a} T. Á. Vámi,⁴⁸ N. Beni,⁴⁹ S. Czellar,⁴⁹ J. Karancsi,^{49,v} A. Makovec,⁴⁹ J. Molnar,⁴⁹ Z. Szillasi,⁴⁹
 M. Bartók,^{50,w} P. Raics,⁵⁰ Z. L. Trocsanyi,⁵⁰ B. Ujvari,⁵⁰ S. Choudhury,⁵¹ J. R. Komaragiri,⁵¹ S. Bahinipati,^{52,x} P. Mal,⁵²
 K. Mandal,⁵² A. Nayak,^{52,y} D. K. Sahoo,^{52,x} S. K. Swain,⁵² S. Bansal,⁵³ S. B. Beri,⁵³ V. Bhatnagar,⁵³ S. Chauhan,⁵³
 R. Chawla,⁵³ N. Dhingra,⁵³ R. Gupta,⁵³ A. Kaur,⁵³ M. Kaur,⁵³ S. Kaur,⁵³ R. Kumar,⁵³ P. Kumari,⁵³ M. Lohan,⁵³ A. Mehta,⁵³
 S. Sharma,⁵³ J. B. Singh,⁵³ G. Walia,⁵³ Ashok Kumar,⁵⁴ Aashaq Shah,⁵⁴ A. Bhardwaj,⁵⁴ B. C. Choudhary,⁵⁴ R. B. Garg,⁵⁴
 S. Keshri,⁵⁴ A. Kumar,⁵⁴ S. Malhotra,⁵⁴ M. Naimuddin,⁵⁴ K. Ranjan,⁵⁴ R. Sharma,⁵⁴ R. Bhardwaj,^{55,z} R. Bhattacharya,⁵⁵
 S. Bhattacharya,⁵⁵ U. Bhawandeep,^{55,z} D. Bhowmik,⁵⁵ S. Dey,⁵⁵ S. Dutt,^{55,z} S. Dutta,⁵⁵ S. Ghosh,⁵⁵ N. Majumdar,⁵⁵
 K. Mondal,⁵⁵ S. Mukhopadhyay,⁵⁵ S. Nandan,⁵⁵ A. Purohit,⁵⁵ P. K. Rout,⁵⁵ A. Roy,⁵⁵ S. Roy Chowdhury,⁵⁵ S. Sarkar,⁵⁵

- M. Sharan,⁵⁵ B. Singh,⁵⁵ S. Thakur,^{55,2} P. K. Behera,⁵⁶ R. Chudasama,⁵⁷ D. Dutta,⁵⁷ V. Jha,⁵⁷ V. Kumar,⁵⁷ A. K. Mohanty,^{57,4} P. K. Netrakanti,⁵⁷ L. M. Pant,⁵⁷ P. Shukla,⁵⁷ A. Topkar,⁵⁷ T. Aziz,⁵⁸ S. Dugad,⁵⁸ B. Mahakud,⁵⁸ S. Mitra,⁵⁸ G. B. Mohanty,⁵⁸ N. Sur,⁵⁸ B. Sutar,⁵⁸ S. Banerjee,⁵⁹ S. Bhattacharya,⁵⁹ S. Chatterjee,⁵⁹ P. Das,⁵⁹ M. Guchait,⁵⁹ Sa. Jain,⁵⁹ S. Kumar,⁵⁹ M. Maity,^{59,aa} G. Majumder,⁵⁹ K. Mazumdar,⁵⁹ N. Sahoo,⁵⁹ T. Sarkar,^{59,aa} N. Wickramage,^{59,bb} S. Chauhan,⁶⁰ S. Dube,⁶⁰ V. Hegde,⁶⁰ A. Kapoor,⁶⁰ K. Kothekar,⁶⁰ S. Pandey,⁶⁰ A. Rane,⁶⁰ S. Sharma,⁶⁰ S. Chenarani,^{61,cc} E. Eskandari Tadavani,⁶¹ S. M. Etesami,^{61,cc} M. Khakzad,⁶¹ M. Mohammadi Najafabadi,⁶¹ M. Naseri,⁶¹ S. Paktinat Mehdiabadi,^{61,dd} F. Rezaei Hosseiniabadi,⁶¹ B. Safarzadeh,^{61,ee} M. Zeinali,⁶¹ M. Felcini,⁶² M. Grunewald,⁶² M. Abbrescia,^{63a,63b} C. Calabria,^{63a,63b} A. Colaleo,^{63a} D. Creanza,^{63a,63c} L. Cristella,^{63a,63b} N. De Filippis,^{63a,63c} M. De Palma,^{63a,63b} A. Di Florio,^{63a,63b} F. Errico,^{63a,63b} L. Fiore,^{63a} A. Gelmi,^{63a,63b} G. Iaselli,^{63a,63c} S. Lezki,^{63a,63b} G. Maggi,^{63a,63c} M. Maggi,^{63a} B. Marangelli,^{63a,63b} G. Minello,^{63a,63b} S. My,^{63a,63b} S. Nuzzo,^{63a,63b} A. Pompili,^{63a,63b} G. Pugliese,^{63a,63c} R. Radogna,^{63a} A. Ranieri,^{63a} G. Selvaggi,^{63a,63b} A. Sharma,^{63a} L. Silvestris,^{63a,q} R. Venditti,^{63a} P. Verwilligen,^{63a} G. Zito,^{63a} G. Abbiendi,^{64a} C. Battilana,^{64a,64b} D. Bonacorsi,^{64a,64b} L. Borgonovi,^{64a,64b} S. Braibant-Giacomelli,^{64a,64b} L. Brigliadori,^{64a,64b} R. Campanini,^{64a,64b} P. Capiluppi,^{64a,64b} A. Castro,^{64a,64b} F. R. Cavallo,^{64a} S. S. Chhibra,^{64a,64b} G. Codispoti,^{64a,64b} M. Cuffiani,^{64a,64b} G. M. Dallavalle,^{64a} F. Fabbri,^{64a} A. Fanfani,^{64a,64b} D. Fasanella,^{64a,64b} P. Giacomelli,^{64a} C. Grandi,^{64a} L. Guiducci,^{64a,64b} F. Iemmi,^{64a} S. Marcellini,^{64a} G. Masetti,^{64a} A. Montanari,^{64a} F. L. Navarreria,^{64a,64b} A. Perrotta,^{64a} T. Rovelli,^{64a,64b} G. P. Siroli,^{64a,64b} N. Tosi,^{64a} S. Albergo,^{65a,65b} S. Costa,^{65a,65b} A. Di Mattia,^{65a} F. Giordano,^{65a,65b} R. Potenza,^{65a,65b} A. Tricomi,^{65a,65b} C. Tuve,^{65a,65b} G. Barbagli,^{66a} K. Chatterjee,^{66a,66b} V. Ciulli,^{66a,66b} C. Civinini,^{66a} R. D'Alessandro,^{66a,66b} E. Focardi,^{66a,66b} G. Latino,^{66a} P. Lenzi,^{66a,66b} M. Meschini,^{66a} S. Paoletti,^{66a} L. Russo,^{66a,ff} G. Sguazzoni,^{66a} D. Strom,^{66a} L. Viliani,^{66a} L. Benussi,⁶⁷ S. Bianco,⁶⁷ F. Fabbri,⁶⁷ D. Piccolo,⁶⁷ F. Primavera,^{67,4} V. Calvelli,^{68a,68b} F. Ferro,^{68a} F. Ravera,^{68a,68b} E. Robutti,^{68a} S. Tosi,^{68a,68b} A. Benaglia,^{69a} A. Beschi,^{69b} L. Brianza,^{69a,69b} F. Brivio,^{69a,69b} V. Ciriolo,^{69a,69b,4} M. E. Dinardo,^{69a,69b} S. Fiorendi,^{69a,69b} S. Gennai,^{69a} A. Ghezzi,^{69a,69b} P. Govoni,^{69a,69b} M. Malberti,^{69a,69b} S. Malvezzi,^{69a} R. A. Manzoni,^{69a,69b} D. Menasce,^{69a} L. Moroni,^{69a} M. Paganoni,^{69a,69b} K. Pauwels,^{69a,69b} D. Pedrini,^{69a} S. Pigazzini,^{69a,69b,gg} S. Ragazzi,^{69a,69b} T. Tabarelli de Fatis,^{69a,69b} S. Buontempo,^{70a} N. Cavallo,^{70a,70c} S. Di Guida,^{70a,70d,q} F. Fabozzi,^{70a,70c} F. Fienga,^{70a,70b} G. Galati,^{70a,70b} A. O. M. Iorio,^{70a,70b} W. A. Khan,^{70a} L. Lista,^{70a} S. Meola,^{70a,70d,q} P. Paolucci,^{70a,q} C. Sciacca,^{70a,70b} F. Thyssen,^{70a} E. Voevodina,^{70a,70b} P. Azzi,^{71a} N. Bacchetta,^{71a} L. Benato,^{71a,71b} A. Boletti,^{71a,71b} R. Carlin,^{71a,71b} A. Carvalho Antunes De Oliveira,^{71a,71b} P. Checchia,^{71a} M. Dall'Osso,^{71a,71b} P. De Castro Manzano,^{71a} T. Dorigo,^{71a} U. Dosselli,^{71a} F. Gasparini,^{71a,71b} U. Gasparini,^{71a,71b} A. Gozzelino,^{71a} S. Lacaprara,^{71a} P. Lujan,^{71a} M. Margoni,^{71a,71b} A. T. Meneguzzo,^{71a,71b} N. Pozzobon,^{71a,71b} P. Ronchese,^{71a,71b} R. Rossin,^{71a,71b} F. Simonetto,^{71a,71b} A. Tiko,^{71a} E. Torassa,^{71a} M. Zanetti,^{71a,71b} P. Zotto,^{71a,71b} G. Zumerle,^{71a,71b} A. Braghieri,^{72a} A. Magnani,^{72a} P. Montagna,^{72a,72b} S. P. Ratti,^{72a,72b} V. Re,^{72a} M. Ressegotti,^{72a,72b} C. Riccardi,^{72a,72b} P. Salvini,^{72a} I. Vai,^{72a,72b} P. Vitulo,^{72a,72b} L. Alunni Solestizi,^{73a,73b} M. Biasini,^{73a,73b} G. M. Bilei,^{73a} C. Cecchi,^{73a,73b} D. Ciangottini,^{73a,73b} L. Fanò,^{73a,73b} P. Lariccia,^{73a,73b} R. Leonardi,^{73a,73b} E. Manoni,^{73a,73b} G. Mantovani,^{73a,73b} V. Mariani,^{73a,73b} M. Menichelli,^{73a} A. Rossi,^{73a,73b} A. Santocchia,^{73a,73b} D. Spiga,^{73a} K. Androssov,^{74a} P. Azzurri,^{74a} G. Bagliesi,^{74a} L. Bianchini,^{74a} T. Boccali,^{74a} L. Borrello,^{74a} R. Castaldi,^{74a} M. A. Ciocci,^{74a,74b} R. Dell'Orso,^{74a} G. Fedi,^{74a} L. Giannini,^{74a,74c} A. Giassi,^{74a} M. T. Grippo,^{74a} F. Ligabue,^{74a,74c} T. Lomtadze,^{74a} E. Manca,^{74a,74c} G. Mandorli,^{74a,74c} A. Messineo,^{74a,74b} F. Palla,^{74a} A. Rizzi,^{74a,74b} P. Spagnolo,^{74a} R. Tenchini,^{74a} G. Tonelli,^{74a,74b} A. Venturi,^{74a} P. G. Verdini,^{74a} L. Barone,^{75a,75b} F. Cavallari,^{75a} M. Cipriani,^{75a,75b} N. Daci,^{75a} D. Del Re,^{75a,75b} E. Di Marco,^{75a,75b} M. Diemoz,^{75a} S. Gelli,^{75a,75b} E. Longo,^{75a,75b} B. Marzocchi,^{75a,75b} P. Meridiani,^{75a} G. Organtini,^{75a,75b} F. Pandolfi,^{75a} R. Paramatti,^{75a,75b} F. Preiato,^{75a,75b} S. Rahatlou,^{75a,75b} C. Rovelli,^{75a} F. Santanastasio,^{75a,75b} N. Amapane,^{76a,76b} R. Arcidiacono,^{76a,76c} S. Argiro,^{76a,76b} M. Arneodo,^{76a,76c} N. Bartosik,^{76a} R. Bellan,^{76a,76b} C. Biino,^{76a} N. Cartiglia,^{76a} R. Castello,^{76a,76b} F. Cenna,^{76a,76b} M. Costa,^{76a,76b} R. Covarelli,^{76a,76b} A. Degano,^{76a,76b} N. Demaria,^{76a} B. Kiani,^{76a,76b} C. Mariotti,^{76a} S. Maselli,^{76a} E. Migliore,^{76a,76b} V. Monaco,^{76a,76b} E. Monteil,^{76a,76b} M. Monteno,^{76a} M. M. Obertino,^{76a,76b} L. Pacher,^{76a,76b} N. Pastrone,^{76a} M. Pelliccioni,^{76a} G. L. Pinna Angioni,^{76a,76b} A. Romero,^{76a,76b} M. Ruspa,^{76a,76c} R. Sacchi,^{76a,76b} K. Shchelina,^{76a,76b} V. Sola,^{76a} A. Solano,^{76a,76b} A. Staiano,^{76a} S. Belforte,^{77a} M. Casarsa,^{77a} F. Cossutti,^{77a} G. Della Ricca,^{77a,77b} A. Zanetti,^{77a} D. H. Kim,⁷⁸ G. N. Kim,⁷⁸ M. S. Kim,⁷⁸ J. Lee,⁷⁸ S. Lee,⁷⁸ S. W. Lee,⁷⁸ C. S. Moon,⁷⁸ Y. D. Oh,⁷⁸ S. Sekmen,⁷⁸ D. C. Son,⁷⁸ Y. C. Yang,⁷⁸ H. Kim,⁷⁹ D. H. Moon,⁷⁹ G. Oh,⁷⁹ J. A. Brochero Cifuentes,⁸⁰ J. Goh,⁸⁰ T. J. Kim,⁸⁰ S. Cho,⁸¹ S. Choi,⁸¹ Y. Go,⁸¹ D. Gyun,⁸¹ S. Ha,⁸¹ B. Hong,⁸¹ Y. Jo,⁸¹ Y. Kim,⁸¹ K. Lee,⁸¹ K. S. Lee,⁸¹ S. Lee,⁸¹ J. Lim,⁸¹ S. K. Park,⁸¹ Y. Roh,⁸¹ J. Almond,⁸² J. Kim,⁸² J. S. Kim,⁸² H. Lee,⁸² K. Lee,⁸² K. Nam,⁸² S. B. Oh,⁸² B. C. Radburn-Smith,⁸² S. h. Seo,⁸² U. K. Yang,⁸² H. D. Yoo,⁸² G. B. Yu,⁸² H. Kim,⁸³ J. H. Kim,⁸³ J. S. H. Lee,⁸³ I. C. Park,⁸³

- Y. Choi,⁸⁴ C. Hwang,⁸⁴ J. Lee,⁸⁴ I. Yu,⁸⁴ V. Dudenas,⁸⁵ A. Juodagalvis,⁸⁵ J. Vaitkus,⁸⁵ I. Ahmed,⁸⁶ Z. A. Ibrahim,⁸⁶
 M. A. B. Md Ali,^{86,bb} F. Mohamad Idris,^{86,ii} W. A. T. Wan Abdullah,⁸⁶ M. N. Yusli,⁸⁶ Z. Zolkapli,⁸⁶ R Reyes-Almanza,⁸⁷
 G. Ramirez-Sanchez,⁸⁷ M. C. Duran-Osuna,⁸⁷ H. Castilla-Valdez,⁸⁷ E. De La Cruz-Burelo,⁸⁷ I. Heredia-De La Cruz,^{87,jj}
 R. I. Rabadan-Trejo,⁸⁷ R. Lopez-Fernandez,⁸⁷ J. Mejia Guisao,⁸⁷ A. Sanchez-Hernandez,⁸⁷ S. Carrillo Moreno,⁸⁸
 C. Oropeza Barrera,⁸⁸ F. Vazquez Valencia,⁸⁸ J. Eysermans,⁸⁹ I. Pedraza,⁸⁹ H. A. Salazar Ibarguen,⁸⁹ C. Uribe Estrada,⁸⁹
 A. Morelos Pineda,⁹⁰ D. Kroscheck,⁹¹ S. Bheesette,⁹² P. H. Butler,⁹² A. Ahmad,⁹³ M. Ahmad,⁹³ Q. Hassan,⁹³
 H. R. Hoorani,⁹³ A. Saddique,⁹³ M. A. Shah,⁹³ M. Shoaib,⁹³ M. Waqas,⁹³ H. Bialkowska,⁹⁴ M. Bluj,⁹⁴ B. Boimska,⁹⁴
 T. Frueboes,⁹⁴ M. Górski,⁹⁴ M. Kazana,⁹⁴ K. Nawrocki,⁹⁴ M. Szleper,⁹⁴ P. Traczyk,⁹⁴ P. Zalewski,⁹⁴ K. Bunkowski,⁹⁵
 A. Byszuk,^{95,kk} K. Doroba,⁹⁵ A. Kalinowski,⁹⁵ M. Konecki,⁹⁵ J. Krolkowski,⁹⁵ M. Misiura,⁹⁵ M. Olszewski,⁹⁵ A. Pyskir,⁹⁵
 M. Walczak,⁹⁵ P. Bargassa,⁹⁶ C. Beirão Da Cruz E Silva,⁹⁶ A. Di Francesco,⁹⁶ P. Faccioli,⁹⁶ B. Galinhas,⁹⁶ M. Gallinaro,⁹⁶
 J. Hollar,⁹⁶ N. Leonardo,⁹⁶ L. Lloret Iglesias,⁹⁶ M. V. Nemallapudi,⁹⁶ J. Seixas,⁹⁶ G. Strong,⁹⁶ O. Toldaiev,⁹⁶ D. Vadruccio,⁹⁶
 J. Varela,⁹⁶ S. Afanasiev,⁹⁷ P. Bunin,⁹⁷ M. Gavrilenko,⁹⁷ I. Golutvin,⁹⁷ I. Gorbunov,⁹⁷ A. Kamenev,⁹⁷ V. Karjavin,⁹⁷
 A. Lanev,⁹⁷ A. Malakhov,⁹⁷ V. Matveev,^{97,ll,mm} P. Moisenz,⁹⁷ V. Palichik,⁹⁷ V. Perelygin,⁹⁷ S. Shmatov,⁹⁷ S. Shulha,⁹⁷
 N. Skatchkov,⁹⁷ V. Smirnov,⁹⁷ N. Voytishin,⁹⁷ A. Zarubin,⁹⁷ Y. Ivanov,⁹⁸ V. Kim,^{98,nn} E. Kuznetsova,^{98,oo} P. Levchenko,⁹⁸
 V. Murzin,⁹⁸ V. Oreshkin,⁹⁸ I. Smirnov,⁹⁸ D. Sosnov,⁹⁸ V. Sulimov,⁹⁸ L. Uvarov,⁹⁸ S. Vavilov,⁹⁸ A. Vorobyev,⁹⁸
 Yu. Andreev,⁹⁹ A. Dermenev,⁹⁹ S. Gninenko,⁹⁹ N. Golubev,⁹⁹ A. Karneyeu,⁹⁹ M. Kirsanov,⁹⁹ N. Krasnikov,⁹⁹
 A. Pashenkov,⁹⁹ D. Tlisov,⁹⁹ A. Toropin,⁹⁹ V. Epshteyn,¹⁰⁰ V. Gavrilov,¹⁰⁰ N. Lychkovskaya,¹⁰⁰ V. Popov,¹⁰⁰
 I. Pozdnyakov,¹⁰⁰ G. Safronov,¹⁰⁰ A. Spiridonov,¹⁰⁰ A. Stepenov,¹⁰⁰ V. Stolin,¹⁰⁰ M. Toms,¹⁰⁰ E. Vlasov,¹⁰⁰ A. Zhokin,¹⁰⁰
 T. Aushev,¹⁰¹ A. Bylinkin,^{101,mm} R. Chistov,^{102,pp} M. Danilov,^{102,pp} P. Parygin,¹⁰² D. Philippov,¹⁰² S. Polikarpov,¹⁰²
 E. Tarkovskii,¹⁰² V. Andreev,¹⁰³ M. Azarkin,^{103,mm} I. Dremin,^{103,mm} M. Kirakosyan,^{103,mm} S. V. Rusakov,¹⁰³ A. Terkulov,¹⁰³
 A. Baskakov,¹⁰⁴ A. Belyaev,¹⁰⁴ E. Boos,¹⁰⁴ V. Bunichev,¹⁰⁴ M. Dubinin,^{104,qq} L. Dudko,¹⁰⁴ V. Klyukhin,¹⁰⁴ O. Kodolova,¹⁰⁴
 N. Korneeva,¹⁰⁴ I. Lokhtin,¹⁰⁴ I. Miagkov,¹⁰⁴ S. Obraztsov,¹⁰⁴ M. Perfilov,¹⁰⁴ V. Savrin,¹⁰⁴ P. Volkov,¹⁰⁴ V. Blinov,^{105,rr}
 D. Shtol,^{105,rr} Y. Skovpen,^{105,rr} I. Azhgirey,¹⁰⁶ I. Bayshev,¹⁰⁶ S. Bitioukov,¹⁰⁶ D. Elumakhov,¹⁰⁶ A. Godizov,¹⁰⁶
 V. Kachanov,¹⁰⁶ A. Kalinin,¹⁰⁶ D. Konstantinov,¹⁰⁶ P. Mandrik,¹⁰⁶ V. Petrov,¹⁰⁶ R. Ryutin,¹⁰⁶ A. Sobol,¹⁰⁶ S. Troshin,¹⁰⁶
 N. Tyurin,¹⁰⁶ A. Uzunian,¹⁰⁶ A. Volkov,¹⁰⁶ A. Babaev,¹⁰⁷ P. Adzic,^{108,ss} P. Cirkovic,¹⁰⁸ D. Devetak,¹⁰⁸ M. Dordevic,¹⁰⁸
 J. Milosevic,¹⁰⁸ J. Alcaraz Maestre,¹⁰⁹ I. Bachiller,¹⁰⁹ M. Barrio Luna,¹⁰⁹ M. Cerrada,¹⁰⁹ N. Colino,¹⁰⁹ B. De La Cruz,¹⁰⁹
 A. Delgado Peris,¹⁰⁹ C. Fernandez Bedoya,¹⁰⁹ J. P. Fernández Ramos,¹⁰⁹ J. Flix,¹⁰⁹ M. C. Fouz,¹⁰⁹ O. Gonzalez Lopez,¹⁰⁹
 S. Goy Lopez,¹⁰⁹ J. M. Hernandez,¹⁰⁹ M. I. Josa,¹⁰⁹ D. Moran,¹⁰⁹ A. Pérez-Calero Yzquierdo,¹⁰⁹ J. Puerta Pelayo,¹⁰⁹
 I. Redondo,¹⁰⁹ L. Romero,¹⁰⁹ M. S. Soares,¹⁰⁹ A. Triossi,¹⁰⁹ A. Álvarez Fernández,¹⁰⁹ C. Albajar,¹¹⁰ J. F. de Trocóniz,¹¹⁰
 J. Cuevas,¹¹¹ C. Erice,¹¹¹ J. Fernandez Menendez,¹¹¹ S. Folgueras,¹¹¹ I. Gonzalez Caballero,¹¹¹ J. R. González Fernández,¹¹¹
 E. Palencia Cortezon,¹¹¹ S. Sanchez Cruz,¹¹¹ P. Vischia,¹¹¹ J. M. Vizan Garcia,¹¹¹ I. J. Cabrillo,¹¹² A. Calderon,¹¹²
 B. Chazin Quero,¹¹² J. Duarte Campderros,¹¹² M. Fernandez,¹¹² P. J. Fernández Manteca,¹¹² J. Garcia-Ferrero,¹¹²
 A. García Alonso,¹¹² G. Gomez,¹¹² A. Lopez Virto,¹¹² J. Marco,¹¹² C. Martinez Rivero,¹¹² P. Martinez Ruiz del Arbol,¹¹²
 F. Matorras,¹¹² J. Piedra Gomez,¹¹² C. Prieels,¹¹² T. Rodrigo,¹¹² A. Ruiz-Jimeno,¹¹² L. Scodellaro,¹¹² N. Trevisani,¹¹²
 I. Vila,¹¹² R. Vilar Cortabitarte,¹¹² D. Abbaneo,¹¹³ B. Akgun,¹¹³ E. Auffray,¹¹³ P. Baillon,¹¹³ A. H. Ball,¹¹³ D. Barney,¹¹³
 J. Bendavid,¹¹³ J. F. Benitez,¹¹³ M. Bianco,¹¹³ A. Bocci,¹¹³ C. Botta,¹¹³ T. Camporesi,¹¹³ M. Cepeda,¹¹³ G. Cerminara,¹¹³
 E. Chapon,¹¹³ Y. Chen,¹¹³ D. d'Enterria,¹¹³ A. Dabrowski,¹¹³ V. Daponte,¹¹³ A. David,¹¹³ M. De Gruttola,¹¹³
 A. De Roeck,¹¹³ N. Deelen,¹¹³ M. Dobson,¹¹³ T. du Pree,¹¹³ M. Dünser,¹¹³ N. Dupont,¹¹³ A. Elliott-Peisert,¹¹³
 P. Everaerts,¹¹³ F. Fallavollita,^{113,tt} G. Franzoni,¹¹³ J. Fulcher,¹¹³ W. Funk,¹¹³ D. Gigi,¹¹³ A. Gilbert,¹¹³ K. Gill,¹¹³ F. Glege,¹¹³
 D. Gulhan,¹¹³ J. Hegeman,¹¹³ V. Innocente,¹¹³ A. Jafari,¹¹³ P. Janot,¹¹³ O. Karacheban,^{113,t} J. Kieseler,¹¹³ V. Knünz,¹¹³
 A. Kornmayer,¹¹³ M. Krammer,^{113,b} C. Lange,¹¹³ P. Lecoq,¹¹³ C. Lourenço,¹¹³ M. T. Lucchini,¹¹³ L. Malgeri,¹¹³
 M. Mannelli,¹¹³ A. Martelli,¹¹³ F. Meijers,¹¹³ J. A. Merlin,¹¹³ S. Mersi,¹¹³ E. Meschi,¹¹³ P. Milenovic,^{113,uu} F. Moortgat,¹¹³
 M. Mulders,¹¹³ H. Neugebauer,¹¹³ J. Ngadiuba,¹¹³ S. Orfanelli,¹¹³ L. Orsini,¹¹³ F. Pantaleo,^{113,q} L. Pape,¹¹³ E. Perez,¹¹³
 M. Peruzzi,¹¹³ A. Petrilli,¹¹³ G. Petrucciani,¹¹³ A. Pfeiffer,¹¹³ M. Pierini,¹¹³ F. M. Pitters,¹¹³ D. Rabady,¹¹³ A. Racz,¹¹³
 T. Reis,¹¹³ G. Rolandi,^{113,vv} M. Rovere,¹¹³ H. Sakulin,¹¹³ C. Schäfer,¹¹³ C. Schwick,¹¹³ M. Seidel,¹¹³ M. Selvaggi,¹¹³
 A. Sharma,¹¹³ P. Silva,¹¹³ P. Sphicas,^{113,ww} A. Stakia,¹¹³ J. Steggemann,¹¹³ M. Stoye,¹¹³ M. Tosi,¹¹³ D. Treille,¹¹³
 A. Tsirou,¹¹³ V. Veckalns,^{113,xx} M. Verweij,¹¹³ W. D. Zeuner,¹¹³ W. Bertl,^{114,a} L. Caminada,^{114,yy} K. Deiters,¹¹⁴
 W. Erdmann,¹¹⁴ R. Horisberger,¹¹⁴ Q. Ingram,¹¹⁴ H. C. Kaestli,¹¹⁴ D. Kotlinski,¹¹⁴ U. Langenegger,¹¹⁴ T. Rohe,¹¹⁴
 S. A. Wiederkehr,¹¹⁴ M. Backhaus,¹¹⁵ L. Bäni,¹¹⁵ P. Berger,¹¹⁵ B. Casal,¹¹⁵ N. Chernyavskaya,¹¹⁵ G. Dissertori,¹¹⁵

- M. Dittmar,¹¹⁵ M. Donegà,¹¹⁵ C. Dorfer,¹¹⁵ C. Grab,¹¹⁵ C. Heidegger,¹¹⁵ D. Hits,¹¹⁵ J. Hoss,¹¹⁵ T. Klijnsma,¹¹⁵
 W. Lustermann,¹¹⁵ M. Marionneau,¹¹⁵ M. T. Meinhard,¹¹⁵ D. Meister,¹¹⁵ F. Michel, ¹¹⁵ P. Musella,¹¹⁵ F. Nessi-Tedaldi,¹¹⁵
 J. Pata,¹¹⁵ F. Pauss,¹¹⁵ G. Perrin,¹¹⁵ L. Perrozzi,¹¹⁵ M. Quitnat,¹¹⁵ M. Reichmann,¹¹⁵ D. Ruini,¹¹⁵ D. A. Sanz Becerra,¹¹⁵
 M. Schönenberger,¹¹⁵ L. Shchutska,¹¹⁵ V. R. Tavolaro,¹¹⁵ K. Theofilatos,¹¹⁵ M. L. Vesterbacka Olsson,¹¹⁵ R. Wallny,¹¹⁵
 D. H. Zhu,¹¹⁵ T. K. Aarrestad,¹¹⁶ C. Amsler,^{116,zz} D. Brzhechko,¹¹⁶ M. F. Canelli,¹¹⁶ A. De Cosa,¹¹⁶ R. Del Burgo,¹¹⁶
 S. Donato,¹¹⁶ C. Galloni,¹¹⁶ T. Hreus,¹¹⁶ B. Kilminster,¹¹⁶ I. Neutelings,¹¹⁶ D. Pinna,¹¹⁶ G. Rauco,¹¹⁶ P. Robmann,¹¹⁶
 D. Salerno,¹¹⁶ K. Schweiger,¹¹⁶ C. Seitz,¹¹⁶ Y. Takahashi,¹¹⁶ A. Zucchetta,¹¹⁶ V. Candelise,¹¹⁷ Y. H. Chang,¹¹⁷
 K. y. Cheng,¹¹⁷ T. H. Doan,¹¹⁷ Sh. Jain,¹¹⁷ R. Khurana,¹¹⁷ C. M. Kuo,¹¹⁷ W. Lin,¹¹⁷ A. Pozdnyakov,¹¹⁷ S. S. Yu,¹¹⁷
 Arun Kumar,¹¹⁸ P. Chang,¹¹⁸ Y. Chao,¹¹⁸ K. F. Chen,¹¹⁸ P. H. Chen,¹¹⁸ F. Fiori,¹¹⁸ W.-S. Hou,¹¹⁸ Y. Hsiung,¹¹⁸ Y. F. Liu,¹¹⁸
 R.-S. Lu,¹¹⁸ E. Paganis,¹¹⁸ A. Psallidas,¹¹⁸ A. Steen,¹¹⁸ J. f. Tsai,¹¹⁸ B. Asavapibhop,¹¹⁹ K. Kovitanggoon,¹¹⁹ G. Singh,¹¹⁹
 N. Srimanobhas,¹¹⁹ A. Bat,¹²⁰ F. Boran,¹²⁰ S. Damarseckin,¹²⁰ Z. S. Demiroglu,¹²⁰ C. Dozen,¹²⁰ E. Eskut,¹²⁰ S. Girgis,¹²⁰
 G. Gokbulut,¹²⁰ Y. Guler,¹²⁰ I. Hos,^{120,aaa} E. E. Kangal,^{120,bbb} O. Kara,¹²⁰ A. Kayis Topaksu,¹²⁰ U. Kiminsu,¹²⁰
 M. Oglakci,¹²⁰ G. Onengut,¹²⁰ K. Ozdemir,^{120,ccc} S. Ozturk,^{120,ddd} A. Polatoz,¹²⁰ B. Tali,^{120,eee} U. G. Tok,¹²⁰ S. Turkcapar,¹²⁰
 I. S. Zorbakir,¹²⁰ C. Zorbilmez,¹²⁰ G. Karapinar,^{121,fff} K. Ocalan,^{121,ggg} M. Yalvac,¹²¹ M. Zeyrek,¹²¹ I. O. Atakisi,¹²²
 E. Gülmез,¹²² M. Kaya,^{122,hhh} O. Kaya,^{122,iii} S. Tekten,¹²² E. A. Yetkin,^{122,jjj} M. N. Agaras,¹²³ S. Atay,¹²³ A. Cakir,¹²³
 K. Cankocak,¹²³ Y. Komurcu,¹²³ B. Grynyov,¹²⁴ L. Levchuk,¹²⁵ F. Ball,¹²⁶ L. Beck,¹²⁶ J. J. Brooke,¹²⁶ D. Burns,¹²⁶
 E. Clement,¹²⁶ D. Cussans,¹²⁶ O. Davignon,¹²⁶ H. Flacher,¹²⁶ J. Goldstein,¹²⁶ G. P. Heath,¹²⁶ H. F. Heath,¹²⁶ L. Kreczko,¹²⁶
 D. M. Newbold,^{126,kkk} S. Paramesvaran,¹²⁶ T. Sakuma,¹²⁶ S. Seif El Nasr-storey,¹²⁶ D. Smith,¹²⁶ V. J. Smith,¹²⁶ K. W. Bell,¹²⁷
 A. Belyaev,^{127,iii} C. Brew,¹²⁷ R. M. Brown,¹²⁷ D. Cieri,¹²⁷ D. J. A. Cockerill,¹²⁷ J. A. Coughlan,¹²⁷ K. Harder,¹²⁷ S. Harper,¹²⁷
 J. Linacre,¹²⁷ E. Olaiya,¹²⁷ D. Petyt,¹²⁷ C. H. Shepherd-Themistocleous,¹²⁷ A. Thea,¹²⁷ I. R. Tomalin,¹²⁷ T. Williams,¹²⁷
 W. J. Womersley,¹²⁷ G. Auzinger,¹²⁸ R. Bainbridge,¹²⁸ P. Bloch,¹²⁸ J. Borg,¹²⁸ S. Breeze,¹²⁸ O. Buchmuller,¹²⁸
 A. Bundock,¹²⁸ S. Casasso,¹²⁸ D. Colling,¹²⁸ L. Corpe,¹²⁸ P. Dauncey,¹²⁸ G. Davies,¹²⁸ M. Della Negra,¹²⁸ R. Di Maria,¹²⁸
 Y. Haddad,¹²⁸ G. Hall,¹²⁸ G. Iles,¹²⁸ T. James,¹²⁸ M. Komm,¹²⁸ R. Lane,¹²⁸ C. Laner,¹²⁸ L. Lyons,¹²⁸ A.-M. Magnan,¹²⁸
 S. Malik,¹²⁸ L. Mastrolorenzo,¹²⁸ T. Matsushita,¹²⁸ J. Nash,^{128,mmm} A. Nikitenko,^{128,h} V. Palladino,¹²⁸ M. Pesaresi,¹²⁸
 A. Richards,¹²⁸ A. Rose,¹²⁸ E. Scott,¹²⁸ C. Seez,¹²⁸ A. Shtipliyski,¹²⁸ T. Strebler,¹²⁸ S. Summers,¹²⁸ A. Tapper,¹²⁸
 K. Uchida,¹²⁸ M. Vazquez Acosta,^{128,nnn} T. Virdee,^{128,q} N. Wardle,¹²⁸ D. Winterbottom,¹²⁸ J. Wright,¹²⁸ S. C. Zenz,¹²⁸
 J. E. Cole,¹²⁹ P. R. Hobson,¹²⁹ A. Khan,¹²⁹ P. Kyberd,¹²⁹ A. Morton,¹²⁹ I. D. Reid,¹²⁹ L. Teodorescu,¹²⁹ S. Zahid,¹²⁹
 A. Borzou,¹³⁰ K. Call,¹³⁰ J. Dittmann,¹³⁰ K. Hatakeyama,¹³⁰ H. Liu,¹³⁰ N. Pastika,¹³⁰ C. Smith,¹³⁰ R. Bartek,¹³¹
 A. Dominguez,¹³¹ A. Buccilli,¹³² S. I. Cooper,¹³² C. Henderson,¹³² P. Rumerio,¹³² C. West,¹³² D. Arcaro,¹³³ A. Avetisyan,¹³³
 T. Bose,¹³³ D. Gastler,¹³³ D. Rankin,¹³³ C. Richardson,¹³³ J. Rohlf,¹³³ L. Sulak,¹³³ D. Zou,¹³³ G. Benelli,¹³⁴ D. Cutts,¹³⁴
 M. Hadley,¹³⁴ J. Hakala,¹³⁴ U. Heintz,¹³⁴ J. M. Hogan,^{134,ooo} K. H. M. Kwok,¹³⁴ E. Laird,¹³⁴ G. Landsberg,¹³⁴ J. Lee,¹³⁴
 Z. Mao,¹³⁴ M. Narain,¹³⁴ J. Pazzini,¹³⁴ S. Piperov,¹³⁴ S. Sagir,¹³⁴ R. Syarif,¹³⁴ D. Yu,¹³⁴ R. Band,¹³⁵ C. Brainerd,¹³⁵
 R. Breedon,¹³⁵ D. Burns,¹³⁵ M. Calderon De La Barca Sanchez,¹³⁵ M. Chertok,¹³⁵ J. Conway,¹³⁵ R. Conway,¹³⁵ P. T. Cox,¹³⁵
 R. Erbacher,¹³⁵ C. Flores,¹³⁵ G. Funk,¹³⁵ W. Ko,¹³⁵ R. Lander,¹³⁵ C. McLean,¹³⁵ M. Mulhearn,¹³⁵ D. Pellett,¹³⁵ J. Pilot,¹³⁵
 S. Shalhout,¹³⁵ M. Shi,¹³⁵ J. Smith,¹³⁵ D. Stolp,¹³⁵ D. Taylor,¹³⁵ K. Tos,¹³⁵ M. Tripathi,¹³⁵ Z. Wang,¹³⁵ F. Zhang,¹³⁵
 M. Bachtis,¹³⁶ C. Bravo,¹³⁶ R. Cousins,¹³⁶ A. Dasgupta,¹³⁶ A. Florent,¹³⁶ J. Hauser,¹³⁶ M. Ignatenko,¹³⁶ N. Mccoll,¹³⁶
 S. Regnard,¹³⁶ D. Saltzberg,¹³⁶ C. Schnaible,¹³⁶ V. Valuev,¹³⁶ E. Bouvier,¹³⁷ K. Burt,¹³⁷ R. Clare,¹³⁷ J. Ellison,¹³⁷
 J. W. Gary,¹³⁷ S. M. A. Ghiasi Shirazi,¹³⁷ G. Hanson,¹³⁷ G. Karapostoli,¹³⁷ E. Kennedy,¹³⁷ F. Lacroix,¹³⁷ O. R. Long,¹³⁷
 M. Olmedo Negrete,¹³⁷ M. I. Paneva,¹³⁷ W. Si,¹³⁷ L. Wang,¹³⁷ H. Wei,¹³⁷ S. Wimpenny,¹³⁷ B. R. Yates,¹³⁷ J. G. Branson,¹³⁸
 S. Cittolin,¹³⁸ M. Derdzinski,¹³⁸ R. Gerosa,¹³⁸ D. Gilbert,¹³⁸ B. Hashemi,¹³⁸ A. Holzner,¹³⁸ D. Klein,¹³⁸ G. Kole,¹³⁸
 V. Krutelyov,¹³⁸ J. Letts,¹³⁸ M. Masciovecchio,¹³⁸ D. Olivito,¹³⁸ S. Padhi,¹³⁸ M. Pieri,¹³⁸ M. Sani,¹³⁸ V. Sharma,¹³⁸
 S. Simon,¹³⁸ M. Tadel,¹³⁸ A. Vartak,¹³⁸ S. Wasserbaech,^{138,ppp} J. Wood,¹³⁸ F. Würthwein,¹³⁸ A. Yagil,¹³⁸
 G. Zevi Della Porta,¹³⁸ N. Amin,¹³⁹ R. Bhandari,¹³⁹ J. Bradmiller-Feld,¹³⁹ C. Campagnari,¹³⁹ M. Citron,¹³⁹ A. Dishaw,¹³⁹
 V. Dutta,¹³⁹ M. Franco Sevilla,¹³⁹ L. Gouskos,¹³⁹ R. Heller,¹³⁹ J. Incandela,¹³⁹ A. Ovcharova,¹³⁹ H. Qu,¹³⁹ J. Richman,¹³⁹
 D. Stuart,¹³⁹ I. Suarez,¹³⁹ J. Yoo,¹³⁹ D. Anderson,¹⁴⁰ A. Bornheim,¹⁴⁰ J. Bunn,¹⁴⁰ J. M. Lawhorn,¹⁴⁰ H. B. Newman,¹⁴⁰
 T. Q. Nguyen,¹⁴⁰ C. Pena,¹⁴⁰ M. Spiropulu,¹⁴⁰ J. R. Vlimant,¹⁴⁰ R. Wilkinson,¹⁴⁰ S. Xie,¹⁴⁰ Z. Zhang,¹⁴⁰ R. Y. Zhu,¹⁴⁰
 M. B. Andrews,¹⁴¹ T. Ferguson,¹⁴¹ T. Mudholkar,¹⁴¹ M. Paulini,¹⁴¹ J. Russ,¹⁴¹ M. Sun,¹⁴¹ H. Vogel,¹⁴¹ I. Vorobiev,¹⁴¹
 M. Weinberg,¹⁴¹ J. P. Cumalat,¹⁴² W. T. Ford,¹⁴² F. Jensen,¹⁴² A. Johnson,¹⁴² M. Krohn,¹⁴² S. Leontsinis,¹⁴²
 E. MacDonald,¹⁴² T. Mulholland,¹⁴² K. Stenson,¹⁴² K. A. Ulmer,¹⁴² S. R. Wagner,¹⁴² J. Alexander,¹⁴³ J. Chaves,¹⁴³

- Y. Cheng,¹⁴³ J. Chu,¹⁴³ A. Datta,¹⁴³ K. Mcdermott,¹⁴³ N. Mirman,¹⁴³ J. R. Patterson,¹⁴³ D. Quach,¹⁴³ A. Rinkevicius,¹⁴³
 A. Ryd,¹⁴³ L. Skinnari,¹⁴³ L. Soffi,¹⁴³ S. M. Tan,¹⁴³ Z. Tao,¹⁴³ J. Thom,¹⁴³ J. Tucker,¹⁴³ P. Wittich,¹⁴³ M. Zientek,¹⁴³
 S. Abdullin,¹⁴⁴ M. Albrow,¹⁴⁴ M. Alyari,¹⁴⁴ G. Apollinari,¹⁴⁴ A. Apresyan,¹⁴⁴ A. Apyan,¹⁴⁴ S. Banerjee,¹⁴⁴
 L. A. T. Bauerwick,¹⁴⁴ A. Beretvas,¹⁴⁴ J. Berryhill,¹⁴⁴ P. C. Bhat,¹⁴⁴ G. Bolla,^{144,a} K. Burkett,¹⁴⁴ J. N. Butler,¹⁴⁴ A. Canepa,¹⁴⁴
 G. B. Cerati,¹⁴⁴ H. W. K. Cheung,¹⁴⁴ F. Chlebana,¹⁴⁴ M. Cremonesi,¹⁴⁴ J. Duarte,¹⁴⁴ V. D. Elvira,¹⁴⁴ J. Freeman,¹⁴⁴
 Z. Gecse,¹⁴⁴ E. Gottschalk,¹⁴⁴ L. Gray,¹⁴⁴ D. Green,¹⁴⁴ S. Grünendahl,¹⁴⁴ O. Gutsche,¹⁴⁴ J. Hanlon,¹⁴⁴ R. M. Harris,¹⁴⁴
 S. Hasegawa,¹⁴⁴ J. Hirschauer,¹⁴⁴ Z. Hu,¹⁴⁴ B. Jayatilaka,¹⁴⁴ S. Jindariani,¹⁴⁴ M. Johnson,¹⁴⁴ U. Joshi,¹⁴⁴ B. Klima,¹⁴⁴
 M. J. Kortelainen,¹⁴⁴ B. Kreis,¹⁴⁴ S. Lammel,¹⁴⁴ D. Lincoln,¹⁴⁴ R. Lipton,¹⁴⁴ M. Liu,¹⁴⁴ T. Liu,¹⁴⁴ R. Lopes De Sá,¹⁴⁴
 J. Lykken,¹⁴⁴ K. Maeshima,¹⁴⁴ N. Magini,¹⁴⁴ J. M. Marraffino,¹⁴⁴ D. Mason,¹⁴⁴ P. McBride,¹⁴⁴ P. Merkel,¹⁴⁴ S. Mrenna,¹⁴⁴
 S. Nahn,¹⁴⁴ V. O'Dell,¹⁴⁴ K. Pedro,¹⁴⁴ O. Prokofyev,¹⁴⁴ G. Rakness,¹⁴⁴ L. Ristori,¹⁴⁴ A. Savoy-Navarro,^{144,qqq}
 B. Schneider,¹⁴⁴ E. Sexton-Kennedy,¹⁴⁴ A. Soha,¹⁴⁴ W. J. Spalding,¹⁴⁴ L. Spiegel,¹⁴⁴ S. Stoynev,¹⁴⁴ J. Strait,¹⁴⁴ N. Strobbe,¹⁴⁴
 L. Taylor,¹⁴⁴ S. Tkaczyk,¹⁴⁴ N. V. Tran,¹⁴⁴ L. Uplegger,¹⁴⁴ E. W. Vaandering,¹⁴⁴ C. Vernieri,¹⁴⁴ M. Verzocchi,¹⁴⁴ R. Vidal,¹⁴⁴
 M. Wang,¹⁴⁴ H. A. Weber,¹⁴⁴ A. Whitbeck,¹⁴⁴ W. Wu,¹⁴⁴ D. Acosta,¹⁴⁵ P. Avery,¹⁴⁵ P. Bortignon,¹⁴⁵ D. Bourilkov,¹⁴⁵
 A. Brinkerhoff,¹⁴⁵ A. Carnes,¹⁴⁵ M. Carver,¹⁴⁵ D. Curry,¹⁴⁵ R. D. Field,¹⁴⁵ I. K. Furic,¹⁴⁵ S. V. Gleyzer,¹⁴⁵ B. M. Joshi,¹⁴⁵
 J. Konigsberg,¹⁴⁵ A. Korytov,¹⁴⁵ K. Kotov,¹⁴⁵ P. Ma,¹⁴⁵ K. Matchev,¹⁴⁵ H. Mei,¹⁴⁵ G. Mitselmakher,¹⁴⁵ K. Shi,¹⁴⁵
 D. Sperka,¹⁴⁵ N. Terentyev,¹⁴⁵ L. Thomas,¹⁴⁵ J. Wang,¹⁴⁵ S. Wang,¹⁴⁵ J. Yelton,¹⁴⁵ Y. R. Joshi,¹⁴⁶ S. Linn,¹⁴⁶ P. Markowitz,¹⁴⁶
 J. L. Rodriguez,¹⁴⁶ A. Ackert,¹⁴⁷ T. Adams,¹⁴⁷ A. Askew,¹⁴⁷ S. Hagopian,¹⁴⁷ V. Hagopian,¹⁴⁷ K. F. Johnson,¹⁴⁷ T. Kolberg,¹⁴⁷
 G. Martinez,¹⁴⁷ T. Perry,¹⁴⁷ H. Prosper,¹⁴⁷ A. Saha,¹⁴⁷ A. Santra,¹⁴⁷ V. Sharma,¹⁴⁷ R. Yohay,¹⁴⁷ M. M. Baarmand,¹⁴⁸
 V. Bhopatkar,¹⁴⁸ S. Colafranceschi,¹⁴⁸ M. Hohlmann,¹⁴⁸ D. Noonan,¹⁴⁸ T. Roy,¹⁴⁸ F. Yumiceva,¹⁴⁸ M. R. Adams,¹⁴⁹
 L. Apanasevich,¹⁴⁹ D. Berry,¹⁴⁹ R. R. Betts,¹⁴⁹ R. Cavanaugh,¹⁴⁹ X. Chen,¹⁴⁹ S. Dittmer,¹⁴⁹ O. Evdokimov,¹⁴⁹
 C. E. Gerber,¹⁴⁹ D. A. Hangal,¹⁴⁹ D. J. Hofman,¹⁴⁹ K. Jung,¹⁴⁹ J. Kamin,¹⁴⁹ I. D. Sandoval Gonzalez,¹⁴⁹ M. B. Tonjes,¹⁴⁹
 N. Varelas,¹⁴⁹ H. Wang,¹⁴⁹ Z. Wu,¹⁴⁹ J. Zhang,¹⁴⁹ B. Bilki,^{150,trr} W. Clarida,¹⁵⁰ K. Dilsiz,^{150,sss} S. Durgut,¹⁵⁰
 R. P. Gandrajula,¹⁵⁰ M. Haytmyradov,¹⁵⁰ V. Khristenko,¹⁵⁰ J.-P. Merlo,¹⁵⁰ H. Mermerkaya,^{150,ttt} A. Mestvirishvili,¹⁵⁰
 A. Moeller,¹⁵⁰ J. Nachtman,¹⁵⁰ H. Ogul,^{150,uuu} Y. Onel,¹⁵⁰ F. Ozok,^{150,vvv} A. Penzo,¹⁵⁰ C. Snyder,¹⁵⁰ E. Tiras,¹⁵⁰ J. Wetzel,¹⁵⁰
 K. Yi,¹⁵⁰ B. Blumenfeld,¹⁵¹ A. Cocoros,¹⁵¹ N. Eminizer,¹⁵¹ D. Fehling,¹⁵¹ L. Feng,¹⁵¹ A. V. Gritsan,¹⁵¹ W. T. Hung,¹⁵¹
 P. Maksimovic,¹⁵¹ J. Roskes,¹⁵¹ U. Sarica,¹⁵¹ M. Swartz,¹⁵¹ M. Xiao,¹⁵¹ C. You,¹⁵¹ A. Al-bataineh,¹⁵² P. Baringer,¹⁵²
 A. Bean,¹⁵² S. Boren,¹⁵² J. Bowen,¹⁵² J. Castle,¹⁵² S. Khalil,¹⁵² A. Kropivnitskaya,¹⁵² D. Majumder,¹⁵² W. Mcbrayer,¹⁵²
 M. Murray,¹⁵² C. Rogan,¹⁵² C. Royon,¹⁵² S. Sanders,¹⁵² E. Schmitz,¹⁵² J. D. Tapia Takaki,¹⁵² Q. Wang,¹⁵² A. Ivanov,¹⁵³
 K. Kaadze,¹⁵³ Y. Maravin,¹⁵³ A. Modak,¹⁵³ A. Mohammadi,¹⁵³ L. K. Saini,¹⁵³ N. Skhirtladze,¹⁵³ F. Rebassoo,¹⁵⁴
 D. Wright,¹⁵⁴ A. Baden,¹⁵⁵ O. Baron,¹⁵⁵ A. Belloni,¹⁵⁵ S. C. Eno,¹⁵⁵ Y. Feng,¹⁵⁵ C. Ferraioli,¹⁵⁵ N. J. Hadley,¹⁵⁵ S. Jabeen,¹⁵⁵
 G. Y. Jeng,¹⁵⁵ R. G. Kellogg,¹⁵⁵ J. Kunkle,¹⁵⁵ A. C. Mignerey,¹⁵⁵ F. Ricci-Tam,¹⁵⁵ Y. H. Shin,¹⁵⁵ A. Skuja,¹⁵⁵ S. C. Tonwar,¹⁵⁵
 D. Abercrombie,¹⁵⁶ B. Allen,¹⁵⁶ V. Azzolini,¹⁵⁶ R. Barbieri,¹⁵⁶ A. Baty,¹⁵⁶ G. Bauer,¹⁵⁶ R. Bi,¹⁵⁶ S. Brandt,¹⁵⁶ W. Busza,¹⁵⁶
 I. A. Cali,¹⁵⁶ M. D'Alfonso,¹⁵⁶ Z. Demiragli,¹⁵⁶ G. Gomez Ceballos,¹⁵⁶ M. Goncharov,¹⁵⁶ P. Harris,¹⁵⁶ D. Hsu,¹⁵⁶ M. Hu,¹⁵⁶
 Y. Iiyama,¹⁵⁶ G. M. Innocenti,¹⁵⁶ M. Klute,¹⁵⁶ D. Kovalskyi,¹⁵⁶ Y.-J. Lee,¹⁵⁶ A. Levin,¹⁵⁶ P. D. Luckey,¹⁵⁶ B. Maier,¹⁵⁶
 A. C. Marini,¹⁵⁶ C. Mcginn,¹⁵⁶ C. Mironov,¹⁵⁶ S. Narayanan,¹⁵⁶ X. Niu,¹⁵⁶ C. Paus,¹⁵⁶ C. Roland,¹⁵⁶ G. Roland,¹⁵⁶
 G. S. F. Stephans,¹⁵⁶ K. Sumorok,¹⁵⁶ K. Tatar,¹⁵⁶ D. Velicanu,¹⁵⁶ J. Wang,¹⁵⁶ T. W. Wang,¹⁵⁶ B. Wyslouch,¹⁵⁶
 S. Zhaozhong,¹⁵⁶ A. C. Benvenuti,¹⁵⁷ R. M. Chatterjee,¹⁵⁷ A. Evans,¹⁵⁷ P. Hansen,¹⁵⁷ S. Kalafut,¹⁵⁷ Y. Kubota,¹⁵⁷
 Z. Lesko,¹⁵⁷ J. Mans,¹⁵⁷ S. Nourbakhsh,¹⁵⁷ N. Ruckstuhl,¹⁵⁷ R. Rusack,¹⁵⁷ J. Turkewitz,¹⁵⁷ M. A. Wadud,¹⁵⁷ J. G. Acosta,¹⁵⁸
 S. Oliveros,¹⁵⁸ E. Avdeeva,¹⁵⁹ K. Bloom,¹⁵⁹ D. R. Claes,¹⁵⁹ C. Fangmeier,¹⁵⁹ F. Golf,¹⁵⁹ R. Gonzalez Suarez,¹⁵⁹
 R. Kamaliuddin,¹⁵⁹ I. Kravchenko,¹⁵⁹ J. Monroy,¹⁵⁹ J. E. Siado,¹⁵⁹ G. R. Snow,¹⁵⁹ B. Stieger,¹⁵⁹ A. Godshalk,¹⁶⁰
 C. Harrington,¹⁶⁰ I. Iashvili,¹⁶⁰ D. Nguyen,¹⁶⁰ A. Parker,¹⁶⁰ S. Rappoccio,¹⁶⁰ B. Roozbahani,¹⁶⁰ G. Alverson,¹⁶¹
 E. Barberis,¹⁶¹ C. Freer,¹⁶¹ A. Hortiangtham,¹⁶¹ A. Massironi,¹⁶¹ D. M. Morse,¹⁶¹ T. Oriimoto,¹⁶¹ R. Teixeira De Lima,¹⁶¹
 T. Wamorkar,¹⁶¹ B. Wang,¹⁶¹ A. Wisecarver,¹⁶¹ D. Wood,¹⁶¹ S. Bhattacharya,¹⁶² O. Charaf,¹⁶² K. A. Hahn,¹⁶² N. Mucia,¹⁶²
 N. Odell,¹⁶² M. H. Schmitt,¹⁶² K. Sung,¹⁶² M. Trovato,¹⁶² M. Velasco,¹⁶² R. Bucci,¹⁶³ N. Dev,¹⁶³ M. Hildreth,¹⁶³
 K. Hurtado Anampa,¹⁶³ C. Jessop,¹⁶³ D. J. Karmgard,¹⁶³ N. Kellams,¹⁶³ K. Lannon,¹⁶³ W. Li,¹⁶³ N. Loukas,¹⁶³
 N. Marinelli,¹⁶³ F. Meng,¹⁶³ C. Mueller,¹⁶³ Y. Musienko,^{163,II} M. Planer,¹⁶³ A. Reinsvold,¹⁶³ R. Ruchti,¹⁶³ P. Siddireddy,¹⁶³
 G. Smith,¹⁶³ S. Taroni,¹⁶³ M. Wayne,¹⁶³ A. Wightman,¹⁶³ M. Wolf,¹⁶³ A. Woodard,¹⁶³ J. Alimena,¹⁶⁴ L. Antonelli,¹⁶⁴
 B. Bylsma,¹⁶⁴ L. S. Durkin,¹⁶⁴ S. Flowers,¹⁶⁴ B. Francis,¹⁶⁴ A. Hart,¹⁶⁴ C. Hill,¹⁶⁴ W. Ji,¹⁶⁴ T. Y. Ling,¹⁶⁴ W. Luo,¹⁶⁴
 B. L. Winer,¹⁶⁴ H. W. Wulsin,¹⁶⁴ S. Cooperstein,¹⁶⁵ O. Driga,¹⁶⁵ P. Elmer,¹⁶⁵ J. Hardenbrook,¹⁶⁵ P. Hebda,¹⁶⁵

S. Higginbotham,¹⁶⁵ A. Kalogeropoulos,¹⁶⁵ D. Lange,¹⁶⁵ J. Luo,¹⁶⁵ D. Marlow,¹⁶⁵ K. Mei,¹⁶⁵ I. Ojalvo,¹⁶⁵ J. Olsen,¹⁶⁵ C. Palmer,¹⁶⁵ P. Piroué,¹⁶⁵ J. Salfeld-Nebgen,¹⁶⁵ D. Stickland,¹⁶⁵ C. Tully,¹⁶⁵ S. Malik,¹⁶⁶ S. Norberg,¹⁶⁶ A. Barker,¹⁶⁷ V. E. Barnes,¹⁶⁷ S. Das,¹⁶⁷ L. Gutay,¹⁶⁷ M. Jones,¹⁶⁷ A. W. Jung,¹⁶⁷ A. Khatiwada,¹⁶⁷ D. H. Miller,¹⁶⁷ N. Neumeister,¹⁶⁷ C. C. Peng,¹⁶⁷ H. Qiu,¹⁶⁷ J. F. Schulte,¹⁶⁷ J. Sun,¹⁶⁷ F. Wang,¹⁶⁷ R. Xiao,¹⁶⁷ W. Xie,¹⁶⁷ T. Cheng,¹⁶⁸ J. Dolen,¹⁶⁸ N. Parashar,¹⁶⁸ Z. Chen,¹⁶⁹ K. M. Ecklund,¹⁶⁹ S. Freed,¹⁶⁹ F. J. M. Geurts,¹⁶⁹ M. Guilbaud,¹⁶⁹ M. Kilpatrick,¹⁶⁹ W. Li,¹⁶⁹ B. Michlin,¹⁶⁹ B. P. Padley,¹⁶⁹ J. Roberts,¹⁶⁹ J. Rorie,¹⁶⁹ W. Shi,¹⁶⁹ Z. Tu,¹⁶⁹ J. Zabel,¹⁶⁹ A. Zhang,¹⁶⁹ A. Bodek,¹⁷⁰ P. de Barbaro,¹⁷⁰ R. Demina,¹⁷⁰ Y. t. Duh,¹⁷⁰ T. Ferbel,¹⁷⁰ M. Galanti,¹⁷⁰ A. Garcia-Bellido,¹⁷⁰ J. Han,¹⁷⁰ O. Hindrichs,¹⁷⁰ A. Khukhunaishvili,¹⁷⁰ K. H. Lo,¹⁷⁰ P. Tan,¹⁷⁰ M. Verzetti,¹⁷⁰ R. Ciesielski,¹⁷¹ K. Goulianios,¹⁷¹ C. Mesropian,¹⁷¹ A. Agapitos,¹⁷² J. P. Chou,¹⁷² Y. Gershtein,¹⁷² T. A. Gómez Espinosa,¹⁷² E. Halkiadakis,¹⁷² M. Heindl,¹⁷² E. Hughes,¹⁷² S. Kaplan,¹⁷² R. Kunnawalkam Elayavalli,¹⁷² S. Kyriacou,¹⁷² A. Lath,¹⁷² R. Montalvo,¹⁷² K. Nash,¹⁷² M. Osherson,¹⁷² H. Saka,¹⁷² S. Salur,¹⁷² S. Schnetzer,¹⁷² D. Sheffield,¹⁷² S. Somalwar,¹⁷² R. Stone,¹⁷² S. Thomas,¹⁷² P. Thomassen,¹⁷² M. Walker,¹⁷² A. G. Delannoy,¹⁷³ J. Heideman,¹⁷³ G. Riley,¹⁷³ K. Rose,¹⁷³ S. Spanier,¹⁷³ K. Thapa,¹⁷³ O. Bouhali,¹⁷⁴ A. Castaneda Hernandez,¹⁷⁴^{www} A. Celik,¹⁷⁴ M. Dalchenko,¹⁷⁴ M. De Mattia,¹⁷⁴ A. Delgado,¹⁷⁴ S. Dildick,¹⁷⁴ R. Eusebi,¹⁷⁴ J. Gilmore,¹⁷⁴ T. Huang,¹⁷⁴ T. Kamon,¹⁷⁴^{xxx} R. Mueller,¹⁷⁴ Y. Pakhotin,¹⁷⁴ R. Patel,¹⁷⁴ A. Perloff,¹⁷⁴ L. Perniè,¹⁷⁴ D. Rathjens,¹⁷⁴ A. Safonov,¹⁷⁴ A. Tatarinov,¹⁷⁴ N. Akchurin,¹⁷⁵ J. Damgov,¹⁷⁵ F. De Guio,¹⁷⁵ P. R. Dudero,¹⁷⁵ J. Faulkner,¹⁷⁵ E. Gurpinar,¹⁷⁵ S. Kunori,¹⁷⁵ K. Lamichhane,¹⁷⁵ S. W. Lee,¹⁷⁵ T. Mengke,¹⁷⁵ S. Muthumuni,¹⁷⁵ T. Peltola,¹⁷⁵ S. Undleeb,¹⁷⁵ I. Volobouev,¹⁷⁵ Z. Wang,¹⁷⁵ S. Greene,¹⁷⁶ A. Gurrola,¹⁷⁶ R. Janjam,¹⁷⁶ W. Johns,¹⁷⁶ C. Maguire,¹⁷⁶ A. Melo,¹⁷⁶ H. Ni,¹⁷⁶ K. Padeken,¹⁷⁶ J. D. Ruiz Alvarez,¹⁷⁶ P. Sheldon,¹⁷⁶ S. Tuo,¹⁷⁶ J. Velkovska,¹⁷⁶ Q. Xu,¹⁷⁶ M. W. Arenton,¹⁷⁷ P. Barria,¹⁷⁷ B. Cox,¹⁷⁷ R. Hirosky,¹⁷⁷ M. Joyce,¹⁷⁷ A. Ledovskoy,¹⁷⁷ H. Li,¹⁷⁷ C. Neu,¹⁷⁷ T. Sinthuprasith,¹⁷⁷ Y. Wang,¹⁷⁷ E. Wolfe,¹⁷⁷ F. Xia,¹⁷⁷ R. Harr,¹⁷⁸ P. E. Karchin,¹⁷⁸ N. Poudyal,¹⁷⁸ J. Sturdy,¹⁷⁸ P. Thapa,¹⁷⁸ S. Zaleski,¹⁷⁸ M. Brodski,¹⁷⁹ J. Buchanan,¹⁷⁹ C. Caillol,¹⁷⁹ D. Carlsmith,¹⁷⁹ S. Dasu,¹⁷⁹ L. Dodd,¹⁷⁹ S. Duric,¹⁷⁹ B. Gomber,¹⁷⁹ M. Grothe,¹⁷⁹ M. Herndon,¹⁷⁹ A. Hervé,¹⁷⁹ U. Hussain,¹⁷⁹ P. Klabbers,¹⁷⁹ A. Lanaro,¹⁷⁹ A. Levine,¹⁷⁹ K. Long,¹⁷⁹ R. Loveless,¹⁷⁹ V. Rekovic,¹⁷⁹ T. Ruggles,¹⁷⁹ A. Savin,¹⁷⁹ N. Smith,¹⁷⁹ W. H. Smith,¹⁷⁹ and N. Woods¹⁷⁹

(CMS Collaboration)

¹*Yerevan Physics Institute, Yerevan, Armenia*

²*Institut für Hochenergiephysik, Wien, Austria*

³*Institute for Nuclear Problems, Minsk, Belarus*

⁴*Universiteit Antwerpen, Antwerpen, Belgium*

⁵*Vrije Universiteit Brussel, Brussel, Belgium*

⁶*Université Libre de Bruxelles, Bruxelles, Belgium*

⁷*Ghent University, Ghent, Belgium*

⁸*Université Catholique de Louvain, Louvain-la-Neuve, Belgium*

⁹*Centro Brasileiro de Pesquisas Fisicas, Rio de Janeiro, Brazil*

¹⁰*Universidade do Estado do Rio de Janeiro, Rio de Janeiro, Brazil*

^{11a}*Universidade Estadual Paulista, Universidade Federal do ABC, São Paulo, Brazil*

^{11b}*Universidade Estadual Paulista*

^{11c}*Universidade Federal do ABC*

¹²*Institute for Nuclear Research and Nuclear Energy, Bulgarian Academy of Sciences, Sofia, Bulgaria*

¹³*University of Sofia, Sofia, Bulgaria*

¹⁴*Beihang University, Beijing, China*

¹⁵*Institute of High Energy Physics, Beijing, China*

¹⁶*State Key Laboratory of Nuclear Physics and Technology, Peking University, Beijing, China*

¹⁷*Tsinghua University, Beijing, China*

¹⁸*Universidad de Los Andes, Bogota, Colombia*

¹⁹*University of Split, Faculty of Electrical Engineering, Mechanical Engineering and Naval Architecture, Split, Croatia*

²⁰*University of Split, Faculty of Science, Split, Croatia*

²¹*Institute Rudjer Boskovic, Zagreb, Croatia*

²²*University of Cyprus, Nicosia, Cyprus*

²³*Charles University, Prague, Czech Republic*

²⁴*Universidad San Francisco de Quito, Quito, Ecuador*

- ²⁵Academy of Scientific Research and Technology of the Arab Republic of Egypt,
Egyptian Network of High Energy Physics, Cairo, Egypt
- ²⁶National Institute of Chemical Physics and Biophysics, Tallinn, Estonia
- ²⁷Department of Physics, University of Helsinki, Helsinki, Finland
- ²⁸Helsinki Institute of Physics, Helsinki, Finland
- ²⁹Lappeenranta University of Technology, Lappeenranta, Finland
- ³⁰IRFU, CEA, Université Paris-Saclay, Gif-sur-Yvette, France
- ³¹Laboratoire Leprince-Ringuet, Ecole polytechnique, CNRS/IN2P3, Université Paris-Saclay,
Palaiseau, France
- ³²Université de Strasbourg, CNRS, IPHC UMR 7178, F-67000 Strasbourg, France
- ³³Centre de Calcul de l'Institut National de Physique Nucléaire et de Physique des Particules,
CNRS/IN2P3, Villeurbanne, France
- ³⁴Université de Lyon, Université Claude Bernard Lyon 1, CNRS-IN2P3,
Institut de Physique Nucléaire de Lyon, Villeurbanne, France
- ³⁵Georgian Technical University, Tbilisi, Georgia
- ³⁶Tbilisi State University, Tbilisi, Georgia
- ³⁷RWTH Aachen University, I. Physikalisches Institut, Aachen, Germany
- ³⁸RWTH Aachen University, III. Physikalisches Institut A, Aachen, Germany
- ³⁹RWTH Aachen University, III. Physikalisches Institut B, Aachen, Germany
- ⁴⁰Deutsches Elektronen-Synchrotron, Hamburg, Germany
- ⁴¹University of Hamburg, Hamburg, Germany
- ⁴²Institut für Experimentelle Teilchenphysik, Karlsruhe, Germany
- ⁴³Institute of Nuclear and Particle Physics (INPP), NCSR Demokritos, Aghia Paraskevi, Greece
- ⁴⁴National and Kapodistrian University of Athens, Athens, Greece
- ⁴⁵National Technical University of Athens, Athens, Greece
- ⁴⁶University of Ioánnina, Ioánnina, Greece
- ⁴⁷MTA-ELTE Lendület CMS Particle and Nuclear Physics Group, Eötvös Loránd University,
Budapest, Hungary
- ⁴⁸Wigner Research Centre for Physics, Budapest, Hungary
- ⁴⁹Institute of Nuclear Research ATOMKI, Debrecen, Hungary
- ⁵⁰Institute of Physics, University of Debrecen, Debrecen, Hungary
- ⁵¹Indian Institute of Science (IISc), Bangalore, India
- ⁵²National Institute of Science Education and Research, Bhubaneswar, India
- ⁵³Panjab University, Chandigarh, India
- ⁵⁴University of Delhi, Delhi, India
- ⁵⁵Saha Institute of Nuclear Physics, HBNI, Kolkata, India
- ⁵⁶Indian Institute of Technology Madras, Madras, India
- ⁵⁷Bhabha Atomic Research Centre, Mumbai, India
- ⁵⁸Tata Institute of Fundamental Research-A, Mumbai, India
- ⁵⁹Tata Institute of Fundamental Research-B, Mumbai, India
- ⁶⁰Indian Institute of Science Education and Research (IISER), Pune, India
- ⁶¹Institute for Research in Fundamental Sciences (IPM), Tehran, Iran
- ⁶²University College Dublin, Dublin, Ireland
- ^{63a}INFN Sezione di Bari, Università di Bari, Politecnico di Bari, Bari, Italy
- ^{63b}INFN Sezione di Bari
- ^{63c}Università di Bari
- ^{63d}Politecnico di Bari
- ^{64a}INFN Sezione di Bologna, Università di Bologna, Bologna, Italy
- ^{64b}INFN Sezione di Bologna
- ^{64c}Università di Bologna
- ^{65a}INFN Sezione di Catania, Università di Catania, Catania, Italy
- ^{65b}INFN Sezione di Catania
- ^{65c}Università di Catania
- ^{66a}INFN Sezione di Firenze, Università di Firenze, Firenze, Italy
- ^{66b}INFN Sezione di Firenze
- ^{66c}Università di Firenze
- ⁶⁷INFN Laboratori Nazionali di Frascati, Frascati, Italy
- ^{68a}INFN Sezione di Genova, Università di Genova, Genova, Italy
- ^{68b}INFN Sezione di Genova
- ^{68c}Università di Genova

- ^{69a}*INFN Sezione di Milano-Bicocca*
^{69b}*Università di Milano-Bicocca*
- ^{70a}*INFN Sezione di Napoli, Università di Napoli 'Federico II', Napoli, Italy,*
Università della Basilicata, Potenza, Italy, Università G. Marconi, Roma, Italy
- ^{70b}*INFN Sezione di Napoli*
^{70c}*Università di Napoli 'Federico II'*
^{70d}*Università della Basilicata*
^{70e}*Università G. Marconi*
- ^{71a}*INFN Sezione di Padova, Università di Padova, Padova, Italy,*
Università di Trento, Trento, Italy
- ^{71b}*INFN Sezione di Padova*
^{71c}*Università di Padova*
^{71d}*Università di Trento*
- ^{72a}*INFN Sezione di Pavia*
^{72b}*Università di Pavia*
- ^{73a}*INFN Sezione di Perugia, Università di Perugia, Perugia, Italy*
^{73b}*INFN Sezione di Perugia*
^{73c}*Università di Perugia*
- ^{74a}*INFN Sezione di Pisa, Università di Pisa, Scuola Normale Superiore di Pisa, Pisa, Italy*
^{74b}*INFN Sezione di Pisa*
^{74c}*Università di Pisa*
- ^{74d}*Scuola Normale Superiore di Pisa*
- ^{75a}*INFN Sezione di Roma, Sapienza Università di Roma, Rome, Italy*
^{75b}*INFN Sezione di Roma*
^{75c}*Sapienza Università di Roma*
- ^{76a}*INFN Sezione di Torino, Università di Torino, Torino, Italy,*
Università del Piemonte Orientale, Novara, Italy
- ^{76b}*INFN Sezione di Torino*
^{76c}*Università di Torino*
- ^{76d}*Università del Piemonte Orientale*
- ^{77a}*INFN Sezione di Trieste, Università di Trieste, Trieste, Italy*
^{77b}*INFN Sezione di Trieste*
^{77c}*Università di Trieste*
- ⁷⁸*Kyungpook National University*
- ⁷⁹*Chonnam National University, Institute for Universe and Elementary Particles, Kwangju, Korea*
⁸⁰*Hanyang University, Seoul, Korea*
⁸¹*Korea University, Seoul, Korea*
- ⁸²*Seoul National University, Seoul, Korea*
⁸³*University of Seoul, Seoul, Korea*
- ⁸⁴*Sungkyunkwan University, Suwon, Korea*
⁸⁵*Vilnius University, Vilnius, Lithuania*
- ⁸⁶*National Centre for Particle Physics, Universiti Malaya, Kuala Lumpur, Malaysia*
- ⁸⁷*Centro de Investigacion y de Estudios Avanzados del IPN, Mexico City, Mexico*
⁸⁸*Universidad Iberoamericana, Mexico City, Mexico*
- ⁸⁹*Benemerita Universidad Autónoma de Puebla, Puebla, Mexico*
⁹⁰*Universidad Autónoma de San Luis Potosí, San Luis Potosí, Mexico*
⁹¹*University of Auckland, Auckland, New Zealand*
- ⁹²*University of Canterbury, Christchurch, New Zealand*
- ⁹³*National Centre for Physics, Quaid-I-Azam University, Islamabad, Pakistan*
⁹⁴*National Centre for Nuclear Research, Swierk, Poland*
- ⁹⁵*Institute of Experimental Physics, Faculty of Physics, University of Warsaw, Warsaw, Poland*
⁹⁶*Laboratório de Instrumentação e Física Experimental de Partículas, Lisboa, Portugal*
⁹⁷*Joint Institute for Nuclear Research, Dubna, Russia*
- ⁹⁸*Petersburg Nuclear Physics Institute, Gatchina (St. Petersburg), Russia*
⁹⁹*Institute for Nuclear Research, Moscow, Russia*
- ¹⁰⁰*Institute for Theoretical and Experimental Physics, Moscow, Russia*
¹⁰¹*Moscow Institute of Physics and Technology, Moscow, Russia*
- ¹⁰²*National Research Nuclear University 'Moscow Engineering Physics Institute' (MEPhI),
 Moscow, Russia*
- ¹⁰³*P.N. Lebedev Physical Institute, Moscow, Russia*

¹⁰⁴*Skobeltsyn Institute of Nuclear Physics, Lomonosov Moscow State University, Moscow, Russia*¹⁰⁵*Novosibirsk State University (NSU), Novosibirsk, Russia*¹⁰⁶*State Research Center of Russian Federation, Institute for High Energy Physics of NRC "Kurchatov Institute", Protvino, Russia*¹⁰⁷*National Research Tomsk Polytechnic University, Tomsk, Russia*¹⁰⁸*University of Belgrade, Faculty of Physics and Vinca Institute of Nuclear Sciences, Belgrade, Serbia*¹⁰⁹*Centro de Investigaciones Energéticas Medioambientales y Tecnológicas (CIEMAT), Madrid, Spain*¹¹⁰*Universidad Autónoma de Madrid, Madrid, Spain*¹¹¹*Universidad de Oviedo, Oviedo, Spain*¹¹²*Instituto de Física de Cantabria (IFCA), CSIC-Universidad de Cantabria, Santander, Spain*¹¹³*CERN, European Organization for Nuclear Research, Geneva, Switzerland*¹¹⁴*Paul Scherrer Institut, Villigen, Switzerland*¹¹⁵*ETH Zurich - Institute for Particle Physics and Astrophysics (IPA), Zurich, Switzerland*¹¹⁶*Universität Zürich, Zurich, Switzerland*¹¹⁷*National Central University, Chung-Li, Taiwan*¹¹⁸*National Taiwan University (NTU), Taipei, Taiwan*¹¹⁹*Chulalongkorn University, Faculty of Science, Department of Physics, Bangkok, Thailand*¹²⁰*Cukurova University, Physics Department, Science and Art Faculty, Adana, Turkey*¹²¹*Middle East Technical University, Physics Department, Ankara, Turkey*¹²²*Bogazici University, Istanbul, Turkey*¹²³*Istanbul Technical University, Istanbul, Turkey*¹²⁴*Institute for Scintillation Materials of National Academy of Science of Ukraine, Kharkov, Ukraine*¹²⁵*National Scientific Center, Kharkov Institute of Physics and Technology, Kharkov, Ukraine*¹²⁶*University of Bristol, Bristol, United Kingdom*¹²⁷*Rutherford Appleton Laboratory, Didcot, United Kingdom*¹²⁸*Imperial College, London, United Kingdom*¹²⁹*Brunel University, Uxbridge, United Kingdom*¹³⁰*Baylor University, Waco, USA*¹³¹*Catholic University of America, Washington DC, USA*¹³²*The University of Alabama, Tuscaloosa, USA*¹³³*Boston University, Boston, USA*¹³⁴*Brown University, Providence, USA*¹³⁵*University of California, Davis, Davis, USA*¹³⁶*University of California, Los Angeles, USA*¹³⁷*University of California, Riverside, Riverside, USA*¹³⁸*University of California, San Diego, La Jolla, USA*¹³⁹*University of California, Santa Barbara - Department of Physics, Santa Barbara, USA*¹⁴⁰*California Institute of Technology, Pasadena, USA*¹⁴¹*Carnegie Mellon University, Pittsburgh, USA*¹⁴²*University of Colorado Boulder, Boulder, USA*¹⁴³*Cornell University, Ithaca, USA*¹⁴⁴*Fermi National Accelerator Laboratory, Batavia, USA*¹⁴⁵*University of Florida, Gainesville, USA*¹⁴⁶*Florida International University, Miami, USA*¹⁴⁷*Florida State University, Tallahassee, USA*¹⁴⁸*Florida Institute of Technology, Melbourne, USA*¹⁴⁹*University of Illinois at Chicago (UIC), Chicago, USA*¹⁵⁰*The University of Iowa, Iowa City, USA*¹⁵¹*Johns Hopkins University, Baltimore, USA*¹⁵²*The University of Kansas, Lawrence, USA*¹⁵³*Kansas State University, Manhattan, USA*¹⁵⁴*Lawrence Livermore National Laboratory, Livermore, USA*¹⁵⁵*University of Maryland, College Park, USA*¹⁵⁶*Massachusetts Institute of Technology, Cambridge, USA*¹⁵⁷*University of Minnesota, Minneapolis, USA*¹⁵⁸*University of Mississippi, Oxford, USA*¹⁵⁹*University of Nebraska-Lincoln, Lincoln, USA*¹⁶⁰*State University of New York at Buffalo, Buffalo, USA*¹⁶¹*Northeastern University, Boston, USA*¹⁶²*Northwestern University, Evanston, USA*

¹⁶³*University of Notre Dame, Notre Dame, USA*¹⁶⁴*The Ohio State University, Columbus, USA*¹⁶⁵*Princeton University, Princeton, USA*¹⁶⁶*University of Puerto Rico, Mayaguez, USA*¹⁶⁷*Purdue University, West Lafayette, USA*¹⁶⁸*Purdue University Northwest, Hammond, USA*¹⁶⁹*Rice University, Houston, USA*¹⁷⁰*University of Rochester, Rochester, USA*¹⁷¹*The Rockefeller University, New York, USA*¹⁷²*Rutgers, The State University of New Jersey, Piscataway, USA*¹⁷³*University of Tennessee, Knoxville, USA*¹⁷⁴*Texas A&M University, College Station, USA*¹⁷⁵*Texas Tech University, Lubbock, USA*¹⁷⁶*Vanderbilt University, Nashville, USA*¹⁷⁷*University of Virginia, Charlottesville, USA*¹⁷⁸*Wayne State University, Detroit, USA*¹⁷⁹*University of Wisconsin - Madison, Madison, WI, USA*^aDeceased.^bAlso at Vienna University of Technology, Vienna, Austria.^cAlso at IRFU, CEA, Université Paris-Saclay, Gif-sur-Yvette, France.^dAlso at Universidade Estadual de Campinas, Campinas, Brazil.^eAlso at Federal University of Rio Grande do Sul, Porto Alegre, Brazil.^fAlso at Universidade Federal de Pelotas, Pelotas, Brazil.^gAlso at Université Libre de Bruxelles, Bruxelles, Belgium.^hAlso at Institute for Theoretical and Experimental Physics, Moscow, Russia.ⁱAlso at Joint Institute for Nuclear Research, Dubna, Russia.^jAlso at Cairo University, Cairo, Egypt.^kAlso at Zewail City of Science and Technology, Zewail, Egypt.^lAlso at Fayoum University, El-Fayoum, Egypt.^mAlso at Department of Physics, King Abdulaziz University, Jeddah, Saudi Arabia.ⁿAlso at Université de Haute Alsace, Mulhouse, France.^oAlso at Skobeltsyn Institute of Nuclear Physics, Lomonosov Moscow State University, Moscow, Russia.^pAlso at Tbilisi State University, Tbilisi, Georgia.^qAlso at CERN, European Organization for Nuclear Research, Geneva, Switzerland.^rAlso at RWTH Aachen University, III. Physikalischs Institut A, Aachen, Germany.^sAlso at University of Hamburg, Hamburg, Germany.^tAlso at Brandenburg University of Technology, Cottbus, Germany.^uAlso at Institute of Nuclear Research ATOMKI, Debrecen, Hungary.^vAlso at Institute of Physics, University of Debrecen, Debrecen, Hungary.^wAlso at MTA-ELTE Lendület CMS Particle and Nuclear Physics Group, Eötvös Loránd University, Budapest, Hungary.^xAlso at IIT Bhubaneswar, Bhubaneswar, India.^yAlso at Institute of Physics, Bhubaneswar, India.^zAlso at Shoolini University, Solan, India.^{aa}Also at University of Visva-Bharati, Santiniketan, India.^{bb}Also at University of Ruhuna, Matara, Sri Lanka.^{cc}Also at Isfahan University of Technology, Isfahan, Iran.^{dd}Also at Yazd University, Yazd, Iran.^{ee}Also at Plasma Physics Research Center, Science and Research Branch, Islamic Azad University, Tehran, Iran.^{ff}Also at Università degli Studi di Siena, Siena, Italy.^{gg}Also at INFN Sezione di Milano-Bicocca, Università di Milano-Bicocca, Milano, Italy.^{hh}Also at International Islamic University of Malaysia, Kuala Lumpur, Malaysia.ⁱⁱAlso at Malaysian Nuclear Agency, MOSTI, Kajang, Malaysia.^{jj}Also at Consejo Nacional de Ciencia y Tecnología, Mexico city, Mexico.^{kk}Also at Warsaw University of Technology, Institute of Electronic Systems, Warsaw, Poland.^{ll}Also at Institute for Nuclear Research, Moscow, Russia.^{mm}Also at National Research Nuclear University 'Moscow Engineering Physics Institute' (MEPhI), Moscow, Russia.ⁿⁿAlso at St. Petersburg State Polytechnical University, St. Petersburg, Russia.^{oo}Also at University of Florida, Gainesville, USA.^{pp}Also at P.N. Lebedev Physical Institute, Moscow, Russia.

- ^{qq} Also at California Institute of Technology, Pasadena, USA.
^{rr} Also at Budker Institute of Nuclear Physics, Novosibirsk, Russia.
^{ss} Also at Faculty of Physics, University of Belgrade, Belgrade, Serbia.
^{tt} Also at INFN Sezione di Pavia, Università di Pavia, Pavia, Italy.
^{uu} Also at University of Belgrade, Faculty of Physics and Vinca Institute of Nuclear Sciences, Belgrade, Serbia.
^{vv} Also at Scuola Normale e Sezione dell'INFN, Pisa, Italy.
^{ww} Also at National and Kapodistrian University of Athens, Athens, Greece.
^{xx} Also at Riga Technical University, Riga, Latvia.
^{yy} Also at Universität Zürich, Zurich, Switzerland.
^{zz} Also at Stefan Meyer Institute for Subatomic Physics.
^{aaa} Also at Istanbul Aydin University, Istanbul, Turkey.
^{bbb} Also at Mersin University, Mersin, Turkey.
^{ccc} Also at Piri Reis University, Istanbul, Turkey.
^{ddd} Also at Gaziosmanpasa University, Tokat, Turkey.
^{eee} Also at Adiyaman University, Adiyaman, Turkey.
^{fff} Also at Izmir Institute of Technology, Izmir, Turkey.
^{ggg} Also at Necmettin Erbakan University, Konya, Turkey.
^{hhh} Also at Marmara University, Istanbul, Turkey.
ⁱⁱⁱ Also at Kafkas University, Kars, Turkey.
^{jjj} Also at Istanbul Bilgi University, Istanbul, Turkey.
^{kkk} Also at Rutherford Appleton Laboratory, Didcot, United Kingdom.
^{lll} Also at School of Physics and Astronomy, University of Southampton, Southampton, United Kingdom.
^{mmm} Also at Monash University, Faculty of Science, Clayton, Australia.
ⁿⁿⁿ Also at Instituto de Astrofísica de Canarias, La Laguna, Spain.
^{ooo} Also at Bethel University.
^{ppp} Also at Utah Valley University, Orem, USA.
^{qqq} Also at Purdue University, West Lafayette, USA.
^{rrr} Also at Beykent University.
^{sss} Also at Bingol University, Bingol, Turkey.
^{ttt} Also at Erzincan University, Erzincan, Turkey.
^{uuu} Also at Sinop University, Sinop, Turkey.
^{vvv} Also at Mimar Sinan University, İstanbul, İstanbul, Turkey.
^{www} Also at Texas A&M University at Qatar, Doha, Qatar.
^{xxx} Also at Kyungpook National University.